10-19-2023

Genetic and Pharmacological Factors Control Aging in Caenorhabditis elegans.

Brian McNally Egan
Washington University in St. Louis

WASHINGTON UNIVERSITY IN ST. LOUIS
Division of Biology and Biomedical Sciences
Program in Molecular Cell Biology

Dissertation Examination Committee:
Kerry Kornfeld, Chair
Abhinav Diwan
Roberta Faccio
Michael Nonet
Heather True

Genetic and Pharmacological Factors Control Aging in *Caenorhabditis elegans.*

by
Brian M. Egan

A dissertation presented to
Washington University in St. Louis
in partial fulfillment of the
requirements for the degree
of Doctor of Philosophy

December 2023
St. Louis, Missouri

Table of Contents

List of Figures

List of Tables

List of Abbreviations

Aß	Amyloid Beta
ACE	Angiotensin-converting enzyme
ACE2	Angiotensin-converting enzyme 2
Acer	Angiotensin-converting enzyme-related
ACN-1	ACE-like non-metallopeptidase
AD	Alzheimer's Disease
AGT	Angiotensinogen
AGT1R	Angiotensin II type-1 receptor
AGT2R	Angiotensin II type-2 receptor
Ance	ANgiotensin-converting enzyme
Ang I	Angiotensin I
Ang II	Angiotensin II
APP	Amyloid precurser protein
Daf-c	Dauer constitutive
Daf-d	Dauer defective
DR	Dietary restriction
GWAS	Genome-wide association study
GFP	Green fluorescent protein
EMS	Ethylmethanesulfanate
HID	High-temperature induction of dauer
HPLC/MS	High-performance liquid chromatography/mass spectroscopy
IGF	Insulin-like growth factor
IIS	Insulin/IGF-1 signaling
INSR	Insulin receptor (human, mouse)
InR	Insulin receptor (*Drosophila*)
LB	Lysogeny broth
METC	Mitochondrial electron transport chain

MTOR	Mechanistic target of rapamycin
NGM	Nematode growth medium
RAS	Renin-angiotensin system
RAAS	Renin-angiotensin-aldosterone system
RNAi	RNA interference
ROS	Reactive oxygen species
RT-qPCR	Reverse transcription quantitative polymerase chain reaction
SDS	sodium dodecyl sulfate
SOD	Superoxide dismutase
TOR	Target of rapamycin
WGS	Whole-genome sequencing
WT	Wild type

Acknowledgements

In my many long years as a graduate student I have been fortunate enough to accumulate a great many people to thank. I apologize in advance to anyone whose names I have inadvertently omitted. I would like to thank you, the reader, for taking the time to read something that I have spent so much time and energy on. I hope this document will in some way help you during your own scientific journey.

First, my mentor Kerry Kornfeld. I first met Kerry by chance at a poster session, where he introduced me to the concept that aging could be studied scientifically. I have been continually inspired by his ability to recognize both the big-picture idealist qualities of our research, as well as the down-to-earth applications. He has supported me both professionally and personally throughout my graduate school career. He has a great talent in seeing the silver lining in anything, and has often been able to tease out useful insights when I was all too ready to give up. He has allowed me to grow as a scientist, and has been incredibly supportive of my future career in science communication; I am very fortunate to have had Kerry's mentorship.

Second, the many people whose mentorship and guidance helped me throughout my career. Sandeep Kumar, John Murphy, Andrea Scharf, Zuzana Kocsisova, and others who originated many of the projects that I pursued; I hope that I have left some of these projects in a state that allows others to continue them as I did. My thesis committee, Heather True, Abhinav Diwan, Mike Nonet, and Roberta Faccio for their insight and encouragement, even during those times that I had no useable data to show after months of work. My program coordinator Stacy Kiel, whose organization and support is instrumental for our success. Tim Schedl, Shin Imai, and many others in the worm and aging fields for sharing their experience and expertise during our many seminars and journal clubs. My fellow graduate students in DBBS, for your constant

reassurances that none of you knew what you were doing either. Luke Schneider, who makes all the work we do possible, and who kept me well supplied with honey throughout my career. And all the members of the Kornfeld laboratory, past, present, and future, for making the laboratory such a wonderful environment.

Third, to my parents and the rest of my extended family, who have helped and supported me for many years, despite not really understanding what I do; don't worry, neither do I, really. Holidays and celebrations at home with my family kept me going through the many years of failed experiments and few breaks. To answer the question they've been asking me for the last five years ("When will you graduate?"), I guess I can finally answer that question. To my friends, both local and distant; I will always cherish our late-night dinner parties and tabletop gaming sessions. I look forward to making you much more barbecue in the future.

Fourth, the many individuals and groups that have helped me materially. Jim Skeath and Heather True, for helping me get a (much needed) NIH T32 GM007067-43 training grant; Irving Boime, for supporting me with the Irving Boime Graduate Student Fellowship. Wormbase and Wormbook, for the invaluable knowledge and resources on every aspect of nematode biology. The *Ceanorhabditis* Genome Center, for the dozens of genotypes that I have ordered over the years. And all the laboratories whose equipment and resources I have been allowed to use.

Finally, I would like to thank my fiancé and best friend Sarah. I cannot overstate how much her support has been instrumental to my success, and I will be forever thankful for her unquestioning and unwavering support.

Brian Egan

Washington University in St. Louis
December 2023

ABSTRACT OF THE DISSERTATION

Genetic and pharmacological factors control aging in *Caenorhabditis elegans.*
by
Brian M. Egan

Doctor of Philosophy in Biology and Biomedical Sciences

Molecular Cell Biology

Washington University in St. Louis, 2023

Professor Kerry Kornfeld, Chair

Aging is a time-dependent decline in organismal structure and function that ultimately results in death. Aging occurs in nearly all metazoan organisms, and is a major risk factor for many human diseases including cancer, diabetes, hypertension, heart disease, and Alzheimer's Disease. The genetic pathways and mechanistic factors that underly the aging process are poorly understood. Control of aging in the nematode *C. elegans* can be accomplished via modulation of gene activity by genetic knockdown or by the introduction of inhibitory pharmaceutical compounds. While many such interventions have been described in the literature, understanding the underlying mechanisms that control aging remains a critical goal of aging research.

Here, I advance the field by characterizing genetic and pharmacological mechanisms which control aging in *C. elegans*. Among these factors are *phm-2* and *eat-2*, genes necessary for pharynx development and function that control aging via a unique interaction between dietary restriction and the innate immune system; the human amyloid beta peptide, the proposed causative agent of Alzheimer's Disease, which enhances survival under pathogenic stress conditions; the ACE-inhibitor drug captopril and its mechanistic target *acn-1*, which control aging via interaction with the molting and developmental decision making pathways, and represent a highly conserved mechanism for lifespan extension across the animal kingdom; a

novel allele of the well-studied *daf-2* receptor tyrosine kinase gene that recapitulates human insulin receptoropathies; and osmotic stress response to sodium chloride concentration, which highlights a previously unrecognized role in nematode culture conditions that controls aging. These discoveries further our understanding of the mechanistic basis of aging in *C. elegans*.

Chapter I: Introduction

1.1 Understanding aging

What is aging, and why does it occur? This is the central question of the field of aging biology. After reaching adulthood, organisms undergo a characteristic time-dependent decline that results in loss of homeostatic capability, reduction of stress resistance, degradation of tissue structure and function, and, ultimately, death; this process is referred to as 'aging'. Despite decades of research, however, the precise mechanisms underlying the aging process remain largely unknown. The aim of this thesis is to uncover and characterize mechanistic factors underlying the aging process.

With few exceptions, all metazoan organisms age; however, the rate at which aging occurs can vary drastically between species. Some, like the Greenland shark, can live for centuries, while others, such as the mayfly, have adult lifespans of only a few days [1,2]. Like other factors of an animal's biology, an individual's lifespan is partly controlled by its genes. Similarly, the mean lifespan of a population or species is also determined by genetics. However, the precise genetic mechanisms that control the aging process remain poorly understood.

The free-living, non-parasitic nematode *Caenorhabditis elegans* has long been used as a model to study genetic factors that control the aging process [3–5]. Like other animals, *C. elegans* undergo a characteristic age-related decline resulting in lowered stress resistance, reduced movement and feeding behavior, loss of homeostatic capability, increased tissue disorganization, reduced fecundity, and death [5]. This process occurs in as little as two weeks, making *C. elegans* a convenient model to study interventions which affect aging. Approximately 70% of *C. elegans* genes have a homolog in humans, allowing simple translation of research into mammalian

contexts [6,7]. A variety of techniques allow modulation of *C. elegans* genes and gene expression, and loss-of-function mutations are available for most genes [8–10]. Administration of potential anti-aging compounds is simple and scalable, allowing rapid screening of large amounts of candidate compounds; indeed, several compounds that were first shown to extend lifespan in nematodes have also been shown to function in mammals [11–13]. Here, I use the nematode *C. elegans* as a model to better understand the genetic mechanisms underlying the aging process, and how genetic and pharmacological manipulation of these systems can control aging.

1.1.2 Age-related changes in *C. elegans*

Throughout the last several decades of research into *C. elegans*, hundreds of articles have been published describing dozens of phenotypes that change throughout the animal's lifespan (reviewed in [5]). While lifespan is the gold standard measurement for aging, measuring other age-related degenerative phenotypes allows one to better understand the aging process as a whole. The ideal anti-aging treatment will not only extend the animal's total lifespan, but will also extend the period of healthy functioning, the so-called "healthspan". Movement rate is an especially useful measure of healthspan, as it has been shown to correlate to healthy aging in a number of species [14–17]. Similarly, measurements of fecundity and reproductive output allow better insight into reproductive aging (reviewed in [18]). Other commonly measured phenotypes include pharyngeal pumping rate, heat and oxidative stress resistance, tissue function and integrity, proteostasis, DNA repair, etc.

When categorizing age-related phenotypes, it quickly becomes apparent that aging is an animal-wide phenomenon, with no tissue or organ being immune from its effects. Even at the cellular, subcellular, and molecular levels, the effects of aging are readily apparent; aging is

fractal, degrading the organism at every level of organization. Understanding the results of the aging process is crucial to understanding its mechanistic basis. In **Chapter 2**, I categorize age-related changes in *C. elegans* and summarize current strategies for aging research.

1.1.3 The Evolution of Aging

We have come to a detailed understanding of what aging looks like, but we are still far from understanding how aging came to be. It is simple to observe that different animals have different lifespans, and that these differences in the rate of aging likely result from adaptation to different ecological niches. Animal lifespan is correlated with various physiological traits, including body size and metabolic rate [19,20]; lifespan is also correlated phylogenetically, with more closely related organisms having similar lifespans [19]. It is probable, then, that traits related to aging undergo natural selection in much the same manner as other physiological traits. However, it is as yet unclear whether aging is "programmed" in the sense that it is an adaptive trait that is selected to promote fitness, or is simply the result of integrative evolutionary pressures failing to keep animals alive past a certain point. It is important to keep in mind that the degree to which aging is "programmed" likely varies depending on the species, with different environmental factors, ecological niches, or reproductive strategies exerting different evolutionary pressures.

In general, though, evolutionary game theory predicts that organisms will adopt the best available strategies for survival and reproduction that maximize their fitness payoffs [21,22]. Aging is one of these strategies; animals must remain alive and healthy long enough to reproduce, but further survival past this point offers diminishing payoffs. Thus, a general hypothesis for why aging exists might be that animals survive only as long as they need to in order to pass on their

genes and ensure the survival and success of their progeny, maximizing fitness payoffs while minimizing unneeded expenditures of scarce resources. Some more detailed models for the evolution of aging are briefly discussed here, and elaborated upon further in **Chapter 2**.

Genes are passed on at the moment of reproduction, an event that usually occurs fairly early relative to an animal's maximum lifespan [23,24]. Absent factors such as parental investment or other methods of indirect fitness, only those traits which exert their effect on fitness prior to reproduction can be influenced by natural selection. Thus, heritable traits which negatively impact an animal's ability to survive late in life will not be selected against, as those traits will have already been passed on to the next generation. This "shadow of selection" describes a situation of preferential selection for early-life fitness benefits at the expense of late-life somatic degradation [25]. This may also help explain why certain diseases, such as cancer, are rare early in life but become more common as an individual ages.

This also brings to mind the possibility of traits which both positively and negatively affect fitness, but at different points in an animal's lifespan. This "antagonistic pleiotropy" (AP) hypothesis suggests that traits which enhance fitness early in life but reduce fitness late in life will still be adaptive, as traits which exert their effect earlier are more likely to affect an organism's reproductive success [26]. Furthermore, comparatively few organisms in the wild live long enough to die of old age anyway, instead succumbing more frequently to extrinsic causes of death such as disease or predation [27–29]. Thus, the paradigm of "live fast, die young" seems to be a winning strategy for reproductive success in the wild.

According to a gene-centered view of evolution, the ultimate function of an organism is to pass on its genes to the next generation. In this view, an organism is simply a vessel of somatic tissues whose purpose is to maximize the success of the germline. Indeed, many examples exist

of animals sacrificing their own survival in order to maximize their reproductive success [30]. This "disposable soma" model predicts that there exists preferential selection for traits which improve reproductive success over long-term individual survival, and thus traits which maximize lifespan may not be adaptive at all. In *C. elegans*, genetic mutations which extend lifespan often concurrently reduce fecundity, implying that there exists a sort of tradeoff in the expenditure of resources: animals can allocate energy and resources into either reproduction of the germline or maintenance of the soma, but not both at the same time [31].

A final hypothesis is that extrinsic causes of mortality are simply so great that no organism, no matter how fit, is able to overcome them. Thus, over time, irreversible damage accumulates in the form of damage to DNA, proteins, and other macromolecules. Aging, then, cannot be halted, but can only be delayed long enough for an organism to reproduce itself. This model predicts that longer-lived animals are better at dealing with these damaging factors, a function necessitated by a given ecological niche or reproductive strategy. This would help explain why larger animals are generally longer lived: these animals must survive long enough to reach a size appropriate for reproduction [19,20,32].

1.2 Genetic factors control aging

It has long been recognized that the aging process is controlled by genes. In humans, lifespan is partially genetically controlled, accounting for ~20-30% of variability in lifespan [33–37]. Several heritable progeroid syndromes appear to phenotypically mimic premature aging, suggesting that genes can both positively and negatively regulate aging [38]. Genetic pathways that control aging have been identified in both mammalian and invertebrate animal models; many of these pathways function in multiple organisms, indicating a conserved role for genetic

pathways that regulate aging [39–43]. Thus, the study of genes that control aging in model organisms can help us to better understand human aging.

C. elegans is an especially useful in this regard: its short lifespan and large library of genetic tools allow large-scale screening for longevity-inducing genes. Indeed, throughout several decades of research, numerous genetic mutations have been identified that can extend *C. elegans* lifespan. Here, I briefly describe several well-characterized aging pathways and discuss how my research advances our understanding of their mechanism.

1.2.1 Dietary Restriction

Historically, resource deprivation in general, and dietary restriction (DR) in particular, has been one of the most highly conserved mechanisms for extending lifespan throughout *Animalia*. First described in rodents in 1935 [44], reduction of caloric intake reproducibly extends lifespan in numerous organisms, including yeast, arthropods, mammals, and *C. elegans* [45–52]. Though the mechanism is not thoroughly understood, one compelling hypothesis suggests that deprivation of resources activates genetic programs associated with stress resistance and somatic maintenance, resulting in a net increase in lifespan and a reduction in age-related degeneration [53–55]. This is not without its tradeoffs, however, as DR is often associated with reduced fecundity in multiple organisms [46–48], though this effect may not be mechanistically connected [56]. Numerous pathways are associated with DR-induced control of aging including *sir-2* and its various homologs [41], mTOR signaling [57], and autophagy [58], suggesting that DR controls aging by influencing a variety of metabolic pathways [52].

Many methods for inducing DR in worms, such as intermittent feeding and dilution of the bacterial food source, are complex and difficult to reliably implement [48,56,59–61]. Thus, *eat-2(lf)*

mutants are commonly used as genetic models for DR [49]. The *eat-2* nicotinic acetylcholine receptor subunit gene functions to regulate pumping of the pharynx, a digestive organ located at the worm's mouth. This organ rapidly pumps as the animal feeds, drawing in bacteria and grinding it before transporting it into the intestine. In *eat-2(lf)* mutants, pharynx pumping rate is severely reduced; this results in reduced food intake and DR [49,62].

phm-2(lf) mutants were recently shown to have extended lifespan due to a mechanism which integrates DR and the innate immune system [63]. The pharyngeal muscle gene *phm-2* encodes a protein homologous to human scaffold attachment factor B (SAFB), and is necessary for the proper morphological development of the pharynx. *phm-2(lf)* animals display defective pharynges, resulting in improper grinding of the bacterial food source. This allows live bacteria to enter and colonize the intestine. In wild-type animals, the *E. coli* OP50 bacterial food source is nonpathogenic, as complete grinding by the pharynx ensures no live bacteria enter the intestine. In *phm-2(lf)* mutants, however, live *E. coli* OP50 bacteria are able to colonize the intestine, resulting in an activation of the innate immune response. Part of this response is bacterial food avoidance behavior: the animal is able to sense that it is sick, and responds by actively moving away from the bacterial lawn. This behavior results in reduced caloric intake and lifespan extension by DR.

In **Chapter 3**, we discuss the characterization of this novel pathway to lifespan extension in *phm-2(lf)* mutants, integrating aging, dietary restriction, the innate immune system, and the gut microbiome. Furthermore, we recharacterize *eat-2(lf)* mutant aging as not solely influenced by DR alone, but also by bacterial colonization of the intestine and innate immune activation. This discovery recontextualizes previous research on DR using *eat-2(lf)* mutants.

In **Chapter 4**, I further characterize *phm-2(lf)* mutants, and use the pathogen hypersensitivity phenotype to study the human amyloid beta (Aß) peptide, the causative factor underlying Alzheimer's Disease; I describe Aß as an antimicrobial peptide, and show that it promotes survival under pathogenic stress, thus integrating aging, stress resistance, and the innate immune system.

1.2.2 Inulin/IGF-1 Signaling

The insulin/IGF-1 signaling (IIS) pathway was one of the first genetic pathways that was observed to control aging [4,64], and is homologous to the mammalian insulin signaling pathway. In worms, this pathway controls a wide variety of cellular processes, including stress resistance, aging, molting, and development [65]. Many components of the IIS pathway control aging; perhaps the best studied of these is *daf-2*, a receptor tyrosine kinase gene and homolog of the mammalian insulin receptor [64,66,67]. DAF-2 binds to a variety of extracellular insulin-like ligands, and then activates a signaling pathway which terminates with the DAF-16/FOXO transcription factor. DAF-16 promotes transcription of genes responsible for survival and stress resistance. Under conditions which are favorable for development into reproductive adults, DAF-16 is inhibited; under stressful conditions, DAF-16 localizes to the nucleus and upregulates transcription of stress response and dauer-promoting genes. Partial loss-of-function mutations in *daf-2* result in constitutive activation of DAF-16, resulting in extended lifespan, reduced age-related degenerative phenotypes, reduced fecundity, elevated stress resistance, and ectopic entry into the dauer diapause state.

Regulation of dauer entry is one of primary functions of the IIS [65,68]. The dauer diapause state is an alternative L3 larval developmental stage that worms enter into under conditions

which are suboptimal for development into reproductive adults. These conditions include low food availability, high population density, and elevated temperature. Dauer animals are physically and physiologically distinct from other larval stages, and are analogous to a hibernative or spore-like state. Physically, dauers are longer and thinner than other larvae, possess a buccal plug which seals the oral cavity and prevents ingestion of food, and appear darker due to accumulation of fat stores [68,69]. Physiologically, dauers have drastically extended lifespan of over two months, much longer than the mean adult lifespan of ~14 days [70]. Dauer are stress resistant, likely due to activation of genes involved in heat and oxidative stress resistance [68]. However, dauers are sterile: in order to reproduce, worms must exit the dauer stage, continue larval development, and ultimately develop into reproductive adults. Improper dauer entry under conditions which are permissive for successful reproduction would drastically reduce an individual's fitness; and, conversely, improperly exiting the dauer state under conditions that are unable to support survival and reproduction also reduces fitness. Worms have therefore developed sophisticated mechanisms for sensing external conditions and integrating this information into their internal decision-making. The IIS pathway is an important member of this developmental decision-making machinery. Much research has been done to characterize the interaction between the IIS and aging, and numerous long-lived loss-of-function alleles of *daf-2* have been characterized [66,67].

In **Chapter 6**, I discuss the discovery and characterization of *daf-2(am326)* [71]. This mutant was first observed in a forward-genetic screen for hypersensitivity to high doses of the ACE-inhibitor drug captopril (further discussed in **Introduction 1.3.1**). The primary discoveries related to *daf-2(am326)* are threefold. First, that *daf-2(am326)* is a novel long-lived allele of *daf-2* that lacks many of the negative pleiotropies associated with other *daf-2(lf)* mutants, such as

reduced development rate and delayed reproductive period. Second, that it recapitulates mutations observed in the human insulin receptor, and thus serves as a model for human diseases associated with insulin resistance in the experimentally simple nematode system. Third, that *daf-2(am326)* reveals the role of captopril and its target, ACN-1, in the control not only of aging, but also dauer entry and developmental decision-making.

1.2.3 Other genetic pathways control aging

Several other genetic pathways control aging in *C. elegans* and other organisms; these will be described briefly here, but further elaboration is beyond the scope of this document. Dysfunction of the mitochondrial electron transport chain (METC) extends lifespan in many organisms, and controls aging independently of other types of resource deprivation in *C. elegans* [72–77]. Initial hypotheses suggested that this effect was related to reduction of mitochondrial reactive oxygen species (ROS), but current models dispute the role of ROS in aging [78–80]. Other interventions include reducing protein translation efficiency [81–83], and manipulating the activity of the mechanistic target of rapamycin (mTOR) and mTOR interacting proteins (reviewed in [84]).

1.3 Pharmacological factors control aging in *C. elegans*

The ultimate goal of the field of aging biology is to delay or reduce the burden of age-related degeneration in humans. Despite the identification and characterization of numerous genetic interventions that delay aging in model organisms, their effectiveness as treatments for aging in humans remains unclear: given current technology, there is limited ability to directly introduce longevity-modulating mutations into the human genome *in vivo*. Thus, identifying and studying pharmacological compounds that control aging is highly desirable, as they present a simple and tractable mechanism for modulating cellular functions absent genetic interventions,

and are therefore likely candidates for future treatments of human aging. *C. elegans* is a useful platform for the identification and study of anti-aging compounds due to its rapid lifespan and simple culture conditions, making it ideal for large-scale screens. To date, dozens of compounds have been identified that control aging in nematodes [12,13]. Several compounds first identified in worms also control aging in mammals and other model organisms, including captopril and trehalose [85,86], indicating the translatability of this model. Current research into anti-aging compounds often focuses on previously identified compounds that are known to interact with human biology and which are prescribed for the treatment of human diseases. Compounds which meet these criteria and also control aging in model organisms are ideal candidate compounds for potential future studies of anti-aging compounds in humans. The diabetes medication metformin and the immunosuppresent compound rapamycin are prime candidates for these studies, as both extend lifespan in multiple model organisms [87–90,81,91–93]. Here, I describe captopril as another anti-aging compound which controls aging in rodents and *C. elegans* [71,85,94].

1.3.1 The ACE-inhibitor drug captopril controls aging and development via inhibition of ACN-1

Recent evidence has identified the ACE-inhibitor compound captopril as a powerful regulator of aging. Captopril is the first in a series of ACE-inhibitor compounds that were identified following research into the venom of the Brazilian pit viper [95]. These compounds are now commonly prescribed for the treatment of hypertension, or high blood pressure, in humans. In mammals, captopril functions by modulating the activity of the renin-angiotensin-aldosterone system (RAAS), which is responsible for the regulation of vasoconstriction and vasodilation (reviewed in [96–100]). Captopril binds to and inhibits the activity of ACE, the angiotensin-converting enzyme. ACE functions to proteolytically cleave the peptide angiotensin I (Ang I)

into angiotensin II (Ang II); Ang II binds to a variety of targets, most notably the angiotensin II type-I receptor (AGT1R), resulting in vasoconstriction and an increase in blood pressure. Significant evidence from model organisms has identified a secondary role for genetic and pharmacological inhibition of the RAAS in aging. Other ACE inhibitors, like enalapril and lisinopril, delay aging in rodents and *Drosophila*; furthermore, genetic knockdown of RAAS pathway components also delays aging in these models (reviewed in [101]). In **Chapter 5**, I discuss current perspectives on the RAAS and its role in aging in humans, rodents, *Drosophila*, and *C. elegans*.

Captopril was first discovered to control aging in *C. elegans* [85]. Administration of captopril results in an extended mean lifespan of ~20%, a reduction in age-related degeneration of movement and pharyngeal pumping, and increased heat and oxidative stress resistance. Captopril likely functions by inhibiting ACN-1, the nematode homolog of ACE: treatment with *acn-1* RNAi phenocopies captopril treatment, and fails to further extend lifespan in worms treated with captopril, indicating that they likely function via a shared mechanism. *acn-1* has previously been shown to control spatial and temporal control of molting and development [102,103], suggesting a integration of aging and development.

Worms are especially useful for studying the effect of the RAAS on aging, as they possess neither blood nor a closed circulatory system; thus, the effects of captopril on aging may be studied in isolation from its effects on blood pressure. Indeed, recent evidence from the National Institute on Aging Interventions Testing Program confirmed that captopril also extends lifespan in mice [94]. Thus, inhibition of the RAAS represents a well-supported but understudied paradigm for aging regulation. Many questions remain open regarding captopril/*acn*-1-mediated control of aging, however, including the mechanistic function of *acn-1* in aging. In **Chapter 6**, I

discover that inhibition of *acn-1* via RNAi or captopril administration induces dauer entry and characterize the interaction of *acn-1* with developmental decision-making.

1.3.2 Concentration of sodium chloride controls aging

In the wild, nematodes live in a chemically heterologous soil environment, and thus have adapted to respond to changes in temperature, pH, oxidative stress, osmotic stress, and other factors. Mechanisms of osmoregulation in particular have evolved to maintain equilibrium in osmotic pressure with the external environment, and adapt to changes in the concentration of external osmolytes [104,105]. The primary methods of dealing with high osmolyte concentrations are, first, to sense and move away from regions of high concentration, and second, to regulate the production of internal organic osmolytes such as glycerol in order to maintain equilibrium between the internal and external environments [104,105]. Sodium chloride is a common osmolyte and necessary dietary nutrient for *C. elegans*. In the laboratory, nematodes are most commonly cultured on Petri dishes of nematode growth medium (NGM) containing approximately 50 mM supplemental NaCl [3]. However, it has been shown that excess NaCl concentration can reduce lifespan in *C. elegans* as a result of increased osmotic stress [106].

In **Chapter 7**, I discuss new observations regarding the role of salt (NaCl) concentration and activation of the osmotic stress response on lifespan in *C. elegans.* We observe that removal of excess salt from the medium serves to extend lifespan; or, rather, that the standard concentration of supplemental salt in NGM reduces lifespan. Historically, this salt concentration was not chosen based on what would be optimal for *C. elegans* lifespan; rather, it was based on common formulations of LB agar media optimized for the growth of the *E. coli* OP50 bacterial food source. We propose that this supplemental salt serves to reduce survival, and suggest a

mechanism of osmotic stress. This research has important implications for future research, as it suggests that nearly all previous research on aging in *C. elegans* was performed under conditions of mild osmotic stress.

Chapter 2: How to measure, analyze, and interpret age-related changes in *Caenorhabditis elegans*: lessons for mechanistic and evolutionary theories of aging

The work presented in Chapter 2 is a review article manuscript under preparation with the following authors:

Zuzana Kocsisova[1,2*]; **Brian M. Egan[1*]**; Andrea Scharf[1,3]; Xavier Anderson[1]; Franziska Pohl[1,4]; Kerry Kornfeld[1]

[1]Department of Developmental Biology, Washington University School of Medicine, St. Louis, MO, United States

[2]Department of Genetics, Washington University School of Medicine, St. Louis, MO, United States

[3]Department of Biological Sciences, Missouri University of Science and Technology, Rolla, MO, United States

[4]Department of Medicine, Washington University School of Medicine, St. Louis, MO, United States

[*] **Co-first author**

I was jointly responsible for the writing, editing, and revision of this review article with Zuzana Kocsisova; my major contributions were to the section discussing age-related changes in morphological structure and function, and to the discussion section, primarily with respect to evolutionary theories of aging.

2.1 Abstract

Aging is characterized by progressive degenerative changes in tissue organization and function that increase the probability of mortality. Major goals of aging research include elucidating the series of events that cause degenerative changes and analyzing environmental and genetic factors that modulate these changes. Mechanistic studies of aging depend on accurate and precise descriptions of age-related changes, since these descriptions define the aging phenotype. Here we review studies that describe age-related changes in C. elegans, including measurements of integrated functions such as behavior and reproduction, microscopic analyses of tissue organization, and biochemical studies of macromolecules. Studies that analyze the relationships between different age-related changes are discussed. The results are considered in light of mechanistic and evolutionary theories of aging. Together these studies provide fundamental insights into aging in C. elegans that may be relevant to aging in other animals.

2.2 Introduction

2.2.1 Overview

Aging is a fundamental aspect of animal biology that resonates deeply with humans, as we can witness the aging process in others and experience our own aging. Because aging is characterized by degenerative changes that progressively diminish organismal function and increase the probability of death from intrinsic causes, people have a strong desire to understand aging so that it can be ameliorated or delayed [25,107]. In contrast to many other synthetic processes in biology that are known to be mediated by complex patterns of gene expression and intricate molecular mechanisms, aging is not well characterized. The causes of aging and the potential plasticity of age-related degeneration are active areas of research.

While gaining a deeper understanding of human aging is the ultimate goal of aging research, the experimental challenges of studying aging in humans or other vertebrates are substantial, primarily due to their long lifespans and the high costs associated with investigating them in a laboratory environment. By contrast, the free-living nematode *Caenorhabditis elegans* is a leading model system for studies of aging due to their short lifespans and simple culture conditions. Numerous mutations, drugs, and environmental factors have been identified that extend the adult lifespan significantly. Mechanistic studies of how these factors influence aging are critical, and the foundation for these studies are measurements of age-related changes. Here we review the current understanding of age-related changes in *C. elegans*.

This review is divided into three sections: **(1)** a consideration of the approaches used to measure age-related changes, **(2)** a description of the specific age-related changes that have been reported for *C. elegans*, and **(3)** conclusions about aging that have emerged from these studies.

The **first section** focuses on **(a)** which age-related changes should be measured; **(b)** why it is important to measure age-related changes; **(c)** how age-related changes are measured; **(d)** tools and methods employed for these measurements; **(e)** how these measurements provide a foundation to study mutations and interventions which delay aging; and **(f)** how these measurements can define the relationships between age-related changes.

The **second section** describes specific age-related changes that occur in *C. elegans*, including behaviors mediated by the neuromuscular system, reproduction, tissue morphology, and biochemical properties (**Table 1**). As is common in *C. elegans* research, most studies focus on the hermaphrodite. Several studies have examined age-related changes in the *C. elegans* male, specifically focused on its behavior and tail morphology (**Table 2**). This section also describes the relationships between age-related changes (**Table 3**) (see **Tables 1-3** at end of **section 2.2**).

The **third section** highlights major conclusions from these studies, including the significance of relationships between age-related changes, and the relevance of these studies to mechanistic and evolutionary theories of aging.

2.2.2 Distinguishing age-related changes pertinent to development and senescence

Changes over an animal's lifespan are widespread, yet not every change is due to aging or senescence, and not every change is an appropriate focus for aging studies. It is important to draw a distinction between age-related changes that represent development and growth, and age-related changes that represent senescence. While several criteria are useful for distinguishing these changes, establishing definitions that precisely distinguish these two types of changes is challenging.

One useful criterion is whether the age-related change increases organization or function of an organ or tissue (typical of development) or decreases organization and function (typical of aging). While this is a simple criterion, it is not definitive. For example, older adults display an induction of stress response genes, which seems likely to be a functional response that improves survival. However, this is likely in response to an overall decrease in stress resistance as the animal ages. By contrast, young hermaphrodites lose the ability to generate sperm when the gonad switches to egg production; this change results in a loss of functional capacity, yet is typically considered a developmental change.

A second criterion is the point in the life cycle at which the change occurs. Events in the embryo will typically be developmental whereas changes in older adults will typically be aging-related. While the onset of reproductive maturity is often used as the final event of development and earliest point of comparison for aging studies, it is clear that the distinction is artificial, since

the peak of function typically occurs at a time after the onset of reproductive maturity in a variety of organisms. In fact, there is no time in midlife that clearly separates development from aging, and it is likely that developmental changes and age-related changes occur simultaneously. For example, damage accumulation, which is typically considered an age-related change, begins in young animals that are undergoing development and growth.

A third criterion is the existence of a genetic program that specifies the change. Time-dependent developmental changes require a genetic program. If age-related degenerative changes also require a genetic program, then this criterion cannot distinguish development from aging. By contrast, if age-related changes do not require a genetic program, then this would be a distinguishing characteristic. As the relationships between genetic programs and age-related changes are better characterized, this criterion may become more valuable.

The passage of time results not only in aging, but other changes in the organism as well. For example, adult hermaphrodites have a limited number of sperm, and as time progresses they experience both aging and feminization due to sperm depletion (**Figure 7C**). Some studies separate these two variables by using female animals or by providing sperm through mating to avoid feminization [108].

Although a consideration of these issues does not lead to a definition of age-related changes that represent aging, these criteria are useful, and most studies focus on changes that occur late in adult life and diminish tissue function or organization.

2.2.3 Measuring age-related changes is the foundation for mechanistic aging studies

Measuring age-related changes is important for several reasons. First, these studies provide a description of normal aging in wild-type animals, and this description is the basis for

the current understanding of aging. These descriptive studies have revealed that age-related changes are widespread, affecting many different tissues. Furthermore, age-related changes occur at all levels of organization. At the level of integrated systems that require multiple tissues, there are declines in survival, stress resistance, and function, such as diminished body movement and reproduction. At the level of tissues and cells, there are changes in morphology, such as a decline in intestinal and vulval integrity, and increased disorganization of the nucleus and mitochondrial networks. At the molecular level there are structural changes of macromolecules, such as DNA, proteins, and metabolites.

Second, the identification of specific age-related changes has been the source of hypotheses regarding the causes of aging. For example, the observation of age-related increases in oxidative damage to macromolecules such as proteins and nucleic acids suggests the hypothesis that these structural changes are a cause of age-related functional declines[109]. Similarly, the observation of age-related increases in yolk protein in the body cavity or apoptotic corpses in the germline suggests the hypothesis that some developmental processes may become detrimental when they continue during adulthood and are a cause of age-related functional declines [110,111].

Third, measurements of age-related changes can provide markers of aging. Such markers allow assessments of the extent of aging in live animals and can be used to predict lifespan or used to evaluate short-lived strains for evidence of premature aging [112,113,15,114,115].

Fourth, the measurement of age-related changes is a necessary starting point for studies that can define causal relationships during aging. The ultimate goal of aging research is to provide a comprehensive description of age-related changes that includes the causal relationships between the different changes. While measurements of age-related changes alone do not define

these causal relationships, these measurements are an essential element of experiments that have the potential to define causal relationships. These experiments include the analysis of genetic, environmental, dietary, and pharmacological factors that influence aging, and longitudinal studies that define relationships between different age-related changes [15]. In the past decade, a vast number of genetic and pharmacological factors have been reported to influence aging. In this review, we will focus on descriptions of age-related changes in wild-type animals and on longitudinal studies that define the relationships between age-related changes.

For these reasons, measurements of age-related changes are a critical component of every mechanistic aging study.

2.2.4 How to measure age-related changes

Any property of a biological system that can be measured can in principle be analyzed as a function of time during the animal's life stages.

The **first** important issue is the time axis; relevant considerations are the starting time, the ending time, and the number of intermediate times that are analyzed (**Figure 1**). For *C. elegans*, the starting times that are frequently selected are egg deposition, the emergence of the L1 larvae or the L4 larvae, or the appearance of the first embryos in the uterus, since these developmental stages can be accurately determined by morphological criteria. The simplest study involves measuring one time point. If two or more time points are analyzed, then it is possible to derive a graph of the property versus time. Two time points can be analyzed with a linear regression (**Figure 1A,C**), whereas more time points can be analyzed with a linear, polynomial, or exponential regression (**Figure 1A-D**). *C. elegans* studies frequently involve daily measurements until the end of life. For example, a lifespan analysis typically involves daily assessments of

whether the animal is alive or dead. When designing a study, the tradeoffs between temporal resolution, sample size, and statistical power should be carefully considered [116]. In this review, we summarize the reported age-related changes regardless of the number of time points analyzed in the study.

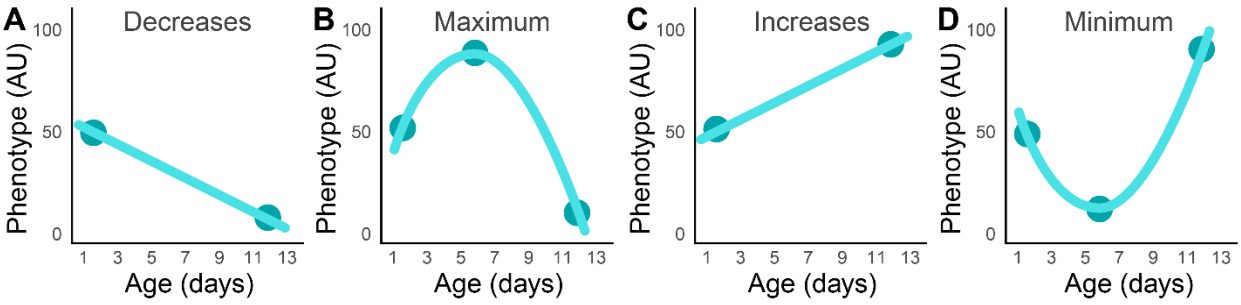

Figure 1: Values that display age-related change may increase steadily, decrease steadily, or curve with a maximum or minimum

Only two points are required to define a line **(A,C)**, but three or more points are required to define a more complex pattern **(B,D)**. If a study measured a phenotype at only two time points and reported a decrease **(A)**, then the underlying reality might include an initial increase followed by a decrease **(B)**, and a subsequent study with increased temporal resolution may reveal the more complex pattern. Similarly, if a study measured a phenotype at only two time points and reported an increase **(C)**, then the underlying reality might include an initial decrease followed by an increase **(D)**, and a subsequent study with increased temporal resolution may reveal the more complex pattern.

The **second** important issue is whether the study has a longitudinal or cross-sectional study design. Cross-sectional studies typically involve a single measurement of each young individual and a single measurement of each old individual (**Figure 2**). Any differences between the group of young animals and the group of old animals are attributed to age. However, it is not possible to rule out that differences existed between the groups for reasons other than age. Cross-sectional studies are used for invasive measurements, such as electron microscopy, and for experiments that require combining multiple animals (bulk measurements), such as protein analysis by mass spectrometry or western blot.

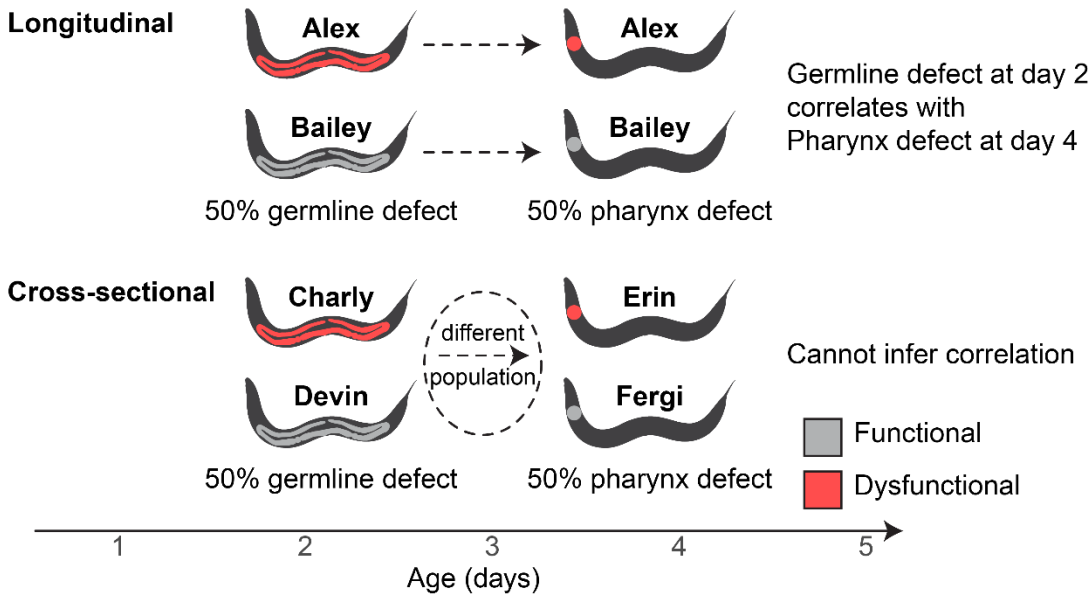

Figure 2: Aging studies can be longitudinal or cross-sectional

In this example of study designs, a longitudinal **(upper)** and a cross sectional **(lower)** approach were used to measure germline defects at day 2 and pharynx defects at day 4 (N=2 animals per time point). In both studies, 50% of day 2 animals displayed the germline defect, and 50% of day 4 animals displayed the pharynx defect.

In the longitudinal study, the same individuals (Alex and Bailey) were observed at day 2 and 4, and the analysis demonstrated a positive correlation between a germline defect at day 2 and a pharynx defect at day 4. In the cross-sectional study, different individuals were measured at day 2 (Charly and Devin) and day 4 (Erin and Fergi); thus, correlations cannot be inferred.

In a longitudinal study, individual animals are observed at a young age and the same individuals are observed again later at an old age (**Figure 2**). Because the same individual is observed at all time points, it is more straightforward to distinguish which changes existed between individuals and which changes occurred as a result of age. Because longitudinal studies involve serial measurements of the same individual, the measurements must be non-invasive (except for the final measurement, which can be invasive). Longitudinal studies provide the same information as cross-sectional studies, as well as opportunities for data analysis that are not

possible with cross-sectional studies, including correlations among age-related changes. *C. elegans* are well suited to longitudinal studies because of their relatively short lifespan.

The **third** important issue is the measurement itself. While in principle any measurable property of the animal can be analyzed as a function of time, in practice aging studies of *C. elegans* tend to focus on rhythmic behaviors, tissue and cell morphology, and changes in biochemical properties. Each of these measurements is discussed in detail below.

A general issue is the extent to which the measurement is quantitative. **(i)** Some measurements are highly quantitative, such as the rate of pharyngeal pumping or the number of copies of a particular mRNA. For highly quantitative measurements, it is possible to graph the quantity versus time (**Figure 3A,C,E**). Image analysis tools like ImageJ and FIJI can be vital in extracting quantitative information from microscopic analyses. **(ii)** For measurements that are not highly quantitative, the typical approach is to establish ordered categories (**Figure 3G,H**). For example, tissue organization is not easily quantified, so categories such as well organized, partly disorganized, and highly disorganized might be used [113,117,118]. Numbers may be assigned to these ordered categories (e.g. well organized = 1, partly disorganized = 2, highly disorganized = 3) to allow the generation of summary statistics. However, because these numbers are assigned somewhat arbitrarily, this approach is limited to non-parametric statistics. **(iii)** Other non-quantitative measurements may not lend themselves to ordered categories, so unordered categories are used. For example, germline defects may include cavities, misshapen oocytes, mislocated oocytes, and cellularization, yet is it not clear which defect is more severe than another. **(iv)** Finally, some measurements are binary. For example, vitality is not easily quantified or categorized, so animals are classified as alive or dead. Statistical methods developed for survival analysis are often used with binary measurements.

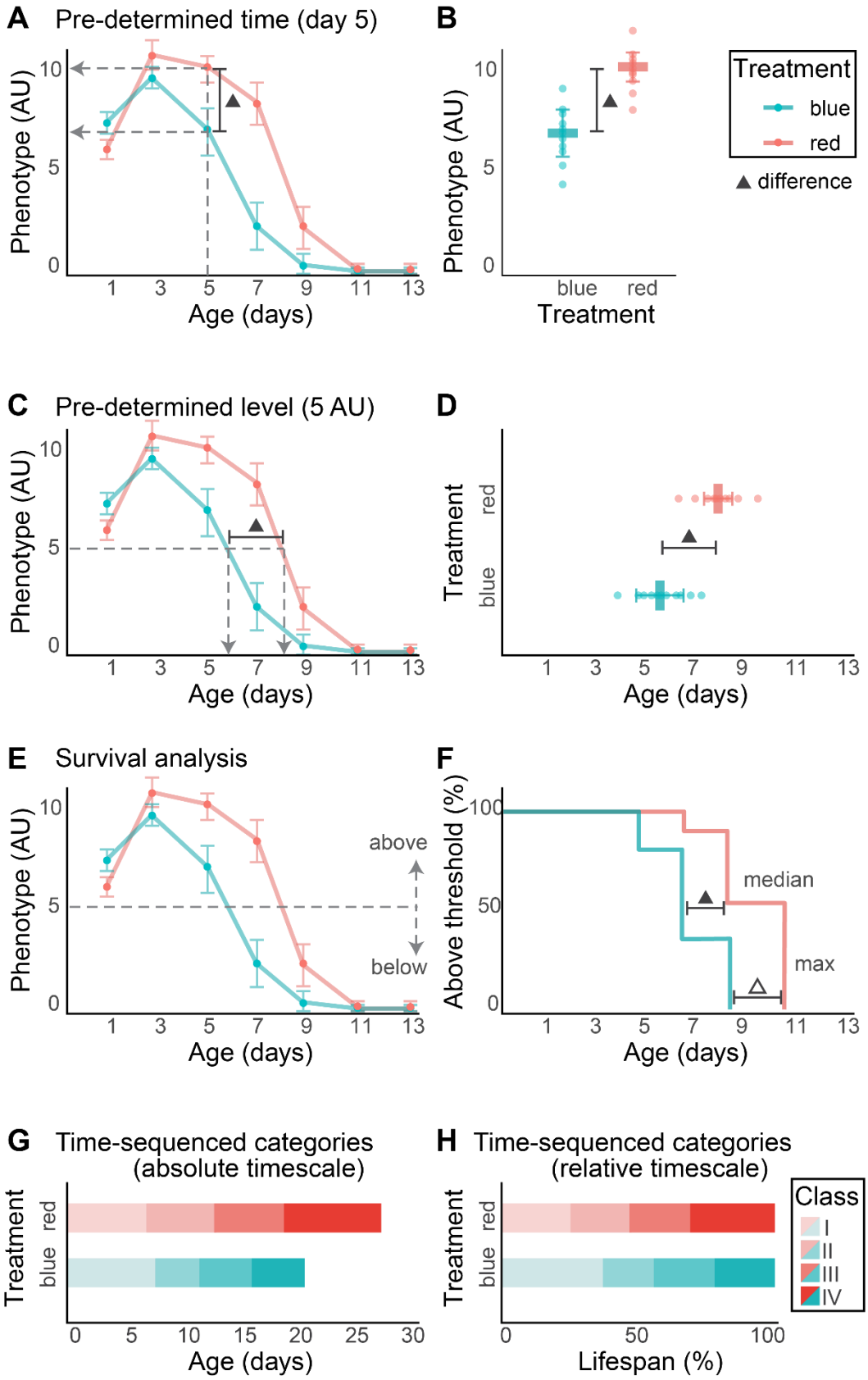
A
Pre-determined time (day 5)
Phenotype (AU)
Age (days)
B
Treatment
blue
red
difference
C
Pre-determined level (5 AU)
D
E
Survival analysis
above
below
F
Above threshold (%)
median
max
G
Time-sequenced categories
(absolute timescale)
H
Time-sequenced categories
(relative timescale)
Class
I
II
III
IV
Lifespan (%)

Figure 3: Analysis of age-related changes

A comprehensive description of an age-related decline involves a large set of phenotypic measurements taken at many different times. These data sets can be analyzed, summarized, and compared using several different approaches illustrated here.

(A,C,E) Blue and red lines are hypothetical examples of data sets generated by measuring a quantitative phenotype in arbitrary units (AU) as a function of time (days) for two groups of animals; these data are identical in the three panels. The blue animals displayed a more rapid age-related decline than the red animals. The dashed lines and notations indicate the analysis approach shown in accompanying panels **B**, **D**, and **F**.

(A, B) Red and blue animals were compared by determining the phenotypic value for each group at one time (e.g., day 5). The typical summary statistic is the average phenotypic value at the specified time (bold horizontal line), +/- the standard deviation (whiskers). For data which are not normally distributed, the median and inter-quartile range may be more appropriate and may be visualized as a box and whiskers plot. In either case, individual data points may be displayed as shown here. Black triangle indicates the difference between the means of the blue and red group. The average phenotypic value of the blue group is lower, indicating a more rapid decline. Note that red and blue values are similar at earlier (day 3) and later (day 11) times; thus, the difference only exists during mid-life (days 5, 7, and 9).

(C, D) Blue and red animals were compared by analyzing the time when each group transitioned to a specified phenotypic value (e.g., below 5 AU, which is ~50% of the maximum value). The typical summary statistic is the average (or median) span of time from the start of the experiment to the transition time. Black triangle indicates the difference between the means of the blue group and the red group. The transition time of the blue group occurred at an earlier time, indicating a more rapid decline. This approach is well suited to measure healthspan – if a value above 5 AU is defined as good health, then blue and red displayed healthspans of ~6 and ~8 days, respectively.

(E, F) If a phenotypic value is specified as shown in panels **C** and **D**, then each animal can be classified as above or below that value. The fraction of animals above (or below) the value can be plotted. This is the standard approach for survival data, where the specified phenotypic value is alive (versus dead), and the typical summary statistic is the mean (or median) lifespan. This approach can be used for continuously varying phenotypes by specifying an above/below value such as fertility (e.g., 1 or more eggs produced), pharyngeal pumping (e.g., 10 or more pumps per minute), or body movement (e.g., 5 or more bends per minute). A staircase-style graph is often used to indicate that the data represent a "survival" analysis. Non-parametric statistics, such as the Kaplan-Meier estimator, are typically used because survival data rarely fit a normal distribution or the assumptions of parametric tests and often contain "censored" events. Black triangle indicates the difference between the medians and "maximums" (90^{th} percentile) of the blue group and the red group. The graph shows that the fraction of animals above the specified value declines more slowly in the red group, and the red group has a higher mean age with 50% above the specified value and a higher maximum age with at least one animal above the specified value.

(G) If there is a continuous variable or multiple time-dependent variables, then it is possible to define three or more categories that represent consecutive stages of aging. This

approach was used by [15]. Stage I is a period from onset of adulthood until the end of self-fertile progeny production; Stage II is a post-reproductive period characterized by vigorous motor activity; Stage III is a period of reduced motor activity with continued pharyngeal pumping; Stage IV is a period of minimal motor activity until the end of lifespan. A similar approach was used by Herndon *et al.* (2002) and Newell Stamper *et al.* (2018) to classify animals into three stages: voluntary coordinated mobility, uncoordinated mobility in response to stimulation, and head/tail mobility in response to stimulation [117,119]. In this plot, the time axis is in absolute values of days. The blue group spent a longer time in stage I and a shorter time in stage IV compared to red.

(H) The same data as panel **G** can be normalized to maximum lifespan to show the proportion of life spent in each stage [15]. This type of approach was used by Bansal *et al.* (2015) to compare the proportion of life in healthspan versus gerospan [120]. The blue group spent a larger percentage of its life in healthspan.

A **fourth** important issue in analyzing these data is the generation of summary statistics for the purpose of making comparisons. **Figure 3** shows the basic approaches that have been used to generate summary statistics. One approach is to analyze the pattern of the declining function. For example, the data can be fit to a straight line and the slope of the line and intercepts where the line crossed the x- or y-axis can be used as summary statistics [14,121]. An important issue with the approach of fitting data to a straight line is that these data may fit better to another shape. A second approach is to predetermine a time and then compare the values (see **Figure 3A,B**). This approach is almost always used for studies of biochemical properties and tissue morphology, and is often used for studies of behavior. A third approach is to predetermine a transition point in the value and then compare the times (see **Figure 3C,D**). A related approach is to predetermine the value and compare the number of individuals in the population above or below the value (see **Figure 3E,F**). This is the approach used for lifespan, where the predetermined value is the transition from alive to dead. This approach can also be used to analyze other transitions, such as the cessation of pharyngeal pumping or reproduction [15,31,122]. Several transitions can be combined to represent stages of aging (**Figure 3G,H**), and the time

axis can be normalized to maximum lifespan to show the proportion of life spent in each stage [15,120].

2.2.5 Tools and methods

Classical tools for measuring age-related changes in *C. elegans* include microscopy, biochemistry, and nucleic acid sequencing. As discussed above, some techniques lend themselves to **quantitative** measurements while others are **qualitative**. Some techniques, like counting pharyngeal pumping, are **non-invasive**; some techniques, like differential interference contrast (DIC) microscopy, also known as Nomarski microscopy, are **invasive but non-lethal**; some techniques, like immunohistochemistry, are **invasive and lethal**. Some methods such as microscopy provide **spatially-resolved** information, while other methods such as Western blot analysis and RNA-seq require homogenization of the tissue, thus losing the spatial aspects. A related aspect of such techniques is the amount of tissue required for analysis. Due to recent advances in DNA sequencing technologies, it is becoming possible to use techniques like RNA-seq on individual *C. elegans*. Other techniques, like mass spectrometry, require pooling several hundred, thousand, or million animals in order to obtain a **bulk measurement** on a sufficiently large sample. This review highlights the features and limitations as each method is introduced and in the fourth column of **Tables 1 and 2**.

An important recent advance in this field is the development of tools and methods for **automating measurements**. Automated techniques help researchers achieve a larger sample size and a more consistent environment. These techniques generally rely on automated serial image capture and image recognition tools that must distinguish information about the animal from background noise. Standard approaches for *C. elegans* culture and analysis - Petri dishes with nematode growth medium seeded with *E. coli* OP50 and visualized on the stage of a dissecting

microscope - are well-suited to manipulation by human hands and observation by human eyes, but are difficult to automate. Stroustrup *et al.* (2013) used Petri dishes, but substituted scanners instead of the dissecting microscope [123]. Solis and Petrascheck (2011) turned to liquid culture to increase throughput of lifespan assays, and placed animals in 96-well microtiter plates that can be observed under a microscope manually or automatically [124]. Hulme *et al.* (2010) also used liquid culture of animals, but each individual was maintained in a separate microfluidics chamber for lifelong microscopic observation [125]. Zhang *et al.* (2016) isolated individual animals in droplets of *E. coli* OP50 in sealed polymer compartments for lifelong microscopic observation [126]. Churgin *et al.* (2017) also isolated individual animals in droplets of *E. coli* OP50 for lifelong microscopic observation but used a molded polymer [127]. Additional automation and culture techniques are reviewed by [128]. All of these techniques have been demonstrated to automate the measurement of lifespan, and techniques that maintain animals under near-constant surveillance can measure additional age-related changes non-invasively.

2.2.6 Statistical analysis of lifespans

The analysis of survival data requires special techniques and non-parametric statistics, because survival data rarely fit a normal distribution or the assumptions of parametric tests. The survival curve displays the probability of being alive at a particular age and is often displayed as a Kaplan-Meier survival curve, which accounts for censored events as explained below [129]. A survival curve can be summarized by its mean (or median), maximum, and variance. The amount of variation in lifespan of individuals can be described by how “steep” or “square” the survival curve appears: a steep curve means less variation. Two or more survival curves can be compared based on these parameters. When very large sample sizes are available, it may be possible to

mathematically model the survival curve, for example by fitting a Gompertz or a Weibull function [130], or to compare whether two survival curves scale [131].

Whether one is measuring a nematode's lifespan or another binary phenotype, some animals that were measured at the start of the study will never reach the measured endpoint (**Figure 4**). They may crawl off the Petri dish, die for a reason not under study (e.g. matricidal hatching or vulval extrusion), or may not have reached the endpoint (e.g. death) by the time the result is being analyzed. This poses a challenge to analyzing survival datasets. As displayed in **Figure 4B,C**, these animals can be (1) **excluded** from the entire dataset (purple) or, (2) included until the time they bag, extrude, flee, or the experiment ends (green), because the fact that they were alive at earlier timepoints is, in fact, informative. The second approach is called **censoring**. Both approaches are commonly used in the *C. elegans* literature.

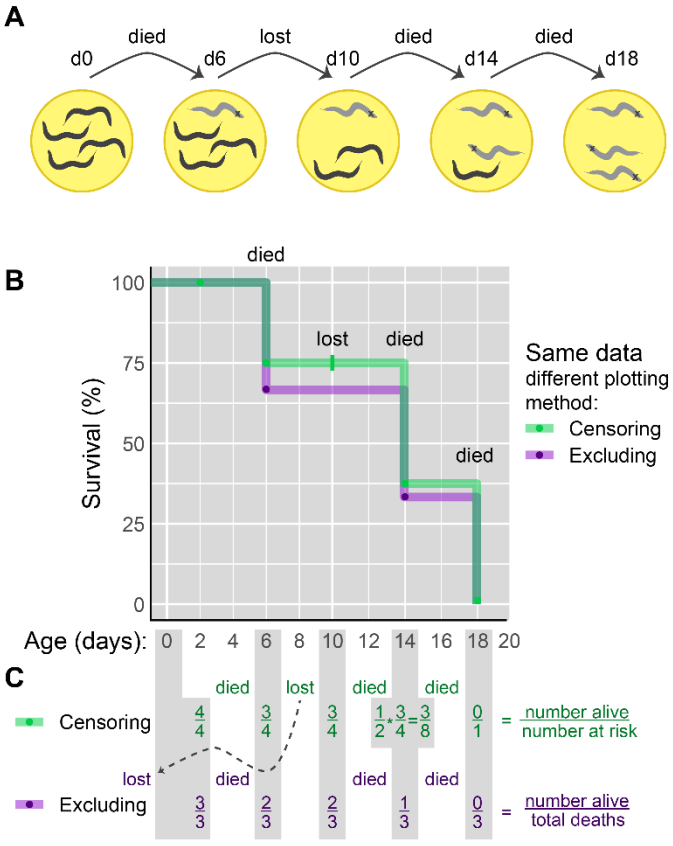

Figure 4: Approaches to censoring or excluding data in survival analysis
(A) Diagrams show a time sequence of worms on a Petri dish. The lifespan experiment began with 4 animals on day 0: one died day 6, one was lost day 10, one died day 14, and one died day 18 to end the experiment. 'died' indicates verified death (observation of a dead animal), whereas 'lost' indicates an animal that disappeared with an unknown fate. **(B)** The two survival curves illustrate this same lifespan dataset analyzed using either excluding (purple) or censoring [129] (green) of animals that did not reach the measured endpoint (death). Censored events are indicated with a '|' on the graph. **(C)** Fractions below the plot indicate the calculation of the survival curve. In the excluded method, the lost animal is considered lost before the start of the experiment; thus, it is never part of the graph, and the purple line values are 100 (3 live animals), 67 (2 live animals), 33 (1 live animals) and 0 (no live animals). In the censored method, the lost animal is included in days 1-12 but not in days 14-18, and the green line values are 100 (4 live animals), 75 (3 live animals), 37 (1.5 live animals) and 0 (no live animals). Notice the effect on the survival curve at days 6-14 and 14-18.

Not including censored data leads to under-estimates of lifespan, and could lead to bias if the censored events occurred in a non-random way. For example, if censoring occurs due to animals crawling off the Petri dish, the genotype with the healthiest and most motile animals may be more prone to crawl off the Petri dish than wild-type controls. Excluding, rather than censoring, these animals biases the dataset and decreases the sample size. Even when these events occur in a random fashion, exclusion decreases the sample size, leading to reduced statistical power. On the other hand, censoring animals requires the assumption that their likelihood of natural death at any age was the same as the rest of the population [129]. Optimally, very few animals would be excluded or censored.

In wild-type unmated animals, ~8% die due to matricidal hatching [132]. Animals which died due to matricide or vulval extrusion are typically excluded or censored because their early death may not be informative about the aging process under study. However, several recent studies have examined matricide and vulval extrusion, finding them to be predictive of lifespan [133,134]. Sterilizing animals chemically or genetically may reduce the number that need to be censored for matricidal hatching.

Animals that crawl off the agar and desiccate on the plastic dish are also censored. When an experimental treatment increases the rate of "fleeing" to intolerably high levels or unequally among treatments, adjusting culture conditions may reduce fleeing. A physical barrier of palmitic acid applied to the border of agar dishes works admirably well [135,136]. Worm Corrals, WorMotels, microfluidics, and liquid culture also prevent fleeing, making censoring and excluding nearly unnecessary [125,124,126,127].

Software is available to perform survival analyses. The *survival* library in the R software environment can be used for all statistical analyses and basic graphing. Additional libraries, such as *ggplot2*, *ggfortify*, and *survminer* are useful for adjusting the graphics. The same R analysis can be performed without needing to learn R by using the Online Application for Survival analysIS, OASIS [137,138]. In Python, the relevant library is *lifelines*. Finally, commercial software for statistical analysis also contains tools for survival analysis.

Because of variation in approaches to censoring and excluding, it is important to pay attention to the methods used by each study. It is helpful to the reader when the methods clearly state whether animals were censored or excluded, the censoring criteria, and the number of animals censored or excluded by group, in addition to the sample size. It is also helpful to cite the software used for graphing and statistical analysis.

2.2.7 Important aspects of nematode culture

A powerful aspect of *C. elegans* studies is a single defined wild-type genotype and a widely-used set of culture conditions: Bristol N2 grown at 20°C on Petri dishes with Nematode Growth Medium (NGM) inoculated with *E. coli* OP50 [3,139]. However, many studies of age-related changes have modified the genotype or culture conditions for various reasons.

Temperatures besides 20°C may be used so that experimental time-points align more conveniently with the typical workday and work week, or because the genotypes and phenotypes are most robust at temperatures other than 20°C. In addition, development and aging are accelerated at 25°C, which reduces the time necessary for lifespan studies.

In aging studies it is important to separate the animals under study from their progeny. One method to achieve this requires moving the adult animals away from their progeny daily. Because this method is labor-intensive, it may be prohibitive for large sample sizes, and it may be incompatible with techniques that limit access to the animals. An alternative approach is to use only female or sterile animals which cannot produce progeny. Common mutant genotypes include: *fog-2, spe-8, spe-9, daf-2, glp-1, glp-4*, etc. While convenient, these genotypes are not neutral to aging. For example, the temperature-sensitive *daf-2(e1370)* allele in the dauer entry pathway provides a convenient method to separate the parental generation from progeny and also causes the animal to live twice as long as wild-type [64]. Studies of the aging male sometimes use *him-5* strains in order to make the collection of males easier.

Another method to avoid mixing generations involves using drugs to selectively kill or sterilize progeny. The antimetabolite drug floxuridine (FUdR) has been used since the earliest aging studies in nematodes [140]. FUdR at concentrations up to 400 μM does not affect the lifespan in wild-type animals, but causes a lifespan extension in some mutants, including *gas-1* and *tub-1* [141–144]. FUdR can make aging experiments possible in strains otherwise prone to extremely high levels of matricidal hatching [132].

While *E. coli* OP50 has historically been the primary food source for nematode culture, many other dietary conditions can cause changes in lifespan (reviewed in [143]). It has long been known that decreasing caloric intake can increase the lifespan in *C. elegans* [48,59,49]. Common

methods of inducing dietary restriction in nematodes are food dilution [48], reducing bacterial growth [59,60], and removal of food [56,61].

Feeding *E. coli* OP50 that has been killed via heat, antibiotics, or UV-light treatment can increase lifespan in adult animals [145,113]. Some have suggested caloric restriction as a cause, but no difference in morphology or fecundity has been observed in animals fed dead *E. coli* [145], and this effect is still observed with bacteria grown on carbenicillin, which simply arrests bacterial growth [113]. Variability in male lifespan of animals grown on crowded plates was reduced when animals were fed dead *E. coli*, and also reduced when males were maintained on the same bacterial lawn for their whole life compared to transferring every few days [145].

Other bacterial food sources can increase or decrease lifespan compared to *E. coli* OP50. *E. coli* strains HB101 and HT115 increase lifespan compared to OP50 [146–148], and *E. coli* HB101 can also reduce reproductive lifespan, but not brood size [149]. Bacterial species other than *E. coli* can extend lifespan [150–154] or reduce lifespan [155–157]. The soil bacteria *Comamonas* DA1877 has been shown by some to reduce fecundity and lifespan in adult animals and accelerate their development [158], while others have found no effect on fecundity or lifespan [63,159].

Besides bacterial diet, other conditions can affect *C. elegans* lifespan. Gems and Riddle (2000) showed that isolated males lived longer than males raised with other males; this effect occurred with as few as 2 males living on the same dish, and was not observed in hermaphrodites [145]. Avery and Shtonda (2003) reported that bacterial cell size affected growth rate; animals raised on larger bacteria grew slower than animals raised on smaller bacteria [160].

The bacterial food source is often used to deliver double-stranded RNA for RNAi feeding experiments [161–163]. Previously, *E. coli* HT115 was used for this purpose, but recent advancements have made it possible for *E. coli* OP50 to be used for RNAi feeding [164].

2.2.8 Using measurements of age-related changes to characterize factors that influence aging.

In *C. elegans*, factors that have been demonstrated to influence aging include mutations, drugs, diet, and environmental conditions such as temperature. A major goal of aging research is to characterize the mechanisms that cause these factors to influence aging. One important approach to addressing these mechanisms of action is the analysis of how these factors affect age-related changes. A typical approach is to compare an age-related change in wild-type and mutant animals. If, for example, animals with a loss-of-function mutation display a delay of the age-related change, then it suggests that the gene activity causes an acceleration of that age-related change.

So many genes, drugs, and environmental manipulations have been found to extend lifespan and delay age-related changes, that describing them in full is beyond the scope of this review; Son *et al.* (2019) and Kenyon (2010) provide excellent reviews of mutations and treatments which delay aging [165,166].

2.2.9 How to define relationships between age-related changes

A fundamental question in this field is: what are the relationships between age-related changes? In principle, two age-related changes might be independent, they might share a common cause, or they might be linked in a causal relationship such that one age-related change causes the second age-related change (**Figure 5**). This issue is particularly important for the age-related increase in the probability of mortality that is measured by lifespan; a major goal of aging

studies is to identify the age-related changes that contribute to the increasing probability of mortality. Thus, studies that distinguish age-related changes that are independent of survival probability from age-related changes that are correlated with survival probability are important.

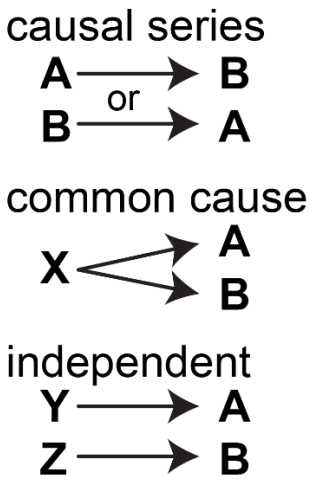

Figure 5: Correlation and Causation

If two age-related changes, A and B, are positively correlated in longitudinal studies (value >0), then they are likely to be a causal series **(top)** or share a common cause X **(middle)**, indicated by positive arrows. If A and B are negatively correlated in longitudinal studies (value <0), then they are likely to be a causal series **(top)** or share a common cause X **(middle)** and be related by negative bars (not shown). If A and B are not correlated in longitudinal studies (value ~0), then their age-related changes likely result from independent causes **(bottom)**.

Several approaches can be used to experimentally address the relationship between two age-related changes. First, in some cases it is possible to use an experimental intervention to specifically modify one age-related change, and then measure the effect on the second age-related change. For example, a drug with antioxidant activity might be used to specifically delay age-related oxidative damage and the effects on lifespan could be monitored. This approach is conceptually appealing, but in practice it is difficult to specifically affect age-related degenerative changes – especially to prevent, delay, or decrease the extent of one specific age-related change.

A second approach is to characterize the correlation between two age-related changes. For example, Johnson (1987) analyzed multiple recombinant inbred strains and showed that strains with an extended lifespan also displayed an extended period of body movement [14]. Another method is to use longitudinal studies to analyze variation within a genetically homogeneous population. Huang *et al.* (2004) used this approach to show that animals with an extended period of pharyngeal pumping also displayed an extended period of body movement[15]. This review highlights experimentally determined relationships as each age-related change is considered, and **Table 3** summarizes the relationships between age-related changes that have been defined using these approaches.

Table 1: Catalog of changes in hermaphrodites

Age-related phenotype	**Age-related change**	**Method**	**Features and limitations**	**References**
Survival				
Lifespan	Probability of death increases	Manual observation of animals on NGM with dissecting microscope	Categorical Non-invasive	[140,167,168,48]
		Automated 1) Lifespan-on-a-chip in microfluidics 2) 96-well plate in liquid medium 3) Lifespan Machine on standard NGM		1-[125] 2-[124] 3-[123] 4-[126]

		4) Worm corrals in sealed hydrogel 5) WorMotel on NGM in sealed compartments		5-[127]
Stress tolerance and response				
Heat shock tolerance and response	Decreased survival; decreased transcriptional response	Survival assay; western blot; RT-qPCR (reverse-transcription quantitative polymerase chain reaction); *hsf-1::gfp* with fluorescent microscopy	Invasive	[169,170]
Unfolded protein tolerance and response	Decreased survival; decreased transcriptional response	Survival assay; RT-qPCR	Invasive	[170]
Oxidative stress tolerance and response	Decreased survival; decreased transcriptional response; decreased enzymatic response	Survival assay; RT-qPCR; enzymatic activity	Invasive	[170,171]
DNA damage tolerance and response	Decreased survival; decline in transcriptional response	Survival assay; biochemical assays of extracts; RT-qPCR	Invasive	[172,173]
Male exposure	Decreased survival;	Survival assay; dissecting	Invasive	[174]

tolerance and response	decrease in body size	microscope; body size		
Pathogen exposure, tolerance, and immune response	Decreased survival; decreased transcriptional response	Survival assay; RT-qPCR; western blot	Invasive	[175]
Behavior				
Body movement	Decrease in rate	Dissecting microscope, machine vision, CeleST *(C. elegans* Swimming Test)	Quantitative Non-invasive	[176,177,14,117,15,178,179,120,180,119]
Habituation (spontaneous locomotion)	Decrease in response time and reversal rate	Dissecting microscope, video recording equipment	Quantitative Non-invasive	[181]
Isothermal tracking	Decrease in response	Dissecting microscope, radial thermal gradient	Qualitative Non-invasive (except temperature shift)	[182]
Pharyngeal pumping	Decrease in rate	Dissecting microscope	Quantitative Non-invasive Non-spatial	[168,183,176,15,118,120]
Pharynx pumping function	Decrease in function	Electropharyngeogram	Quantitative Invasive	[184]
Defecation	Decrease in rate	Dissecting microscope	Quantitative Non-invasive	[168,177,185,186]
Chemotaxis	Decrease in response	Dissecting microscope,	Quantitative Non-invasive	[183,187]

		chemical attractant on NGM dish		
Neurobiology				
Neuronal structure	Remains relatively intact for a long time; appearance of morphological defects; increase in neurite branching	Fluorescent reporter protein with microscopy; electron microscopy	Qualitative Invasive Spatial	[117,188–190]
Synapse structure	Decrease in synapse integrity	Fluorescent reporter protein with microscopy; electron microscopy	Qualitative Invasive Spatial	[190]
Neural mitochondrial structure	Size, shape, density, and load of mitochondria peaks between days 4 and 8, then declines; inter-mitochondrial distance troughs at day 8 then progressively increases	Fluorescent reporter protein with microscopy	Quantitative Invasive Spatial	[191]
Synapse function	Progressive decline in rate of spontaneous post-synaptic currents	Patch-clamp recordings	Quantitative Invasive Spatial	[192]

Neural mitochondrial function	Decrease in mitochondrial trafficking	Fluorescent reporter protein with microscopy, time-lapse imaging	Quantitative Invasive Spatial	[191]
Neural mitochondrial oxidative stress tolerance	Decrease in resistance to oxidative stress	Fluorescent reporter protein with microscopy	Quantitative Invasive Spatial	[191]
Reproduction				
Self-progeny production	Decrease in rate	Dissecting microscope	Quantitative Non-invasive	[168,48,14,15,193,31,194,126]
Cross-progeny production	Decrease in rate	Dissecting microscope	Quantitative Non-invasive	[31,133,195]
Embryo viability	Decrease in viability	Dissecting microscope	Quantitative Non-invasive	[196]
Oocyte morphology	Appearance of cavities, misshapen oocytes, small oocytes, oocytes in uterus, fewer late-stage oocytes Masses of chromatin in oocytes (endomitotic) in gonad and/or in uterus	DIC microscopy; DAPI (4',6-diamidino-2-phenylindole) DNA stain with fluorescence microscopy	Categorical Invasive (lethal or non-lethal)	[197–200,110,201,202]

Proximal gonad morphology	Decrease in organization; appearance of debris and opaque masses from day 5	DIC microscopy; DAPI DNA stain with fluorescence microscopy	Qualitative Invasive	[113,199,202]
Distal gonad morphology	Decrease in organization; appearance of cavities, graininess, cellularization, atrophy, narrowing, fragmentation, and swollen nuclei from day 5	DIC microscopy; DAPI DNA stain with fluorescence microscopy	Qualitative Invasive	[113,199,202]
Apoptosis	Decreases from day 4 (in unmated)	CED-1::GFP or SYTO 12 with fluorescence microscopy	Quantitative Invasive (except GFP)	[110]
RNA granules	Increased periuclear staining of RNA-rich P granules in the germline of aged adult hermaphrodites	SYTO 14 live cell dye with fluorescence microscopy	Qualitative Invasive Spatial	[203]

Meiotic prophase progression	Progressive slowing begins by day 1.5 of adulthood, occurs in mated animals	DAPI DNA stain, EdU or BrdU labeling of S-phase with fluorescence microscopy	Quantitative Invasive	[202,204]
Germ cell number	Number of germ cells in unmated animals remains relatively constant for 6 days; Number of rows of cells in distal gonad decreases by day 5	DAPI DNA stain with confocal fluorescence microscopy	Quantitative Invasive	[202,205]
Progenitor zone size	Decreases by day 3 in mated and unmated animals	Antibody staining of progenitor or meiotic markers; DAPI DNA stain with confocal fluorescence microscopy	Quantitative Invasive	[206,205,198,207–209,202]
Progenitor zone cell cycle	M-phase index decreases in unmated animals; Cell cycle speed decreases by day 3 in mated animals.	pH3 antibody stain, DAPI DNA stain, EdU labeling of S-phase with fluorescence microscopy	Quantitative Invasive (lethal)	[210,208,202]
Notch effector domain (stem cell number)	Domain of expression decreases	Antibody stain of tagged Notch pathway effector proteins LST-1 and	Quantitative Invasive (lethal)	[202]

		SYGL-1 with fluorescence microscopy		
DTC nucleus position	Mislocalizes away from distal tip	WAPL-1 antibody stain and DAPI DNA stain with fluorescence microscopy	Quantitative Invasive (lethal)	[202]
Body and Tissue Morphology				
Body size	Increase in early adulthood; decrease in late adulthood	Dissecting microscope with camera, images analyzed in ImageJ with an optional WormSizer plug-in	Quantitative Non-invasive	[168,177,117]
Head and pharynx	Decrease in organization	DIC microscopy; Harlick texture entropy	Qualitative Invasive	[113,118,211]
Pharynx size	Enlarged or atrophied pharynx in a subset of the population	DIC microscopy	Quantitative Invasive Spatial	[212]
Pharynx deterioration	Increase in entropy	DIC microscopy	Quantitative Non-invasive	[113,117]
Body wall muscle	Decrease in myosin fiber organization; loss of sarcomeric density	Electron microscopy; DIC microscopy	Qualitative Invasive	[117,187]
Bacterial accumulation	Accumulation in the pharynx and intestine	Electron microscopy; DIC microscopy	Qualitative Invasive	[113,118,213]

Intestinal integrity	Loss of intestinal nuclei; loss of microvilli; breakdown of plasma membrane; cytoplasmic shrinking	Transmission electron microscopy; DAPI DNA stain with fluorescence microscopy	Qualitative Invasive Spatial	[213]
Tissue appearance	Acquisition of granular appearance	Dissecting microscope	Qualitative Non-invasive	[113]
Vulval integrity	Increase in probability and severity of vulval rupture in a subset of the population	Dissecting microscope	Quantitative Non-invasive	[134]
Hypodermis	Loss of three nuclei in tail	DAPI DNA stain with fluorescence microscopy	Qualitative Invasive Spatial	[197]
Midsection, body cavity	Masses of DNA accumulated	DAPI DNA stain with fluorescence microscopy, DNA synthesis confirmed by BrdU	Qualitative Invasive Spatial	[197]
Subcellular Morphology				
Mitochondria	Loss of tubular morphology; mtDNA copy number declines; functional and structural decline	Transmission electron microscopy; qPCR; fluorescent reporter protein with fluorescence microscopy	Qualitative Invasive Spatial	[214–216]

Nucleus	Reduction in the number of nuclei	DAPI DNA stain with fluorescence microscopy; fluorescent reporter protein with fluorescence microscopy	Quantitative Invasive Spatial	[197,213]
Nuclear envelope	Decrease in organization of the nuclear envelope	Fluorescent reporter protein with fluorescence microscopy; confocal microscopy; electron microscopy	Categorical Invasive Spatial	[117,217]
Nucleolus	Increase in size relative to the whole nucleus	Fluorescent reporter protein with fluorescence microscopy; DIC microscopy	Quantitative Invasive (non-lethal) Spatial	[117]
Processing bodies	Accumulation	Fluorescent fusion protein with fluorescence microscopy	Quantitative Invasive (lethal)	[218]
Ectopic fat depositions and lipid droplets	Increase; change in spatial distribution	Fluorescence microscopy; transmission electron microscopy; Third Harmonic Generation microscopy	Quantitative Invasive Spatial	[117,219–221]

Autophagosomes	Increase in the number of autophagosomes	Confocal microscopy	Quantitative Invasive	[222]
Biochemical – gene and chromatin				
Genome copy number	Increase in genome copy number in germline; decrease in mitochondrial genome copy number	qPCR; DAPI DNA stain with fluorescence microscopy	Quantitative Invasive Non-spatial	[197,215]
DNA integrity	Increase in single strand breaks; methylation increases	*In vitro* assay for single strand breaks; High-performance liquid chromatography (HPLC)	Quantitative Invasive Non-spatial	[172]
Chromatin	Histone methylation profile changes	H3K4m3 Chip-Seq	Quantitative Invasive Non-spatial	[172,223,224]
RNA expression/transcriptomics	Gene expression changes; RNA expression changes	RNA-seq microarray	Quantitative Invasive	[225–228,108,229]; reviewed in [230]
mRNA splicing	Splicing efficiency declines	mCherry/GFP reporter and transcriptomics	Quantitative Invasive	[231]

Small noncoding RNAs, including microRNAs	Changes in expression profile	Microarray	Quantitative Invasive	[227,232,233]
Circular RNAs	Upregulation	RNA-seq	Quantitative Invasive	[234]
Biochemical – protein				
Posttranslational modifications	Increase in levels of protein carbonylation content, especially in mitochondria and germline	Biochemical assays of extracts; Immunofluorescence	Quantitative Invasive Spatial	[235,214,236]
Proteome	Protein levels increase and decrease	SILAC-based deep Proteome Analysis	Quantitative Invasive	[237,238]
Protein structure	Protein misfolding; loss of protein function; protein aggregation	Expression of metastable proteins fused to fluorescent proteins (temperature-sensitive mutations); mass spectrometry microscopy	Quantitative Invasive/Non-invasive; Some spatial	[170,239,240]; useful references: [241–243]
Clustered change in protein levels	Yolk redistribution; increase in Yolk	Electron microscopy; DIC microscopy; western blot	Qualitative Invasive Spatial	[113,117,111]

Enzymatic activity	Decrease in protein tyrosine kinase activity; increase in lysosomal hydrolases	Biochemical assay of enzymatic activity; western blot	Quantitative Invasive	[121,244,245]
Biochemical – metabolism				
Autofluorescence	Increase	Spectrofluorometry; fluorescence microscopy; electron microscopy	Quantitative Invasive Spatial	[167,48,246,247,113,114,233,248,249]
Metabolic activity	Decrease	Various assays	Quantitative Invasive Non-spatial	[250–254,215]
Metabolites	Changes in metabolite concentrations (Amino acids, lipids, etc.)	Nuclear magnetic resonance (NMR); mass spectrometry (GC-MS)	Quantitative Invasive Non-spatial	[251–253,215,255–260]
Metallostasis	Changes in metal profile	Inductively coupled plasma atomic emission spectroscopy (ICP-AES) analysis	Quantitative Invasive Non-spatial	[261]

Table 2: Catalog of male-specific changes

Age-related change	Description over age	Method	Features and Limitations	References
Behavior				
Mating behavior	Decrease in successfully completed mating events	Dissecting microscope	Quantitative Non-invasive	[262]
Body movement	Decrease in rate	Dissecting microscope	Quantitative Non-invasive	[262]
Body and Tissue Morphology				
Male tail morphology	Progressive deterioration of tail structure	DIC microscopy	Quantitative Invasive (non-lethal)	[262]
Body size	Mated males show decreased body length later in life compared to unmated males	Dissecting microscope, camera, and ImageJ	Quantitative Non-invasive	[263]
Sperm	Decrease in viability	Dissecting microscope, counting of progeny	Quantitative Non-invasive	[172]

Table 3: Correlations between age-related changes

	Survival probability	**Pharyngeal pumping**	**Body movement**	**Body/tissue morphology**
Self-fertile reproduction	no correlation [14,15]	no correlation [15]	no correlation [14,15]	
Mated reproduction	positive [133,264]			
Body movement	positive [176,177,14,117,15,114,178,179]	positive [15,176]	positive [178,181]	

Maximum body movement velocity	positive [180]			
Pharyngeal pumping	positive [14,15,265]			
Defecation	no correlation [177]		no correlation [177]	
Pharynx morphology	positive [212]	positive [212,266]		positive [111]
Uterine morphology				positive [111]
Synaptic deterioration			positive [190]	
Neurite morphology			positive [189]	positive [267]
Pseudocoelomic morphology				positive [111]
Intestinal morphology				positive [111]
'Smurf' phenotype (intestinal permeability)	positive [268]			
Mitochondria	positive [180]	positive [180]	positive [180]	positive [191]
Mitochondrial copy number			negative [215]	
Nuclear morphology			positive [117,217]	
Nucleolar size	negative [269]			
Body wall muscle			positive [117]	
Autofluorescence	positive [233,249]		positive [114]	

Splicing efficiency	positive [231]			
Metabolism			positive [245]	

Blue: positive correlation
Red: negative correlation
Gray: no correlation
Empty: not determined

2.3 Discussion: Description of age-related changes

2.3.1 Survival

The most pivotal age-related change is survival; the cumulative probability of death eventually reaches 100% (**Table 1, Survival**). Gershon (1970) chose the nematode as a convenient model for aging studies and measured the lifespan of *Turbatrix aceti* nematodes [140]. Shortly after, Epstein *et al.* (1972) measured the lifespan of *Caenorhabditis briggsae* in axenic culture [167]. *C. elegans* lifespans were measured in both axenic and standard NGM culture by [48,168]. Since then, countless studies have measured the lifespan of millions of *C. elegans* with numerous genotypes in varied environmental conditions.

It is difficult to determine the time of death with precision; if death is defined as the permanent cessation of all vital functions, measuring the live to dead transition lacks precision because all vital functions cannot be measured non-invasively at all times in *C. elegans* aging experiments. The working definition of death in a lifespan analysis is the cessation of visible body and pharyngeal movement, either spontaneous or in response to a stimulus such as light or prodding with a platinum wire.

Substantial variability in lifespan exists, even among isogenic populations in a consistent environment. In defined liquid medium named *C. elegans* maintenance medium (CeMM), the mean lifespan is 30 ± 20 days with a maximum of 93 days. In standard nematode growth

medium (NGM) and *E. coli* OP50 diet, the mean lifespan is 16 ± 6 days with a maximum of 30 days [193]. Reproducibility within and between laboratories (e.g. in the *Caenorhabditis* Intervention Testing Program) can be a challenge; therefore, a rigorous experimental design includes a concurrent control in every lifespan experiment [270].

2.3.2 Stress Response

Despite attempts to maintain a constant laboratory environment, any environment, including standard NGM culture, involves fluctuating levels of stress to some degree. One way to conceptualize death in standard conditions is that it occurs when an individual's level of stress resistance decreases to the point that a small fluctuation that increases environmental stress overwhelms and kills the individual. Stress resistance experiments intentionally increase the level of a stressor (e.g. heat, oxidation, radiation, pathogen, etc.) at a particular time and measure the ability of individuals to survive the stress. Conceptually, stress resistance experiments and standard lifespan experiments are very similar, as they both measure the survival of animals over time.

When an animal dies under high-stress conditions, it is not clear whether that death occurred as a result of stress, or whether the animal would have died of old age even under low-stress conditions. For this reason, some studies include a no-additional-stress control (i.e., survival from the starting point with no additional stress) [171].

Survival time in heat stress and oxidative stress conditions decreases with age (**Table 1, Stress tolerance and response**) [170,171]. The transcriptional response to heat stress and the unfolded protein response also decreases with age. Survival time in DNA damage conditions decreases with age, and the DNA damage response (including transcription of nucleotide excision repair machinery) also decreases with age [172,173].

Sensitivity to the nematocidal effects of nile blue, a presumed measure of stress resistance, was positively correlated with the decline in body movement [15,176]. Resistance to stress positively correlates with lifespan between strains [120].

In the laboratory, *C. elegans* is typically fed *E. coli* OP50. *E. coli* is a weak pathogen for *C. elegans*, and resistance to its pathogenic effects are age-related [271]. Indeed, *E. coli* OP50 accumulates in the intestines of aged animals [113,118,213], and this may represent a prevalent cause of death late in life [272].

C. elegans resists pathogenic stress via activation of an innate immune response [273,274], and the ability to respond to pathogens declines with age. Youngman *et al.* (2011) measured survival of aged animals cultured on *E. coli* OP50 then transferred to pathogenic *P. aeruginosa* PA14 bacteria [175]. Adults at days 3, 6, and 9 displayed a progressive decrease in survival and an increase in bacterial colonization of the intestine. Similarly, Laws *et al.* (2006) observed a significant reduction in survival time between animals transferred to four different strains of pathogenic bacteria on days 0 and 7 [275]. Conversely, Burns *et al.* (2017) did not observe an age-related decrease in pathogen resistance to *S. enterica*, although this study only measured up to day 5 of adulthood [276].

2.3.3 Behavior

2.3.3.1 Body Movement

The well-coordinated sinusoidal body movement characteristic of young hermaphrodites becomes progressively slower and less coordinated and ultimately ceases altogether in old hermaphrodites (**Table 1, Behavior**). Two approaches have been used to measure body movement during aging. First, it is possible to quantify movement as waves per minute observed with a dissecting microscope. Several studies found that the wave frequency declines regularly

with age and fit the data to a straight line [168,177,14,4,187]. Second, it is possible to define categories of movement ability [176,117,15]. Herndon *et al.* (2002) and Hosono *et al.* (1980) defined three categories: Class A (Herndon) or Type I (Hosono) animals progress with rhythmic sinusoidal movement, Class B (Herndon) or Type II (Hosono) are not active and are uncoordinated, and Class C (Herndon) or Type III (Hosono) are unable to progress but spontaneously move their head or tail and respond to touch [176,117]. "No visible movement" is not a category here because it is defined as death. Huang *et al.* (2004) defined two categories: fast moving corresponding to Type I/Class A and not fast moving corresponding to type II/class B and type III/class C [15].

With advances in technology, automated methods to measure body movement have been developed. Restif *et al.* (2014) identified novel features of age-associated changes in swimming and analyzed a variety of phenotypes from wave initiation rate to reverse swimming at day 4 and day 11 using the *C. elegans* Swimming Test (CeleST) program [179]. Some phenotypes, such as wave initiation rate, travel speed, brush stroke, and activity index, decline with age; by contrast, body wave number, asymmetry, and curling increase with age. Other phenotypes such as stretch, reverse swimming, and attenuation displayed minimal age-related change. Bansal *et al.* (2015) measured movement in liquid medium by performing a thrashing experiment and compared the distance traveled by individual animals by analyzing tracks during a finite period [120]. Results from both experiments corresponded to previous results [15,117]: as adults age they move less. Using the same classification system as Herndon *et al.* (2002) and Hosono *et al.* (1980) [176,117], Newell Stamper *et al.* (2018) performed a longitudinal study on individual animals [119]; as animals age they gradually traverse from Class A to Class B to Class C to death.

The relationships between the decline of body movement and several other age-related changes have been characterized. Several studies have analyzed the relationship between the

age-related change of body movement and the declining survival probability measured by lifespan. Herndon *et al.* (2002) and Hosono *et al.* (1980) showed that dividing wild-type animals into movement classes was predictive of lifespan [176,117]. Huang *et al.* (2004) showed in a longitudinal study that the fast body movement span was positively correlated with lifespan in wild-type animals and several mutants [15]. Johnson (1987) analyzed a series of recombinant inbred strains with differing lifespans, and found that the x-intercept of the age-related movement decline positively correlated with the maximum lifespan [14]. By contrast, Bolanowski *et al.* (1981) found no correlation between the rate of decline in movement frequency and the lifespan in a longitudinal study of wild-type animals [177]. Hsu *et al.* (2009) performed a longitudinal study of wild type from adult day 3 until death and specifically examined the locomotor speed by a nematode tracking system [178]. Age-related change in locomotor speed correlated with lifespan; animals with a slower rate of motor activity decay have a longer lifespan than those with a faster rate of decay [178]. Hahm *et al.* (2015) analyzed the maximum velocity of individual animals over their lifespan using a stereomicroscope [180]. Animals with a higher maximum velocity have a longer lifespan than animals with a lower maximum velocity [180]. The decline in body movement was positively correlated with sensitivity to the nematocidal effects of nile blue, a presumed measure of stress resistance [15,176]. Overall, these studies indicate that the decline in body movement is positively correlated with the decline in the survival probability and can be used to predict lifespan (**Table 3**).

Habituation is the phenomenon that an organism's response decreases after repeated or prolonged presentation of a stimulus. Beck and Rankin (1993) examined spontaneous locomotion and habituation by mechanically tapping the Petri dish [181]. The magnitude and occurrence of reversals stimulated by tapping decreased with age from adult day 4 to day 7 and

12. This can be interpreted as an age-related reduction of sensitivity or an increase in habituation, recovering from habituation slower compared to younger animals. Timbers *et al.* (2013) also used tapping of the Petri dish to examine reversal probability and reversal distance of adults at various ages in the presence and absence of food [277]. Age-dependent changes in short-term habituation occur during the reproductive period: day 2 adults are less likely to respond to tapping both in the presence and absence of food compared to day 0 adults, suggesting an increase in habituation to tapping stimulus and a decrease in the ability to distinguish the intensity of stimuli as the worm ages. Age dependent changes in reversal distance were not observed [277].

2.3.3.2 Pharyngeal Pumping

The pharynx is a neuromuscular organ that undergoes rhythmic contractions that facilitate feeding; contractions can be counted using a dissecting microscope [278]. The pharyngeal pumping rate reaches a maximum of approximately 300 pumps per minute in day 2 adults. Pharyngeal pumping undergoes an age-related decline and typically ceases by about day 12 (**Table 1, Behavior**) [168,176,15,118]. Russel *et al.* (2017) analyzed age-related changes using an electropharyngeogram in a microfluidic device [184]; the frequency of pharyngeal pumping decreases with age, whereas the duration of pharyngeal contractions and the variability of the inter-pump interval increase with age.

Longitudinal studies have been used to characterize the relationships between the decline in pharyngeal pumping and other age-related changes (**Table 3**). The decline in body movement is positively correlated with the decline in pharyngeal pumping [15,176]. Hosono *et al.* (1980) showed that older adults that still displayed rhythmic, sinusoidal body movement (type 1) displayed more rapid pharyngeal pumping than animals of the same age that had diminished

body movement and were unable to progress (type III), indicating a positive correlation between the declines in pharyngeal pumping and body movement [176]. Huang *et al.* (2004) showed that both the fast-pharyngeal pumping span and the pharyngeal pumping span were positively correlated with the fast body movement span [15]. Bansal *et al.* (2015) examined how pharygneal pumping over age correlates with lifespan and with chronological and relative physiological healthspan; pharyngeal pumping decreases to a minimum by day 15 regardless of the health of the animal and is therefore not correlated with healthspan (defined by a combined metric for movement ability and stress resistance) [120].

2.3.4 Neurobiology

Defects in movement might be caused by changes in neuron, muscles, or both. Herndon *et al.* (2002) used neuronally expressed GFP reporters and electron microscopic analysis to determine that the nervous system undergoes minimal age-related morphological changes [117]. Since age-related morphological changes have been observed in many somatic tissues, these results suggested that degeneration in locomotion was more likely to be caused by changes in muscle than changes in the nervous system [117,5].

By contrast, more recent studies have identified various age-related changes in neuronal structure; these include changes in neuron soma morphology, increases in spontaneous neurite branching, and the formation of morphological abnormalities along the axon (**Figure 6C-G**) [188–190,267]. Pan *et al.* (2011) used neuronally expressed GFP reporters and fluorescence microscopy to examine structural changes in the ALM, PLM, AVM, and PVM touch receptor neurons [188]. They categorized several classes of defects in the neuronal processes that increased in frequency with age: formation of “bubble”-like lesions, GFP-rich “beads”, and triangular protrusions (“blebs”). Age-related morphological abnormalities in the soma of ALM neurons associated with increased

disorganization of microtubule bundles. In addition, the ventral nerve cord (VNC) displayed a low frequency increase in the number of fascicles by day 8 and beading along the axon by day 17.

Toth *et al.* (2012) used similar methods and noticed several additional neuronal features that progressively increase with age, including novel branches emerging from neuronal processes (**Figure 6G**), novel outgrowths emerging from the soma (**Figure 6A**), and bending of the neuronal process ("wavy" appearance, **Figure 6D**) [190]. They observed an age-related decrease in the presence of GFP-rich "beads" along the processes; this is different from Pan *et al.* (2011) who reported an age-related increase, but only in PLM neurons [188].

Tank *et al.* (2011) examined age-dependent development of new neuronal outgrowths in mechanosensory neurons and showed that this phenotype also occurred in GABAergic motor neurons, indicating that age-related branching occurs in multiple neuronal cell types [189]. They analyzed the correlation between physiological age (measured by touch response) and branch outgrowth; at day 13, low-mobility animals displayed more branches than high-mobility animals, documenting a correlation between neuronal abnormalities and movement decline (**Table 3**).

Pan *et al.* (2011), Tank *et al.* (2011), and Toth *et al.* (2012) all observed neuronal morphological changes in most, but not all, aged animals, indicating this phenotype only occurs in a subset of the population [188–190]. In addition, different morphological changes occurred in different types of neurons. Overall, these results indicate that while most morphological changes display an age-related increase, the frequency of abnormalities differs between individuals in a population and between neuronal cell types within the same animal.

Quantification is an important goal of any phenotype analysis, and many of the changes observed in neurons are described in qualitative terms. Hess *et al.* (2019) developed an image

analysis pipeline to quantify neuronal morphology [267]. Both the number and length of soma outgrowths in ALM were increased at day 8 compared to day 1, whereas the total soma volume decreased. For age-related neurite outgrowths in PLM, their position along the process was correlated with the presence of neurite "bends" (**Table 3**).

Toth *et al.* (2012) identified a correlation between the degree of synaptic deterioration and decrepitude in aged animals, suggesting a link between the decline of locomotory behavior and neuronal function [190]. Deterioration of the synapse and depletion of presynaptic vesicles were observed by day 15 in the nerve ring and lateral ganglia (**Figure 6H, I**). The severity of these phenotypes was reduced in class A (youthful) compared to class C (decrepit) adults, establishing a correlation between degeneration of the synapse and body movement (**Table 3**). Similarly, Liu *et al.* (2013) and Li *et al.* (2019) showed that motor neurons display age-related functional decline, exhibiting a progressive decline in the frequency of spontaneous post-synaptic currents in motor neurons but not body-wall muscle receptors [192,279].

Morsci *et al.* (2016) showed that mitochondria in the soma of mechanosensory neurons display phasic changes during aging [191]. They observed increased organization and density in middle age compared to both early and late life (**Figure 6B**), an age-related decrease in mitochondrial trafficking along the ALM process from day 1 to day 11, and an age-dependent decrease in mitochondrial resistance to oxidative stress. Mitochondrial size, density, and load in day 11 decrepit animals were reduced compared to youthful-looking day 11 animals (**Table 3**).

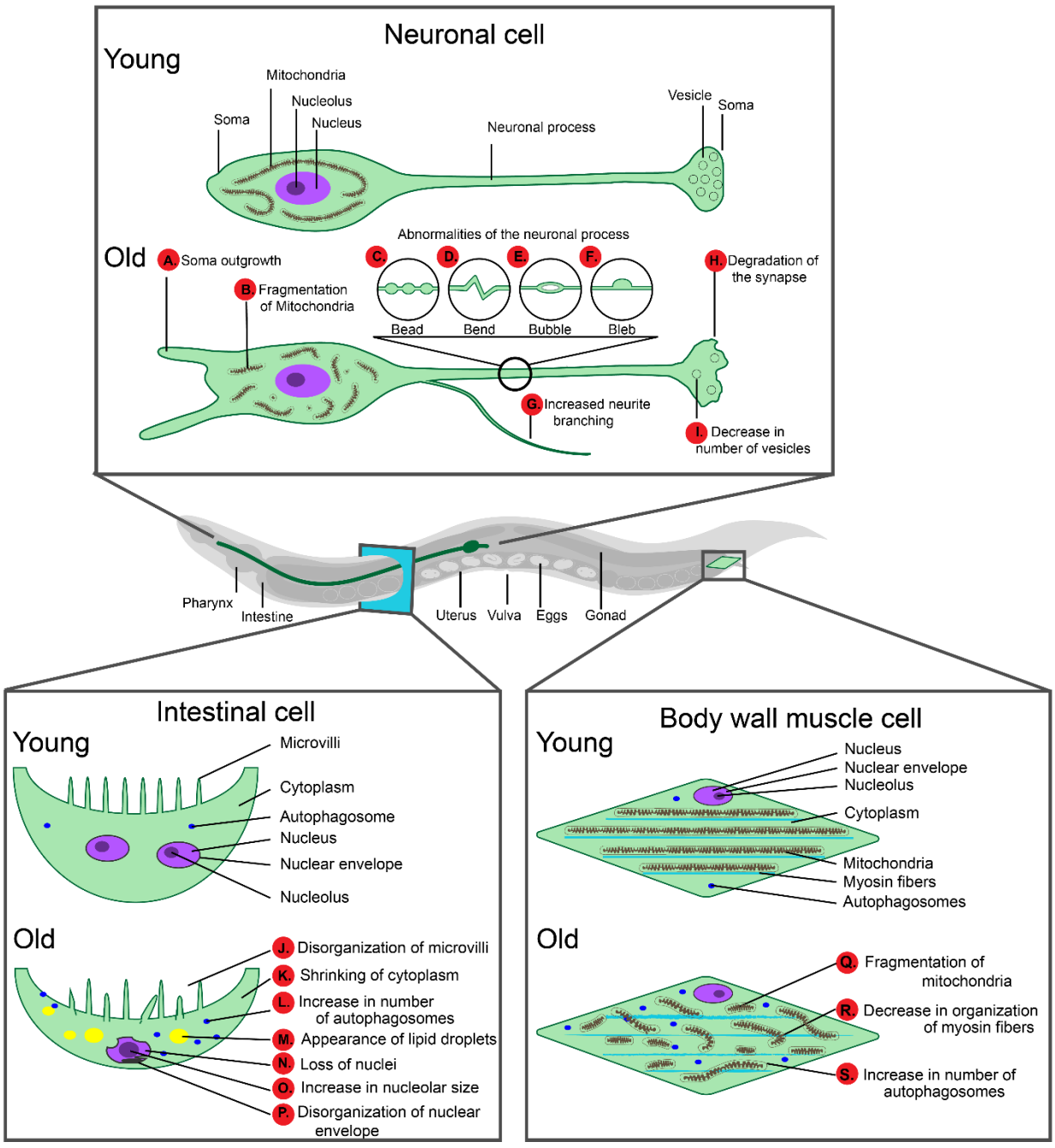

Figure 6: Age-related degenerative changes in cell morphology
The cartoon shows a worm with a generic neuron (expanded above), cross section of a generic intestinal cell (expanded below left) and a generic muscle cell (expanded below right). Young and old diagrams illustrate prominent age-related changes reported in one or more of these cell types. In general, a single cell type has not been documented to display all of these changes.

Neuronal cell (A-I)

(A) Aged animals display an increase in the number and length of soma outgrowths in the ALM neuron [188–190,267]. **(B)** Mitochondrial networks become progressively smaller and more fragmented with age in mechanosensory neurons [191]. **(C-F)** Neuronal processes display age-related morphological defects that are primarily observed in mechanosensory neurons [188–190]. **(G)** Spontaneous branching of new neurite outgrowths increases with age, primarily in the PLM [188–190,267]. **(H-I)** The integrity of the synapses of the nerve ring and lateral ganglia deteriorates with age, and there is a decrease in the number of synaptic vesicles [190]. These phenotypes were more pronounced among Class C (decrepit, poorly aged) nematodes.

Intestinal cell (J-P)

(J) Intestinal cell microvilli display regular organization and uniform length in young animals. As *C. elegans* age, microvilli lose their regularity and become degraded [117,213]. **(K)** In aged *C. elegans* the cytoplasm shrinks and the intestinal lumen is enlarged [213]. **(L,S)** Autophagosomes increase in intestinal and muscle cells with age [222]. **(M)** Lipid droplets accumulate in aged animals and appear in the cytoplasm of intestinal cells [117,213]. **(N)** Intestinal cells typically have two nuclei in young *C. elegans*, and nuclei number displays age-related decline. Day 4 animals exhibit about 30 nuclei, whereas in day 20 animals the number of intestinal nuclei can be as low as 10 [213]. **(O)** The nucleolar size increases with age and is especially easy to observe in intestinal cells due to their large cell size [117]. **(P)** The intestinal nuclear envelope dramatically loses its integrity and displays abnormal shapes, fragmentation, and extensive stretching [217].

Body wall muscle cell (Q-S)

(Q) Mitochondria undergo fragmentation, decrease in length, and become more spherical with age in body wall muscle cells [216]. **(R)** Body wall muscle cells exhibit a decrease in organization in myosin fibers [117,187]. **(S,L)** Autophagosomes increase in intestinal and muscle cells with age [222].

2.3.5 Reproduction – function and morphology

2.3.5.1 Self-Progeny and Cross-Progeny Production

Successful reproduction is the ultimate goal of an organism. Therefore, the age-related decline of reproductive function is likely to be critical for the evolution of aging. From a single fertilized egg, the *C. elegans* hermaphrodite develops its entire soma and both arms of its reproductive tract and begins laying eggs at ~65 hours at 20°C [280]. At the peak of reproduction, oocytes are ovulated every ~23 min [281], resulting in an average of ~150 progeny per day.

It is notable that self-fertile reproduction ceases relatively early in life: for wild-type hermaphrodites at 20°C on standard nematode growth medium seeded with live *E. coli* OP50, the self-fertile reproductive span is 5.8 days and the lifespan is 15.2 days [15]. A description of age-related changes in the germline can be found in **Figure 7A,B**.

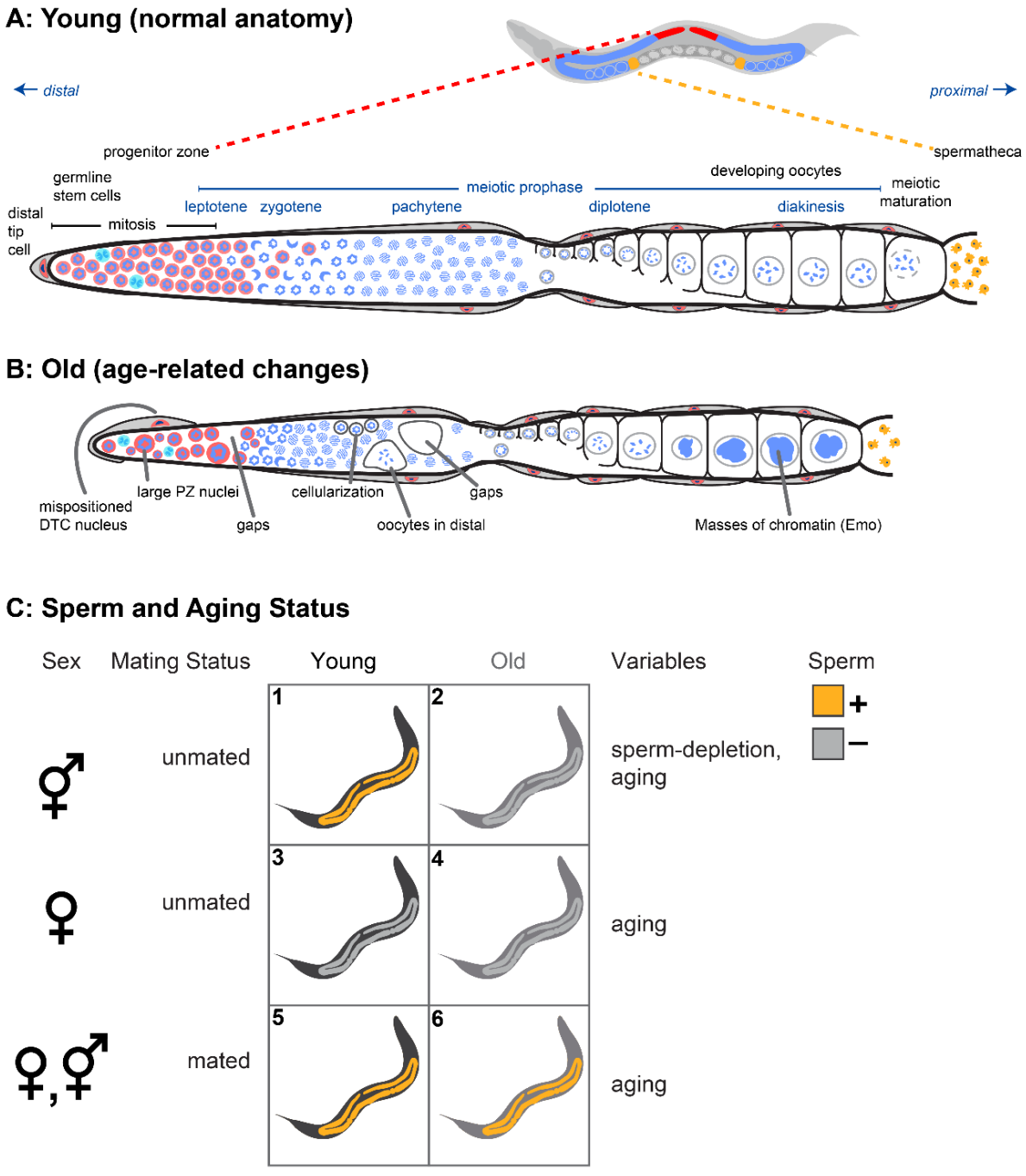

Figure 7: Germline develops defects with age

(A) Normal anatomy of *C. elegans* germline. **Top**: *C. elegans* hermaphrodites have two U-shaped germlines: distal is red, proximal is blue, spermatheca is yellow, and uterus with developing embryos is dark gray. **Bottom**: Diagram of one straightened *C. elegans* hermaphrodite germline. Nuclear morphology can be visualized by staining DNA with DAPI (blue). The distal progenitor zone (red) contains mitotically cycling stem and progenitor cells. The distal tip cell (DTC) provides the GLP-1/Notch ligand to maintain the stem cell fate of these cells. As cells migrate away from the DTC, they exit the progenitor zone and enter meiotic prophase.

(B) Numerous age-related changes in the germline have been reported. Several are illustrated here.

(C) Diagrams illustrate worms with sperm adequate for reproduction (yellow) or lacking sperm (gray). In wild-type self-fertile hermaphrodites **(1,2)**, the number of sperm is limiting for self-reproduction. Therefore, two major changes occur with the passage of time: aging and sperm-depletion. By contrast, unmated females change only by aging, since sperm are never available **(3,4)**, and hermaphrodites or females mated to males change only by aging, since sperm are continuously available for reproduction **(5,6)**.

In self-fertile *C. elegans* hermaphrodites the first ~300 germ cells differentiate as sperm, and the remaining germ cells differentiate as oocytes. Ward and Carrel (1979) showed that there is an age-related decrease in the number of sperm in or near the spermatheca which corresponds with the fertilization of oocytes [282]. Klass (1977) and Croll *et al.* (1977) documented that there is an age-related peak and decline in fertilized eggs laid that corresponds with the depletion of sperm [48,168]. There is a delayed, slightly overlapping, and much smaller peak of unfertilized oocytes deposited. However, the germline responds to sperm depletion by arresting the development of oocytes, a phenotype known as oocyte "stacking". These age-related changes are modulated by temperature, and the self-fertile reproductive span is extended by cold temperatures[48,15]. The decline in fertilized eggs laid by self-fertile hermaphrodites is caused by the depletion of self-sperm, since mating to males can significantly increase the number of fertilized eggs laid[282,283]. Mating increases duration of reproduction, while the peak remains relatively unchanged [31,264].

Reproduction requires both the germ line and somatic tissues, and it is important to understand how age-related changes in both the reproductive tract and in somatic tissues affect reproductive function. It is notable that even when sperm are not limiting, reproduction ceases relatively early in life: at 20°C on standard nematode growth medium seeded with live *E. coli* OP50, in wild-type hermaphrodites with excess sperm from mating to males, the reproductive span is 8.8 ± 1.8 days and the lifespan is 15.6 ± 3.3 days [264]. Further, progeny production declines from a peak of ~150 progeny per day on adult day 2 to ~40 progeny per day on adult day 5 and to ~12 progeny per day on adult day 7, while the animals are all still alive, moving, and feeding [202]. This suggests that the age-related decline in reproductive function may not be caused primarily by a decline in somatic functions that maintain survival.

The relationship between the age-related decline in self-fertile reproduction and other age-related changes has been analyzed. Johnson (1987) analyzed the length of the self-fertile reproductive period in many recombinant inbred lines and found no correlation with the mean lifespan of these lines (**Table 3**) [14]. Huang *et al.* (2004) conducted a longitudinal analysis of wild-type and mutant hermaphrodites, and there was no correlation between the self-fertile reproductive span and the lifespan, the fast body movement span, or the pharyngeal pumping span (**Table 3**) [15]. The self-fertile reproductive span appears to be determined by the number of sperm that are generated, which is controlled by a developmental switch, and the rate of sperm utilization. The absence of correlation observed in multiple studies indicates that these processes are independent of the processes that influence the decline of body movement, pharyngeal pumping, and survival probability [15,193].

Because self-fertile hermaphrodites completely deplete self-sperm, measurements of live progeny production do not accurately measure the reproductive capacity of these hermaphrodites

late in life. To address this issue, Hughes *et al.* (2007) and Pickett *et al.* (2013) analyzed progeny production in mated hermaphrodites that have sufficient sperm [31,264]. Compared to self-fertile hermaphrodites, mated hermaphrodites generate more progeny, but still display an age-related decline in progeny production that results in the cessation of progeny production at ~day 8. These studies demonstrate formally that hermaphrodites undergo an age-related decline of reproductive function that is independent of sperm depletion.

Progeny production is typically assayed on standard NGM petri dishes with lawns of live *E. coli* OP50. Individual P0 animals, "mother worms," are placed on a dish, allowed to produce progeny for 24 hours, then transferred to a fresh dish. Progeny are counted either immediately as eggs and larvae or after 2-3 days when the progeny have developed into adults that are easier to count. Alternative approaches to assaying progeny production include maintaining "mother worms" in 96-well dishes of *C. elegans* minimal medium (CeMM) [193], hanging drops of culture medium [194], or droplets of bacteria sealed in a hydrogel [126]. Progeny production, when analyzed as the number of progeny produced on each day of life, is a quantitative phenotype. It is possible to analyze it as a discrete phenotype: fertile (> 1 progeny) versus sterile (0 progeny). However, this approach can equate an animal producing 1 egg per day to an animal producing 150 eggs per day. Another assay of reproduction is the ability to produce progeny when mated to a male after a period of sperm depletion. While nearly 100% of wild-type hermaphrodites regain fertility when mated on adult day 8, only 50% do so when mated on day 10, and none regain fertility when mated on day 15 [195].

2.3.5.2 Progeny viability and morphology

C. elegans embryos exhibit a remarkably low rate of lethality: typically less than 1%. The lethality of embryos from older mothers can increase for two reasons: extended arrest in

diakinesis (only for embryos which developed from stacked oocytes) and/or due to older germline tissue. Anduz and Ellis (2008) reported that lethality increased to ~20% in embryos which developed from stacked oocytes. However, lethality among embryos which developed from non-stacked oocytes produced by older mothers was ~3% [196].

The size of *C. elegans* embryos and L1 larvae is tightly regulated. Hibshman *et al.* (2016) report that L1 larvae hatched from embryos deposited by older mothers are slightly longer [284].

2.3.5.3. Gonad morphology

C. elegans contain two U-shaped assembly-line-like germlines in which stem cells proliferate in the distal region (distal to the vulva). Stem cells then differentiate into oocytes in the proximal region (proximal to the vulva), which are ovulated into the spermatheca, fertilized, and begin embryonic development in the uterus.

The oocytes and germline viewed by DIC microscopy undergo multiple age-related changes in appearance that are suggestive of deterioration. Garigan *et al.* (2002) defined five categories of deterioration and used this scoring system to document progressive, age-related deterioration of germ line morphology [113].

Proximal germline and oocyte morphology deteriorate with age. In unmated hermaphrodites, the gonad responds to sperm depletion by stopping oocyte maturation and arresting oocytes in diakinesis, a process referred to as oocyte "stacking" or feminization. By DIC, stacked oocytes appear as narrow rectangles [199]. Luo *et al.* (2010) report an increased incidence of small oocytes, clusters of oocytes, and cavities in the uterus of day 8 post-reproductive animals [198]. Clusters of oocytes were also observed in day 8 reproductive animals [198]. Hughes *et al.* (2011) report in increased incidence of debris, vacuole-like structures, and

opaque masses visible by DIC in the proximal gonad [199]. By using DAPI to visualize DNA, Kocsisova *et al.* (2019) reported gaps and oocytes in the pachytene region [202].

Multiple groups have reported swollen nuclei (detected by DIC) and masses of chromatin (detected by DAPI) in the proximal gonad arm and/or uterus of older (day 5, day 8) sperm-depleted animals. These are sometimes called hypertrophic nuclei, hypertrophic oocytes, hypertrophic embryos, hyperplasia, and tumors [285,197,198,200,110,201]. It is hypothesized that they result from the endoreduplication of unfertilized oocytes [285]. In sperm-replete animals, endomitotic oocytes were reported in 10% of the population at day 5 [202].

The distal germline contains the mitotic stem cells, progenitor cells, and meiotic cells in leptotene, zygotene, and pachytene. These cells exhibit incomplete separation of the cytoplasm, forming a syncytium, yet maintaining asynchronous cell cycles [286]. Garigan *et al.* (2002) reported increased spacing of mitotic nuclei, nucleoplasm disrupted by cavities and grainy material, and nuclei that appear to be cellularized [113]. Luo *et al.* (2010) also reported cavities, graininess, and cellularization [198]. Hughes *et al.* (2011) reported a narrow distal gonad and swollen nuclei in the distal gonad [199]. de la Guardia *et al.* (2016) reported narrowing of the distal gonad and distal gonad fragmentation [110]. By using DAPI to visualize DNA, Kocsisova *et al.* (2019) reported enlarged progenitor zone nuclei and small distal germlines [202].

2.3.5.4 Meiotic prophase progression and apoptosis

In L4 hermaphrodites, germ cells differentiate into sperm; by contrast, in adult hermaphrodites, germ cells differentiate into oocytes. In young adults, the process of meiotic prophase progression and oogenesis takes ~2 days [204]. Measuring meiotic progression requires injecting or feeding a nucleoside analog (such as BrdU or EdU) which is incorporated during S-phase, retained by cells as they differentiate, and detected by fluorescent microscopy. Meiotic

progression is defined from the last S-phase in the distal germline to meiotic maturation of the most proximal oocyte. As reported by Jaramillo-Lambert *et al.* (2007) meiotic progression begins to slow by adult day 1.5 [204]. Meiotic progression in older sperm-replete animals requires significantly longer than 48 hours [202].

A large proportion (~87%) of germ cells that enter meiosis in the adult function as nurse cells that provide essential constituents to growing oocytes but do not become oocytes themselves; they undergo apoptosis in late pachytene [287–289]. The number of apoptotic germ cells per gonad arm (detected by CED-1::GFP) displayed an increase from day 1 to day 4, then a decrease from day 4 to day 8 [110].

Schisa *et al.* (2001) used fluorescence microscopy of the live cell dye SYTO 14 and reported increased perinuclear staining of RNA-rich P granules in the germline of aged adult hermaphrodites [203].

2.3.5.5 Germ cell number and Progenitor Zone size

The total number of germ cells in the entire germline remains relatively constant for 6 days in unmated hermaphrodites [205] but decreases slightly in sperm-replete mated hermaphrodites [202].

The progenitor zone, sometimes called the proliferative zone or mitotic zone, is the most distal region of the germline located next to the distal tip cell. This region contains all germ cells which have not yet entered meiosis, including mitotically-cycling germline stem cells and progenitor cells undergoing pre-meiotic S-phase (**Figure 7A**). The cells in the progenitor zone can be identified by immunohistochemistry and approximated by DAPI morphology [290,205,291–293]. Methods to accelerate and automate the detection of germ cell nuclei and DNA content have been reported [294,209].

Some variability in progenitor zone measurements exists between laboratories. Crittenden *et al.* (2006) reported that PZ cell number remained unchanged up to day 6 of adulthood (day 1 ~243, day 2 ~227, day 3 ~214) in unmated hermaphrodites [205]. Luo *et al.* (2010) report that the number of cells in the progenitor zone peaks at ~220 at day 2, then decreases to ~150 at day 6 of adulthood in unmated hermaphrodites [198]. Killian and Hubbard (2005) and Qin and Hubbard (2015) report that the number of cells in the progenitor zone peaks at ~250 cells, decreases to ~150 cells by day 3, ~100 cells by day 6, and ~50 cells by day 12 of adulthood in unmated hermaphrodites [206,208]. Narbonne *et al.* (2015) reported that the number of cells in the progenitor zone peaks at ~190 at day 2 and decreases to ~80 at day 7 in unmated hermaphrodites [210]. Shi and Murphy (2014) noted that 50 µM FUdR, which did not affect lifespan, reduced the number of germ cell nuclei [207].

In mated hermaphrodites, Shi and Murphy (2014) found a decrease in the number of progenitor zone cells with age, from ~150 at day 1 to ~100 at days 2-4 [207]. Qin and Hubbard (2015) report that mating, via germ cell flux, accelerates the decline of the progenitor zone to ~60 cells at day 6 [208]. Narbonne *et al.* (2015) reported that the number of cells in the progenitor zone peaks at ~190 at day 1 and decreases to ~90 at day 8 in continuously mated hermaphrodites [210]. Kocsisova *et al.* (2019) reported that in mated hermaphrodites the total number of progenitor zone cells was ~220 in day 1 adults, ~160 at day 3 and ~130 at day 5 [202]. These experiments indicate that the progenitor zone may become depleted more rapidly in sperm-replete animals than in sperm-depleted animals (**Figure 7C**).

2.3.5.6 Progenitor Zone Cell Cycle

In young adult hermaphrodites, the mitotic cell cycle of germline stem cells in the progenitor zone takes 6.5-8 hours and consists of a very short or non-existent G1-phase, long S-

phase, long G2-phase, and a short mitotic division [291]. The germ cells do not undergo transit-amplifying divisions [293], and quiescent cells are not observed [205].

Methods to visualize cell cycle phase in living cells have not been reported to work in the *C. elegans* germline to date [295]. Cells in M-phase can be detected in fixed tissues by staining with mouse anti-phospho-histone H3 antibody. Cells in S-phase can be detected by feeding the nucleoside analog EdU, which is incorporated into DNA during S-phase and detected by click chemistry in fixed tissues. While the number of cells in each phase and the proportion of the progenitor zone in M-phase (M-phase index) or S-phase (S-phase index) can be calculated for individual animals, the measurement of the rate of the cell cycle requires pooling data from many individuals and several EdU-feeding duration experiments, then performing a regression [296].

Narbonne *et al.* (2015) and Qin and Hubbard (2015) reported that the M-phase index gradually decreases with age in unmated hermaphrodites, suggesting the germ cells arrest their cell cycle, likely in G2 phase [208,210]. Narbonne *et al.* (2015) found that mating hermaphrodites delays the decline of the M-phase index. Kocsisova *et al.* (2019) examined mated hermaphrodites and found no significant difference in either the M-phase or the S-phase index between day 1 and day 5 adults [202]. Rather, they report that the rate of progression through the cell cycle slows with age, requiring ~12 hours in day 3 and 5 adults.

2.3.5.7 DTC nucleus

The distal tip cell is a somatic cell that alone provides the stem cell niche for the germline. Hughes (2005) reported that the distal tip cell, detected with *plag-2*::GFP, occasionally shifts and/or disappears in day 6-12 unmated hermaphrodites [285]. Byrd *et al.* (2014) reported that the extent of the distal tip cell plexus, visualized by *plag-2*::myrGFP, remains unchanged by day 4 in unmated hermaphrodites [297]. Kocsisova *et al.* (2019) reported that the distal tip cell nucleus,

detected by antibody staining, occasionally mislocalizes away from the distal tip in day 5 mated hermaphrodites [202]. It is not known whether age-related changes in the distal tip cell affect the level of Notch signaling in germline stem cells.

2.3.5.8 Notch effector domain (stem cell number)

As germ cells move away from and lose contact with the distal tip cell, they lose Notch signaling, complete their ongoing mitotic cell cycle, and then begin meiotic S-phase [293]. The distal tip cell provides the ligand to activate the Notch signaling pathway which permits the stem cell fate and blocks differentiation and entry into meiosis. Two direct transcriptional targets of GLP-1 are the *sygl-1* and *lst-1* genes, which are redundantly necessary and individually sufficient to promote germline stem cell fate and block differentiation [298–300]. Thus, the extent of LST-1 and SYGL-1 accumulation provides a readout that is correlated with stem cell identity, though detectable LST-1 and SYGL-1 accumulation cannot currently be used to define the number of stem cells. In day 1 adults, LST-1 and SYGL-1 are expressed in ~38 and ~81 cells, respectively [300,202], but the number of cells expressing these proteins decreased two-fold by day 5 in mated hermaphrodites [202].

2.3.6 Body and Tissue Morphology

2.3.6.1 Body Size

C. elegans adults display an age-related increase in size [168,177]. Croll *et al.* (1977) noted a progressive increase from day 3 to day 14 in length (~70%), width (~30%), and volume (~280%) [168]. Bolanowski *et al.* (1981) noted an increase in volume from day 3 to day 9 (~170%) with little further change [177]. The age-related changes in size may be an example of programmed growth

rather than a degenerative change, although the period of body growth overlaps with periods characterized by functional declines.

2.3.6.2 Head and Pharynx

Chow *et al.* (2006) analyzed age-related changes in pharynx morphology by categorizing DIC images based on the extent of deterioration (least, somewhat, or most) [118]. This analysis revealed an age-related increase in pharynx deterioration [118]. Electron microscopy showed that the pharynx of older adults loses its smooth, rounded shape and has an irregular appearance [117].

Shamir *et al.* (2009) described a new method for quantifying age-associated deterioration of pharyngeal tissue [211]. They used an algorithm to measure morphological changes in the pharynx by quantifying image entropy to measure the animal's physiological age.

Zhao *et al.* (2017) categorized two separate death-associated pharyngeal bulb morphologies, termed "P" (enlarged) and "p" (atrophied) [212]. On average, animals that displayed enlarged pharynxes died earlier than animals that displayed atrophied pharynxes, suggesting a possible role for bacterial infection in pharyngeal pathology [212].

2.3.6.3 Bacterial accumulation

C. elegans is typically cultured with live *E. coli.* There appears to be an age-related increase in the amount of bacteria in the pharynx and the anterior and posterior intestine [113,118]. Interestingly, treatments that reduce bacterial proliferation, such as UV light treatment and antibiotics, extend lifespan, indicating that live *E. coli* are pathogenic in older animals [113].These interventions had a minimal effect on the decline of pharyngeal pumping, leading Chow *et al.* (2006) to conclude that bacterial accumulation is not a major contributor to this functional decline [113,118].

McGee *et al.* (2011) concurred with Garigan *et al.* (2002) that undigested bacteria accumulate in the intestine [113,213]. The authors used electron microscopy to section and visualize the localization of bacteria and found that bacteria localized to the grinder, suggesting that the cause is a decline in pharyngeal pumping. The authors observed that bacteria can move through the lumenal membrane or invade via the vulva, and that this is associated with age-related changes in intestinal tissue integrity and morphology.

2.3.6.4 Body wall muscle

The analysis of Herndon *et al.* (2002) demonstrated that *C. elegans* experience sarcopenia, an age-related decline in muscle structure and function [117]. One approach to visualizing muscle morphology is to express GFP in the nuclei of body wall muscle cells; there is an age-related change in nuclear GFP distribution characterized by a highly fragmented appearance [117]. The cell bodies of body wall muscles can be visualized by staining with phalloidin. Alternatively, GFP localized to the sarcomeres of the body wall muscles can be used to visualize muscle structure. These approaches reveal a progressive, age-related disorganization of sarcomeres with less dense packing and irregular orientation (**Figure 6R**) [117,187]. Electron microscopy revealed multiple changes in sarcomeres including fewer myosin thick filaments, bent or broken thick filaments, shrunken cells due to cytoplasmic loss, and accumulation of lipid droplets [117]. The disorganization of the body wall muscles was positively correlated with the decline in body movement [117] (**Table 3**).

2.3.6.5 Tissue appearance

Garigan *et al.* (2002) used DIC microscopy to analyze age-related changes in tissue appearance in the region of the head and pharynx [113]. These changes include (1) a progressive

lack of definition of nuclear boundaries; (2) progressive loss of the smooth and uniform appearance of the cytoplasm and nucleoplasm and the appearance of necrotic cavities and a curdled texture; (3) accumulation of shiny, mobile particles (likely to be yolk) and less mobile material [113]. Garigan *et al.* (2002) defined categories to describe the extent of deterioration (none, low, medium, high, and very high) [113]. A cross-sectional analysis showed that there is an age-related increase in the extent of deterioration.

2.3.6.6 Vulval integrity

Leiser *et al.* (2016) quantified a commonly observed phenotype, vulval extrusion, which they termed 'age-associated vulval integrity defects', or "Avid", first described in Leiser *et al.* (2011) [301,134]. This phenotype, sometimes described as "vulval rupture" or "vulval extrusion", occurs commonly under standard culture conditions, and animals that die from this problem are typically censored from aging experiments [60,81,302,303]. Leiser *et al.* (2016) argued that Avid is a useful measure of healthspan, as animals that display Avid live significantly shorter than non-Avid animals [134]. The frequency of Avid increased with age, and primarily occurs in "middle age", after completion of the reproductive period [134].

2.3.6.7 Intestinal Integrity

McGee *et al.* (2011) used electron microscopy and DAPI DNA staining to document age-related changes in intestinal morphology: degradation of the intestinal lumen, shrinking of the cytoplasm, loss of microvilli, loss of nuclei, and bacterial invasion (**Figure 6J,K,N**) [213]. This senescent phenotype is defined as intestinal atrophy and correlates positively with the formation yolky lipoprotein pools in the body cavity [111] (**Figure 6M, Table 3**). The authors suggested that bacterial invasion was caused by the breakdown of intestinal lumen.

Dambroise *et al.* (2016) reported an age-related onset of the permeability of blue fluorescein dye through the intestine [268]. This "Smurf" phenotype was interpreted as a sudden increase in the overall permeability of the intestine that had a positive correlation with survival probability; that is, the presence of the Smurf phenotype was associated with earlier death. Measurements were conducted in a longitudinal fashion on a population of animals throughout their lifespan via the use of non-destructive dye. The correlation of the onset of Smurf phenotype and overall survival was also present in wild isolates which had higher or lower lifespan than wild-type.

2.3.6.8 Hypodermis

Golden *et al.* (2007) used DAPI staining and fluorescence microscopy to reveal age-related loss of nuclei in H9 and H10 hypodermal cells of the tail [197]. At day 4, most animals displayed 2-3 visible nuclei; at day 14, some animals displayed 1-3 nuclei, while most displayed zero; and by day 19, no animals displayed visible nuclei. Measurements of genomic DNA copy number by qPCR in individual hermaphrodites showed a progressive increase from day 4 to day 21. Males and FUdR-treated hermaphrodites displayed no change in genomic DNA copy number, suggesting the copy number increase derives from the germline [197].

2.3.6.9 Midsection, Body cavity

Golden *et al.* (2007) reported that DAPI-stained material accumulates along the midsection of wild-type animals; first observed at day 14, this material eventually fills the body cavity [197]. BrdU was incorporated into the same region at day 11 compared to day 9, indicating these masses likely require active DNA synthesis, but co-staining with DAPI was not possible [197].

In young adult hermaphrodites, yolk protein is primarily in the intestine, where it is synthesized, and in late-stage oocytes and embryos, where it is accumulated. Older hermaphrodites accumulate shiny, mobile patches of yolk protein in the body cavity that appear to form yolky lipoprotein pools [113,117,111]. For more details see the *Biochemical* section.

2.3.7 Cellular Morphology

2.3.7.1 Mitochondrial Morphology

Using electron microscopy, Yasuda *et al.* (2006) observed that mitochondria in body wall muscles displayed an age-related 'swollen' morphology that was first observed in day 10 adults and was more pronounced in day 15 adults [214]. 'Swollen" mitochondria correlated with decreases in oxygen consumption and the activities of complex I and II of the mitochondrial electron transport chain. Using qRT-PCR, Gruber *et al.* (2011) observed a decline in mtDNA copy number from day 3 to day 14 [215]. mtDNA copy number correlated with decrepitude in day 12 animals; class A (youthful) animals had higher copy number compared to class B and C (decrepit) animals. Thus, high mitochondrial number was correlated with delayed physiological decline (**Table 3**).

Regmi *et al.* (2014) measured mitochondrial morphology using mitochondrial membrane-targeted GFP [216]. Mitochondrial morphology displayed age-related changes from day 1 to 16; fragmentation and circularity increased, whereas length decreased. Mitochondrial networks in body wall muscle cells become increasingly fragmented from day 1 to 16 (**Figure 6Q**).

2.3.7.2 Nucleus

The nucleus harbors the cell's genetic information and is spatially organized to promote multiple functions including securing DNA integrity, DNA damage repair, DNA replication,

transcription, splicing, ribosome assembly, and controlled import and export. Age-related changes in the spatial organization of the nucleus could have far-reaching effects due to the central importance of nuclear functions. The first evidence of age-related nuclear changes in *C. elegans* was reported in [117]. Muscle nuclei displayed age-related loss of integrity and shape. And nucleoli increased in size in relation to the nucleus in day 7 animals (**Figure 6O**). These nuclear changes correlated with a decline in locomotion - mobility class C animals displayed a more drastic change in nuclear shape. These findings are supported by Haithcock *et al.* (2005), who used a LMN-1::GFP reporter to analyze the nuclear envelope [217]. The typical circular nuclear envelope was lost in day 8 animals. Continuing up to day 18, the nuclear envelope dramatically lost its integrity, and nuclei displayed abnormal shapes, fragmentation, and extensive stretching (**Figure 6P**) [217]. Animals with severely impaired mobility (class III) displayed more severe changes in nuclear envelope morphology compared to animals with more youthful locomotion, establishing a correlation between cellular morphology and movement physiology (**Table 3**).

Another age-related change is a loss of visible nuclei in the tail and intestine of adults observed by DAPI staining and fluorescence microscopy. Young animals exhibit 2-3 tail nuclei - the number is reduced on day 14, and none are visible on day 19 [197]. Young animals display 30 uniform-appearing intestinal nuclei. After day 8 the number of intestinal nuclei decreases. Some 20-day-old animals have fewer than 10 intestinal nuclei, and nuclei that are visible appear to be smaller. Notably, the severity of these age-related changes varies between animals, and the heterogeneity of animals increases with age [213].

Tiku *et al.* (2017) measured the size of hypodermal nucleoli of day 1 adult animals, recovered the animals, and monitored lifespan [269]. Smaller nucleoli in day 1 adults were a

predictor of longer lifespans [269]. Thus, the size of nucleoli measured by microscopy is negatively correlated with the physiology of lifespan (**Table 3**).

2.3.7.3 Processing bodies

Processing bodies and stress granules are RNA-protein complexes involved in post-transcriptional gene regulation. Using GFP reporters (*dcap-1::GFP*) and fluorescence microscopy, Rousakis *et al.* (2014) observed an age-related accumulation of processing bodies from days 1 to 5 and an increase in processing body size [218].

2.3.7.4 Ectopic fat depositions and lipid droplets

C. elegans contain lipid droplets in the intestine which constitute the main fat storage in the animal. Tserevelakis *et al.* (2014) reported that the fat content reaches a maximum in young adults [219], whereas Herndon *et al.* (2002) and McGee *et al.* (2011) described cytoplasmic lipid accumulations in the intestinal cells in post reproductive animals (**Figure 6M**) [117,213]. Herndon *et al.* (2002) used electron microscopy to document age-related accumulation of fat inside and outside the intestine in both muscle and the hypodermis [117]. Tserevelakis *et al.* (2014) developed a non-invasive and dye-free tool for analysis of lipids in biological samples based on higher harmonic generation imaging techniques; this technical innovation facilitated a more detailed and quantitative study [219]. Lipid accumulation was visualized and quantified in L1 and L4 larval stages, and day 1, 5, 10, and 15 adults. Lipid droplets in the intestine increased during development and decreased during aging [219]. By contrast, lipid droplets display age-related accumulation up to threefold in the pharyngeal muscles, body wall muscles, and neurons [220,221]. Since the intestine is the canonical fat storage tissue, age-related increase of lipids outside of the intestine is defined as ectopic fat.

2.3.7.5 Autophagosomes

Autophagy is a major recycling pathway associated with longevity. Double-membrane vesicles are formed in the cytoplasm and transport macromolecules to the lysosome, where these autophagosomes fuse to autolysosomes, and hydrolases degrade the contents. A GFP::LGG-1 reporter was used to quantify fluorescent foci on days 1, 3, 5, 7, and 10 in the intestine, body-wall muscles, pharynx, and nerve-ring neurons. The number of GFP::LGG-1 foci displayed an age-related increase in all tissues, up to 9-fold in muscle cells, which can be interpreted as an increase in autophagosomes (**Figure 6L,S**) [222]. Chang *et al.* (2017) developed an additional reporter, mCherry::GFP::LGG-1, to distinguish between autophagosomes (red and green foci) and autolysosomes (red foci) in day 1, 3, 5, 7, and 10 animals [222]. Red and green foci displayed an age-related increase in the intestine, muscle, and pharynx throughout the time course, whereas red foci displayed an age-related increase until day 5 and then decreased in day 7 and day 10 animals. In contrast to results from the GFP::LGG-1 reporter strain, green and red foci in neurons decrease from day 1 to day 3 and then increase at day 7 to reach a plateau; the number of green foci displayed an age-related decrease in neurons [222].

2.3.8 Biochemical – gene and chromatin

2.3.8.1 Genome copy number

Golden *et al.* (2007) reported that masses of DNA accumulate in the midbody and germline of day 14 and 19 animals compared to day 4 [197]. BrdU incorporation indicates the regions are transcriptionally active in day 11 animals compared to day 9. Nuclear genome copy number was analyzed by qPCR from day 4 until 21. Young adults displayed a nuclear genome copy number of ~4000-5000, whereas older adults (> day 10) displayed variable nuclear genome copy number from close to zero to more than 25,000 [197]. By contrast to this age-related increase

in nuclear genome copy number, Gruber *et al.* (2011) reported an age-related decline in mitochondrial DNA copy number, which negatively correlated with body movement [215]: adults classified in mobility class A displayed a higher mtDNA copy number compared to adults in mobility-impaired classes B and C [215] (**Table 3**). However, Brys *et al.* (2010) did not detect an age-related change in mtDNA copy number, suggesting further analysis is warranted [254].

2.3.8.2 DNA integrity

Klass *et al.* (1983) demonstrated multiple age-related changes in DNA. DNA extracted from pools of adults displays an age-related increase in the number of single-stand breaks [172]. Furthermore, there is an age-related decline in the ability of DNA to function as a template for transcription *in vitro* [172]. Whereas Klass *et al.* (1983) described an age-related increase in the levels of 5-methylcytosine [172], Simpson *et al.* (1986) conducted a sensitive analysis and failed to detect 5-methylcytosine in *C. elegans* during either development or senescence [304]. Melov *et al.* (1995) used a PCR strategy to assess deletions in the mitochondrial genome [305]. The frequency of deleted mitochondrial DNA increases with chronological age in four different populations of *C. elegans*.

2.3.8.3 Chromatin

Histone modifications alter chromatin structure and affect gene expression. Chromatin immunoprecipitation combined with deep sequencing (ChIP-seq) can be used to analyze histone modifications genome-wide, and these data can be corelated with gene expression analyzed by RNA-seq.

H3K36m3 is mainly found in transcriptional regions of genes (exons and introns without start and stop sites as well as regulatory regions) and is associated with active transcription. The

pattern of H3K36m3 in the genome is described as stable with age in experiments comparing L3 larvae and day 2, 4, and 12 adults. However, the data are complex: in old animals, 624 genes display new H3K36 trimethylation and 1,930 genes display a loss of trimethylation. Notably, these genes exhibit extremely low H3K36m3 or high levels of H3K36m3 in young animals, and the observed changes are considered small [223].

The H3K4m3 level also appeared to not change dramatically comparing L3 larvae and day 2 and 12 adults. H3K4m3 is associated with active transcription and displays a general enrichment at the transcriptional start site and the 5' promotor region where it does not change with age. In contrast, uncommon H3K4m3 in the gene body appeared to change with age and positively correlated with age-related gene expression changes [224] (**Table 3**).

2.3.8.4 mRNA splicing

Splicing is a fundamental step in gene expression. Using an *in vivo* fluorescent alternative splicing reporter, Heintz *et al.* (2017) reported that day 5 adults displayed altered and more heterogeneous fluorescent patterns compared to day 1, which is due to increased splicing defects such as exon skipping [231]. Nearly all animals skipped exons after day 7, and the "youthful" fluorescent pattern disappeared. Furthermore, animals with the "youthful" fluorescent pattern on day 6 of adulthood display a 23% longer lifespan than animals with the pattern indicating splicing defects. Therefore, splicing efficiency on day 6 is a predictor of lifespan [231] (**Table 3**).

2.3.8.5 RNA Expression

A variety of approaches have been used to analyze age-related changes of RNA levels. Fabian and Johnson (1995) analyzed the abundance of total RNA, rRNA, and poly(A)+ RNA; no

consistent age-related changes were detected [306]. In a related study, these authors identified twelve specific transcripts that display a change in abundance over the adult life span [225]. Cherkasova *et al.* (2000) concentrated on genes that display high expression in dauer larvae [307]. They used a subtracted cDNA library that was enriched for dauer-specific poly(A)+ RNA to analyze age-related changes in their expression levels. Five genes with higher transcript levels in dauer larvae, including *hsp-1* and *daf-21,* also displayed an age-related increase in transcript levels. Microarray technology made it possible to analyze genome-wide profiles of transcript levels [308,226,309]. Lund *et al.* (2002) identified 164 genes that displayed statistically significant age-related changes in transcript levels [226]. Age-related gene expression changes detected by microarrays are described in detail in [230].

Small and noncoding RNAs, including micro RNAs (miRNA), regulate gene expression and are candidates to influence aging. Ibáñez-Ventoso *et al.* (2006) analyzed the miRNA expression levels of day 6, 8, 11, 13, and 15 animals [232]. 50 out of 114 miRNAs displayed age-related changes in expression. A longitudinal study featuring single animal vermiculture, daily imaging, and semi-automated data analysis was performed with animals containing *mir-71*, *mir-239*, and *mir-246* promotor::GFP constructs. While GFP levels increased with age in all three strains, lifespan was positively correlated with expression levels of *mir-71* and *mir-239* promoters and inversely correlated with expression levels of the *mir-246* promoter [233]. Deep-sequencing approaches revealed that other small and noncoding RNAs also undergo age-related expression changes [227].

Circular RNAs (circRNAs) are a recently identified RNA species. Cortés-López *et al.* (2018) reported that levels of 1,052 circRNA increase at least 1.5-fold in day 10 adults compared to L4 larvae [234]. Several were classified as age-specific, since 28 and 51 circRNAs were detected

only in day 7 and day 10 animals, respectively. Analysis of linear RNA levels did not copy the results of the age-related changes in circRNA levels [234].

The ongoing development of better "omics" techniques, such as deep sequencing, combined with improved data analysis and modeling approaches, is likely to provide detailed descriptions of age-related changes of RNA expression levels and correlations with metabolites and proteins [228,229,310].

2.3.9 Biochemical – protein

2.3.9.1 Posttranslational modifications

Oxygen free radicals and other reactive oxygen species (ROS) can damage macromolecules, and oxidative damage has been proposed to cause age-related pathologies [109]. One specific measure of this damage is the level of protein carbonylation. Adachi *et al.* (1998) measured protein carbonylation per milligram of protein in extracts of pooled animals [235]. In wild-type animals the level of protein carbonylation increased ~3-fold from day 4-8 to day 20. In a more detailed analysis, Yasuda *et al.* (2006) compared mitochondrial and cytoplasmic fractions of day 4, 8, 12, and 15 adults [214]. Both fractions displayed an age-related increase of carbonylated proteins. In mitochondria, carbonylated proteins increased 4-fold, which might be related to production of ROS in this organelle [214].

The spatial pattern of carbonylated proteins can be determined in animals using freeze-crack, methanol/acetone fixation, and immunostaining after treatment with dinitrophenylhydrazine (DNHP). Goudeau and Aguilaniu (2010) reported that the germline contains more carbonylated proteins than somatic tissue [236]. The most proximal oocytes that are close to fertilization displayed less antibody staining then the rest of the gonad, which could be

due to a clearing mechanism. Day 2 and 5 adults displayed an age-related increase in oxidized proteins in both the germline and somatic tissue [236].

2.3.9.2 Proteome

Quantitative proteomic approaches can be used to establish a detailed description of the aging proteome in *C. elegans*. Two methods based on the SILAC (stable isotope labeling by/with amino acids in cell culture) approach have been used to identify age-related changes in the proteome:

(1) To label the proteome, worms were fed *E. coli* cells labelled with heavy lysine isotopes [237]. Twenty-two different *C. elegans* lysates from day 1 to 22 were analyzed, and more than 5,000 different proteins were identified. About 30% of the analyzed proteins displayed age-related abundance changes of at least 2-fold.

(2) *E. coli* cells were labelled with arginine and lysine containing light, medium, or heavy isotopes and fed to *C. elegans*. In addition, RNAi feeding was used to reduce *orn-1* transcript levels to prevent the enzymatic conversion of arginine to proline [238]. Day 1, 5, and 10 adults were analyzed, and about 10,000 proteins were identified. 627 proteins displayed a significant age-related change in abundance.

In combination, these two studies provide extensive data sets that can be mined to understand age-related changes in the proteome. Further analysis to uncover GO groups and protein networks that impact aging might be fruitful avenues for future studies.

2.3.9.3 Protein stability

Quantitative analysis of insoluble proteins via mass spectrometry of day 3 versus day 10 adults revealed a significant age-related increase of aggregated proteins [240]. These data were

confirmed by an independent study that analyzed proteome-wide changes in protein insolubility of day 1 versus day 11 adults via mass spectrometry [311]. In a more detailed analysis, aggregated proteins in day 1, 6, 12, and 17 adults were analyzed in relation to their abundance in the proteome: the most abundant proteins constituted the majority of the insoluble protein fraction [237]. In combination, these quantitative studies of the insoluble proteome provide extensive data for future studies.

In agreement with these quantitative analyses of aggregated proteome, Ben-Zvi *et al.* (2009) reported aggregated paramyosin in muscles of day 12 adults of a temperature-sensitive fluorescent reporter strain [239]. These data indicate that the stability of the proteome is reduced with age in *C. elegans*.

2.3.9.4 Enzymatic activity

The activity of specific enzymes has been shown to display age-related changes. Protein tyrosine kinase activity in *C. elegans* extracts decreases about 60% from day 5 to day 15 of adulthood [244]. The activity of several acid hydrolases that are likely to be localized to lysosomes were examined in aging hermaphrodites by [121]. β-N-acetyl-D-glucosaminidase, β-glucosidase, α-mannosidase, and acid hydrolase displayed age-related increases in activity. These changes are somewhat specific, since several other lysosomal enzymes did not display age-related changes in activity [121].

Phosphoenolpryruvate carboxykinase activity increases from L4 to adulthood, peaks on day 6, and decreases in older adults [245]. Similarly, the abundance of this enzyme increased from L4 to adulthood, peaked on day 3, and decreased in older adults. Another metabolic enzyme, pyruvate kinase, exhibited a continuous increase in activity with age. Furthermore,

phosphoenolpryruvate carboxykinase abundance was positively correlated with motor activity during days 3-12 of adulthood (**Table 3**). The motor activity was measured as locomotory speed [245].

2.3.9.5 Clustered change in protein levels

In young adult hermaphrodites, yolk protein is localized primarily in the intestine, where it is synthesized, and in late-stage oocytes and embryos, where it accumulates. Older hermaphrodites accumulate shiny, mobile patches of yolk protein in the body cavity [113]. Immunoelectron microscopy showed that yolk protein YP170 (vitellogenin) was distributed in electron dense lipid-like droplets and large accumulations throughout the body cavity of older hermaphrodites [117]. Similar observations have been made by visualizing GFP-tagged yolk protein [111]. These studies suggest that the intestine continues to synthesize and secrete yolk protein after the time when oocyte production declines, resulting in accumulation of yolk protein in the body cavity, a hypothesis supported by [111]. Herndon *et al.* (2002) speculated that yolk protein expression is left on in older hermaphrodites because there is little (if any) selective pressure to modify patterns of gene expression in post-reproductive animals [117], a hypothesis further elaborated on in [25,26]. Vitellogenin accumulates especially in self-fertile animals after sperm depletion, whereas mating reduces the accumulation of vitellogenin [285].

In a systematic study, Ezcurra *et al.* (2018) analyzed lipid pools in the body cavity [111]. VIT-2 (YP170) and VIT-6 (YP115 and YP88) localized in these pools. Therefore, they were defined as yolky lipoprotein pools. YP170, YP115, and YP88 levels increased from day 1 to 5 of adulthood; in day 5 adults YP170, YP115, and YP88 represented 30-40% of all proteins. Furthermore, intestinal atrophy was positively correlated with yolky lipoprotein pools in the

body cavity, which supports the hypothesis that intestinal biomass is converted into yolk in older adults via intestinal autophagy [111].

2.3.10 Biochemical – metabolism

2.3.10.1 Autofluorescence

The age-related increase in autofluorescence in postmitotic cells is a premier biomarker of aging, because it is easy to observe, robust, and occurs across phyla. Lipofuscin, also called age-pigment, is a frequently studied fluorescent compound [312]. Oxidized proteins and lipids accumulate with age, forming aggregates that are visible as brown spots and emit yellow-orange fluorescence with wavelengths of 570 to 605 nm when excited with UV light [313].

Epstein *et al.* (1972) provided the initial report of granules in the intestine that resemble lipofuscin in a *Caenorhabditis* species; cross-sections of *C. briggsae* were analyzed by electron microscopy [167]. Michael Klass then discovered an age-related increase of autofluorescence in *C. elegans* extracts measured with a fluorometer [48]. Since then, autofluorescence has been an established and widely used marker of aging in *C. elegans*. The recent development of semi-automated microscopic devices that allow longitudinal experiments with higher throughput show that blue fluorescence (excitation: 350/50 nm, emission 460/50 nm) increases specifically 6-12 hours before an animal dies [248,249], whereas red fluorescence (excitation: 545/30 nm, emission: 610/70 nm) increases throughout life and predicts future lifespan [249].

There are two main methods to measure autofluorescence and define age-related changes: (1) using a fluorometer to measure bulk autofluorescence of *C. elegans* extracts [48,246,247,251,252], or (2) using a fluorescence microscope to measure spatially resolved autofluorescence in intact animals [247,113,114,233,248,249].

(1) Using *C. elegans* extract is a simple way to measure pooled animals and to get an average change of autofluorescence. The pooled animal extracts need to be normalized using dry weight and volume or protein concentration [48,247]. The disadvantage is that, aside from fractionated samples, it is impossible to get spatial information and to do longitudinal studies.

(2) Fluorescence microscopy makes it possible to monitor changes in autofluorescence of single individuals over time with spatial resolution. The disadvantage of this technique is that it is limited to a small number of animals, but the recent development of a semi-automated culture system allows longitudinal studies with higher throughput [233].

Autofluorescence is positively correlated with an age-related decline in body movement and lifespan (**Table 3**). Gerstbrein *et al.* (2005) measured autofluorescence in day 11 animals that were divided into three body movement classes [114]. The severely impaired group showed a significantly higher level of autofluorescence than the youthful and partially impaired group. Moreover, longer lived animals exhibit lower levels of autofluorescence, and especially red autofluorescence can be used to predict lifespan as early as 7 days post hatching [233,249].

2.3.10.2 Metabolic activity

Several measurements of metabolic activity have been demonstrated to display age-related changes (see **Table 1**). Carbon dioxide generation by populations of *C. elegans* grown on dishes can be measured by gas respirometry. Carbon dioxide generation declines about 50% from day 6 to 12 [250]. Oxygen consumption by populations of *C. elegans* in liquid culture were monitored polarographically using Clark type electrodes. Oxygen consumption of wild-type animals declines about 60% from adult day 0 to 12 [251,252,254]. Heat produced by populations of live *C. elegans* can be monitored by microcalorimetry, and it is a measure of the rate of catabolic processes. Heat production of wild-type *C. elegans* declines about 80% from adult day 0 to 12.

ATP levels, a measure of instantly available energy, can be monitored in animal extracts using enzyme reactions that require ATP. ATP levels decline about 80% from adult day 0 to 12 [254]. ADP levels decline about 70% [254]. The amount of superoxide anion, an estimate of the potential for metabolic activity, can be measured in animal extracts using lucigenin-mediated luminescence; this declines about 95% from adult day 0 to 12.

2.3.10.3 Metabolites

Prior to the development of high throughput metabolomics approaches, only a few age-related changes in metabolite levels were reported, such as a decrease of cardiolipin accompanied by an increase of phosphatidylcholines in mitochondria [215], or the change in lactate/pyruvate ratio [260]. However, the increasing power of mass spectrometry and NMR spectroscopy combined with advanced data processing accelerated the field of metabolomics and the comprehensive analysis of changes of metabolic pathways [314,315]. Now several groups have reported comparisons of metabolites in young versus old animals using a variety of *C. elegans* culture methods, animal lysate procedures, and analysis techniques. Pontoizeau *et al.* (2014) cultured wild-type animals on NGM dishes in the presence of FUdR and used NMR spectroscopy analysis of intact young adults before egg production versus day 7 adults to create a footprint of 22 metabolites [255]. Copes *et al.* (2015) cultured *glp-4* mutant animals in liquid medium at 25°C and compared day 4 versus day 10 adults using GC-MS [256]. They analyzed 186 metabolites and 1,937 proteins to focus on affected pathways. Davies *et al.* (2015) cultured wild-type animals on NGM dishes with FUdR and used NMR to compare 33 metabolites in animals 2.5, 6, 8, 10, 13, 16, and 20 days after hatching to define a metabolic age [257]. Gao *et al.* (2017) cultured wild type and *glp-4* mutant animals on NGM dishes with fluorouracil (5-FU) and analyzed 44 fatty acids, 18 amino acids, and over 600 phospholipids using MS, UPLC-MS/MS,

and HPLC-MS in wild-type eggs, L1, L2, L3, L4, and day 1-10 adults [258]. In addition, they analyzed a fraction of these metabolites in *glp-4* L3, day 1, 3, 5, 7, and 9 animals to document metabolic changes. Wan *et al.* (2017) were interested in metabolic changes related to reproduction; they cultivated wild type and *glp-1* mutant animals on NGM dishes with FUdR and used UPLC-MS and NMR to compare 45 metabolites in young adults before egg-laying versus day 10 adults after egg-laying [259].

The limitations of all these approaches are: 1) small numbers of biological replicates due to the difficulty and expense of these procedures, and 2) the choice of different sets of metabolites made by each investigator, making comparisons of different studies challenging. The strengths of these approaches are the large and useful databases of age-related metabolic changes that enable future aging network analysis.

2.3.10.4 Metal homeostasis

Organisms tightly control metal concentrations in cells, tissues and organs. Networks of transporters, metal binding factors, and stress response proteins protect against overload and deficiency. Klang *et al.* (2014) compared metal concentrations of day 1, 5, 9, and 11 adults; calcium, iron, copper, and manganese increase with age, potassium and phosphorus decrease with age, and magnesium, sodium, sulfur, strontium, and zinc don't display age-related changes [261].

2.3.11 Male Behavior, Reproduction, and Morphology

While behavioral, reproductive, and morphological changes in *C. elegans* hermaphrodites have been extensively analyzed, only a few studies have examined age-related changes in males. Male mating requires robust motility, the ability to interact with a hermaphrodite and insert the

male tail, and sperm viability. Thus, mating success depends on the integrated function of neurons, muscles, and the gonad.

Klass *et al.* (1983) analyzed sperm depletion and viability in the presence and absence of "females" using DH26 mutant hermaphrodites that do not produce sperm and thus are functionally self-sterile. Males cultured in the absence of females had significantly more sperm at adult days 10 and 15 compared to males cultured in the presence of self-fertile hermaphrodites, suggesting males accumulate sperm in the absence of mating [172]. Males were allowed to mate, and after 24 hours the number of fertilized eggs and the proportion that hatched were quantified. Day 10 and 15 males produced fewer viable progeny than day 5 males when mated to young (day 3) females [172]. This occurs in males cultured with and without females, although the rate of decline is faster in males cultured with females. The authors propose that the age-related decrease in male fertility is not the result of an accumulation of old sperm, but rather results from changes in precursor cells, as males cultured with females are continually voiding and differentiating new sperm. Chatterjee *et al.* (2013) evaluated age-related changes in male fertility by mating males to wild-type hermaphrodites; the proportion of cross-progeny versus self-progeny decreased as males aged [262].

The male tail is crucial for mating and is comprised of cuticular fans, sensory spicules, and the hook. Chatterjee *et al.* (2013) examined the morphology of male tails on adult days 1, 3, and 5, and categorized tails as normal, semi-normal, or abnormal based on visual appearance [262]. Male tail morphology displayed a trend of deterioration by day 5 based on changes to the cuticle and rays; however, this change was not statistically significant. Thus, the rapid decline in brood size was not explained by degradation of the tail structure visualized microscopically at this level of detail.

Chatterjee *et al.* (2013) examined behaviors required for male reproductive success from adult day 1 to 5 [262]. In day 5 males, the efficiency of locating the vulva, the percentage of responding males, and the percentage of males that maintained contact with the vulva significantly decreased; response time increased slightly, and difficulty in turning increased dramatically. Aging in *C. elegans* is associated with a decrease in body movement, and males move vigorously over various ages even when infertile. Because the ability of males to produce cross progeny decreased significantly by day 7, while no appreciable decrease in movement ability was observed, the authors concluded that body movement capability plays a minor part in male reproductive aging [262].

2.4 Conclusions

2.4.1 What have we learned of value?

Our main goals are to: (1) describe age-related changes that have been reported in the literature; (2) discuss techniques to measure, analyze, and interpret these age-related changes; and (3) raise awareness of important factors in designing studies to measure aging. We hope this article will be a useful guide to designing experiments that measure aging and encourage best practices for data analysis for the community of scientists that study nematode aging.

One value of documenting age-related changes is their utility in characterizing interventions that influence aging. Genetic or pharmacological interventions that extend lifespan often delay the onset and progression of age-related degenerative changes, and monitoring a variety of age-related changes enriches the understanding of the intervention.

When designing an experiment to measure an age-related change, one should consider both the amount of useful data that will be generated and the time and resources necessary to conduct the experiment – is the juice worth the squeeze? Ideally, the experiment yields lots of

high-quality data with minimal effort. Some measurements (pharyngeal pumping, body movement, etc.) are simple and rapid, requiring relatively small investments of time and resources; other measurements (DNA damage, nuclear morphology, meiotic cell-cycle progression) are complex and time consuming, requiring advanced expertise and specialized reagents and equipment. It is important to consider the balance between the simplicity of the measurement and the usefulness of the resulting data.

In some cases, tradeoffs exist between effort expended and the ability to interpret the data. For example, there are multiple approaches to address the complexity of self-progeny when measuring lifespan, which is often considered the gold standard measurement of aging research. An approach that is more laborious but also easier to interpret is to observe a population of hermaphrodites cultured on standard NGM-agar dishes seeded with *E. coli* OP50; the population is observed daily, and deaths are noted. Each animal is manually transferred to a fresh dish daily throughout the reproductive period, which prevents the test animal from being confused with progeny. Approaches that are less laborious but more difficult to interpret include adding drugs such as FUdR to arrest adult reproduction, or using mutants that have temperature-dependent sterility [316]. However, these approaches introduce confounding factors that may independently influence aging – a drug or a mutation – which makes the results more difficult to interpret.

In this review, we discussed the differences between cross sectional and longitudinal study designs. In summary, longitudinal studies measure the same animal at different time points, whereas cross-sectional studies measure distinct animals or populations at different time points. In principle, longitudinal measurements are more informative for identifying effects of aging, since all animals are part of the same cohort; in addition, they offer unique opportunities for data analysis. Cross sectional studies have the caveat that differences between young and old cohorts

might reflect differences in cohort experience in addition to differences in chronological age. For example, if we compare 85-year-old to 35-year-old Europeans in 2023, during childhood only the older cohort experienced the deprivation of World War II, whereas only the younger cohort experienced the Internet. However, some measurements require destructive interventions, which precludes subsequent measurements and are incompatible with a longitudinal study design. For example, measuring DNA damage requires lysing worms and extracting DNA, so it is not possible to also measure lifespan. If you are measuring a non-invasive phenotype, we recommend considering a longitudinal study design so that you can establish correlations with other aging end points such as lifespan.

Another important factor in experimental design is the time of the measurement. Measurements early in life are useful for phenotypes that decline more rapidly compared to the animal's overall lifespan. For example, egg production peaks early in the hermaphrodite lifespan and declines rapidly while the animal is still alive and moving vigorously [48,168]. The best approach to understanding this age-related decline is to focus on changes in young adults. By contrast, measurements later in life are beneficial for slowly progressive age-related degeneration, because the magnitude of the change steadily increases, becoming easier to measure. For example, body movement displays a relatively steady decline throughout an animal's lifespan [121]; thus, the magnitude of the change progressively increases until the end of life. In this case, maximizing the time between the first and final measurements captures the largest change in this phenotype. Choices about times to begin and end measurements vary depending on the laboratory and techniques; therefore, it is important to take this into account when considering comparisons of results published by different groups.

Some studies need to confront the issue that age-dependent changes may result from developmental programs or age-related degenerative changes. This raises intriguing questions: Does development end, and if so, when? Does aging begin, and if so, when? Do development and aging occur sequentially or simultaneously? Commonly used breakpoints between development and aging are at the onset of adulthood (following the final larval molt) or the onset of reproduction (time of first egg lay, etc.). Because no single timepoint objectively delineates development and aging, the choice of a time to define as the start of adulthood ("time 0" of a measurement) is ultimately arbitrary. Changes observed in very young animals are more likely to be the result of development, whereas changes later in life are more likely to be the result of aging. For example, young hermaphrodites display an age-related decline in sperm production when the gonad switches to making eggs. This is typically considered a developmental transition, but because it is the loss of the capacity to make sperm, it satisfies many definitions of aging.

Our primary focus is the documentation of progressive and degenerative age-related changes. An important consideration is that these types of observational studies do not formally establish cause; specifically, documenting an age-related degenerative change does not prove that it is a cause of a physiological endpoint, such as death. For example, documenting progressive, age-related disorganization of pharynx morphology using microscopy does not prove that this change is the cause of the progressive, age-related decline of pharynx pumping rate. Rather, it establishes that the two changes are correlated in time. Alternative models that are also consistent with this type of temporal correlation include (1) the age-related decline of pharynx pumping rate is the cause of the age-related disorganization of pharynx morphology, (2) there is a shared cause that drives both age-related changes, (3) the age-related changes are unrelated, and it is merely a

coincidence that they occur in the same time frame. It is tempting to tell "just so" stories – it appeals to our intuition to propose that the morphology change is the cause of the functional change. While this may be a useful working hypothesis, it is important to understand that further experiments are necessary to distinguish correlation and cause, and in the absence of further experiments it is wise to consider alternative models. Furthermore, age-related changes may have complex interactions, since different parts of an animal body are deeply interdependent. For example, the age-related decline of pharyngeal pumping rate reduces nutrient intake, which is likely to affect physiology, and reduces bacterial grinding efficiency, which allows live bacteria to enter the intestine [113,118,211]. Live bacteria in the intestine can lead to infections, intestinal degeneration, and death, illustrating the potential for cascades of failure as the decline of one organ increases the stress on other organs [113,118,213].

2.4.2 What are the relationships between age-related changes

One major accomplishment of studies in *C. elegans* is the definition of relationships between age-related changes. Age-related changes in tissue morphology and function have been documented in many animals, but few studies have rigorously addressed relationships between these changes. The experimental advantages of the *C. elegans* system that facilitate longitudinal studies have made it possible to address this important question (**Figure 2**).

Table 3 summarizes experimentally defined relationships. There is a strong positive correlation between the declines of pharyngeal pumping, body movement, and survival probability. The decline of body movement is positively correlated with increased appearance of disorganized body wall muscles and increased accumulation of fluorescent compounds in the body. On a cellular level, the decline of body movement is positively correlated with declines in synaptic and neurite morphology, increased changes in mitochondrial and nuclear morphology,

and metabolic defects; the decline of body movement is negatively correlated with increased mitochondrial copy number. Age-related reduction in pharyngeal pumping rate is positively correlated with increased degradation of pharynx morphology and mitochondrial morphology. Survival probability is the gold standard phenotype of aging; a rapid decline in survival probability correlates with rapid declines in mated reproductive potential, degradation in pharyngeal morphology, decline in mitochondrial morphology, declines in maximum velocity and splicing efficiency, and increased accumulation of autofluorescence. A rapid decline in survival probability is negatively associated with increased nucleolar size. Declines in the organization of body and tissue morphology are a classic symptom of aging in many organisms. In nematodes, declining tissue morphology has been reported for pharynx, uterus, intestine, pseudocoelom, and neurons, whereas declining cellular morphology is associated with changes in mitochondria.

One interpretation of positive correlations between age-related changes is that these changes are causally connected in series. For example, the age-related increase in disorganization of body wall muscles may cause the age-related decline in body movement. The age-related increase in frequency of endomitotic oocytes in the gonad may cause the age-related increase in sterility. A second interpretation is that a shared mechanism influences the timing of two correlated processes. For example, the age-related decline in body movement and pharyngeal pumping may both be caused by an age-related decline of a hormone that stimulates the activity of both systems. Overall, these results indicate that age-related changes in tissue morphology and function are controlled by shared mechanisms and/or causally linked in series (**Figure 5**).

The age-related decline of self-fertile reproduction and the age-related decline of defecation cycle displayed no correlations with other age-related changes. One explanation for

these results is that these age-related changes report on developmental transitions rather than age-related degeneration. For example, the decline in self-fertile reproduction results, at least in part, from depletion of the finite supply of sperm produced during larval development. Thus, animals that make more sperm during development will display a delayed decline, whereas animals that make less sperm will display an earlier decline. A similar pattern might be observed for other factors that are produced in a limited supply during development and gradually exhausted during adulthood. Because the lack of a correlation is a type of negative result, other possible explanations include a lack of sensitivity to detect a small positive correlation, or that the longitudinal studies were performed in the wrong timeframe to detect the positive correlation.

Peter Medawar observed, "It is a curious thing that there is no word in the English language that stands for…ageing silenced of its overtones of increasing deterioration and decay" [25]. Because organisms exist that do not appear to degenerate as they increase in chronological age, such as *Planaria*, the absence of this word is not merely a semantic issue – it likely guides the way that we think in a manner that is not conducive to understanding biology. The analysis of age-related degeneration has led the field to the concept of healthspan. Healthspan, defined as the period during which an animal displays good health, is a useful concept. But it begs the question – how do we define good health? From a biomedical perspective, it raises the question of whether it is possible to extend the duration of the healthspan, and how this affects the proportion of an organism's life in which it is in a healthy state. An intervention that extends lifespan might increase the proportion of life spent in good health, or it might decrease it. Ultimately, "good health" is an arbitrary definition of some proportion of the capacity of a youthful animal. If a healthy young person can run 100 meters in 20 seconds, we might define good health as running 100 meters in less than 40 seconds and bad health as more than 40

seconds. If a young worm pumps its pharynx 150 times per minute, we might define good health as pumping more than 120 times per minute, or 100, or 75, or 50. While the position of the good health line is arbitrary, the concept of good health is useful.

To determine whether an organism is undergoing "healthy aging", it is necessary to define aging in terms other than the organism's chronological age. A biomarker is defined as a trait that predicts remaining lifespan (or healthspan) similar to or better than chronological age [112,115]. A commonly used biomarker for aging is mobility, which can be readily observed [176,117,317]. The age-related decline in mobility is highly predictive of aging severity in several animal species (reviewed in [318]), and is correlated with several age-related phenotypes in nematodes (**Table 3**). However, because cessation of motor function is often used as a definition of death (i.e., lack of spontaneous or induced movement), using the level of motor function to predict lifespan has an element of circular logic [115] (the organism that is moving slowest in the group will be the first to cease movement altogether). Bansal *et al.* (2015) suggested the terms "healthspan" and "gerospan" to differentiate healthy and unhealthy aging, defining them as the periods when an animal has greater than 50% or less than 50% of its maximal functional capacity for a given phenotype, respectively [120]. Considering aging in these terms allows one to understand the extent to which interventions extend chronological age and affect the proportion of life spent in a healthy state.

2.4.3 How do studies in *C. elegans* relate to mechanistic theories of aging?

Over the last five decades, the understanding of age-related changes in *C. elegans* has vastly increased. In addition to the increased risk of death with increased chronological age, more than 70 different aging phenotypes have been described in *C. elegans* so far, including morphological deteriorations in most organs and tissues, behavioral alterations, and biochemical

changes (**Table 1**). One advantage of the *C. elegans* model is the ability to readily study age-related changes in longitudinal studies and thereby establish correlations between different phenotypes. However, by contrast to the long list of publications that document age-related changes, only 32 studies address the correlations between these changes (**Table 3**). The aging field is still a long way from solving one of the biggest puzzles in biomedical research: what is the mechanistic cause of all these age-related changes? The hallmarks of aging in diverse organisms include genetic instability, impairment of tissue function, and failure of key cellular processes and components (reviewed in [319]). Interestingly, most species exhibit similar aging phenotypes. With the discovery of age-related changes in various species, scientists have developed new theories about the underlying cause of aging. But how do we assess these theories? Do the major theories provide robust explanations for all species, or only some species? Do theories accurately predict interventions that influence the extension of lifespan? In this section, we review the current prominent mechanistic theories of aging in light of what has been learned by analyzing age-related changes in *C. elegans*.

2.4.3.1 Telomere shortening

Telomere attrition is a hallmark of aging in mammals, and it is proposed to contribute to the age-related decline of somatic stem cells by limiting the proliferative capacity [319]. Because all somatic cells in adult *C. elegans* are postmitotic, it seems unlikely that telomere shortening influences aging in worms. In some *C. elegans* strains, natural variations in telomere length correlate with altered structure of the human homolog of the telomere-capping shelterin complex subunit; however, these variations do not correlate with differences in lifespan [320]. Therefore, telomere shortening is unlikely to be a mechanistic cause of aging in *C. elegans*.

2.4.3.2 Cellular Senescence

Senescent cells arrest proliferation, resist apoptosis, and exhibit a characteristic senescence-associated secretory phenotype (SASP). These cells accumulate in tissues of older animals and are induced by certain diseases. They have been discussed as drivers of organismal aging, and are targets for intervention strategies [321]. Since *C. elegans* is a post-mitotic organism in which senescent cells have not been observed, cellular senescence is unlikely to be a mechanistic cause of aging in *C. elegans*.

2.4.3.3 Oxidative damage theory / mitochondrial free radical theory of aging

Originally proposed by Denham Harman in 1956, the oxidative damage theory exemplifies a common logic used to link the observation of age-related changes with mechanistic theories of aging [322]. According to this theory, reactive-oxygen species (ROS) that damage molecules in cells are a mechanistic cause of age-related deterioration. Superoxide free radical (O^{2-}) and hydrogen peroxide (H_2O_2) are byproducts of mitochondrial oxidative phosphorylation and accumulate with age due to mitochondrial dysfunction [322,323,321]. The theory rests on two pillars: (1) there is an age-related increase in oxygen radicals and oxidatively damaged macromolecules, and (2) exposure to high levels of oxygen radicals shortens lifespan. This plausible sounding theory dominated the field for decades and is still widely invoked to sell antioxidant remedies such as skin creams. However, it has been extremely difficult to test rigorously, because the definitive experiment is to remove oxygen radicals and measure aging, but this is not possible in the obligate aerobic species used to study aging.

Studies in *C. elegans* have been important in evaluating this theory. Some of the identified mitochondrial mutants, such as *mev-1* [324] and *gas-1* [325], display shorter lifespans consistent with this hypothesis. By contrast, several mutants with dysfunctional mitochondria are long-lived, such as the *clk-1* mutant, contradicting the hypothesis [186,326]. Yang and Hekimi (2010)

showed that the long-lived mutants with mitochondrial dysfunction caused by mutations in *nuo-6* and *isp-1* have higher levels of mitochondrial superoxide. The theory predicts that antioxidants will increase the lifespan of animals. However, treatment with antioxidants such as N-acetyl cysteine (NAC) or vitamin C reduce the lifespan of *nuo-6* and *clk-1* mutants [327]. In this situation, it appears that superoxide has a life *prolonging* effect, which is supported by the discovery that treatment with 0.1 mM paraquat increases the life span of wild type, *eat-2*, *daf-2* and *sod-2* mutants. Furthermore, *C. elegans* mutants that lack all superoxide dismutase genes and have a higher level of ROS still display a wild-type lifespan [327]. A current view is that endogenous mitochondrial ROS are signaling molecules that induce a stress response that can induce longer lifespans, whereas treatments with high levels of exogenous ROS that induce damage and a reduction in lifespan do not reflect normal physiology [326]. More detailed studies are needed to definitively establish whether ROS are a mechanistic cause of organismal aging, but studies in *C. elegans* have raised significant doubts about this theory.

2.4.3.4 Green theory of aging / loss of proteostasis

According to the green theory of aging, a mechanistic cause of age-related declines are damage that results from endogenous metabolic waste products and exogenous xenobiotics [328]. In addition to toxic byproducts/waste products that the organism accumulates with increasing age or due to dysfunctional processes, this hypothesis includes the effects of externally produced industrial products, byproducts, and waste that accelerate age-related changes and lifespan [329,261]. This theory is grounded in the idea that cells and organisms have protective strategies, such as detoxification mechanisms, chaperones, and the proteolytic system, and these protective systems are adequate to maintain homeostasis in young animals but decline during aging and can no longer protect the animals against these insults. In *C. elegans*, Morimoto and colleagues showed

that during the first day of adulthood, *C. elegans* loses the ability to prevent protein misfolding and aggregation [239]. The system that is responsible for maintaining proteostasis is the heat shock response. The transcription factor HSF-1 induces the expression of molecular chaperones that maintain the structure of metastable proteins. Surprisingly, this system is repressed in early adulthood [170], apparently leaving the organism unprotected from metabolic waste products and xenobiotics. Mitochondrial stress can delay the early repression of the heat shock response, thereby maintaining proteostasis [330]. Thus, in *C. elegans* there seems to be a programmed withdrawal of a robust proteostasis response, and this may be a mechanistic cause of aging. An important future goal is to develop approaches to maintain the proteostasis response during aging and determine if this can extend lifespan or healthspan as predicted by the theory.

2.4.3.5 "Run on" functions

The basis of this theory is that synthetic functions that are adaptive early in adult life continue beyond the point in time they are useful, becoming deleterious because they consume limited resources and/or produce a product that causes age-related degeneration [331,332]. For example, growth pathways that are necessary in development are not switched off after maturity or the cessation of reproduction. These programs "run on" without purpose, thereby damaging the older organism. The relationship of such a process to genetically "programmed" aging is complex and may be in the eye of the beholder. If one ascribes to the view that aging is deleterious and cannot be selected for by evolution, then run on programs can be interpreted as an unintentional "quasi-program" that was selected as a developmental program but causes age-related degenerative changes. If one entertains the idea that aging might be genetically programmed, then the absence of an "off switch" might be interpreted as a programmed mechanism of aging. One prominent example that supports this theory is yolk production in the

C. elegans intestine and export of yolk protein into the body cavity to supply the gonad. Gems and colleagues showed that *C. elegans* hermaphrodites continue producing yolk after reproduction ceases, leading to accumulation of this product in the body cavity. As a consequence, post-reproductive *C. elegans* turn intestinal biomass into yolk, which is proposed to be a mechanistic cause of age-related intestinal atrophy and ectopic yolk deposition [111].

2.4.4 How do studies of *C. elegans* relate to evolutionary theories of aging?

The question of the evolution of aging is as old as evolutionary theory itself. Erasmus Darwin, the grandfather of both Charles Darwin and Francis Galton and author of a poem explaining his early theory of evolution, commented "*How short the span of life*," [333]. Charles Darwin listed many questions that he hoped his theory of evolution by natural selection would answer, including, "*Why is life short?*" [334]. George C. Williams explained the reason we continue to be baffled by the existence of aging: "*It is indeed remarkable that after a seemingly miraculous feat of morphogenesis a complex metazoan should be unable to perform the much simpler task of merely maintaining what is already formed*," [26]. These musings raise two fundamental questions about aging that have not been resolved: (1) Why does aging occur in DNA life forms that exist today as a result of evolution and natural selection? Specifically, is aging a beneficial trait chosen by natural selection or a deleterious trait which natural selection cannot overcome? (2) How does aging occur mechanistically? Is aging caused by genetic programs that actively promote degenerative change or actively withdraw maintenance functions necessary for continued survival? Alternatively, is aging caused by the accumulation of damage caused by environmental or metabolic toxins despite the concerted efforts of genetically encoded detoxification mechanisms to fight these insults and promote longevity? While studies of age-

related changes in *C. elegans* do not definitively answer these questions, they do shed light on some of the key issues.

2.4.4.1 Reproductive aging versus somatic aging, and the shadow of selection

According to a gene-centered view of evolution, the ultimate function of an organism is to transmit its genetic information to its descendants via reproduction. Reproduction is accomplished by different organisms in many different ways, and it occurs in different organisms at different points in their lives. Many reproductive strategies have been described wherein organisms may reproduce throughout a significant portion of their lifespan, reproduce only once, or reproduce seasonally or only in certain conditions. However, definitionally, reproduction must occur prior to an organism's death; thus, regardless of factors like reproductive strategy or age of reproductive viability, essentially all species display a post-reproductive lifespan to some extent. Some species (such as Pacific Salmon), experience a very short post-reproductive lifespan in comparison to their total lifespan [335]; but in some species, this period can represent a significant portion of maximum lifespan (such as human females). Absent factors such as parental investment wherein such a trait can be adaptive, an organism's continued existence after it has reproduced does not confer additional fitness benefits to its progeny (and in some cases, such as resource competition, may actively hinder it). Why, then, does an organism's total lifespan so often extend beyond its period of reproductive viability? In the case of *C. elegans*, its maximal rate of self-fertile reproduction occurs on day 2-3, and it continues reproducing until day 5-6 [31]; yet, its lifespan continues until day 15 [48,168], and it maintains structural and functional integrity in its soma and the somatic components of its germline long after it ceases reproduction.

Current evolutionary theories are well equipped to explain why the soma degenerates after reproduction ceases – there is no reproductive advantage to continued survival. However, this shifts the key evolutionary question to the reproductive system: why does reproductive function degenerate? This question becomes the crux of the matter. It is clear that evolution can produce organisms with radically different lifespans, and which reach sexual maturity at different times. Richard Law described a thought experiment regarding a hypothetical organism that he called the "Darwinian Demon" [336]. This organism begins reproducing immediately after being born, produces infinite progeny, and has an infinite lifespan; thus, it experiences maximal fitness. In reality, all organisms are constrained by resource limitations, physiological constraints, etc., but the point is clear: if it is possible for animals to have long lifespans, and if longer-lived animals can produce more progeny, and if animals that produce more progeny generally have higher fitness than conspecifics that produce fewer progeny, then why do short-lived animals exist?

One hypothesis to explain this disparity is the so-called "Shadow of Selection", first described by Peter Medawar and J. B. S. Haldane [25]. In 1952, P.B. Medawar delivered a lecture in which he laid out "the origin and evolution of [aging as] a single unsolved problem of biology." Medawar noted there are both extrinsic and intrinsic forces of mortality, and presented a thought experiment in which there was no intrinsic force of mortality. A population of test-tubes, which have a probability of breaking every month, replace themselves. "The older the test-tubes are, the fewer there will be of them - not because they become more vulnerable with increasing age, but simply because the older test-tubes have been exposed more often to the hazard of being broken." The older test tubes contribute less to the replacement of the population, simply because there are fewer of them from the compounded toll of extrinsic

mortality. At this point, Medawar changes the scenario to include sudden disintegration at five years; the effect is nearly negligible, because so few test tubes live that long anyway. This illustrates the inescapable consequence of extrinsic mortality: "the efficacy of natural selection deteriorates with increasing age" – a concept termed the "shadow of selection." Medawar highlights how diseases like Huntington's chorea can only manifest in an environment that has decreased extrinsic mortality sufficiently to allow individuals to reach symptomatic age. The corollary to this argument is that if it is adaptive for an organism to eliminate a detrimental trait, evolution could select for mutants in which symptoms are postponed until the age at which extrinsic mortality is likely to have killed the vast majority of organisms.

This hypothesis is based on the assumption that aging is a deleterious trait. Due to extrinsic factors unique to a given organism's ecological niche, most organisms in the wild will not survive to reach their maximum lifespan; thus, in wild populations death due to intrinsic aging is likely rare compared to death due to extrinsic factors such as disease and predation. As such, the selective pressure on traits that extend lifespan past the average age of death in the wild will be low, and selection for traits which extend an organism's ability to reproduce after their likely death will be rare. Indeed, when isolated from wild sources, *C. elegans* are most often found in the dauer stage, and only rarely in the adult stage [337]; furthermore, the lifespan of *C. elegans* in the soil is drastically reduced compared to worms raised under laboratory conditions [338]. While the shadow of selection theory is appealing, it is difficult to test rigorously. Ultimately, it is an explanation for why something does not exist (genes that promote additional longevity), and there might be many alternative explanations for why something does not exist, including the possibility that it is not adaptive to live longer.

2.4.4.2 Tradeoff theories – antagonistic pleiotropy and disposable soma

Several theories invoke tradeoffs to explain the evolution of aging. These theories assume (1) aging is a deleterious trait, and (2) genetic architectures that obviate the tradeoffs were never available for natural selection. All other factors being equal, a gene which exerts its effect on an organism's fitness early in life will be under a higher degree of selective pressure than a gene which affects fitness later in life. Similarly, a pleiotropic gene which has a positive effect on fitness early in life but an equal and opposite negative effect later in life will still increase an organism's net fitness, as the earlier positive effect of the gene will have a stronger net impact. This observation is central to the Antagonistic Pleiotropy (AP) hypothesis, first described by George C. Williams [26]. In *C. elegans*, antagonistic pleiotropy has been used to explain age-related fitness tradeoffs observed in autophagy [339] and the timing of reproduction [340], and it has been demonstrated that long-lived mutants are outcompeted by their shorter-lived wild-type counterparts in the lab [341]. Many genetic interventions have been described which extend lifespan in *C. elegans*; these long-lived mutants often display reduced progeny production [342,31]. These observations have been argued as consistent with the AP theory, since these genes promote reproduction but inhibit longevity. According to this theory, even though genetic changes exist that can cause *C. elegans* to live longer, such changes have not been selected for in the wild because the co-incident phenotype, reduced progeny production, reduces the animal's fitness.

A correlate to the AP hypothesis is the idea of "run-on programs" that was discussed above: the undirected continuation of developmental programs in the absence of a selective pressure on their deactivation (first proposed in [331,343]). This hypothesis suggests that senescence is "quasi-programmed"; that is, not directed by a developmental program *per se*, but rather the result of the continued action of early-life developmental programs into later life. Such programs are not "turned off" simply because there is no evolutionary pressure to deactivate them due to

the Shadow of Selection. Certain age-related phenotypes in *C. elegans*, such as gonad degeneration, yolk accumulation, oocyte stacking, etc. have been suggested to be caused by hyperfunction of early-life developmental programs [332,110].

An organism's activities are constrained by the limited resources and energy it can obtain from its environment. Therefore, trade-offs must be made regarding the allocation of scarce resources to growth, reproduction, cellular maintenance, and other cellular activities. The disposable soma hypothesis, proposed by Thomas Kirkwood in 1977, posits that aging is caused by differential investment in the maintenance and propagation of the germline at the expense of the soma [344]. Kirkwood observed that accurate replication of germline DNA was essential to reproduction, whereas it is necessary in the soma only insofar as it allows the propagation of the germline. DNA and protein errors are therefore retained in somatic cells to a greater extent, resulting in a progressive breakdown in somatic tissues that is observed as senescence. *C. elegans* hermaphrodites display striking degeneration of the germline prior to somatic degeneration, which does not seem to fit well with predictions of a model arguing that resources were devoted to the reproduction system at the cost of somatic maintenance. The disposable soma hypothesis would seem to predict that during aging the germline would be preserved while the somatic tissues degenerate around it, which is not the pattern in *C. elegans*.

2.4.4.3 Population dynamics and the optimal progeny number theory

Hughes *et al.* (2007) proposed the optimal progeny number theory to explain reproductive senescence in *C. elegans* [31]. Although the theory emerged from studies of worms, it is a general theory that applies to all organisms that age, similar to the theories described above. The optimal progeny number theory is based on the assumption that reproductive aging is a beneficial trait because it limits progeny production and promotes an optimal number of progeny.

According to the theory, maximal progeny production can lead to unstable population dynamics that threatens the survival of the population, whereas an optimal progeny number promotes stable population dynamics and long-term survival of the population. A useful way to conceptualize the theory is to consider each individual as a double strand of DNA enclosed in a shell. The shell is the body produced by growth and development – it is transient, replaced every generation, and displays aging. Indeed, this review catalogs all the ways the shell/worm built around *C. elegans* DNA degenerates. The double strand of DNA is the essence of the life form, and it endures and passes to the next generation by semiconservative replication. The drive of the DNA is to reproduce and make as many copies of itself as possible. This drive is embedded in the very nature of DNA; as Watson and Crick famously suggested, "The complementary nature of [its] structure suggests how it duplicates itself." [345]. However, "as many copies as possible" is determined by the resources available in the niche to support growth, development, and reproduction of the shells; these resources fluctuate but are never infinite – they are always finite and can only support a limited number of individuals. According to the theory, the DNA evolved reproductive restraint to maximize the number of DNA copies over evolutionary time, and reproductive aging is part of the reproductive restraint strategy. According to this theory, the reproductively optimal organism delays the onset of reproduction until the optimal time, produces the optimal number of progeny over the reproductive period, and ceases reproduction due to reproductive aging. A population of these reproductively optimal organisms consists of as many individuals as the niche can support over long periods of time. There is no doubt that the DNA has mastered the challenge, since it coats the surface of the earth with untold numbers of individuals representing a spectacular diversity of shell designs.

The optimal progeny number theory immediately explains the existence of reproductive aging, which is the key evolutionary question. Furthermore, it predicts that reproductive aging is programmed in some manner. It also explains the paradox of post reproductive lifespan, which is a prominent feature of *C. elegans*. To achieve the optimal progeny production curve, the shell must function at a high level until all reproduction has been accomplished. Thus, there is evolutionary pressure to delay somatic aging until reproductive cessation, which results in a post reproductive lifespan. To evaluate the optimal progeny number theory, it is necessary to integrate studies of organismal aging with population dynamics. A recent publication by Scharf *et al.* (2022) is a step in this direction, since it establishes a laboratory ecosystem and simulation model that enable studies of population dynamics to be integrated with individual life history traits such as reproductive and somatic aging [346].

2.4.4.4 The role of genetic programs in aging

An important conceptual issue in the aging field is the role of genetic programs in controlling age-related degenerative changes. Here, we discuss how the analysis of *C. elegans* contributes to understanding this issue by considering **two broad theories: (1)** Age-related degenerative changes are specified by evolved genetic programs. Such a program might involve active degeneration similar to programmed cell death. Alternatively, this program might involve active withdrawal of maintenance or vitality functions. For example, the stem cell niche might secrete a factor necessary for stem cell maintenance in young animals, and secretion could be turned off in older animals, resulting in stem cell senescence. This model is the prediction of the optimal progeny number theory that is based on the assumption that aging is a beneficial trait. Because aging is beneficial, it is possible for programs that cause aging at the appropriate time of life to be selected for by evolution. **(2)** Age-related degenerative changes result from the

accumulation of damage from internal or external sources, and no evolved genetic programs can protect the organism and promote continued survival. For example, humans have neurons that extend from the spinal cord to the tip of the toe; if such a neuron experiences age-related degeneration, it cannot be replaced because it was formed during the unique process of embryonic and childhood development, which cannot be repeated, and no program ever evolved to replace such a neuron in adults. This model is the prediction of the shadow of selection and tradeoff theories that are based on the assumption that aging is a deleterious trait. Because aging is deleterious, programs that promote aging could not have been selected during evolution.

According to the **first theory**, age-related degenerative changes should be relatively reproducible in all individuals and in all tissues, similar to age-related developmental changes, since both types of events are genetically specified. Furthermore, it might be possible to identify mutants that do not undergo specific age-related degenerative changes, by mutating genes that specify these changes (barring pleiotropies). However, even if programs that specify age-related changes are inactivated by mutations, the organism would not be expected to become immortal. It is likely that age-related problems would accumulate for which there are no evolved solutions, leading to degeneration. Indeed, no mutations in *C. elegans* or other aging organisms have been reported to confer immortality. According to the **second theory**, age-related degenerative changes should be relatively chaotic and less reproducible than developmental changes. Furthermore, it should not be possible to identify mutants that do not undergo specific age-related changes, since these changes are not specified by a genetic program.

This review includes all reported age-related changes, regardless of the degree to which the changes are population-wide and reproducible versus sporadic. It has, however, emphasized the reproducible aspects of age-related degenerative changes, including the finding that most

changes become progressively more severe, occur during a characteristic time window, and affect the majority of individuals studied. On the other hand, the pattern of age-related changes reported by Herndon *et al.* (2002) and Kocsisova *et al.* (2019) suggests that some of these changes are mediated by stochastic events, as evidenced by the degree of heterogeneity among aging individuals and the degree of heterogeneity among aging tissues or cells within an individual (**Figure 8**) [117,202]. For example, in a group of animals that are the same chronological age, there can be wide variation in the ability to perform a function such as body movement. At the cellular level, Herndon *et al.* (2002) noted that there is substantial variability in degenerative changes [117]. For example, examining a pair of cells that are left-right symmetrical might reveal that the left cell was extensively degenerated whereas the right cell was intact [115,117]. In *C. elegans*, the germline provides a useful model for just such studies of symmetry and intraclass correlation (**Figure 8**) [347,202]. These studies convincingly document the degree of variability of age-related changes.

Even developmental events that are definitely programmed display some variability. While it appears that age-related changes at the cellular level are more variable than developmental changes, the amount of this variability has not been defined, and it is difficult to quantify variability. Despite these caveats, the observation that some age-related degenerative changes are highly variable and likely to be mediated by stochastic processes is a significant discovery that suggests that some age-related changes result from the absence of a genetic program. By contrast, the existence of some age-related changes that are population-wide, relatively reproducible, and occur relatively early in life is consistent with the model that some age-related changes are specified by genetic programs (**Figure 8**). The age-related reduction in the number and function of germline stem cells is an example of such an age-related change [202].

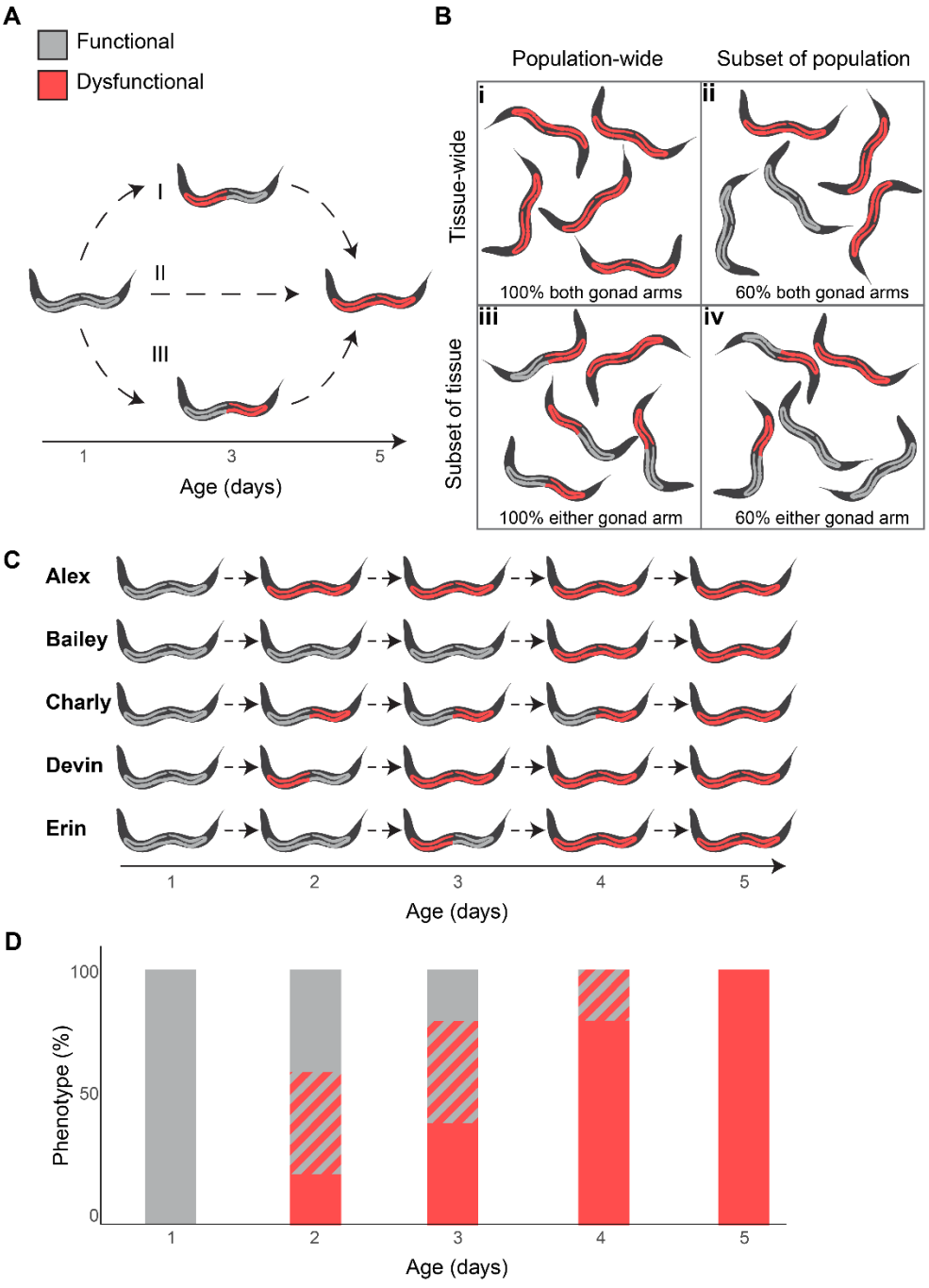

Figure 8: Population-wide versus sporadic nature of age-related changes

(A) Body plan symmetry enables convenient and quantitative approaches to study tissue heterogeneity in aging. An animal that transitions from two functional gonad arms when young (gray) to age-related defects in both gonad arms (red) could have developed defects in both arms simultaneously **(II)**, first in the anterior and next in the posterior arm **(I)**, or first in the posterior and next in the anterior arm **(III)**.

(B) While some age-related degenerative changes are high frequency and population-wide, appearing in every part of a tissue in every individual in a population, other age-related changes are low frequency or sporadic, appearing in some but not all individuals. The pattern can be at the level of the population: 100% of animals display germline defects in panels **i** and **iii**, whereas only a subset of animals (60%) display germline defects in panels **ii** and **iv**. The pattern can be at the level of the tissue: defects affect both gonad arms in panels **i** and **ii**, but affect either or both gonad arms in panels **iii** and **iv**. When the pattern is variable at both the level of the population and the tissue, only some animals are affected, and affected animals may only display defects in part of the tissue, as shown in panel **iv**.

For example, the Endomitotic oocyte phenotype, described in [202], affects only ~10% of day 5 animals, but typically affects both gonad arms (**ii**). In contrast, Herndon *et al.* (2002) reported that sarcomere, hypodermis, and intestinal integrity often suffer random but extreme local crises, described as "wide variability in both the time of onset and the rate of apparent deterioration within an isogenic population reared under uniform environmental conditions," as illustrated in panel iv [117].

Longitudinal observations with fine time resolution reveal the full pattern, whereas these studies with sparse timepoints or cross-sectional observations reveal less detail.

(C) The diagram shows a longitudinal analysis of five individuals (Alex, Bailey, Charly, Devin, and Erin) that develop age-related germline defects over five days. These examples elaborate on the pathways shown in panel **A** and illustrate how different patterns of age-related changes can lead to the same final endpoint of widespread degeneration.

(D) The stacked bar graph summarizes the data in panel **C** by plotting the percentage of individuals at each day which display two functional gonad arms (gray), one functional and one dysfunctional gonad arm (striped), and two dysfunctional gonad arms (red).

Several arguments are often used to suggest that senescence is influenced by genetics. First, certain mutations and natural polymorphisms affect lifespan in a way that suggests the function of these genes is to regulate lifespan. Long-lived mutants have been isolated in both *C. elegans* (e.g. *age-1*, *daf-2*) and *Drosophila melanogaster* (e.g. *methuselah, indy*) [4,64,348]. Also, twin studies in humans show that about a quarter to a third of variation in lifespan is likely genetic, which is higher than what one would expect if senescence were entirely stochastic [349]. Experiments show that artificial selection for longevity can extend lifespan, which also suggests that there is a genetic component which determines longevity [350,351].

Second, in some species (semelparous organisms including salmon, mayflies, bamboo, etc.) rapid senescence and death immediately and invariantly follow reproduction. This has been interpreted by various theorists as either an extreme case of disposable soma or as an example of programmed rapid death similar to apoptosis [352].

Third, similarities in the aging process and in the pattern that reproductive senescence precedes somatic senescence in many species has been interpreted as evidence for a conserved mechanism of aging, because a stochastic aging process is not predicted to produce this type of pattern [31]. Reproductive and somatic senescence are present not only in animals and plants, but also in asymmetrically dividing unicellular eukaryotes (*Saccharomyces cerevisiae*) and even in prokaryotes (*Escherichia coli*). Also, the genes in which mutations extend lifespan in one species are highly conserved through evolution, and mutations in homologous genes also extend lifespan in other species. The interpretation of these observations is that aging is universal to life [353,354].

Fourth, when senescence is accelerated (progerias, certain short-lived mutants) or decelerated (long-lived mutants, castration in Kokanee salmon, caloric restriction), the broad pattern of aging remains the same, which suggests that the treatments do not entirely change aging, but modulate it through existing pathways which normally respond to the nutritional and reproductive environment [335,355,356,199]. On the other hand, classical theories argue that aging is only an artifact of captivity, because aging has rarely been observed to contribute to mortality in the wild [25,357,358]. However, observations of antler flies and other species show that senescence reduces mating success of male antler flies in the wild, which is interpreted to mean that senescence is important to fitness even in the wild [359].

These observations make it clear that genetic programs are, in part, responsible for the control of aging. However, it is likely that the degree to which aging in an individual organism or

population of organisms is influenced by genetic factors rather than stochastic factors is variable. While both factors likely play a role in aging in most organisms, either genetic or stochastic factors may play an increased role depending on the organism's reproductive strategy, environmental conditions, ecological niche, etc. Thus, the question of whether aging is genetically programmed or caused by stochastic deterioration of the soma likely varies between species and under different conditions.

Chapter 3: Lifespan extension in *C. elegans* caused by bacterial colonization of the intestine and subsequent activation of an innate immune response

The work presented in Chapter 3 was published in 2019 in Developmental Cell *with the following authors:*

Kumar, S., **Egan, B. M.**, Kocsisova, Z., Schneider, D. L., Murphy, J. T., Diwan, A., & Kornfeld, K. (2019). *Lifespan extension in* C. elegans *caused by bacterial colonization of the intestine and subsequent activation of an innate immune response*. Developmental Cell, 49(1), 100-117. PMID: 30965033

I contributed primarily to the research regarding the function of the innate immune response in *phm-2(lf)* and *eat-2(lf)* mutants, as well as further characterization of the mechanism of lifespan extension *eat-2(lf)* mutants. I also revised and edited the manuscript and figures for resubmission.

3.1 Abstract

Mechanisms that control aging are important yet poorly defined. To discover longevity control genes, we performed a forward genetic screen for delayed reproductive aging in *C. elegans*. Here we show that *am117* is a nonsense mutation in the *phm-2* gene, which encodes a protein homologous to human scaffold attachment factor B. *phm-2(lf)* mutant worms have an abnormal pharynx grinder, which allows live bacteria to accumulate in the intestine. This defect shortens lifespan on highly pathogenic bacteria but extends lifespan and health span on the standard *E. coli* diet by activating innate immunity pathways that lead to bacterial avoidance behavior and dietary restriction. *eat-2(lf)* mutants displayed a similar phenotype, indicating accumulation of live bacteria also triggers extended longevity in this mutant. The analysis of *phm-2* elucidates connections between pathogen response and aging by defining a mechanism of longevity extension in *C. elegans* - bacterial colonization, innate immune activation and bacterial avoidance behavior.

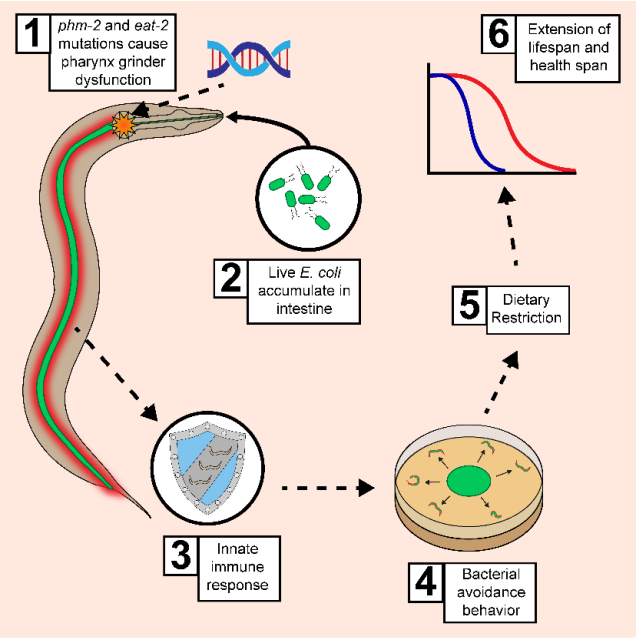

3.2 Introduction

Studies of the microbiome of mammals have begun to elucidate the complex interactions between animal hosts and bacteria, ranging from beneficial commensals to deleterious pathogens. There is currently little information about how these interactions affect aging, which is characterized by progressive degenerative changes of tissue structure and function that impair physiology and ultimately lead to death. *Caenorhabditis elegans* is a terrestrial, non-parasitic nematode that is a powerful genetic system for studies of aging. During its 16-day lifespan, *C. elegans* displays a wide range of age-related changes such as reproductive and musculoskeletal degeneration [360–362]. Tests of environmental, genetic, and pharmacologic interventions have led to the discovery and characterization of a relatively small number of endogenous pathways that can be modified to extend lifespan and health span. Dietary restriction (DR) is the original lifespan extending intervention; first described in rodents [363], it is now established to work in a wide range of organisms including *C. elegans.* Pathways regulated by dietary restriction are beginning to be defined and may include the target of rapamycin (TOR) energy sensing pathway that controls longevity [364]. The insulin/insulin-like growth factor-1 signaling (IIS) pathway plays an evolutionarily conserved role in *C. elegans* and other animals [365,366]. Diminished mitochondrial function can extend lifespan, suggesting that wild-type (WT) levels of mitochondrial activity promote rapid aging [367–369]. The identification of additional mechanisms that extend lifespan is an important goal.

Here we identify *phm-2* as a gene that influences *C. elegans* aging and demonstrate that it functions by a surprising mechanism: *phm-2(lf)* mutants are colonized by bacteria, which triggers an innate immune response that includes behavioral avoidance of bacterial food. Hughes *et. al*. [370] identified the *am117* mutation in a forward genetic screen for delayed reproductive aging, and

here we demonstrate that *am117* also delays somatic aging, displays a scrawny body morphology, and avoids the bacterial lawn. Interaction studies with other aging mutations revealed a strong interaction with *eat-2,* which has been interpreted as a genetic model of dietary restriction [371]. We used positional cloning approaches to identify the affected gene as *phm-2*, previously defined by two mutations that were not molecularly identified [372]. PHM-2 contains two highly conserved protein domains: a SAP domain and an RRM_SAF domain. Both of these domains are also present in the human protein scaffold attachment factor B (SAFB). *phm-2* mutants have a defective pharynx grinder [372] and are hypersensitive to pathogenic bacteria, as the grinder defect allows live bacteria to enter the intestinal lumen [373–376]. Thus, we hypothesized that, in standard culture conditions, *phm-2* mutants allow live *E. coli* to enter the intestinal lumen, resulting in mild pathogenicity and bacterial avoidance behavior. Consistent with this model, we demonstrated that live *E. coli* accumulated in the intestine of *phm-2(lf)* mutant animals, and *phm-2(lf)* mutants cultured on live *E. coli* displayed transcriptional changes and molecular events typical of bacterial infections. This response is important for the delayed aging phenotype, since culture on non-pathogenic bacteria abrogated the scrawny body morphology and aging phenotypes.

eat-2(lf) mutants have been used frequently to analyze dietary restriction in worms since pioneering studies by [371]. Here we demonstrate *eat-2(lf)* mutants accumulated live *E. coli* in the intestine, indicating that they have a defect in pharynx grinder function, and *eat-2(lf)* mutants displayed activation of innate immunity and bacterial avoidance behavior. Furthermore, when *eat-2(lf)* mutants were cultured on nonpathogenic bacteria, the phenotypes were suppressed. Thus, *eat-2* and *phm-2* mutants are not examples of simple dietary restriction, but are a

combination of bacterial colonization, innate immune activation, bacterial avoidance behavior and dietary restriction – an unexpected mechanism of lifespan extension in *C. elegans*.

3.3 Results

am117 mutant hermaphrodites displayed delayed reproductive and somatic aging, bacterial avoidance behavior, decreased body size, and increased stress resistance.

The *am117* mutation was identified in a forward genetic screen for mated hermaphrodites that display extended reproductive spans [370]. The screen was conducted using standard culture conditions: a small lawn of live *E. coli* OP50 on NGM dishes at 20°C. Similar to mated hermaphrodites, self-fertile *am117* hermaphrodites displayed reduced early progeny production and increased late progeny production, resulting in a reduced total brood size and an extended reproductive span (**Figure 1A-C**). To investigate somatic aging, we analyzed adult lifespan. *am117* mutant animals displayed a significant extension of mean (34%) and maximum (24%) lifespan compared to wild type (**Figure 1D, Table S1**). We define maximum adult lifespan as the average lifespan of the 10% of the population that are longest lived. The *am117* extended lifespan phenotype was also observed at 15°C and 25°C, demonstrating that the effect is not temperature dependent (**Figure S1A-B, Table S1**).

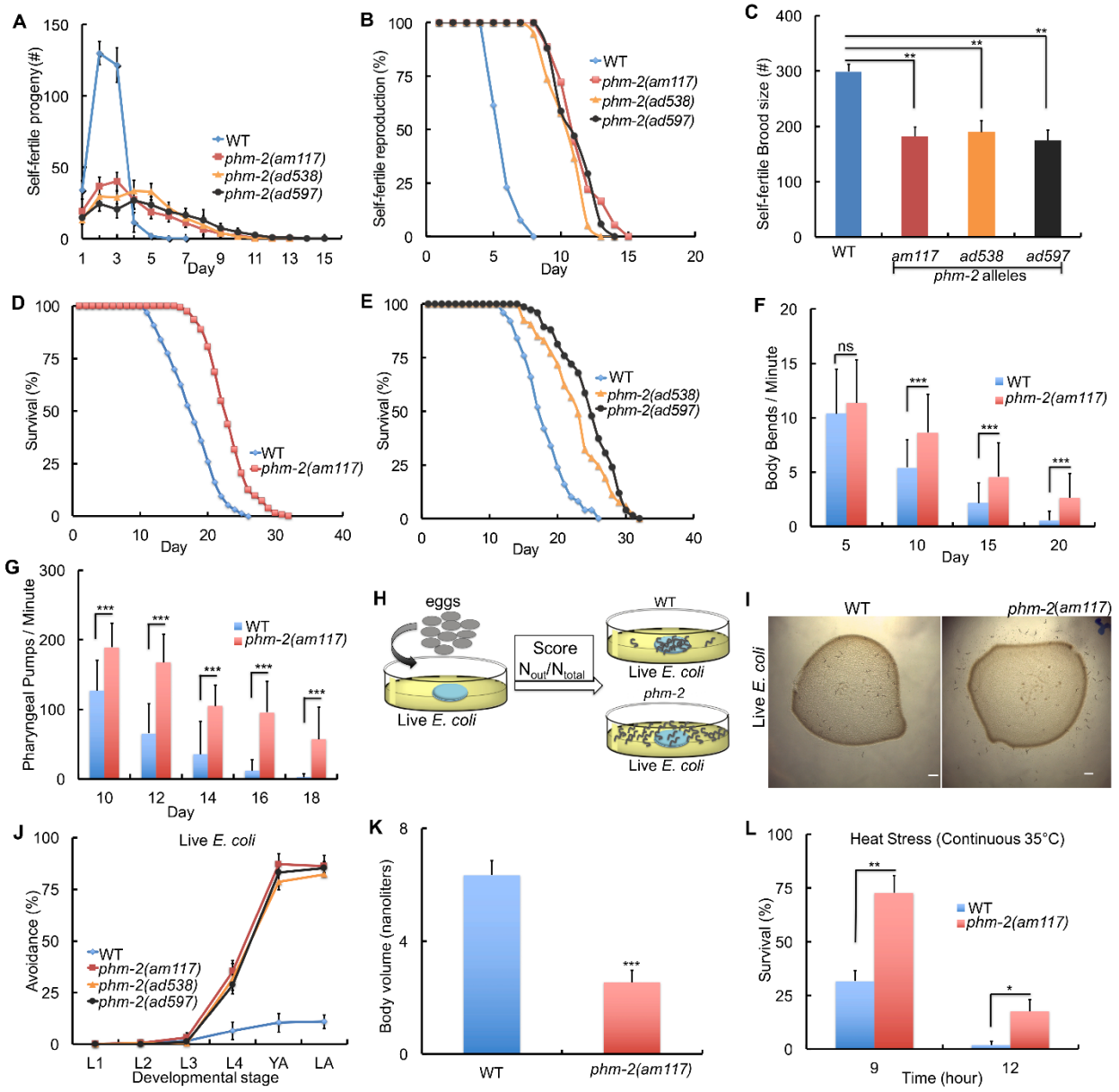

Figure 1: The *am117* mutation delayed reproductive and somatic aging, caused bacterial avoidance behavior, reduced body size and increased stress resistance.

(A-K) Animals were cultured at 20°C on NGM dishes with a small lawn of live *E. coli* OP50 bacteria. **(A-C)** L4 stage hermaphrodites were cultured individually and monitored daily for self-progeny production. Values are the average (+/- S.D.). (N=6-12 animals, Tukey post hoc HSD; **, P <0.01). **(D-E)** Survival curves - see **Table S1** for summary statistics. **(F-G)** Bars represent average (+/-S.D.) body bends per minute **(F)** and pharyngeal pumps per minute **(G)** (N=30-60 animals analyzed in each of 2-3 biological replicates; ***, $P < 0.0001$, not significant (ns), $P >$ 0.05 by Student's t-test). **(H)** Schematic of method used to quantify bacterial avoidance behavior. **(I)** Bright field photographs of dishes with a lawn of live *E. coli* OP50 (dark circle) and the surrounding medium without bacteria; wild-type animals are mostly inside the bacterial lawn, whereas *am117* mutant animals are mostly outside the bacterial lawn. Scale bar = 100 µm. **(J)** "Avoidance" is the average percent of animals (+/- S.D.) outside the bacterial lawn at the larval

stages L1, L2, L3, L4, day 1 adult (YA) and day 2 adult (LA). See **Table S2**. **(K)** Bars represent the average volume of individual worms (+/-S.D.) four days after the L4 stage determined by analyzing dissecting microscope images with the wormsizer algorithm (N=35-66 animals analyzed); ***, $P < 0.0001$ by Student's *t*-test). **(L)** Bars represent average (+/-S.D.) fractional survival. Animals were cultured at 20°C on NGM dishes until day 1 of adulthood, shifted to 35°C, and scored for survival after 9 and 12 hours (N=106-149 animals in each of 3 biological replicates; *, $P < 0.05$; **, $P < 0.005$ by Student's *t*-test).

To investigate the effect of *am117* on age-related degenerative changes [377,378], we analyzed neuromuscular processes that can be monitored non-invasively. Wild-type hermaphrodites display rapid and highly coordinated sinusoidal body movement as young adults, and the speed and coordination of body movements display age-related declines. To analyze body movement quantitatively, we counted body bends of worms on solid medium using a dissecting microscope. *am117* hermaphrodites displayed a significantly higher rate of body movement on days 10, 15, and 20 compared to wild type (**Figure 1F**). The rate of pharyngeal pumping can be analyzed quantitatively using a dissecting microscope and displays age-related decline. *am117* hermaphrodites displayed significantly higher rates of pharyngeal pumping on days 10–18 compared to wild type (**Figure 1G**). Thus, the gene affected by *am117* is necessary to promote rapid somatic aging, including age-related declines of neuromuscular activity and survival probability.

We noticed that *am117* mutant animals were frequently outside the lawn of bacteria, a phenotype called lawn leaving behavior or bacterial avoidance behavior [379] (**Figure 1H-I**). Wild-type animals display this behavior when cultured with pathogenic bacteria or RNAi bacteria that cause toxicity [380]. To quantify this behavior, we counted the number of animals inside and outside the bacterial lawn. Eggs were placed in the center of the bacterial lawn, and animals were scored at the L1, L2, L3, L4, day 1 adult, and day 2 adult stages. *am117* mutant animals displayed bacterial avoidance behavior beginning at the L4 stage and peaking during adulthood

with more than 85% of animals outside the bacterial lawn. By contrast, wild-type animals displayed fewer than 15% of animals outside the bacterial lawn (**Figure 1J, Table S2**). Sensory perception is important for worms to detect and chemotax towards food. There are 60 ciliated neurons in *C. elegans* that function in perception of the external environment [381,382]. Because defects in these neurons might cause animals to wander away from food, we investigated the morphology of amphid neurons in *am117* mutant animals using DiO staining. *am117* mutant animals displayed morphology similar to wild type, indicating that the bacterial avoidance behavior is not likely to be caused by abnormal sensory perception (**Figure S1J-L**). Bacterial avoidance behavior might reduce food ingestion, leading to dietary restriction. Indeed, *am117* mutant animals displayed a scrawny phenotype. To quantify body volume, we used dissecting microscope images and the worm sizer algorithm to analyze live animals 4 days after the L4 stage. Body volume of *am117* animals was reduced 60% compared to wild type (**Figure 1K, S2A-B**). These results indicate that the *am117* mutation causes bacterial avoidance behavior that may result in dietary restriction and a scrawny body morphology.

Many *C. elegans* mutations that delay aging also increase stress resistance [383,384]. To analyze the effect of *am117* on stress resistance, we monitored heat resistance at 35°C. *am117* mutant animals displayed significantly increased survival compared to wild type (**Figure 1L**). Thus, the gene affected by *am117* is necessary to promote the levels of sensitivity to stress observed in wild-type animals.

Lifespan extension caused by *am117* interacted genetically with *eat-2*.

To elucidate the mechanism of action of *am117*, we generated and analyzed double mutant strains with additional mutations that influence lifespan. Multiple genes in the IIS pathway influence *C. elegans* lifespan [385–388]. Mutations that partially reduce the activity of *daf-*

2, which encodes a protein homologous to the vertebrate insulin/IGF-1 receptor, extend lifespan. This signaling pathway controls the activity of a FOXO transcription factor encoded by *daf-16*, and DAF-16 activity is necessary for the lifespan extension caused by mutations in upstream signaling genes [389]. *am117; daf-2(lf)* double mutant animals displayed an extremely long mean lifespan of 58 days that was significantly longer than either single mutant strain (**Figure 2A, Table S1**). *daf-16(lf); am117* double mutant animals displayed a significant extension of mean (58%) and maximum (43%) lifespan compared to *daf-16(lf)* single mutant animals (**Figure 2B, Table S1**). Thus, the *am117* lifespan extension was additive with the *daf-2(lf)* lifespan extension and did not require *daf-16* activity. Furthermore, *am117* extended lifespan and self-fertile reproductive span in the *daf-16(lf); daf-2(lf)* genetic background (**Figure S1C-D, Table S1**). The IIS pathway mediates entry into an alternative third larval stage called dauer, a diapause state that is stress resistant [388,390,391]. *am117* mutant animals did not display an obvious Daf-c phenotype. To test *am117* in a more sensitive assay, we analyzed *am117; daf-2(lf)* double mutant animals. The *am117* mutation did not affect the temperature sensitive Daf-c phenotype caused by *daf-2(lf),* indicating the gene affected by *am117* is not necessary to inhibit formation of dauer larvae (**Figure S1E**).

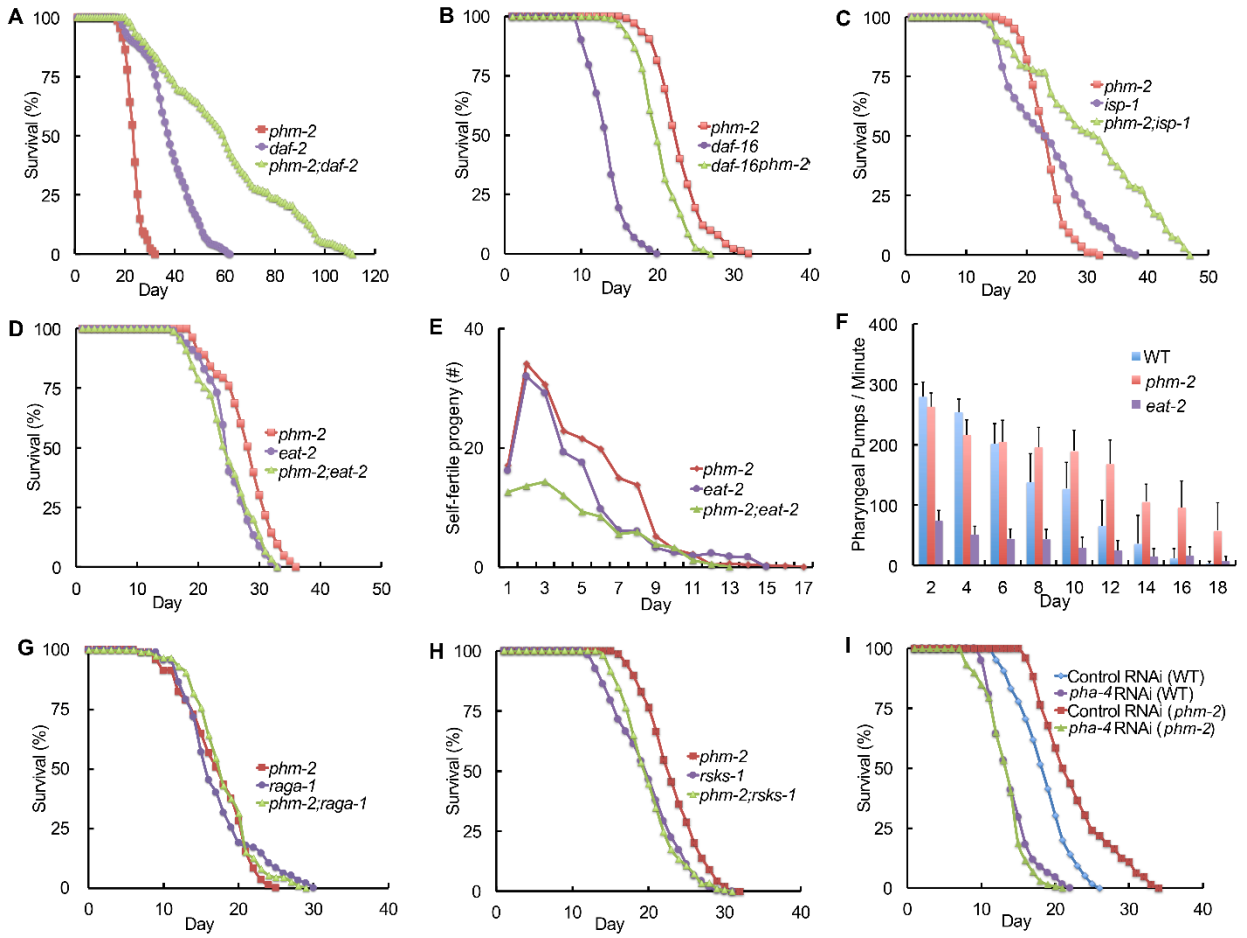

Figure 2. Genetic interactions between *phm-2(am117)* and genes involved in longevity.

(A-D, G-I) Survival curves - see **Tables S1 and S4** for summary statistics. Hermaphrodites had the following genotypes: wild type, *phm-2(am117)*, *daf-2(e1370), daf-16(mu86)*, *isp-1(qm150), eat-2(ad1116)*, *raga-1(ok386),* and *rsks-1*(*ok1255*). **(E)** Self-progeny production as in **Figure 1** (N=8-10 animals). **(F)** Pharyngeal pumping as in **Figure 1** (N=15-55 animals analyzed in each of 2 biological replicates). See **Table S3** for summary statistics. **(I)** Wild-type or *phm-2(am117)* hermaphrodites were cultured on *pha-4* RNAi bacteria or control RNAi bacteria.

Reducing the activity of multiple genes that are critical for mitochondrial activity extends *C. elegans* lifespan. The *isp-1* gene encodes an iron sulfur cluster containing protein that is essential for the function of complex III, and *isp-1(lf)* mutations extend lifespan [369,392]. The *am117*; *isp-1(lf)* double mutant animals displayed an extended lifespan that was significantly

longer than *isp-1(lf)* single mutant animals (**Figure 2C, Table S1**). Thus, the lifespan extensions caused by reducing mitochondrial function and the *am117* mutation were additive.

Energy metabolism genes can influence lifespan. The AMP-activated protein kinase (AMPK) alpha subunit AAK-2 promotes longevity by controlling energy metabolism, since an *aak-2(lf)* mutation reduces lifespan [393,394]. *am117*; *aak-2(lf)* double mutant animals displayed significantly extended mean (42%) and maximum (38%) lifespans compared to *aak-2(lf)* single mutant animals (**Figure S1F, Table S1**). The target of rapamycin (TOR) signaling network plays a critical role in nutrient homeostasis and influences adult longevity [364]. *rict-1(lf)* mutations affect TOR signaling and reduce lifespan. *am117*; *rict-1(lf)* double mutant animals displayed significantly extended mean (93%) and maximum (70%) lifespans compared to *rict-1(lf)* single mutant animals (**Figure S1G, Table S1**). Thus, the activities of *rict-1* and *aak-2* were not necessary for the lifespan extension caused by *am117*. Dietary restriction influences the lifespan of many organisms, demonstrating that *ad libitum* feeding during laboratory culture promotes a rapid lifespan. Mutations of the *eat-2* gene reduce the pharyngeal pumping rate and cause a lifespan extension [371,395]. The lifespan of *am117*; *eat-2(lf)* double mutant animals was not significantly longer than *eat-2(lf)* single mutant animals (**Figure 2D, Table S1**). Furthermore, these double mutant animals did not display an additive extension of reproductive span (**Figure 2E**). These results indicate that *eat-2(lf)* and *am117* may extend lifespan by a similar mechanism. By contrast to *eat-2(lf)* mutant animals, which display a substantial reduction of pharyngeal pumping rate, the *am117* mutant animals displayed a pharyngeal pumping rate similar to wild type in young adults and higher than wild type in older adults (**Figure 2F, Table S3**). To investigate the possibility that *am117* impairs food ingestion even though the pharyngeal pumping rate is normal, we measured feeding by exposing worms to fluorescent beads for 15

minutes and monitoring fluorescence in the intestine. Wild-type and *am117* mutant animals displayed strong fluorescence, indicating robust ingestion, whereas *eat-2(lf)* animals displayed significantly less fluorescence, indicating a reduced ingestion rate (**Figure S1I**).

To further characterize genetic interactions, we analyzed the *raga-1*, *rsks-1,* and *pha-4* genes. The *C. elegans raga-1* gene encodes a highly conserved ras-related GTPase, and *raga-1(lf)* mutations delay aging and age-related degenerative changes [396]. The *C. elegans rsks-1* gene encodes a ribosomal S6 kinase that is evolutionarily conserved and promotes development, metabolism, and autophagy; *rsks-1(lf)* mutant animals display delayed aging and age-related degenerative changes, as well as reduced fertility [364,397–401]. The lifespan of *am117; raga-1(lf)* or *am117*; *rsks-1(lf)* double mutant animals was not significantly longer than *raga-1(lf)* or *rsks-1(lf)* single mutant animals, respectively, indicating that the lifespan extensions are not additive (**Figure 2G-H, Table S1**). *C. elegans pha-4* encodes an ortholog of a mammalian FOXA transcription factor, and *pha-4* is essential for foregut development and necessary for the *eat-2(lf)* lifespan extension phenotype [402,403]. When *pha-4* activity was reduced by feeding RNAi beginning at L1 stage larvae, the lifespan of wild type and *am117* mutant animals was reduced similarly (**Figure 2I, Table S4**). Thus, the lifespan extension caused by the *am117* mutation requires *pha-4* activity. As a control for specificity, we demonstrated that *pha-4* feeding RNAi did not suppress the *daf-2(lf)* lifespan extension phenotype (**Figure S1H, Table S4**). Based on these genetic studies, we hypothesized that the *am117* mutation causes bacterial avoidance behavior, which results in dietary restriction characterized by a scrawny body morphology and delayed aging phenotypes that interact genetically with *eat-2*, *raga-1*, *rsks-1,* and *pha-4*.

Identification of *phm-2* as the gene affected by the *am117* mutation.

To identify the gene affected by the *am117* mutation, we used a positional cloning approach. Hughes *et al.* (2011) used the readily-scored scrawny body morphology phenotype to position *am117* on the right arm of chromosome I by linkage to single nucleotide polymorphism (SNP) markers [370]. Multi-factor mapping experiments indicated *am117* is positioned in a 4.3 map unit interval between a SNP in cosmid F32B4 at +9.0 and *unc-101* at +13.3 (**Figure 3A**). We performed whole-genome sequencing using genomic DNA from the *am117* mutant strain. Candidate mutations in the mapping interval were identified by comparison to the wild-type reference sequence and confirmed by standard DNA sequencing [404]. One candidate mutation caused a nonsense change in the predicted open reading frame F32B4.4. Gene structure predictions indicate that the F32B4.4 locus generates four transcripts; F32B4.4a is the longest and contains nine exons, whereas F32B4.4b.2, F32B4.4c, and F32B4.4b.1 transcripts contain 7, 7, and 6 exons, respectively (**Figure 3B**). The *am117* mutation is a C to T transition in codon 44 of the F32B4.4a transcript that changes an arginine to a stop codon (**Figure 3B**).

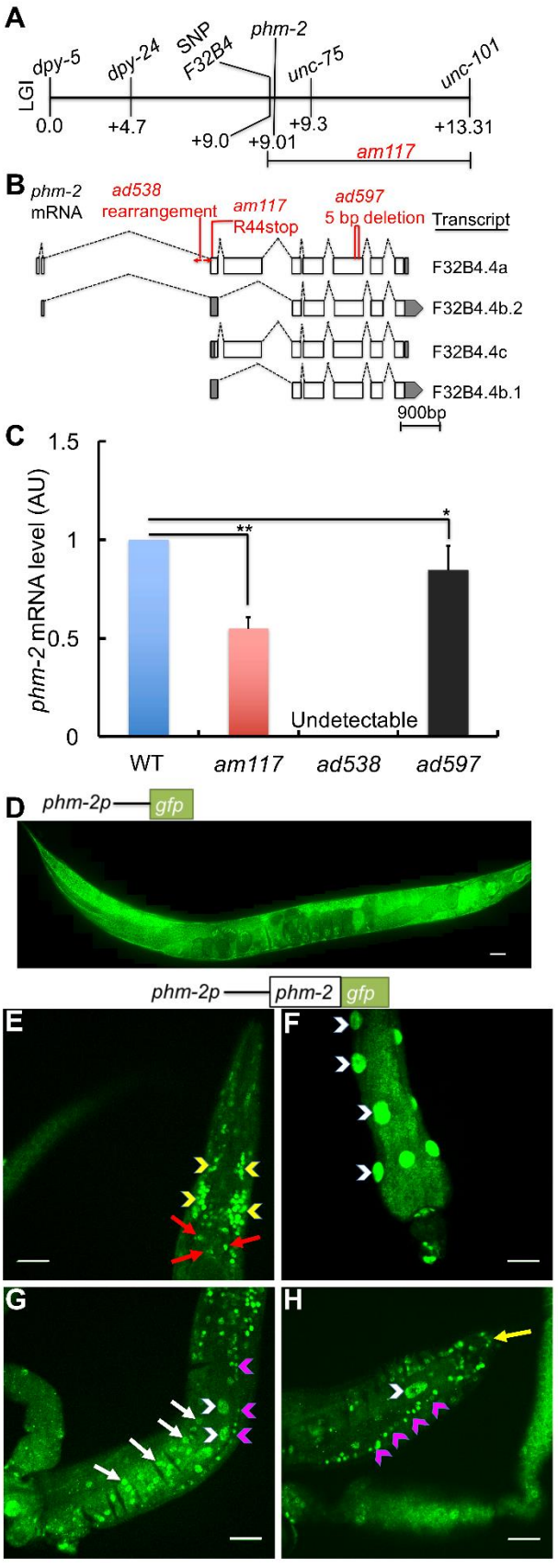
A
LGI
dpy-5
dpy-24
SNP F32B4
phm-2
unc-75
unc-101
0.0
+4.7
+9.0
+9.01
+9.3
+13.31
am117
B
phm-2 mRNA
ad538 rearrangement
am117 R44stop
ad597 5 bp deletion
Transcript
F32B4.4a
F32B4.4b.2
F32B4.4c
F32B4.4b.1
900bp
C
phm-2 mRNA level (AU)
1.5
1
0.5
0
**
*
Undetectable
WT
am117
ad538
ad597
D
phm-2p
gfp
phm-2p
phm-2
gfp
E
F
G
H

Figure 3. The *am117* mutation is an allele of *phm-2.*

(A) A genetic map of the right arm of *C. elegans* linkage group (LG) I. Loci defined by SNPs and mutations that cause visible phenotypes are named above, and map units are shown below. Multi-factor mapping experiments positioned *am117* between a SNP in cosmid F32B4 and *unc-101,* an interval that includes *phm-2*. **(B)** Diagrams of four *phm-2* transcripts. Boxes represent exons, shaded regions are untranslated, and dotted lines indicate introns. Position and nature of mutations is indicated above. **(C)** Bars represent average *phm-2* mRNA levels (+/-S.D.) in arbitrary units (AU) determined by qPCR in wild-type, *phm-2(am117)*, *phm-2(ad538)* and *phm-2(ad597)* animals. The WT value was set equal to 1.0, and mutant values are expressed as fold change over WT (N=4 biological replicates, Tukey post hoc HSD; *, $P < 0.05$; **, $P < 0.01$). **(D-H)** Diagrams of the upstream *phm-2* promoter region (not to scale) extending ~475 bp upstream of the translation start site of F32B4.4a fused to the GFP coding region **(D)** or the *phm-2* and GFP coding regions **(E-H)**. Panel D shows a fluorescence confocal microscope image of a live transgenic animal (genotype *amEx315*) at the adult stage displaying expression in most tissues from head to tail including pharynx, intestine, hypodermis, muscle and tail side neurons. Scale bar = 50 μm. **(E-H)** Fluorescence images show PHM-2::GFP fusion protein detected by immunostaining of fixed transgenic animals (genotype *amEx320)* at the adult stage. Panel E shows pharyngeal nuclei (red arrows) and nerve ring (yellow arrowheads) in the head region; panel F shows intestinal nuclei (white arrowheads); panel G shows ventral nerve cord (pink arrowheads), hypodermis (white arrows) and intestinal nuclei (white arrowheads) in the middle region of the worm; panel H shows tail neurons (yellow arrow), ventral nerve cord (pink arrowheads) and intestinal nuclei (white arrowhead) in the tail region. Scale bar = 20 μm.

We noticed that the *phm-2* gene, which has not been molecularly identified, is positioned on the genetic map in the range of 0.08 – 0.35 map units left of *unc-75*, which is consistent with the position of F32B4.4. Avery (1993) used X-ray mutagenesis to generate two *phm-2* mutations, *ad538* and *ad597*, that were recovered in a screen for eating defective mutants [372]. *phm-2* mutants display morphological defects in the pharyngeal grinder - it is unable to come to its full forward position, the muscle fibers of the terminal bulb appear to be shortened, and the space posterior to the grinder is expanded [372]. To test the model that *phm-2* mutations affect F32B4.4, we determined the DNA sequence of the F32B4.4 locus using genomic DNA from *ad538* and *ad597* mutant animals. The *phm-2(ad597)* allele contains a 5 base pair deletion that eliminates a portion of exon 7 that is common to all four transcripts, and the *phm-2(ad538)* allele

displayed abnormal PCR amplification suggestive of a rearrangement of intron 2 and exon 3 (**Figure 3B**).

To determine how these mutations affect F32B4.4 transcripts, we analyzed mRNA levels by quantitative PCR (qPCR). *phm-2(ad538)* mutants lacked detectable mRNA, consistent with a gross rearrangement of the locus, whereas *phm-2(ad597)* and *am117* mutant animals displayed significantly reduced transcript levels that were nonetheless readily detectable, consistent with a nonsense mutation and a small deletion that may reduce mRNA stability (**Fig. 3C**). These results indicate that the *phm-2* gene corresponds to F32B4.4 and *am117*, *ad538* and *ad597* are each alleles of *phm-2*. The *phm-2(ad597)* mutation is likely to be a strong loss-of function or null allele based on the lack of detectable mRNA.

To analyze the effect of *phm-2* mutations *ad538* and *ad597* on reproduction, we monitored progeny production of self-fertile hermaphrodites. These *phm-2(lf)* mutations caused a decrease of early progeny production, resulting in a smaller self-fertile brood size, and an increase in late progeny production, resulting in an extended self-fertile reproductive span (**Figure 1A-C**). *phm-2(ad538)* and *phm-2(ad597)* mutant animals displayed significant extensions of mean (30%, 33%) and maximum (28%, 27%) lifespan, respectively (**Figure 1E, Table S1**). These *phm-2(lf)* mutations caused bacterial avoidance behavior (**Figure 1J**). Thus, the *phm-2(ad538)* and *phm-2(ad597)* mutations that were identified based on eating defects [372] caused the same reproductive and somatic aging phenotypes used to identify the *am117* mutation [370].

To confirm that the *am117* mutation in *phm-2* causes these phenotypes, we tested a wild-type version of *phm-2*, a cDNA of the F32B4.4a transcript, for rescue ability. We generated five independently derived transgenic strains containing extrachromosomal arrays with wild-type

copies of *phm-2* in the background of *phm-2(am117)*. All these transgenic strains displayed a significant decrease in lifespan compared to non-transgenic *phm-2(am117)* animals (**Figure S3A, Table S1**). Furthermore, expression of wild-type *phm-2* significantly increased the body volume by 42% (**Figure S3B**). Thus, the *phm-2* locus was sufficient to partially rescue the extended lifespan and scrawny body morphology phenotypes, consistent with the model that *phm-2* is the gene affected by the *am117* mutation.

To analyze the predicted PHM-2 protein, we performed a BLAST search to identify related proteins. An alignment of *C. elegans* PHM-2 revealed 19.9%, 20.5%, and 16.7% overall identity to human, mouse, and *Drosophila* proteins, respectively, demonstrating that PHM-2 is an evolutionarily conserved member of the scaffold attachment factor B (SAFB) protein family (**Figure S4**). *C. elegans* PHM-2 protein includes two highly conserved motifs, the SAP domain that may be involved in DNA binding and the RRM_SAF domain that may be involved in RNA recognition [405]. These results suggest that *C. elegans phm-2* and human SAFB are descended from a common ancestral gene.

***phm-2* is broadly expressed, and the PHM-2 protein localizes to the nucleus.**

To determine the expression pattern of *phm-2*, we generated a plasmid that expresses green fluorescent protein (GFP) under the control of the upstream predicted *phm-2* promoter, injected the plasmid into wild-type animals to generate transgenic animals, and monitored fluorescence. The upstream *phm-2* promoter region consisted of ~475 bp of genomic DNA that extends from the start codon *of* F32B4.4a to the 3′ end of the adjacent gene (**Figure 3B**). These transgenic animals displayed GFP expression in multiple tissues including the hypodermis, muscles, neuron, vulva, and intestine, indicating that *phm-2* is expressed in most if not all tissues (**Figure 3D**).

The PHM-2 protein encoded by the F32B4.4a transcript contains 1073 amino acids. To determine the sub-cellular localization of this protein, we generated plasmids that express PHM-2 fused to GFP under the control of the upstream predicted *phm-2* promoter, injected these into *phm-2(am117)* animals to generate transgenic animals, and used immunostaining to detect the fusion protein. PHM-2::GFP was detected in a wide range of cells including the pharynx, nerve ring, intestine, neurons, and ventral nerve cord. The protein displayed punctate staining suggestive of nuclear localization (**Figure 3E-H**).

***phm-2(lf)* mutants displayed abnormal pharynx morphology, live bacteria accumulation in the intestine, and an activated innate immune response.**

A critical function of the *C. elegans* pharynx is to crush live bacteria before they enter the intestine, thus preventing bacterial colonization [406,407]. *phm-2(am117)* mutant animals exhibited abnormal pharynx grinder morphology (**Figure 4A-B**), consistent with the defects observed in the *phm-2(ad538)* and *phm-2(ad597)* mutants identified by Avery (1993) [372]. To determine if this defect allows live bacteria to accumulate in the intestine, we cultured adult animals on *E. coli* OP50-GFP for 24 hours. *phm-2(am117)* mutant animals displayed significantly more fluorescent animals than wild type, demonstrating that live *E. coli* accumulate in the intestine of this mutant strain (**Figure 4C, S5G**). Reducing the activity of *rsks-1* or *pha-4* suppressed the lifespan extension caused by *phm-2(lf)* but did not block bacterial accumulation, indicating these genes function downstream of bacterial accumulation to influence lifespan (**Figure S5H-I**). *phm-2(lf)* mutants have been reported to be hypersensitive to pathogenic bacteria, since the pharynx grinder defect makes them more susceptible to colonization by live bacteria [373,374,376]. Consistent with this observation, *phm-2(am117)* mutant animals were more susceptible than wild-type animals to killing by the pathogenic bacteria *P. aeruginosa* strain

PA14 (**Figure 4D**). Wild-type and *phm-2(am117)* mutants displayed robust avoidance of this pathogenic strain (**Figure 4E**).

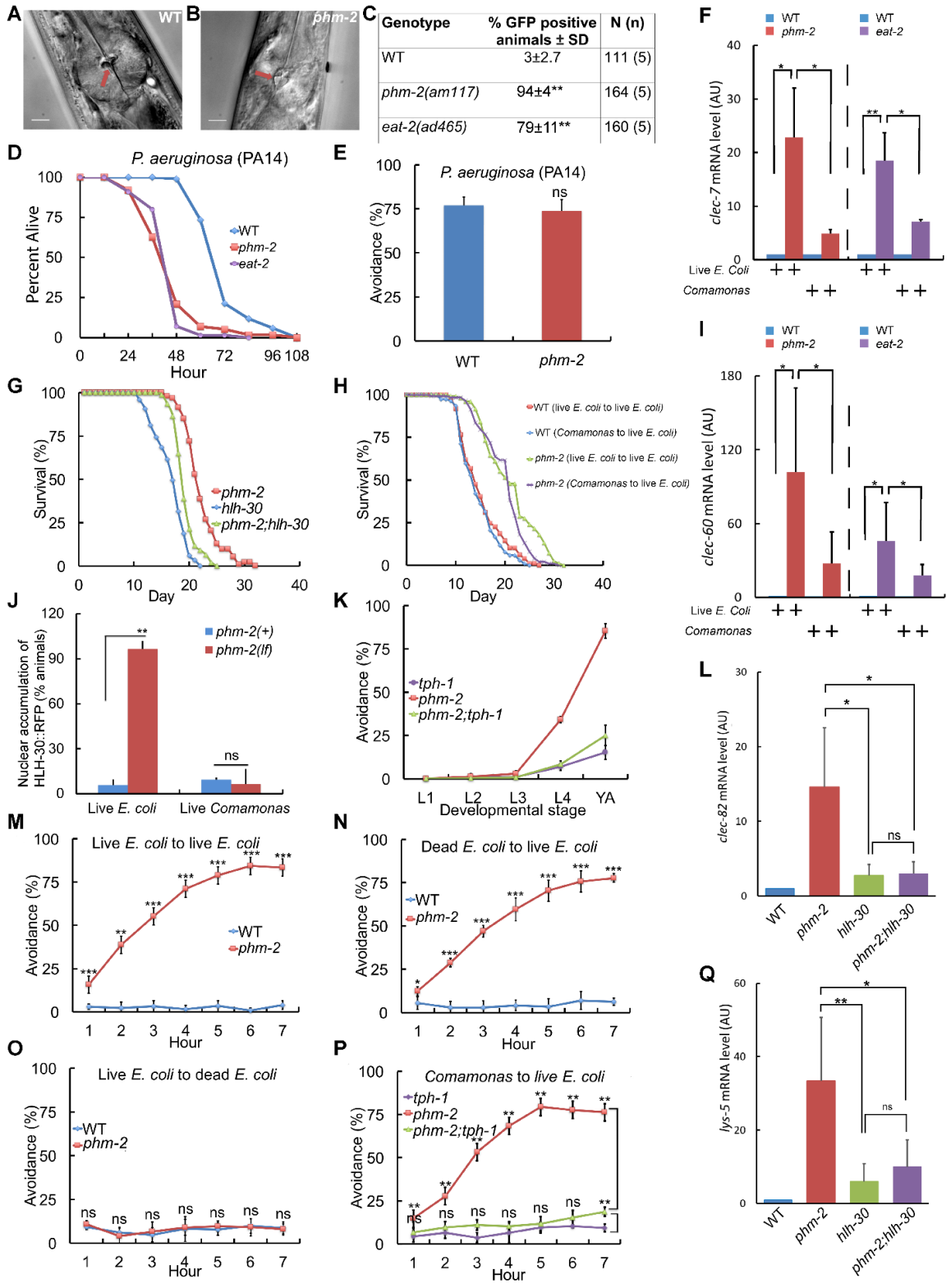

Figure 4. *phm-2(lf)* animals displayed abnormal pharynx morphology, live bacteria accumulation and an innate immune response.

(A,B) Representative bright field photographs of the terminal bulb of the pharynx illustrate an open, abnormal grinder in *phm-2(am117)* mutant animals (red arrow). Scale bar = 10 μm. **(C)** Quantification of number of fluorescent animals for wild-type, *phm-2(am117),* and *eat-2(ad465)* adult animals cultured with green *E. coli* OP50-GFP for 24 hours. N(n) indicates total number of animals and number of independent trials. Tukey post hoc HSD; **, $P < 0.01$ compared to WT. **(D)** Wild-type, *phm-2(am117*), and *eat-2(ad465)* animals were cultured on live *E. coli* OP50 bacteria from egg until the L4 stage, transferred to pathogenic *P. aeruginosa* PA14 bacteria in NGM dishes with FudR at 25°C, and analyzed every 12 hours for survival. *phm-2(am117*) and *eat-2(ad465)* animals had a significantly shorter mean lifespan compared to WT (Five biological experiments, N=98-106 animals, $P < 0.001$ by ANOVA). **(E)** Wild-type and *phm-2(am117*) animals were cultured on live *E. coli* OP50 bacteria from egg until the L4 stage, transferred to pathogenic *P. aeruginosa* PA14 bacteria, and scored after 24 hours. Values are the average (+/- SD) of three biological replicates, N≥100 animals per replicate. Both strains displayed similar, robust avoidance (ns, not significant, $P > 0.05$ by Student's *t*-test). **(F, I, L, Q)** Bars represent mRNA levels (+/-S.D) for *clec-7*, *clec-60, clec-82,* and *lys-5* pathogen response genes determined by qPCR in wild-type, *phm-2(am117), eat-2(ad465), hlh-30(tm1978),* and *phm-2;hlh-30* animals cultured on live *E. coli* OP50 (**F, I** as indicated and **L, Q**) or live *Comamonas* bacteria (**F, I** as indicated). Values in arbitrary units (AU) are the average of three to five biological replicates. ANOVA; *, **, $P < 0.05$, $P < 0.005$; ns, not significant, $P > 0.05$. **(G)** Survival curves for *phm-2(am117)*, *hlh-30(tm1978)*, and *phm-2(am117)*; *hlh-30(tm1978).* See **Table S1** for summary statistics. **(H)** Survival curves of wild type or *phm-2(am117)* animals grown from embryo to adult on either live *E. coli* OP50 or live *Comamonas* DA1877 and then transferred to live *E. coli* OP50 at the adult stage for the remainder of their lifespan. See **Table S6** for summary statistics. **(J)** Quantification of percent of animals that displayed nuclear localized fluorescence for *phm-2(+)* and *phm-2(am117)* animals that express HLH-30::RFP cultured on live *E. coli* OP50 or live *Comamonas* (N≥100 animals). **(K)** *phm-2(am117); tph-1(mg280)* animals did not display bacterial avoidance behavior on live *E. coli* compared to *phm-2(lf)*. See **Table S5** for summary statistics. **(M-O)** Avoidance was measured hourly after wild-type or *phm-2(am117)* adults were transferred to the test dish. Values are the average of five biological replicates, N=148-162 animals **(M)** and three to four biological replicates, N=77-142 animals (N,O). ns, not significant, $P > 0.05$ by Student's *t*-test. **(P)** Animals were cultured on *Comamonas* bacteria from embryo to young adult and then tested on live *E. coli* OP50. *phm-2(am117); tph-1(mg280)* animals displayed less bacterial avoidance behavior compared to *phm-2(lf)* and were similar to *tph-1(lf)* (N=108-146 animals, 4 biological replicates, Tukey post hoc HSD; n.s., not significant, $P > 0.05$).

C. elegans has an innate immune system and responds to bacterial pathogens by expression of protective genes [408,409]. *C. elegans* HLH-30 is the ortholog of vertebrate transcription factor EB (TFEB); *hlh-30* can modulate longevity and plays an important role in

autophagy, lysosomal biogenesis, and regulation of innate immune response genes [410,411]. Exposure to highly pathogenic bacteria induces nuclear accumulation of HLH-30::RFP [411,412]. To test the hypothesis that live *E. coli* in the intestine of *phm-2(lf)* mutant animals activate the innate immune response, we analyzed the transcription of response genes and the nuclear accumulation of HLH-30. The transcript levels of multiple genes involved in the pathogen response were dramatically higher in *phm-2(lf)* mutant animals compared to wild-type animals when cultured on live *E. coli*, including the C-type lectin genes *clec-7, clec-60,* and *clec-82*, the antimicrobial peptide gene *F53A9.8,* and the lysozyme gene *lys-5* (**Figure 4F, I, S5M-O**). This difference in transcript levels between wild type and mutant was largely or completely abrogated when animals were cultured on live *Comamonas,* a non-pathogenic bacteria (**Figure 4F, I, S5M-O**). The *phm-2* promoter was not induced by exposure to highly pathogenic bacteria (**Figure S5A-F**). The HLH-30 transcription factor accumulates in the nucleus when it is activated. Two day old adult *phm-2(lf)* mutant animals displayed nuclear accumulation of HLH-30::RFP compared to wild-type animals when cultured on live *E. coli*, and this difference was not observed when cultured on live *Comamonas* (**Figure 4J, S5J**). To investigate the functional consequences of *hlh-30* activation, we analyzed the expression levels of innate immune genes and the lifespan of *phm-2(lf)*; *hlh-30(lf)* double mutants. *hlh-30* was necessary for the increased transcript levels of *clec-82*, *lys-5*, and *clec-7*, although it was not necessary in the case of *clec-60* (**Figure 4L, Q, S5K-L**). Thus, *hlh-30* appears to mediate at least part of the transcriptional response to bacterial accumulation in *phm-2(lf)* mutant animals. *phm-2(lf)*; *hlh-30(lf)* double mutant animals displayed a lifespan that was intermediate between *phm-2(lf)* and *hlh-30(lf)* single mutants (**Figure 4G, Table S1**). Therefore, *hlh-30* appears to be partially required for the *phm-2(lf)* lifespan

extension. Thus, live *E. coli* accumulate in the intestine of *phm-2(lf)* mutant animals which appears to activate the innate immune response.

Analysis of *phm-2(lf)* bacterial avoidance behavior.

We observed that *phm-2(lf)* mutant animals did not display bacterial avoidance behavior when cultured on UV-killed *E. coli* or non-pathogenic live *Comamonas* bacteria. This raises the question: how do *phm-2(lf)* mutant animals sense that live *E. coli* are pathogenic and implement the bacterial avoidance behavior? To test the possibility that the worms sense a secreted metabolite released by live *E. coli*, we analyzed filtered supernatant from overnight bacterial cultures. Adding supernatant from live *E. coli* OP50 cultures to *Comamonas* bacteria was not sufficient to provoke the bacterial avoidance behavior (**Figure S6C**), and adding supernatant from live *Comamonas* bacteria to *E. coli* bacteria was not sufficient to inhibit bacterial avoidance behavior (**Figure S6D-E**). Furthermore, adding a block of live *E. coli* OP50 to the cover of the dish was not sufficient to provoke the bacterial avoidance behavior (**Figure S6F-G**). Mixtures of live *E. coli* OP50 and *Comamonas* resulted in intermediate levels of bacterial avoidance behavior (**Figure S6H-I**). These results do not support the model that a secreted metabolite caused bacterial avoidance behavior.

We investigated whether *phm-2(lf)* animals learn to avoid live *E. coli*. In the first learning paradigm, animals were trained by culture from egg to adult on one type of bacteria, and then these adults were tested on another type of bacteria (**Figure S6L**). If worms learn avoidance behavior, then the training experience is predicted to influence their behavior during the test. *phm-2(lf)* mutant animals trained on dead *E. coli*, which they do not avoid, and tested on live *E. coli*, displayed robust avoidance behavior that was measurable in one hour and similar to animals trained on live *E. coli* (**Figure 4M-N**). *phm-2(lf)* mutant animals trained on live *E. coli*, which

they avoid, and tested on dead *E. coli* did not display avoidance behavior (**Figure 4O**). Similar results were obtained when *Comamonas* was used instead of dead *E. coli* (**Figure S6J-K**). Thus, in this learning paradigm prior experience had no measurable effect on avoidance behavior, indicating the behavior is not learned.

The second learning paradigm was a binary choice assay; animals were trained by culture from egg to adult on one type of bacteria, adults were tested on dishes with two small lawns with different types of bacteria, and the number of worms in each lawn was scored. Wild type preferred live *E. coli* over *Comamonas* and live *E. coli* over dead *E. coli*, and these preferences were not affected by the training bacteria (**Figure S7**). *phm-2(lf)* mutants preferred *Comamonas* over live *E. coli* and dead *E. coli* over live *E. coli*, and these preferences were not affected by the training bacteria (**Figure S7**). Thus, the *phm-2(lf)* mutants displayed strikingly different bacterial preferences than wild type, consistent with avoidance of live *E. coli*. However, in this learning paradigm prior experience had no measurable effect on avoidance behavior, indicating the behavior is not learned. These experiments indicate that avoidance behavior is a rapid response of *phm-2(lf)* mutant animals to live *E. coli*, since it can be observed after one hour, and it involves a continuous sensing mechanism rather than learning and memory.

To explore the mechanism of bacterial avoidance behavior, we used a candidate gene approach by analyzing double mutant strains. Most of the genes involved in longevity did not strongly influence the bacterial avoidance behavior of *phm-2(lf)* mutant animals, including *daf-16*, *isp-1*, *aak-2*, *rict-1*, and *rsks-1*. However, *daf-2(lf)* caused a modest reduction of avoidance (**Figure S8, Table S5**). We investigated *C. elegans* pathways reported to be involved in avoiding pathogenic bacteria [413–418]. Mutations of *pmk-1*, *mlk-1, hlh-30*, and *npr-1* did not strongly influence the bacterial avoidance behavior of *phm-2(lf)* mutant animals (**Figure S8, Table S5**).

The serotonin biosynthesis enzyme tryptophan hydroxylase is encoded by the *tph-1* gene, which is necessary for avoidance of pathogenic bacteria [379,380]. The analysis of double mutant *phm-2(lf); tph-1(lf)* animals demonstrated that the *tph-1* mutation suppressed the bacterial avoidance behavior caused by *phm-2(lf)* (**Figure 4K, P, Table S5**). A detailed time course revealed that the suppression is partial and most effective in young and old adults, whereas it was less effective in day 2 adults (**Figure S8L**). These results indicate that *tph-1* is necessary to mediate this bacterial avoidance behavior.

Live *E. coli* are pathogenic to *phm-2(lf)* mutant animals, and bacterial avoidance behavior is adaptive.

To test the model that accumulation of live *E. coli* in *phm-2(lf)* mutant animals is deleterious and bacterial avoidance behavior is adaptive, we spread live *E. coli* OP50 bacteria over the entire surface of the NGM dish so that animals could not avoid the bacteria; we refer to such dishes as having a large lawn. By contrast, standard culture dishes have a central spot of bacteria, and we refer to such dishes as having a small lawn. When cultured with live *E. coli* OP50-GFP, *phm-2(lf)* mutant animals displayed significantly increased fluorescence intensity when cultured on the large lawn compared to the small lawn (**Figure 5A, D**). Furthermore, a greater fraction of the animals displayed strong fluorescence (**Figure 5B-C**). Thus, the bacterial avoidance behavior limits the accumulation of live *E. coli* in the intestine.

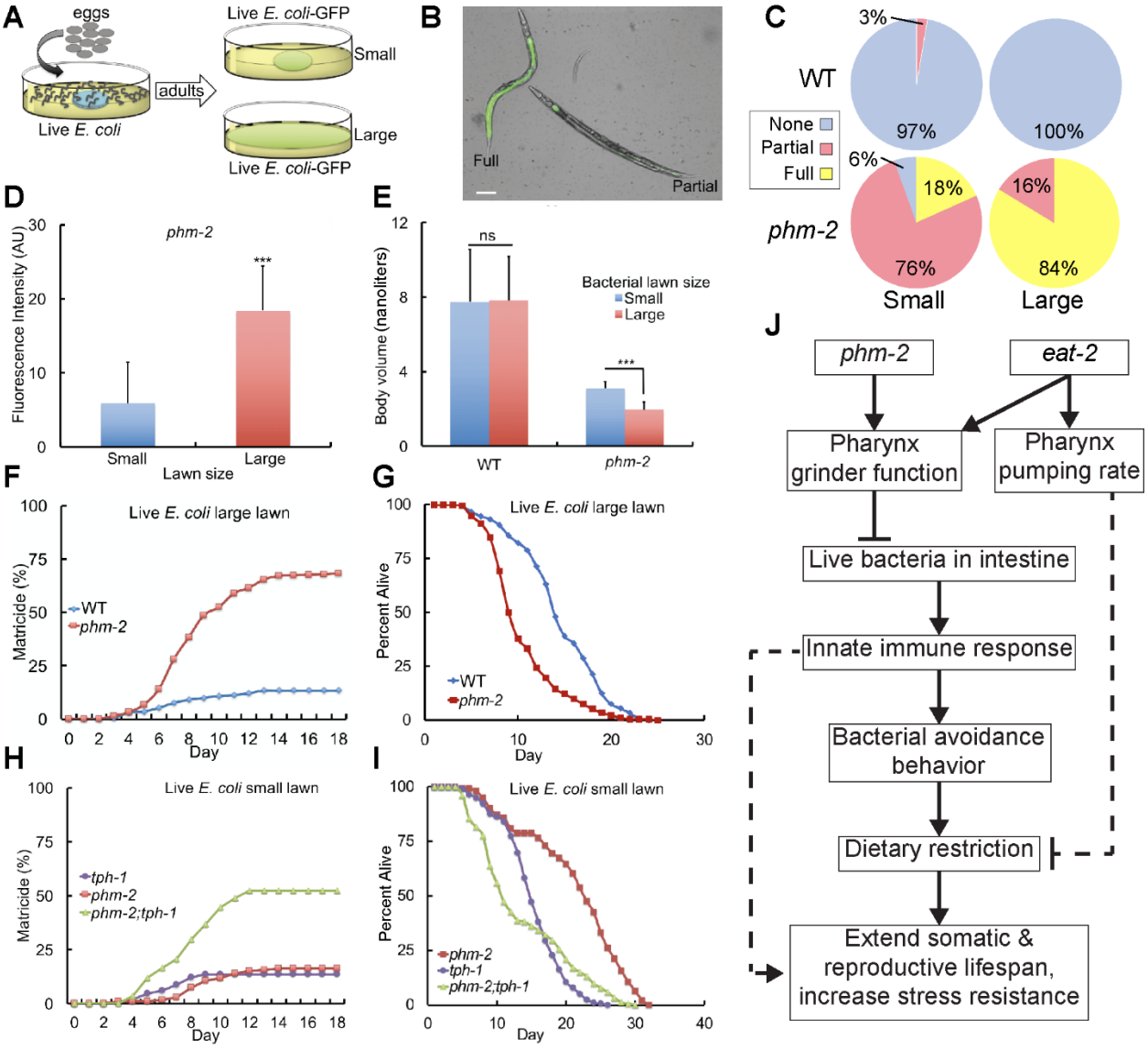

Figure 5. Bacterial avoidance behavior by *phm-2(lf)* animals limits bacterial accumulation in the intestine and increases survival.

(A) Schematic of method. **(B)** Representative bright field photographs and **(C)** Quantification of categories of phenotype severity. Animals were categorized as Full (*E. coli* OP50-GFP throughout the intestine), Partial (*E. coli* OP50-GFP in part of the intestine) or None (no detectable fluorescence in the intestine). Five biological replicates with N≥112 animals were analyzed. Scale bar = 50 µm. **(D)** Quantification of whole animal fluorescence. *phm-2(am117)* adult animals were cultured with a small (blue) or large (red) lawn of *E. coli* OP50-GFP for 24 hours. Values in arbitrary units (AU) are the average (+/-S.D), N≥13 animals. ***, $P < 0.001$, by Student's *t*-test. **(E)** Worm volume as in **Figure 1** (N=40-55 animals analyzed; ns, not significant, $P > 0.05$ by Student's *t*-test). **(F, H)** Values are the cumulative fraction of animals that displayed matricidal hatching versus days of adulthood. Genotypes were wild type, *phm-2(am117),* and *tph-1*(*mg280*). Panel F is based on six to eight biological replicates, N=295-342 animals, and panel H is based on

three biological replicates, N≥168 animals. **(G)** Percent alive for wild type and *phm-2(am117)* animals cultured on a large lawn of live *E. coli,* and **(I)** for *phm-2(am117)*, *tph-1(mg280),* and *phm-2;tph-1* animals cultured on a small lawn of live *E. coli*. Note that animals that died of matricidal hatching were not censored from these data. See **Table S6** for summary statistics. **(J)** Model of the mechanism of *phm-2(lf)* and *eat-2(lf)* lifespan extensions. Dotted lines indicate uncertainty.

To investigate the consequences of increased bacterial accumulation, we monitored the fate of animals cultured on the dishes with large bacterial lawns. *phm-2(lf)* mutant animals displayed a high frequency of early death due to matricidal hatching and a shorter mean lifespan compared to wild type (**Figure 5F-G, Table S6**). Consistent with this finding, *phm-2(lf); tph-1(lf)* double mutant animals displayed a high frequency of matricidal hatching and a shorter mean lifespan when cultured on a small lawn of live *E. coli* OP50, since they do not avoid the bacteria (**Figure 5H-I, Table S6**). *phm-2(lf)* mutant animals cultured on the large lawn of bacteria displayed an enhanced scrawny body morphology compared to animals cultured with a small lawn of bacteria (**Figure 5E**). Reduced body size is a non-specific phenotype that might result from a variety of defects. We interpret that the very small body size of animals cultured on the large lawn results from strong pathogenesis, whereas we interpret that the slightly bigger body size of animals cultured on the small lawn results from mild pathogenesis and dietary restriction caused by food avoidance behavior. Thus, bacterial avoidance behavior of *phm-2(lf)* animals promotes growth and prevents matricidal hatching, and forced exposure to live *E. coli* is indeed deleterious.

Colonization of *phm-2(lf)* mutants by pathogenic *E. coli* causes delayed aging.

We hypothesized that live bacterial accumulation in the intestine causes bacterial avoidance behavior, resulting in dietary restriction that is the cause of the scrawny body morphology and contributes to the delayed aging phenotypes (**Figure 5J**). To test this model, we

tried to identify bacterial food sources that would not trigger the avoidance behavior. When *phm-2(lf)* mutant animals were cultured on another strain of live *E. coli,* the B/K12 hybrid strain HB101, bacterial avoidance behavior, scrawny body morphology and delayed aging phenotypes were still observed (**Figure 6A-D, S2C-D, Table S2, S6**).

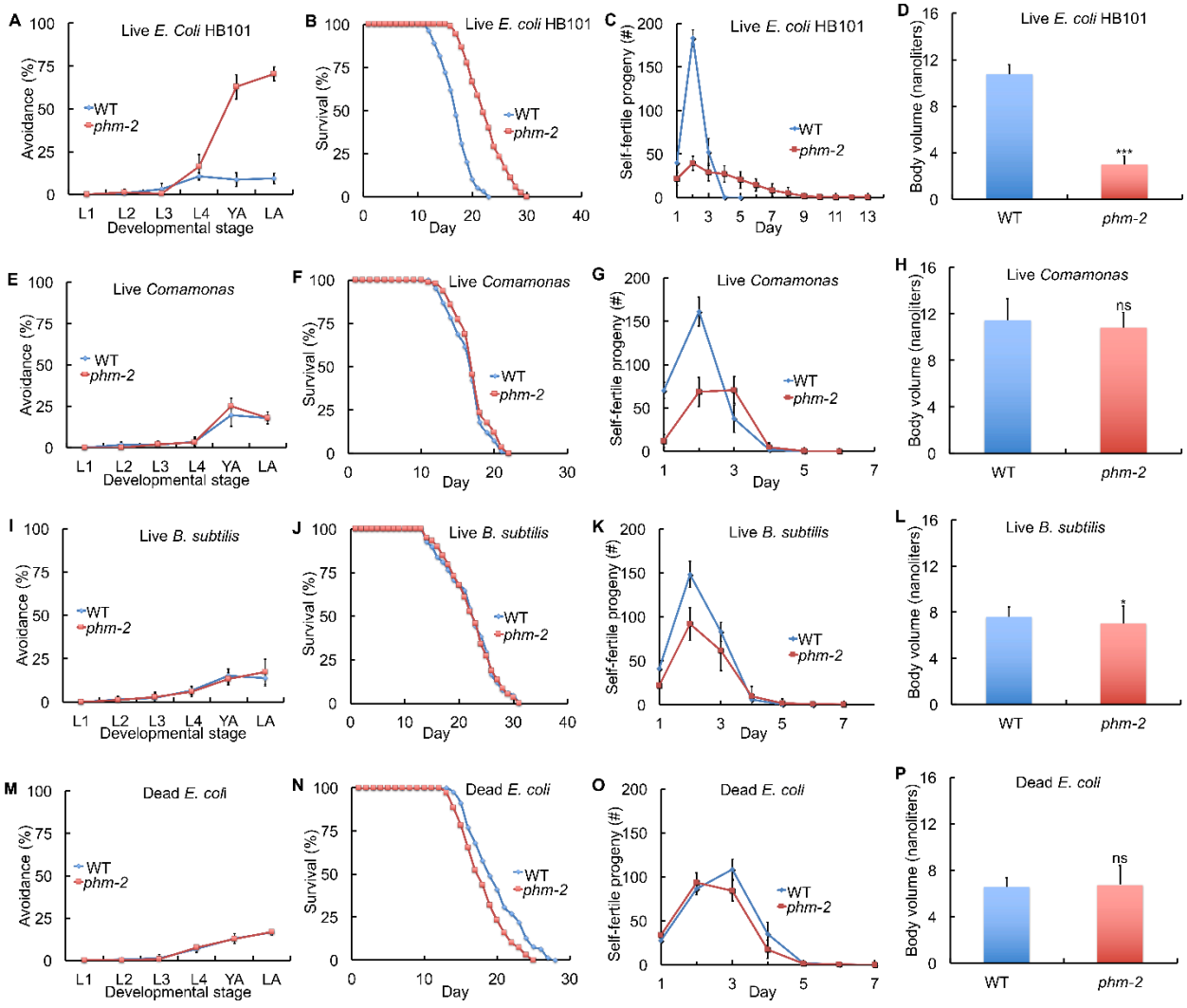

Figure 6. Live *E. coli* accumulation in *phm-2(lf)* mutants caused avoidance behavior, scrawny body morphology, and delayed aging.

WT or *phm-2(am117)* hermaphrodites were cultured with a small bacterial lawn as indicated. **(A, E, I, M)** Avoidance as in **Figure 1** - see **Table S2**. **(B, F, J, N)** Survival curves - see **Table S6** for summary statistics. **(C, G, K, O)** Self progeny production as in **Figure 1** (N=9-16 animals). **(D,**

H, L, P) Worm volume as in **Figure 1** (N=37-58 animals). ***, $P < 0.0001$; *, $P < 0.05$; ns, not significant, $P > 0.05$ by Student's *t*-test.

E. coli is not a natural food source for *C. elegans*, a soil-dwelling animal [419,420]. Furthermore, *E. coli* is a mild pathogen for older adult wild-type *C. elegans* [421]. We analyzed the soil bacteria *Comamonas (*strain DA1877*)* and *Bacillus subtilis,* because they are not pathogenic for *C. elegans*. Strikingly, *phm-2(lf)* mutant animals did not avoid these bacterial lawns and did not display the scrawny body morphology and delayed aging phenotypes (**Figure 6E-L, S2E-H, Table S2, S6**). Furthermore, *phm-2(lf)* mutant animals cultured on dead *E. coli* OP50 that was killed by UV light did not avoid the bacterial lawn or display the scrawny body morphology and delayed aging phenotypes (**Figure 6M-P, S2I-J, Table S2, S6**). Similar results were obtained when *E. coli* OP50 was killed by antibiotic treatment (**Figure S6A-B**). These results suggest that live *E. coli* accumulation is the cause of multiple phenotypes including avoidance behavior, scrawny body morphology, and delayed somatic and reproductive aging.

To investigate whether the extended lifespan of *phm-2(lf)* mutant animals was caused by an effect on development or an effect on adult animals, we compared *phm-2(am117)* animals cultured from embryo to adult on *Comamonas* or live *E. coli* and then transferred to live *E. coli* at adulthood. *phm-2(lf)* mutant animals displayed a similar lifespan in both cases, indicating that the bacterial food source during development does not strongly influence lifespan, whereas the bacterial food source during adulthood is critical (**Figure 4H, Table S6**).

eat-2(lf) animals displayed live *E. coli* accumulation that contributed to the extended lifespan phenotype.

eat-2(lf) mutants were identified by Avery (1993) based on feeding defects and were observed to have slow, strong, often regular pharyngeal pumping [372]. Lakowski and Hekimi

(1998) observed that *eat-2(lf)* mutants display extended longevity [371]. These results led to the model that the reduced pumping rate reduces food ingestion, causing caloric restriction and delayed aging. We confirmed that *eat-2(lf)* mutant animals displayed a reduced rate of pharyngeal pumping and a reduced rate of ingestion as measured by uptake of fluorescent beads compared to wild-type and *phm-2(lf)* animals (**Figure 2F, S1I**). Surprisingly, we observed that *eat-2(lf)* mutant animals accumulated live *E. coli* in the intestine, similar to *phm-2(lf)* mutants (**Figure 4C, S5G**). Based on these results, we hypothesized that *eat-2(lf)* mutant animals have defective pharynx grinder function that allows live bacteria to enter the intestine. This model predicts that *eat-2(lf)* mutant animals will display activation of innate immune genes and hypersensitivity to highly pathogenic bacteria. Indeed, *eat-2(lf)* mutants displayed higher levels of *clec-7*, *clec-60*, *clec-82*, *F53A9.8,* and *lys-5* transcripts compared to wild type, and in four cases these levels were reduced by culture on *Comamonas* (**Figure 4F, I, S5M-O**). Furthermore, *eat-2(lf)* mutant animals were hypersensitive to highly pathogenic *P. auruginosa* strain PA14 (**Figure 4D**). To test additional predictions of this model, we measured bacterial avoidance behavior and analyzed the ability of non-pathogenic food sources to rescue the *eat-2(lf)* aging phenotypes. When cultured on live *E. coli*, *eat-2(ad465)* animals displayed strong bacterial avoidance behavior as well as extended self-fertile reproduction, extended lifespan, and scrawny body morphology (**Figure 7A-D; Table S2, S6**). *eat-2(ad465)* animals cultured on dead *E. coli* displayed mild food avoidance behavior, a small decrease in reproduction, and a small extension of lifespan compared to wild type (**Figure 7E-H; Table S2, S6**). *eat-2(ad465)* animals cultured on *Comamonas* were almost indistinguishable from wild type, since they displayed no bacterial avoidance behavior and reproduction and lifespan returned to wild-type levels; they still displayed a slightly reduced body volume (**Figure 7I-L; Table S2, S6**). These results indicate

that *eat-2(lf)* mutations cause live *E. coli* accumulation in the intestine, which leads to activation of an innate immune response including bacterial avoidance behavior. Live *E. coli* accumulation appears to be the primary cause of *eat-2(lf)* aging phenotypes, since culture on nonpathogenic bacteria abrogated these defects even though it did not abrogate the slow pharyngeal pumping rate.

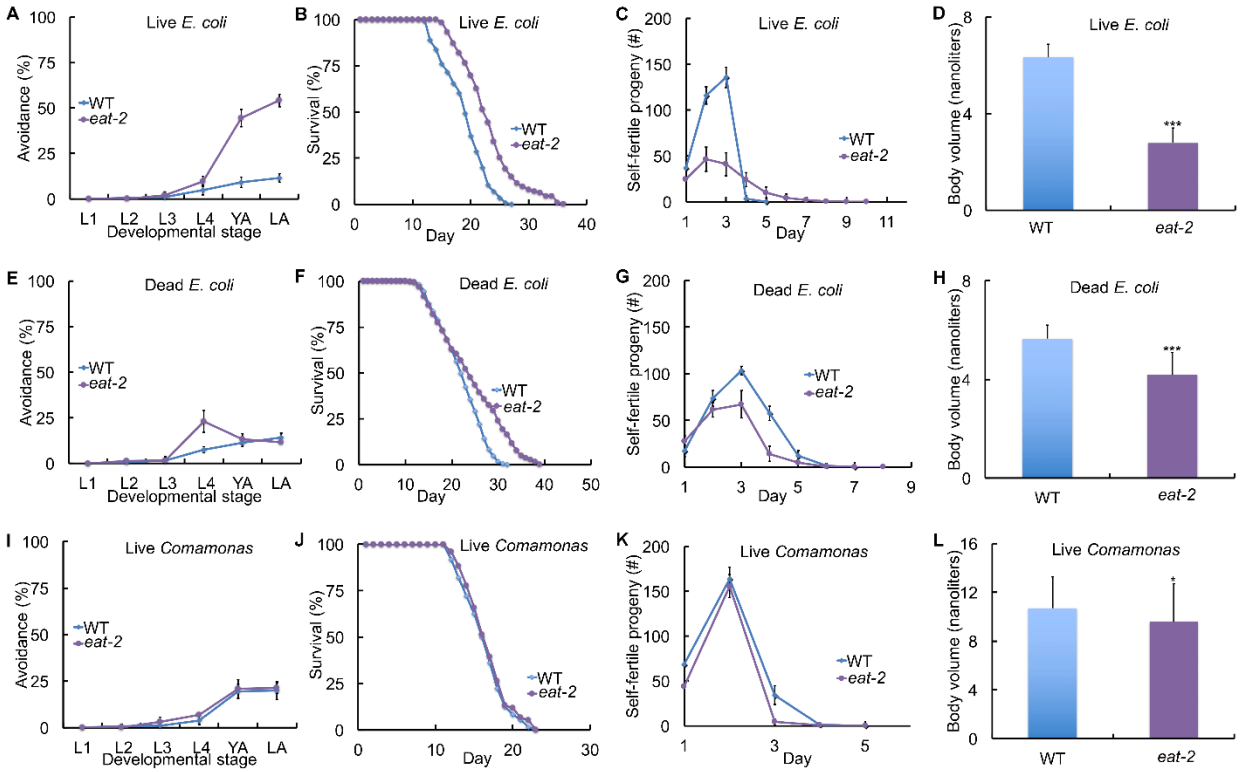

Figure 7. Live *E. coli* accumulation in *eat-2(lf)* mutants caused avoidance behavior, scrawny body morphology, and delayed aging.

WT or *eat-2(ad465)* hermaphrodites were cultured with a small bacterial lawn as indicated. **(A, E, I)** Avoidance as in **Figure 1** - see **Table S2**. **(B, F, J)** Survival curves - see **Table S6** for summary statistics. **(C, G, K)** Self progeny production as in **Figure 1** (N=9-12 animals). **(D, H, L)** Worm volume as in **Figure 1** (N=30-50 animals). ***, $P < 0.0001$; *, $P < 0.05$, by Student's *t*-test.

3.4 Discussion

Identification of *phm-2*, which encodes a SAFB protein conserved in mammals, in a forward genetic screen for delayed reproductive aging.

The main emphasis of aging research has been lifespan, which is determined by age-related degeneration of life-support systems. However, there is increasing appreciation that extending health span as well as lifespan is an important objective of medical research [422–424]. Reproductive aging is an important component of health span; in human females, age-related degenerative changes increase the rate of birth defects and cause a progressive loss of fertility that culminate in menopause [425,426]. Reproductive aging has been well documented in *C. elegans* and is characterized by a progressive decline in the rate of egg laying and increased disorganization of gonad morphology [427]. Whereas many genetic interventions have been reported to extend lifespan, only a subset influence reproductive aging [428–430].

To identify genes that influence reproductive aging, Hughes *et al.* (2011) performed a forward genetic screen for mated hermaphrodites that display an extended reproductive span[370]. The mutation *am117* caused a substantial extension of mated reproductive span, increased the number of progeny generated late in the reproductive period, and delayed age-related degenerative changes in the morphology of the hermaphrodite gonad [370]. Here we demonstrate that the *am117* mutation also influenced somatic aging, since it significantly extended mean and maximum lifespan. Furthermore, *am117* mutant animals displayed significantly increased stress resistance, a phenotype frequently associated with enhanced longevity [383]. The *am117* mutation delayed the age-related decline of body movement and pharyngeal pumping significantly, indicating the mutation affects somatic aging.

We used positional cloning approaches to identify *am117* as a nonsense mutation in F32B4.4. The *phm-2* gene was discovered and named by Avery (1993) [372], who identified the

ad538 and a*d597* alleles based on pharyngeal pumping defects and positioned these mutations on the right arm of chromosome I. Here we demonstrate that *ad597* is a 5 base pair deletion and *ad538* appears to be a gross rearrangement of F32B4.4, and thus we refer to this gene as *phm-2*. Consistent with this model, both *ad597* and *ad538* caused delayed reproductive and somatic aging, similar to the *am117* mutation. These results provide a molecular characterization of *phm-2*, and identify *am117*, *ad597,* and *ad538* as strong loss-of-function or null alleles based on the molecular analysis and the similar phenotypes.

The PHM-2 protein contains two highly conserved domains: a SAP domain and a RRM_SAF domain. The SAP domain is a putative DNA binding domain, whereas the RRM_SAF domain is a putative RNA recognition motif. Both domains are also contained in the human protein scaffold attachment factor B (SAFB). In humans, the SAFB family of proteins has three members: SAFB1, SAFB2, and SALMT. Human SAFB proteins are ubiquitously expressed in most tissues and localized in the nucleus. Similarly, we demonstrated that *C. elegans* PHM-2 is expressed in most or all *C. elegans* tissues and nuclear localized. The function of human SAFB is beginning to be revealed, but many important questions remain. SAFB appears to directly bind promoter regions and regulate transcription of many genes, including hsp27 and repression of the estrogen receptor [431–435]. These data indicate that human *SAFB* and *C. elegans phm-2* are homologous genes that are derived from a common ancestral gene. *phm-2* is the only SAFB homolog in *C. elegans*, as opposed to three proteins in humans that may have redundant functions. Therefore, *C. elegans* is a relevant and powerful model system to investigate this important gene family.

***phm-2* mutations cause a pharyngeal grinder defect that allows live bacteria to accumulate in the intestine, leading to an innate immune response that includes bacterial avoidance behavior.**

The identification of *phm-2* as the affected gene provided two key insights: (1) Avery (1993) showed that *phm-2* mutants have a defective pharynx grinder [372]; (2) subsequent studies of pathogenicity showed *phm-2* mutants are hypersensitive to pathogenic bacteria, because the grinder defect allows live bacteria to enter the intestinal lumen [373,374,376,436]. Thus, we hypothesized that in standard culture conditions, *phm-2* mutants allow live *E. coli* to enter the intestinal lumen, resulting in colonization by a weak pathogen that triggers an innate immune response that includes bacterial avoidance behavior.

Consistent with this model, we demonstrated that (1) Live *E. coli* accumulated in the intestine of *phm-2(lf)* mutant animals, as determined by fluorescently labeled bacteria; (2) *phm-2(lf)* mutants cultured on live *E. coli* displayed transcriptional changes typical of bacterial infections. Innate immune response genes such as C-type lectins, antimicrobial, and lysozyme genes were activated by live *E. coli* in *phm-2(lf)* mutant animals; (3) The HLH-30 transcription factor is the *C. elegans* homolog of mammalian TFEB, the master transcriptional regulator of the autophagy, and in worms HLH-30 protein accumulates in the nucleus in response to pathogenic bacteria [412]. Here we demonstrated that *phm-2(lf)* mutant animals displayed nuclear localization of HLH-30. A *hlh-30(lf)* mutation suppressed the increased transcript levels of multiple innate immune genes, although it did not suppress the bacterial avoidance behavior, indicating that *hlh-30* mediates part but not all of the immune response. An *hlh-30(lf)* mutation partially suppressed the *phm-2(lf)* lifespan extension, indicating that the immune response may contribute to the delayed aging phenotypes. An alternative interpretation is that *hlh-30* activity is necessary for the extended lifespan of *phm-2(lf)* mutants because it promotes autophagy in response to dietary

restriction. (4) Culture on non-pathogenic bacteria such as killed *E. coli*, live *B. subtilis* or live *Comamonas* abrogated the scrawny body morphology and aging phenotypes. Remarkably, on these food sources *phm-2(lf)* mutants closely phenocopied wild type. (5) Forced culture on live *E. coli* caused a shortened lifespan, suggestive of pathogenicity, consistent with previous studies [376]. Forced bacterial exposure was accomplished by using a large lawn that cannot be avoided or creating a double mutant with *tph-1*, which abrogates the bacterial avoidance behavior. These results indicate that the pharyngeal grinder defect allows live *E. coli* to enter the intestine and accumulate, triggering an innate immune response and bacterial avoidance behavior. If the lawn is small and can be avoided, then *phm-2(lf)* mutants display delayed somatic and reproductive aging. If the lawn is large and cannot be avoided, then *phm-2(lf)* mutants display a shortened lifespan due to bacterial pathogenicity. If the lawn consists of non-pathogenic bacteria, then animals do not display bacterial avoidance behavior, and the body morphology and lifespan are similar to wild type. Thus, the lifespan phenotype is conditional upon the level of bacterial pathogenicity: highly pathogenic bacteria result in a shortened lifespan, weakly pathogenic bacteria result in an extended lifespan, and non-pathogenic bacteria result in a wild-type lifespan.

The effects of pathogenic bacteria on *phm-2(lf)* mutants represent an interesting contrast to the effects on wild-type animals. Live *E. coli* are mildly pathogenic for older wild-type animals, which display age-related accumulation of bacteria in the intestine. This contributes to senescent death, since wild-type animals cultured on killed *E. coli* live several days longer than animals cultured on live *E. coli* [421,437,438]. By contrast, *phm-2(lf)* animals cultured on killed *E. coli* live several days shorter than animals cultured on live *E. coli.* In *phm-2(lf)* mutants, live *E. coli* enter the intestine of young animals, triggering bacterial avoidance behavior and an extended lifespan. In wild-type animals, live *E. coli* only enter the intestine of older adults that have

developed pharyngeal dysfunction; these older adults are mobility impaired and do not avoid bacteria, and the accumulation of live bacteria shortens the lifespan.

A role for innate immunity in promoting longevity is beginning to emerge, and our analysis of *phm-2* contributes to this area. *daf-2(lf)* mutants are long lived and resistant to bacterial pathogens, suggesting these two phenotypes might be related [438]. Furthermore, [416] showed that p38 MAPK pathway is important for innate immunity and contributes to the *daf-2(lf)* longevity phenotype. Our results show that colonization with pathogenic bacteria cause the lifespan extension of *phm-2* mutants, directly implicating the innate immune response in enhanced longevity. Part of the response is transcriptional activation of innate immune genes and nuclear localization of HLH-30, and part is bacterial avoidance behavior that leads to dietary restriction (**Figure 5J**). An alternative interpretation that is consistent with the data is that live bacteria in the intestine lead to dietary restriction by impairing nutrient acquisition or otherwise inhibiting growth. Further work is necessary to establish the relative contributions of the damage caused by bacterial colonization versus the innate immune response that consists of molecular and behavioral changes triggered by bacterial colonization and/or damage.

Bacterial lawn avoidance behavior reflects ongoing monitoring of bacterial pathogenicity and requires serotonin signaling.

Bacterial avoidance behavior is a fascinating phenomenon that must involve sensing the pathogenicity of the bacteria and mounting a locomotion response. The behavior was first described in wild-type *C. elegans* in response to highly pathogenic bacteria such as *S. marcescens* and *P. aeruginosa* [379,414]. In addition, the behavior has been documented in response to RNAi bacteria that reduce the activity of many different critical genes [380]. To characterize this behavior, we determined if prior exposure influences subsequent behavior, which might suggest that worms learn to avoid the bacteria. However, *phm-2(lf)* mutant animals initially cultured on

pathogenic live *E. coli* or non-pathogenic killed *E. coli* displayed similar behavior, indicating that bacterial avoidance behavior involves continuous sensing rather than learning. This sensing can occur quickly, since *phm-2(lf)* mutant animals transferred to live *E. coli* displayed measurable avoidance behavior within one hour.

Several innate immune genes and pathways have been linked to bacterial avoidance behavior, such as FSHR-1 [439], the NSY-1/SEK-1/PMK-1 p38 family MAP kinase [415], Toll-like receptor [414,440], and DAF-7/TGF-b [417]. Neuropeptide receptor 1 (*npr-1*) animals fail to avoid pathogen lawns of *P. aeruginosa* [417]. To investigate the role of these pathways in the *phm-2(lf)* bacterial avoidance behavior, we analyzed genetic interactions with *pmk-1*, *mlk-1*, *npr-1*, *daf-2*, *daf-16*, and several other signaling pathways. The results indicate these genes are not necessary for the *phm-2(lf)* bacterial avoidance behavior. Serotonin is a highly conserved neurotransmitter that is used in the gastrointestinal tract and implicated in the response to enteric pathogens. For example, serotonin signaling mediates the Garcia effect, where rats and mammals learn to avoid with activation of nausea [441]. To investigate the role of serotonin signaling, we used a *tph-1(lf)* mutation. *tph-1* encodes a tryptophan hydrolase enzyme critical for serotonin synthesis, and *tph-1(lf)* mutants are defective in serotonin signaling [442]. *tph-1* activity was necessary for the *phm-2(lf)* bacterial avoidance behavior, indicating serotonin signaling plays a critical role in sensing pathogenic bacteria or mounting the locomotion response. This observation is consistent with studies of RNAi bacterial avoidance, which also requires *tph-1* [380]. Furthermore, avoiding the highly pathogenic bacteria *P. aeruginosa* depends on *tph-1*, and continuous exposure to pathogenic bacteria increased transcription of *tph-1* and the biosynthesis of serotonin in ADF neurons that promote avoidance behavior [379]. Together, these results indicate that *phm-2(lf)*

bacterial avoidance behavior requires serotonin signaling but not several other innate immune response genes.

eat-2(lf) mutants displayed live bacterial accumulation in the intestine, activation of innate immunity, and bacterial avoidance that contribute to delayed aging.

Mutations in *eat-2* were identified by Avery (1993) based on a reduced rate of pharyngeal pumping [372]. Lakowski and Hekimi (1998) observed that mutations in multiple *eat* genes cause an extended lifespan and focused on *eat-2* because of the magnitude of the effect [371]. They hypothesized that the reduced pharyngeal pumping rate leads to reduced bacterial ingestion and thereby dietary restriction. *eat-2(lf)* mutants have been used frequently to analyze dietary restriction, resulting in about 70 publications to date. There are alternative methods to achieve dietary restriction in worms, such as dilution of the bacterial food [443]. A puzzling observation that has emerged is that different methods of dietary restriction cause somewhat different phenotypes [444].

Here we demonstrate that *eat-2(lf)* mutants accumulate live *E. coli* in the intestine, indicating they have a defect in pharynx grinder function as well as a reduced rate of pumping. Consistent with this observation, *eat-2(lf)* mutants displayed activation of innate immune genes, bacterial avoidance behavior, and hypersensitivity to highly pathogenic bacteria. Thus, we hypothesized that the *eat-2(lf)* aging phenotype is caused by a mechanism similar to the *phm-2(lf)* phenotype. Indeed, when *eat-2(lf)* mutants were cultured on nonpathogenic bacteria (dead *E. coli* or *Comamonas*), the bacterial avoidance, scrawny body morphology, and longevity phenotypes were all suppressed. Similarly, [445] previously observed that culture on *Comamonas* suppressed the *eat-2* scrawny and extended lifespan phenotypes. Thus, although *eat-2(lf)* mutants have a reduced rate of pharyngeal pumping, the rate is still adequate for full nutrition when these animals do not avoid the bacterial lawn. These observations have implications for the mechanism

of *eat-2* longevity extension and the interpretation of studies that used this reagent. Both *phm-2* and *eat-2* mutants ingest live *E. coli*, which appears to be the root cause of the aging phenotypes. In principle, the aging phenotypes could be caused by damage from live bacteria, the innate immune response, the bacterial avoidance behavior that leads to dietary restriction, or a combination of these effects. Thus, *eat-2* and *phm-2* mutants are not examples of simple dietary restriction (**Figure 5J**). These observations may explain why *eat-2* mutants have been shown to behave differently from dietary restriction achieved by dilution of the bacterial food.

3.5 Materials and Methods

KEY RESOURCES TABLE

REAGENT or RESOURCE	SOURCE	IDENTIFIER
Bacterial and Virus Strains		
Escherichia coli OP50	CGC	OP50
Escherichia coli OP50-GFP	CGC	*E. coli* OP50-GFP
Pseudomonas aeruginosa PA14	Laboratory of Dennis Kim	PA14
Comamonas DA1877	Laboratory of Michael Nonet	DA1877
Escherichia coli HB101	Author's laboratory	HB101
Baccillus subtilis	Author's laboratory	PY79
Ahringer RNAi Libraries in *E. coli* HT115 (D3)	Source BioScience	N/A
Chemicals		
DiO dye	Thermofisher	DiO
Latex microspheres	Polysciences Inc.	Catalog #18242
DAPI	Vector Laboratories	H-1200
Fluorodeoxyuridine (FUdR)	Sigma-Aldrich	F0503
Experimental Models: Organisms/Strains		
C. elegans: WT wild-type	CGC	WT
C. elegans: *phm-2(am117) I*	Author's laboratory	WU740
C. elegans: *phm-2(ad538) I*	CGC	DA538
C. elegans: *phm-2(ad597) I*	CGC	DA597
C. elegans: *daf-16(mu86) I*	CGC	CF1038
C. elegans: *daf-2(e1370) III*	CGC	CB1370
C. elegans: *isp-1(qm150) IV*	CGC	MQ887
C. elegans: *eat-2(ad465) II*	CGC	DA465

C. elegans: *eat-2(ad1116) II*	CGC	DA1116
C. elegans: *aak-2(ok524) X*	CGC	RB754
C. elegans: *rict-1(mg360) II*	CGC	KQ6
C. elegans: *rsks-1(ok1255) III*	CGC	RB1206
C. elegans: *hlh-30(tm1978) IV*	Laboratory of Mitani	TM1978
C. elegans: *tph-1(mg280) II*	CGC	MT15434
C. elegans: *pmk-1(km25) IV*	CGC	KU25
C. elegans: *mlk-1(ok2471) V*	CGC	RB1908
C. elegans: *npr-1(ur89) X*	CGC	IM222
C. elegans: *raga-1(ok386) II*	CGC	VC222
C. elegans: *daf-16(mgDf47);daf-2(e1370)*	CGC	GR1309
C. elegans: *acIs101[(F35E12.5:: gfp);pRF4(rol-6(su1006))]*	CGC	AY101
C. elegans: *agIs17[irg-1::GFP; myo-2::mCherry]*	CGC	AU133
C. elegans: *phm-2(am117) I* (16 times)	This study	WU1686
C. elegans: *phm-2(ad538) I* (3 times)	This study	WU1678
C. elegans: *phm-2(ad597) I* (3 times)	This study	WU1679
C. elegans: *daf-16(mu86) phm-2(am117)*	This study	WU1528
C. elegans: *phm-2(am117);daf-2*	This study	WU1683
C. elegans: *daf-16 phm-2(am117);daf-2*	This study	WU1526
C. elegans: *phm-2(am117);isp-1*	This study	WU1542
C. elegans: *phm-2(am117);eat-2(ad1116)*	This study	WU1543
C. elegans: *phm-2(am117);aak-2*	This study	WU1734
C. elegans: *phm-2(am117);rict-1*	This study	WU1642
C. elegans: *phm-2(am117);rsks-1*	This study	WU1643
C. elegans: *phm-2(am117);hlh-30*	This study	WU1527
C. elegans: *phm-2(am117);pmk-1*	This study	WU1678
C. elegans: *phm-2(am117);mlk-1*	This study	WU1688
C. elegans: *phm-2(am117);npr-1*	This study	WU1668
C. elegans: *phm-2(am117);tph-1*	This study	WU1669
C. elegans: *phm-2(am117);raga-1*	This study	WU1855
C. elegans: *phm-2(am117); acIs101*	This study	WU1677
C. elegans: *phm-2(am117); agIs17*	This study	WU1676
C. elegans: *phm-2(am117);(hlh-30p::hlh-30::RFP);pRF4(rol-6)]*	This study	WU1798
C. elegans: *amEx315[(phm-2p::gfp); pRF4(rol-6)],* Genetic background WT	This study	WU1594
C. elegans: *amEx321[(phm-2p::phm-2::stop codon::gfp);pRF4(rol-6)],* Genetic background *phm-2(am117)*	This study	WU1684
C. elegans: *amEx322[(phm-2p::phm-2::stop codon::gfp);pRF4(rol-6)],* Genetic background *phm-2(am117)*	This study	WU1685

C. elegans: *amEx324[(phm-2p::phm-2::stop codon::gfp);pRF4(rol-6)],* Genetic background *phm-2(am117)*	This study	WU1696
C. elegans: *amEx328[(phm-2p::phm-2::stop codon::gfp);pRF4(rol-6)],* Genetic background *phm-2(am117)*	This study	WU1700
C. elegans: *amEx331[(phm-2p::phm-2::stop codon::gfp);pRF4(rol-6)],* Genetic background *phm-2(am117)*	This study	WU1703
C. elegans: *amEx320[(phm-2p::phm-2::gfp); pRF4(rol-6)],* Genetic background *phm-2(am117)*	This study	WU1671
C. elegans: *amIs13(hlh-30p::hlh-30::RFP);pRF4(rol-6)],* Genetic background *hlh-30(tm1978)*	This study	WU1796
Oligonucleotides quantitative reverse transcription-PCR		
ama-1 Forward: 5′ATCGGAGCAGCCAGGAACTT	This study	N/A
ama-1 Reverse: 5′ GACTGTATGATGGTGAAGCTGG	This study	N/A
phm-2 Forward: 5′ CCATCTCGTCCAGAGTTGATAC	This study	N/A
phm-2 Reverse: 5′ GAGCTCCGAAGTGCTAATGT	This study	N/A
clec-7 Forward: 5′ GGCCGGCTTCAAATGTTTATC	This study	N/A
clec-7 Reverse: 5′ TAGTGGACATTACCATGCAGTC	This study	N/A
clec-60 Forward: 5′ CTGAGCCAAGAACCACAAGA	This study	N/A
clec-60 Reverse: 5′ GAAGTGCTGACTGACGAAAGA	This study	N/A
clec-82 Forward: 5′ TTCCGCCGTTGTCTGTTT	This study	N/A
clec-82 Reverse: 5′ CACTTGAGCTGGCTAGATTGA	This study	N/A
F53A9.8 Forward: 5′GTTCACCATGCAGGAGATCA	This study	N/A
F53A9.8 Reverse: 5′ TCTCCATCTTGGTGTTGAGTTT	This study	N/A
lys-5 Forward: 5′ CGGGAAGTGTAGATACTGTTGG	This study	N/A
lys-7 Reverse: 5′ AGAGACGCCTTAACTTGGTTAG	This study	N/A
Antibodies		
Primary polyclonal rabbit anti-GFP	Laboratory of Swathi Arur	Anti-GFP antibody

Secondary goat anti-rabbit Alexa-594 antibody	Life Technologies	A11012
Software and Algorithms		
Graph, Result and Statistical analysis	Microsoft Office	Excel, Powerpoint
Result and Statistical analysis	Astatsa	http://astatsa.com
Result and Statistical analysis	OASIS	https://sbi.postech.ac.kr/oasis/
Image editing	Adobe	Photoshop and illustrator
Image editing	Fiji ImageJ	https://fiji.sc
WormSizer	Laboratory of L. Baugh	https://github.com/bradtmoore/wormsizer

CONTACT FOR REAGENT AND RESOURCE SHARING

Further information and requests for resources and reagents should be directed to and will be fulfilled by the Lead Contact, Kerry Kornfeld (kornfeld@wustl.edu).

EXPERIMENTAL MODEL AND SUBJECT DETAILS

Caenorhabditis elegans and Bacterial strains

C. elegans were cultured on 6 cm Petri dishes containing NGM agar. To produce a small lawn of live bacteria, we pipetted 200 µL of an overnight culture of *Escherichia coli* strains OP50 or HB101, *Baccillus subtilis*, or *Comamonas* DA1877 and incubated overnight. To produce a small lawn of dead bacteria, we seeded NGM dishes with live *E. coli* OP50, cultured for 24 hours, and exposed to ultraviolet light by placing dishes in a UV Stratalinker 2400 for 15 minutes at maximum power. Bacterial killing was evaluated by inoculating LB medium with UV-treated bacteria; lack of growth at 37°C confirmed effective killing [437]. The wild-type strain was N2 Bristol. The identification and initial characterization of *phm-2*(*am117*) was previously described [370]. *phm-2*(*am117*) was outcrossed to WT up to 16 times. The *phm-2* alleles *ad538* and *ad597* were outcrossed to WT 3 times. The genotypes of all double and triple mutant strains

generated were confirmed by PCR and/or DNA pyrosequencing (Qiagen PSQ96). Additional alleles and strains used in the study are listed in the above Table.

METHOD DETAILS

RNA interference (RNAi)

RNA interference was performed by feeding bacteria that express dsRNA (RNAi bacteria), as described by [446]. Briefly, *E. coli* HT115 bacteria with the control plasmid (L4440) or a plasmid encoding *pha-4* were obtained from the Ahringer library [447]. The identity of the clones was confirmed by DNA sequencing. Single colonies of RNAi bacteria were isolated from LB dishes containing 50 μg/mL ampicillin and used to inoculate overnight starter cultures in LB medium containing 50 μg/mL ampicillin. The starter cultures were used to inoculate larger cultures at 1:100 dilution in LB medium containing 50 μg/mL ampicillin and grown for 6 hours at 37°C. RNAi bacteria were seeded onto NGM agar dishes containing 1 mM isopropyl β-d-1-thiogalactopyranoside (IPTG) and 50 μg/mL carbenicillin. L1 stage larvae were transferred to RNAi dishes and analyzed after reaching adulthood.

Identification of *am117* by whole genome sequencing

To identify the *am117* molecular lesion, we generated genomic DNA from the *am117* strain, performed whole genome sequencing, and compared the results to the WT sequence. In the region close to *unc-75* (+9.3 on chromosome I) where *am117* was positioned by Hughes et al. (2011) [370], three mutations were detected that affect the coding sequence of *F32B4.4, Y53C10.5* and *F56H6.9*.

Plasmid construction and transgenic strain generation

To analyze transcription of *phm-2* isoform a (F32B4.4a), we PCR amplified the 496 bp region between the start codon of *phm-2* and the 3' end of the adjacent upstream gene from genomic DNA of wild-type animals. This promoter region was inserted into plasmid pDG218 to generate pSK1 [*phm-2p::gfp::unc-54 3'UTR*]. Briefly, pDG218 was derived from pBluescript SK+ (Stratagene) by inserting the coding region for green fluorescent protein (GFP) and the *unc-54* 3′-UTR, both amplified from pPD95.77, a gift from A. Fire (Stanford University, Palo Alto, CA).

To analyze expression of PHM-2 protein, we PCR-amplified full length, wild-type *phm-2* coding sequence (3222 bp) from cDNA and ligated into pSK1 to generate pSK2 [*phm-2p::phm-2::stop codon::gfp::unc-54 3'UTR*]. pSK2 encodes PHM-2 protein but the *gfp* coding sequence is out-of-frame following the stop codon of *phm-2.* The stop codon in pSK2 was removed by site directed mutagenesis (New England Biolabs) to generate pSK3 [*phm-2p::phm-2::gfp::unc-54 3'UTR*]. *pSK3* encodes a PHM-2::GFP fusion protein.

Plasmid DNA was prepared using a Miniprep column (Qiagen) and quantified using a Nanodrop (Thermo). Transgenic animals were generated by injecting pSK1 into wild-type hermaphrodites and pSK2 or pSK3 into *phm-2(am117)* hermaphrodites. All injections were performed with the dominant Rol marker pRF4 [448]. We selected independently derived Rol self-progeny that transmitted the Rol phenotype. These transgenes formed extrachromosomal arrays, since the Rol phenotype was transmitted to only a sub-set of the self-progeny.

To measure the expression pattern of HLH-30, we PCR amplified a 1497 bp fragment containing the coding sequence for W02C12.3a from pDONR201 (Dharmacon) and a 2000 bp fragment containing W02C12.3a promoter (Dharmacon) and subcloned these into the

pBlueScript SK+ vector pDG219 to create pJM18 [*hlh-30p::hlh-30::rfp*]. To generate transgenic animals with an extrachromosomal array, we injected pJM18 and pRF4 into *hlh-30(tm1978)* worms. The extrachromosomal array was integrated into the genome by UV irradiation (UV Stratalinker 2400), and we selected RFP positive worms with a roller phenotype that segregated only transgenic animals.

We used standard genetic techniques to construct strains with *phm-2(am117)*; HLH-30::RFP. Eggs were allowed to develop into two-day old adults on live *E. coli* OP50 and live *Comamonas* bacteria, and animals were paralyzed with 1% sodium azide and mounted on a 2% agarose pad for imaging. Images were captured using the 10X objective of a Zeiss Axioplan fluorescent compound microscope equipped with a Zeiss AxioCam MRm digital camera. More than 100 animals were analyzed in three biological replicates.

Measurement of lifespan, reproduction, pharyngeal pumping, and body movement

Studies of lifespan were begun on day zero by placing L4 stage hermaphrodites on a Petri dish. Hermaphrodites were transferred to a fresh Petri dish daily during the reproductive period (approximately the first ten days) to eliminate self-progeny and every 2-3 days thereafter. Each hermaphrodite was examined daily using a dissecting microscope for survival, determined by spontaneous movement or movement in response to prodding with a platinum wire. Dead worms that displayed matricidal hatching, vulval extrusion, or desiccation due to crawling off the agar were excluded from the data analysis. One exception to this data analysis approach was that animals that displayed matricidal hatching were not excluded for experiments shown in **Table S6** rows 21-25. Mean lifespan was calculated as the number of days from the L4 stage to the last day a worm was observed to be alive.

For the experiment described in **Figure 4H**, WT or *phm-2(am117)* embryos were hatched on NGM agar dishes seeded with 200 µL of either *E. coli* OP50 or *Comamonas* DA1877. At adulthood, worms were transferred to plates seeded with *E. coli* OP50 for the remainder of their lifespan.

Daily reproduction, brood size, pharyngeal pumping, and body movement were determined as described in [449]. Briefly, to analyze progeny production, one L4 stage hermaphrodite was placed on a Petri dish (day one) and transferred to a fresh dish daily until at least 4 days without progeny production. Progeny were counted after two days. Pharyngeal pumping was counted during a 10 second interval using a dissecting microscope. Body movement was assayed by observation for 20 seconds using a dissecting microscope. Petri dishes were tapped to stimulate animals to move before scoring.

Measurement of heat stress resistance and dauer formation

Thermotolerance assays were performed as described by McColl *et al.* (2010) [450]. Briefly, WT and *phm-2(am117)* L4 stage hermaphrodites were cultured at 20°C for one day, adults were transferred to 35°C and scored as alive or dead based on responding to prodding with a platinum wire after either 9 or 12 hours.

Dauer formation was assayed as described by Kimura *et al.* (1997) [388]. To analyze dauer formation of *daf-2(e1370)* and *phm-2(am117); daf-2(e1370)* animals, we transferred eggs to 20°C, 22.5°C and 25°C and scored dauer larvae after culturing 3-5 days.

Measurement of worm size

To measure animal size, we captured images of live adult animals four days after the L4 stage on unseeded NGM dishes using a Leica M80 microscope with a 1.25X objective and an IC80 HD camera. Images were batch-processed with IrfanView 4.37 or ImageJ, and worm volume was automatically measured using the WormSizer 1.2.0 plugin for Fiji ImageJ 1.49n, as described in [451]. Roller transgenic animals were paralyzed in a drop of sodium azide on unseeded NGM dishes to prevent the head and tail from touching.

Measurement of bacterial avoidance behavior

We prepared small, uniform circular lawns by pipetting 100 µL of overnight cultures of various bacteria (live *E. coli* OP50 or HB101, live *B. subtillis*, live *Comamonas* DA1877,) on the center of NGM dishes and allowing at least one day to dry. To produce a small lawn of dead bacteria, we seeded NGM dishes with 100 µL of live *E. coli* OP50, cultured for 24 hours, then exposed to ultraviolet light. The next day 50-80 eggs were transferred on top of the bacterial lawn without disturbing or spreading the lawn. Each animal was scored as inside or outside the lawn (Avoidance=N_{out}/N_{total}) at larval stages (L1 to L4) and one (YA) and two (LA) day old adults. For antibiotic dishes, live *E. coli* OP50 bacteria was seeded onto NGM agar dishes containing 12.5 µg/mL tetracycline or 50 µg/mL kanamycin. To generate lawns with a mixture of bacteria, we grew *E. coli* OP50 and *Comamonas* DA1877 overnight, created mixed cultures of various ratios (100:0, 10:90, 50:50, 90:10 and 0:100), and seeded the mixed culture on NGM dishes. To determine whether bacterial secondary metabolites modulate avoidance behavior, we grew *E. coli* OP50 and *Comamonas* DA1877 overnight, pelleted the bacteria at 10,000 RPM for 20 minutes, collected the supernatant, and filtered the supernatant using a 0.22 µm syringe filter.

To generate odorant signals, we cut a square NGM block with either *E. coli* OP50 or *Comamonas* DA1877, attached the block to the inside of a lid, placed the lid over dishes seeded with *E. coli* OP50 or *Comamonas* DA1877, and wrapped the dishes with parafilm. For studies of the pathogenic bacteria *P. aeruginosa* strain PA14, WT and *phm-2(am117)* eggs were allowed to develop to the L4 stage on live *E. coli* OP50, washed 2-3 times in S basal and transferred to a *P. aeruginosa* strain PA14 lawn on NGM dishes. Animals were scored for avoidance after 24 hours.

To determine if experience influences bacterial lawn avoidance behavior, we placed 50-80 eggs on a "training dish" containing a small bacterial lawn (live *E. coli* OP50, live *Comamonas* DA1877, or UV-killed *E. coli* OP50). Young adults (one day after L4 stage) were washed 2-3 times in S basal, transferred to a "testing dish" with a small bacterial lawn and scored as inside or outside the lawn every hour.

Measurement of bacterial lawn choice behavior

To analyze the preference between two bacterial lawn options, we generated dishes with two small lawns by pipetting 90 µL of overnight cultures on either side of a NGM dish. 50-60 eggs were placed on a "training" dish with a small bacterial lawn (live *E. coli* OP50, live *Comamonas* DA1877, or dead *E. coli* OP50). Young adults (one day after L4 stage) were washed 2-3 times in S basal, transferred to a "testing dish" with two small bacterial lawns, and scored as inside lawn 1, inside lawn 2, or outside both lawns after 24 hours.

Measurement of matricidal hatching

We prepared NGM dishes with a large lawn (400 µL of live *E. coli* OP50 spread over the entire surface) or a small lawn (100 µL of live *E. coli* OP50 spotted in the center); dishes were

allowed to dry at least one day. To quantify the prevalence of matricidal hatching, we placed 40-60 eggs (WT or *phm-2(am117))* on these dishes and allowed them to develop to the L4 stage (defined as day 0). Hermaphrodites were transferred to a fresh dish daily during the reproductive period (approximately the first fifteen days) to eliminate self-progeny. Using a dissecting microscope, each hermaphrodite was examined daily for survival, determined by spontaneous movement or movement in response to prodding with a platinum wire. Dead hermaphrodites that displayed live progeny inside the body were scored as matricidal hatching.

Measurement of survival and induction of reporter genes on *P. aeruginosa*

Slow killing was assayed as described [452,453]. Briefly, the *P. aeruginosa* PA14 strain was cultured in LB medium, seeded on 6 cm Petri dishes with 50 µM FUdR, incubated for 24 hours at 37°C and then for 24 hours at room temperature. 20-30 L4 stage hermaphrodites were transferred to these dishes, incubated at 25°C, and scored for survival every 12 hours. Experiments were repeated at least five times.

Two transgenic strains had pathogen responsive promoters driving GFP: *F35E12.5 (acIs101[(F35E12.5::gfp);pRF4(rol-6(su1006))],* and *irg-1* (*agIs17[irg-1::GFP; myo-2::mCherry]*) [416,453]. One transgenic strain had the *phm-2* promoter driving GFP *(amEx315[(phm-2p::gfp); pRF4(rol-6)]*. To measure GFP induction, we placed 30–40 young adult hermaphrodites (one day past the L4 stage) on SK dishes with *P. aeruginosa* PA14 and cultured for 24 hours. Animals were washed 3 times with M9 and placed on a large pre-made 1.5% agarose pad with a 20 µL drop of 1 M sodium azide. A rectangular coverslip was applied, and slides were imaged on a Zeiss Axioplan fluorescent compound microscope equipped with a Zeiss AxioCam MRm digital camera using a 10x objective.

Measurement of fluorescent microsphere ingestion

The protocol was modified from [454]. Briefly, Fluoresbrite Plain YG 45.58µm +/-0.80µm solid latex microspheres in water (Polysciences Inc. 9003-53-6, catalog #18242, lot# 589756) were dissolved in 90% ethanol at a concentration of $3.64x10^{10}$ and diluted 1:1000 in S-basal. 10^8 microspheres were applied to 60 mm NGM dishes and spread with a flame-sterilized glass spreader. The S-basal was allowed to soak into the NGM overnight and protected from light. Worms were washed 3-4 times in a tabletop microcentrifuge with 1 mL of S-basal + 0.1% Tween-20 (SBTw) to remove bacteria, and then applied to a dish. Dishes were incubated with open lids for 15 minutes in the dark, and then 1 mL of 50mM sodium azide in SBTw was added to immobilize the worms. Worms were transferred to an Eppendorf tube and pelleted by centrifugation; the supernatant was removed, and ice-cold methanol was added for 10 minutes. Worms were washed once with SBTw and applied to large pre-made 1.5% agarose pads on glass slides with a rectangular coverslip. Slides were imaged on a Zeiss Axioplan fluorescent compound microscope equipped with a Zeiss AxioCam MRm digital camera using a 5x objective.

Measurement of GFP-labeled *E. coli* in the intestinal lumen

To measure intact bacteria in the intestine, we utilized a strain of *E. coli* labeled with GFP obtained from the CGC that was cultured overnight with 50 µg/mL ampicillin at 37 °C with shaking [373]. Feeding experiments were performed as described above for microsphere ingestion, except that live bacteria were used to seed NGM dishes (100 µL in the center of a dish, or 400 µL spread across the entire surface of a dish), and worms were allowed to feed for 24 hours.

Based on the fluorescent images, we defined three patterns: GFP fluorescence throughout the intestine (full), in some but not all the intestine (partial), and not strongly in the intestine (none).

To measure bacterial ingestion in worms treated with *pha-4* RNAi, we allowed worms to hatch in S-basal + 0.1% cholesterol. L1 animals were transferred to NGM agar dishes containing 1 mM isopropyl β-d-1-thiogalactopyranoside (IPTG) and 50 μg/mL carbenicillin and seeded with *E. coli* HT115 bacteria with either the control plasmid (L4440) or a plasmid encoding *pha-4*. At adulthood, worms were transferred to RNAi dishes seeded with a bacterial solution containing 25% by volume GFP expressing *E. coli* OP50 and 75% by volume control (L4440) or *pha-4* RNAi *E. coli* bacteria. Worms were cultured for 24 hours before being washed and visualized as previously described.

Measurement of DiO staining

To stain animals with DiO, we followed the protocol of [455]) with slight modifications. Briefly, ~2 mg DiO was dissolved in 1mL dimethyl formamide and then diluted in M9 to a final concentration of 20 μg/mL. L4 stage animals were picked into M9, washed once with M9, incubated in DiO solution for 4 hours, washed 3 times with M9, and applied to a large pre-made 1.5% agarose pad with a 20 μL drop of 1 M sodium azide. After applying a rectangular coverslip, the slides were imaged on a Zeiss Axioplan florescent compound microscope equipped with a Zeiss AxioCam MRm digital camera using a 40x objective. *osm-3(p802)* and N2 animals were used as positive and negative controls, respectively, for the Dyf-d phenotype.

Protein imaging *in vivo*

To perform live imaging of fluorescent proteins, we picked >20 animals into S-basal + 4 mM levamisole and placed the animals onto a large pre-made 1.5% agarose pad.

To image intact worms with antibodies, we picked >20 animals into PBS + 0.1% Tween-20 (PBSTw), washed with PBSTw, fixed in 3% PFA (EM grade) for 30-60 minutes, washed twice with PBSTw, incubated with DAPI (1:1000; 0.1 mg/mL) for 5-10 minutes, and mounted the animals on a large pre-made 2.5% agarose pad in DABCO in 90% glycerol. The slide was allowed to dry overnight and then imaged using a PerkinElmer spinning-disc confocal microscope with a 40x or 63x oil-immersion lens.

To image dissected worms with antibodies, we picked >50 animals into PBS, washed twice with PBS, immobilized with levamisole, and dissected by cutting at the pharynx or at the tail with two 25G needles. Worms were fixed in 3% PFA for 10 minutes, post-fixed in ice-cold (-20°C) high-grade methanol (Fisher) for 2 hours, and washed 3 times in PBSTw. Primary polyclonal rabbit anti-GFP antibody (gift from Swathi Arur) was applied at 1:100 in 30% Goat Serum overnight at room temperature. After 3 PBSTw washes, secondary goat anti-rabbit Alexa-594 antibody was applied at 1:400 in 30% Goat Serum overnight at 4°C. After 3 PBSTw washes and a 5 minute DAPI incubation, worms were applied to a large pre-made 2.5% agarose pad in DABCO in 90% glycerol. The slide was allowed to dry overnight and then imaged with a Perkin Elmer spinning-disc confocal microscope using a 40x, 63x, or 100x oil-immersion lens.

Pharynx morphology

To image pharynx morphology, we washed WT and *phm-2(am117)* young adult animals 2-3 times in S basal, paralyzed the animals with 1% sodium azide, mounted the animals on 2%

agarose pads and covered with a coverslip. DIC images were acquired using a Zeiss Axioplan fluorescent compound microscope equipped with a Zeiss AxioCam MRm digital camera.

Quantitative real-time PCR (RT–PCR)

To generate synchronous populations of worms for RNA extraction, we allowed WT, *phm-2(am117), eat-2(ad465), hlh-30(tm1978)* and *phm-2(am117); hlh-30(tm1978)* adults to lay eggs for 4-6 hours at 20°C on NGM dishes seeded with live *E. coli* OP50. Eggs were allowed to develop until 12 hours after the L4 stage. These synchronized young adults were washed and collected for RNA isolation. RNA analysis was performed as previously described with slight modifications [456]. Briefly, RNA was isolated using a Trizol (Invitrogen) and chloroform extraction (GlycoBlue was used to aid precipitation in isopropanol), treated with DNAseI, and further purified using an RNeasy spin column (Quiagen). RNA was quantified using a NanoDrop and diluted in nuclease-free water. cDNA was synthesized using either High Capacity cDNA Reverse Transcription kit (Applied Biosystems) or iScript cDNA Synthesis Kit (BioRad Laboratories, Hercules, CA). Quantitative, real-time PCR was performed using an Applied Biosystems Step One Plus Real-Time PCR system and either SYBR green master mix (Applied Biosystems) or iTaq Universal SYBR Green Supermix (BioRad Laboratories, Hercules, CA). mRNA fold change was calculated using the comparative CT method [457] by comparing mRNA levels of the gene of interest with mRNA levels of the reference gene *ama-1*. A minimum of three biological replicates, each with three technical replicates, were performed.

Statistical Analysis

All data from RT-PCR experiments and measurement of brood size, dauer formation, heat stress resistance, lifespan and bacterial avoidance behavior were analyzed using the two-tailed Student's *t*-test for samples with unequal variances by using Excel. For comparisons of more than two groups, an ANOVA (http://astatsa.com) was used. P-values less than 0.05 were considered statistically significant**.** To determine whether the choice of a statistical test for lifespan affected the conclusions, we used the log-rank (Mantel-Cox) method to analyze a subset of the lifespan experiments https://sbi.postech.ac.kr/oasis/ [458]. Both tests produced similar P-values.

Chapter 4: Expression of human amyloid beta peptide increases survival in a pathogen-hypersensitive mutant

4.1 Abstract

Alzheimer's Disease (AD) is a neurodegenerative condition that is a major cause of debilitation and death worldwide; aging is a primary contributing factor to the development and progression of AD. The suggested cause of AD symptoms is aberrant accumulation of the amyloid beta (Aß) peptide into insoluble plaques within the brain. Despite decades of research, however, our understanding of AD pathogenesis remains limited. Specifically, the nature of Aß and its role in the brain, if any, is poorly understood. Recently, new evidence has emerged suggesting that Aß functions as a component of the innate immune system, and that AD results from aberrant amyloid aggregation in response to bacterial, fungal, and viral infection within the brain. Here, we use a pathogen hypersensitive *C. elegans* model, *phm-2(am117),* to measure the antimicrobial properties of Aß. We expressed the amyloidogenic $A\beta_{1-42}$ isoform in worm muscle tissue and measured its effect on pathogenic infection by *E. coli* OP50. Aß expression rescues pathogen-induced death in *phm-2* mutant animals and reduces matricidal hatching, a common phenotype of pathogen infection. Our results suggest that Aß functions as an antimicrobial peptide to reduce the severity of pathogen infection.

4.2 Introduction

Alzheimer's Disease (AD) is a debilitating neurodegenerative condition characterized by cognitive decline in memory, judgement, reasoning, and orientation that affects more than 47 million people worldwide [459]. Current evidence suggests that the proximal cause of AD

symptoms is aberrant accumulation of the amyloid beta (Aß) peptide into insoluble inclusions within the brain [460–463]. Aß plaques are more common and severe in patients with AD [464–467], and heritable mutations in Aß and the amyloid precursor protein (APP) cause early-onset AD [460,468,469]. However, despite decades of dedicated research, many elements of this interaction are unknown, severely hindering efforts to search for cures or treatments. It is unknown how the size or distribution of amyloid plaques in the brain influence AD development; to date, anti-amyloidogenic drugs have had little success in reducing AD symptoms despite successful clearance of amyloid plaques, suggesting a more complex interaction between AD and Aß [470–472]. Finally, the native function of the Aß peptide itself is unknown. Early research identified it as an inactive cleavage product resulting from the post-translational cleavage of APP, and thus ascribed no function or activity to it [473].

However, recent advances in the field have promoted the idea that Aß is actually a component of the innate immune system, and that its function is to bind to, and prevent the cellular invasion of, viral, bacterial, and fungal pathogens in the brain [474–479]. This has been dubbed the Antimicrobial Peptide Hypothesis: Aß is expressed in the brain in response to pathogen invasion, wherein Aß peptides aggregate around the pathogen, preventing its attachment to cell membranes; the immune system then clears these aggregates along with the pathogens. As humans age, the ability of the immune system to clear Aß aggregates is reduced, resulting in ectopic accumulation of amyloid plaques that disrupt nerve functionality and result in AD symptoms.

Several pieces of evidence support this hypothesis: (1) amyloid plaques have been shown to aggregate around bacterial, viral, and fungal particles [477,480–482]; (2) previous infections by

viruses and bacteria increase the probability of AD development [483–487]; (3) treatment for pathogenic infection reduces the progression or delays the development of AD [488–491].

Previous research in worms has shown that transgenic expression of human Aß promotes survival on the pathogenic fungus *Candida albicans* and the pathogenic bacteria *Salmonella typhimurium* [482]. We wished to further characterize Aß as an innate immune peptide using the *phm-2(am117)* mutant. Our previous studies have revealed *phm-2(am117)* as a model for pathogen hypersensitivity in *C. elegans* (see **Chapter 3** and [63]). Mutations in *phm-2* result in improper development of the pharynx grinder, which results in live bacteria entering the intestine. In wild-type worms, the standard *E. coli* OP50 food source is nonpathogenic, as the pharynx is able to grind the bacteria prior to ingestion. When grown under standard conditions on NGM dishes seeded with a spot of *E. coli* OP50 bacteria, *phm-2(am117)* mutants preferentially avoid the bacterial food lawn; this is due to bacterial infection activating an innate immune response, one component of which is bacterial avoidance behavior. When grown on large lawns of *E. coli* OP50 spread over the entire surface of the agar medium, however, the animals are not able to move away from the bacterial lawn and are unable to avoid consuming the bacteria; this results in reduced survival due to the pathogenic activity of the bacteria. We used this phenotype to measure the antimicrobial activity of the Aß peptide, hypothesizing that expression of Aß would increase survival and reduce the severity of pathogen-induced phenotypes.

4.3 Results

Expression of human Aß$_{1-42}$ rescues survival and reduces matricidal hatching rate in *phm-2(am117)* mutant animals

We measured the lifespan of CL2122 and GMC101 animals on large lawns of bacteria (**Figure 1A, Table 1**). The GMC101 strain expresses human Aß$_{1-42}$ under the control of a body wall muscle-specific *unc-54* promoter [492]; the CL2122 strain acts as a wild type-like vector control, and does not express Aß$_{1-42}$ [493]. Aß$_{1-42}$ is a 42 amino acid isoform of the peptide that more readily forms amyloid plaques in comparison to other isoforms, both in worms and humans [467,494,495]; worms expressing this peptide readily develop insoluble amyloid inclusions when heat shocked [492]. Consistent with our previous observations, the *phm-2(am117)* mutation causes a significant decrease in lifespan in a CL2122 background of 22.6%. Interestingly, however, expression of Aß$_{1-42}$ rescues *phm-2(am117)* survival, resulting in a significant increase in lifespan of 2.7% compared to GMC101 control. GMC101 animals experience a slight yet significant decrease in lifespan of 8% compared to CL2122; this is not the cause of the rescue effect of Aß however, as GMC101;*phm-2(am117)* mutants are still significantly longer lived than CL2122;*phm-2(am117)* mutants, indicating that Aß enhances survival in a *phm-2(am117)* background.

We observed that matricidal hatching was a major cause of death in *phm-2(am117)* mutants (**Figure 1B, Table 2**). Matricidal hatching results in maternal death from internal hatching of embryos, and is a common phenotype resulting from pathogen exposure [63]. Indeed, CL2122;*phm-2(am117)* animals experienced significantly higher matricidal hatching compared to control CL2122. Conversely, matricidal hatching was not significantly increased in *phm-*

2(am117) mutants expressing Aß$_{1-42}$, suggesting that the peptide abrogated phenotypes resulting from pathogen exposure.

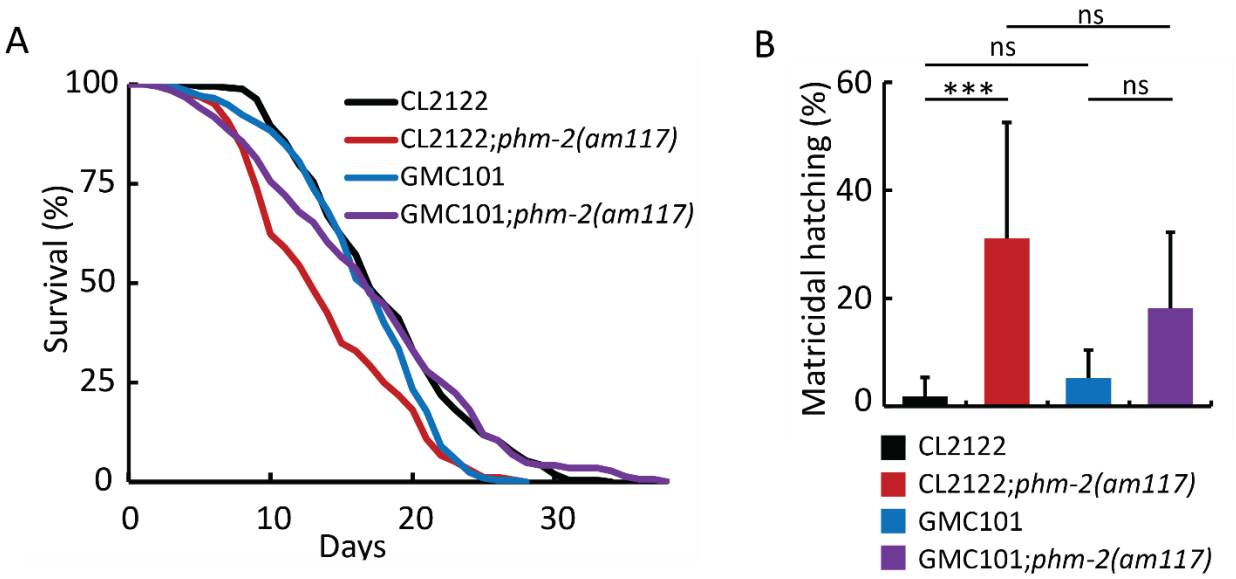

Figure 1: Aß expression increases survival and reduces matricidal hatching in *phm-2(am117)* animals grown on large lawns.

(A,B) Animals were grown at 20°C on NGM dishes with a large lawn of *E. coli* OP50 bacteria. For these experiments, animals which died due to matricidal hatching were not censored, as matricidal hatching was a major cause of death in *phm-2(am117)* animals. **(A)** *phm-2(am117)* significantly reduces lifespan in a control (CL2122) background due to infection by *E. coli* OP50 bacteria. Expression of Aß$_{1-42}$ (GMC101) abrogates *E. coli* pathogenicity in *phm-2(am117)* animals, resulting in a small, significant increase in lifespan compared to GMC101 control. See **Table 1** for detailed statistics. **(B)** The average percentage of animals which died due to matricidal hatching in **(A)** was quantified. Matricidal hatching is a common phenotype resulting from pathogen infection. Matricidal hatching was significantly increased in CL2122;*phm-2(am117)* mutant animals compared to CL2122 control. Conversely, expression of Aß$_{1-42}$ resulted in no significant increase in matricidal hatching, indicating that Aß$_{1-42}$ expression abrogates matricidal hatching in *phm-2(am117)* mutant animals. GMC101;*phm-2(am117)* trended towards reduced matricidal hatching compared to CL2122;*phm-2(am117)*, but did not achieve significance with this sample size (p=0.12) See **Table 2** for detailed statistics. ns, non-significant, p≥0.05; ***, p<0.001. See section **4.5. Materials and Methods** for details on genotypes.

Table 1: Effect of Aß expression on lifespan in *phm-2(am117)* mutant animals.

Genotype[a]	Mean Lifespan (days±s.e.)[b]	Change (%)[c]	N (n)[d]
CL2122	18.03±0.37		426 (11)
CL2122;*phm-2(am117)*	13.95±0.32	-22.6***	438 (11)
GMC101	16.59±0.31	-8.0***	439 (11)
GMC101;*phm-2(am117)*	17.04±0.5	+2.7*	415 (11)

[a] Animals of the indicated genotype were grown on large lawns of *E. coli* OP50. See section **4.5 Materials and Methods** for details on genotypes.

[b] Mean lifespan and standard error (s.e.), determined by Kaplan-Meier survival function. Animals that died due to matricidal hatching were not censored, as this was a major cause of death in *phm-2(am117)* double mutants.

[c] Percent change in mean lifespan. *phm-2(am117)* double mutant-animals are compared to their respective single-mutant controls and GMC101 is compared to CL2122. Negative values indicate lifespan reduction; positive values indicate lifespan extension. *, $p<0.05$; ***, $p<0.001$ by log-rank (Mantel-Cox) test.

[d] N, total number of animals; n, number of independent trials.

Table 2: Effect of Aß expression on matricidal hatching in *phm-2(am117)* mutant animals.

Genotype[a]	Matricidal hatching (%±s.d.)[b]	Significance[c]	N (n)[d]
CL2122	1.8±3.6		247 (11)
CL2122;*phm-2(am117)*	31.1±21.5	0.00005***	275 (11)
GMC101	5.2±5.2	0.93^{ns}	234 (11)
GMC101;*phm-2(am117)*	18.2±14.1	0.12^{ns}	206 (10)

[a] Animals of the indicated genotype were grown on large lawns of *E. coli* OP50 and observed for matricidal hatching. See section **4.5 Materials and Methods** for details on genotype.

[b] Average percentage of animals that died by matricidal hatching and standard deviation (s.d.). Animals were determined to have died from matricidal hatching by observation of hatched larvae inside the gonad. Percent matricidal hatching and s.d. was calculated by dividing the number of animals that died of matricidal hatching by the total number of animals that died of non-censored causes for each trial.

[c] p-value and statistical significance; *phm-2(am117)* double-mutant animals are compared to their respective single-mutant controls, and GMC101 was compared to CL2122 using one-way ANOVA with post-hoc Tukey HSD. ns, $p\geq0.05$; ***, $p<0.001$.

[d] N, total number of animals; n, number of independent trials.

4.4 Conclusions

Here, we discover that expression of human Aß peptide enhances survival and reduces pathogen-induced phenotypes in a worm model of pathogen hypersensitivity. We interpret these results as Aß functioning in an antimicrobial fashion to reduce the pathogenicity of the *E. coli* bacteria. These results lend further support to the Antimicrobial Protection Hypothesis, and for the first time show that Aß can increase *C. elegans* survival on the opportunistic pathogen *E. coli*. Previous studies on Aß and its protective effects in *C. elegans* have focused on highly pathogenic fungi and bacteria [482]. Nematodes, as soil-dwelling bacterivores, have developed strong resistance to pathogen infection; thus, exposure to highly pathogenic fungi or bacteria is required in order to measurably impact their survival. Conversely, *E. coli* is nonpathogenic to wild-type animals, and only reduces the lifespan of hypersensitive mutants by ~20%. This model allows us to more easily titrate the degree of pathogenicity, and allows more fine-grained analysis of the effect of Aß on survival. By increasing the average lifespan to the order of weeks, rather than days, we are more able to measure small changes in lifespan that result from Aß. Furthermore, the *phm-2(am-117)* model of pathogen hypersensitivity opens the door to further studies of infection using pathogens that are otherwise non-infectious in wild-type animals.

E. coli is an especially relevant model for studying the interplay of aging, the immune system, and Aß. It has increasingly been recognized that reactivation of latent infections in the brain of aged patients is a major risk factor for the development of AD: as an individual ages, the ability of their immune system to control latent infections is reduced, resulting in reactivation late in life [487,496,497]. This, in addition to increased Aß aggregation and the reduced ability of the brain to clear amyloid plaques, is thought to accelerate AD development. Similarly, in *E. coli* is non-pathogenic in young wild-type *C. elegans*. As the animal ages, the structural integrity of

their digestive system breaks down, resulting in invasion of *E. coli* into the intestinal lumen and invasion of the bacteria into intestinal cells [213]. Thus, a pathogen which is non-pathogenic early in life becomes pathogenic late in life due to the reduced ability of the organism to maintain the structural and functional integrity of its organ systems. In this manner, challenging animals with an otherwise neutral pathogen mirrors a common factor involved in AD development in humans, and recapitulates it in the experimentally simple nematode model.

4.5 Materials and Methods

Culture conditions and strain construction

Nematodes were cultured under standard conditions as described in Brenner (1974) [3]. Briefly, nematodes were grown in 20°C incubators on dishes containing nematode growth medium (NGM) seeded with 200 µL *E. coli* OP50 bacterial food source in a spot on the center of the dish. For animals grown on large lawns, 500 µL of *E. coli* OP50 was spread such that the entire surface of the dish was covered in a bacterial lawn. Bacteria were allowed to dry covered at room temperature overnight and then stored at 4°C.

Some strains were obtained from the *Caenorhabditis* Genetics Center (CGC) at the University of Minnesota. Strains WU1941 and WU1942 were constructed by crossing WU740 *phm-2(am117)* to GMC101 and Cl2122, respectively. The presence of the transgene was confirmed by observation of intestinal GFP expression and Sanger sequencing. The presence of the *phm-2(am117)* mutation was confirmed by pyrosequencing.

Genotype	Strain	Source
Wild type	N2 Bristol	CGC
phm-2(am117) I	WU740	Kornfeld laboratory [63,199]
dvIs100 [unc-54p::A-beta-1-42::unc-54 3'-UTR + mtl-2p::GFP]	GMC101	CGC [492]

dvIs15 [(pPD30.38) unc-54(vector) + (pCL26) mtl-2::GFP]	CL2122	CGC [493]
phm-2(am117) I ; dvIs100 [unc-54p::A-beta-1-42::unc-54 3'-UTR + mtl-2p::GFP]	WU1941	This study
phm-2(am117) I ; dvIs15 [(pPD30.38) unc-54(vector) + (pCL26) mtl-2::GFP]	WU1942	This study

Measurement of survival and matricidal hatching

Lifespan (survival) assays and determination of matricidal hatching rate were performed as previously described in Kumar *et al.* (2019) [63]. L4 hermaphrodites were picked from gravid populations onto NGM dishes seeded with large lawns of *E. coli* OP50. Animals were moved to new dishes daily throughout the reproductive period and as needed thereafter. Animals were observed for spontaneous movement daily; if none was observed, each animal was gently stimulated with a platinum wire. If neither induced nor spontaneous movement was observed, animals were scored as dead. Animals which died from extrusion of the gonad or desiccation on the side of the dish were censored. Animals which died due to matricidal hatching were not censored from the lifespan assay, as this was observed to be a primary cause of death in mutants containing the *phm-2(am117)* allele. Matricidal hatching percentage was calculated by dividing the number of worms that experienced matricidal hatching by the number of worms that died from non-censored conditions. The experiments continued until all animals had died. Statistical analysis was performed using Kaplan-Meier survival function and log-rank (Mantel-Cox) test (lifespan assay) or one-way ANOVA with post-hoc Tukey HSD (matricidal hatching assay) [129,498].

Chapter 5: Control of aging by the renin-angiotensin-aldosterone system: a review of *C. elegans, Drosophila*, and mammals

The work presented in Chapter 5 was published as a review article in 2022 in Frontiers in Pharmacology *with the following authors:*

Egan, B. M., Scharf, A., Pohl, F., & Kornfeld, K. (2022). *Control of aging by the renin–angiotensin system: a review of* C. elegans, Drosophila, *and mammals*. Frontiers in Pharmacology, 3056. PMID 36188619

I contributed to this review article by outlining the scope, performing the majority of the research and writing of the article, and creating and organizing the figures.

5.1 Abstract

The free-living, non-parasitic nematode *Caenorhabditis elegans* is a premier model organism for the study of aging and longevity due to its short lifespan, powerful genetic tools, and conservation of fundamental mechanisms with mammals. Approximately 70 percent of human genes have homologs in *C. elegans*, including many that encode proteins in pathways that influence aging. Numerous genetic pathways have been identified in *C. elegans* that affect lifespan, including the Dietary Restriction (DR) pathway, the Insulin/insulin-like growth factor (IGF) signaling pathway, and disruption of components of the mitochondrial electron transport chain. *C. elegans* is also a powerful system for performing drug screens, and many lifespan-extending compounds have been reported; notably, several FDA-approved medications extend lifespan in *C. elegans*, raising the possibility that they can also extend lifespan in humans.

The renin-angiotensin system (RAS) in mammals is an endocrine system that regulates blood pressure and a paracrine system that acts in a wide range of tissues to control physiological processes; it is a popular target for drugs that reduce blood pressure, including angiotensin-converting enzyme (ACE) inhibitors and angiotensin II receptor blockers (ARBs). Emerging evidence indicates this system influences aging. In *C. elegans*, decreasing activity of the ACE homolog *acn-1* or treatment with the ACE-inhibitor Captopril significantly extends lifespan. In *Drosophila*, treatment with ACE inhibitors extend lifespan. In rodents, manipulating the RAS with genetic or pharmacological interventions can extend lifespan. In humans, polymorphisms in the ACE gene are associated with extreme longevity. These results suggest the RAS plays a conserved role in controlling longevity. Here, we review studies of the RAS and aging, emphasizing the potential of *C. elegans* as a model for understanding the mechanism of lifespan control.

5.2 Introduction

Caenorhabditis elegans is a powerful model system for aging pharmacology

Age-related degenerative changes are a major issue for human health[499]. A wide variety of systems are affected including the reproductive, central, and peripheral nervous, musculoskeletal, immune, cardiac, renal, and respiratory. The age-related reduction of muscular strength, or sarcopenia, is a serious problem for many elderly people. Although the quest for methods to delay aging is a longstanding human endeavor, no pharmacological agents have yet been demonstrated to delay human aging. One of the biggest challenges to understanding and treating human aging is the fact that humans live so long and age so slowly. Thus, a critical need in aging research is model organisms that are short lived, amenable to experimentation, and relevant to humans.

The analysis of genetically tractable model organisms with short life spans, such as yeast, worms, and flies, has resulted in the identification of genes that can modulate longevity[500]. Studies of mice have provided substantial evidence that at least some mechanisms that affect the rate of age-related degeneration have been conserved during animal evolution (reviewed in [343,499]). Thus, short-lived animals may provide meaningful guides to the biology of human aging and serve as the proving grounds where interventions that delay age-related degeneration can be identified and characterized. The report by the Intervention Testing Program (ITP) of the National Institutes of Aging that Rapamycin extends life span of mice is a compelling example, since Rapamycin was first demonstrated to influence life span in yeast[92,501,502].

C. elegans is a powerful and relevant experimental system that is excellent for the identification of genes and drugs that modulate the rate of aging. *C. elegans* is a free-living,

hermaphroditic nematode that displays extensive conservation of fundamental biological processes with other animals. Pioneering studies by Sydney Brenner and colleagues established *C. elegans* as a powerful experimental model system for forward genetics, reverse genetics, and molecular analysis supported by a fully sequenced genome[3,503]. *C. elegans* has been used to characterize fundamental and highly conserved biological processes such as RNA interference (RNAi) and apoptosis[9,504]. It has been used to develop innovative experimental techniques such as in vivo expression of green fluorescent protein (GFP)[505]; these and other discoveries have had a major impact on understanding mammalian biology. *C. elegans* is extremely well understood at the cellular anatomical level, since the entire cell lineage of the 959 somatic nuclei has been determined[504].

C. elegans is excellent for studies of aging because the adults display the progressive, degenerative changes that are typical of aging in larger animals, but the adult life span is only about 15 days[14]. Age-related degenerative changes in *C. elegans* have been characterized extensively, and genetic analysis of *C. elegans* has resulted in the discovery of genes and pathways that modulate longevity[500,506]. Many well characterized mutations that influence aging by affecting known pathways are reagents that can be used to investigate the mechanism of action of newly discovered genes and drugs that influence aging. *C. elegans* has been used successfully to analyze the molecular targets of drugs[507,508]. Since nearly 75% of all *C. elegans* genes have human counterparts, there is a good chance that the molecular target of a drug in the worm will be similar to the target in humans[503].

The first of what is now a large class of ACE inhibitors, Captopril is an oligopeptide derivative developed in 1975 based on a peptide found in the venom of a snake, *Bothrops jararaca*, the Brazilian pit viper[509]. ACE inhibitors modulate the renin-angiotensin system

(RAS), a mechanism by which the body adapts to hypotension[97,99]. In this review we focus on emerging evidence from *C. elegans*, *Drosophila* and mammals that the RAS controls longevity and drugs that target this system might be useful agents in the quest to extend human lifespan.

The RAS is an endocrine system that controls blood pressure and a paracrine system that mediates a wide range of physiological processes

High blood pressure, or hypertension, is defined as a systolic blood pressure over 140 mmHg and/or diastolic blood pressure over 90 mmHg[510]. It is a common malady throughout the world, affecting more than 31% of the adult population (~1.4 billion people); the percentage of the population suffering from hypertension continues to increase, creating an accelerating health crisis[510]. High blood pressure is associated with, and is a likely cause of, many cardiovascular and renal diseases[510], and is estimated to result in more than 10 million deaths per year worldwide[511]. What causes hypertension? Dietary factors such as sodium are one cause; genetics can be a second cause[512]. Age has been identified as a major risk factor for hypertension, with incidences rising in aging populations[512]. Understanding the interaction between age and hypertension is important for maintaining the health of an aging population.

The RAS was first identified as a crucial regulator of blood pressure in the mid-20th century ([513], reviewed in [97,99]). The classic understanding was that the RAS is an endocrine system. In response to low blood pressure, the kidney secretes renin, an aspartyl protease. Renin cleaves the peptide Angiotensinogen (AGT), which the liver releases into the blood stream, into Angiotensin I (Ang I), a 10 amino acid peptide. Ang I is cleaved into Angiotensin II (Ang II), an 8 amino acid peptide, by the Angiotensin-converting enzyme (ACE), a metallopeptidase secreted by the lungs. Ang II binds to the Angiotensin II type 1 receptor (AGT1R) on vascular endothelial cells. AGT1R is a G-protein coupled receptor that initiates a signal transduction pathway resulting in vasoconstriction and increased blood pressure (**Figure 1A**) (reviewed in [98,100,514,515]).

In the last 30 years, exciting new discoveries have shown that the RAS is significantly more complicated in two dimensions: the endocrine system has many additional components, including some that promote vasodilation, and the RAS functions as a paracrine/autocrine system in many organs to mediate a wide range of physiological responses.

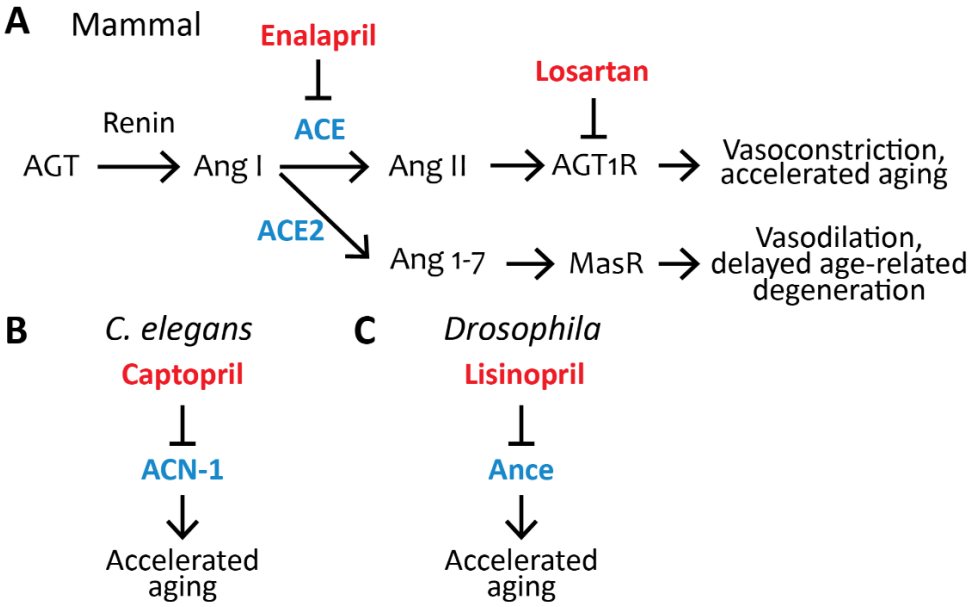

Figure 2: **Pharmacological inhibition of the renin-angiotensin system influences aging in *C. elegans*, *Drosophila*, and mammals. (A)** The RAS pathway in mammals; the ACE inhibitor Enalapril and Angiotensin II type-1 receptor blocker Losartan are FDA approved drugs that control aging in non-human mammals (see **Table 1**). AGT, Angiotensinogen; Ang I, Angiotensin I; ACE, Angiotensin-converting enzyme; Ang II, Angiotensin II; AGT1R, Angiotensin II type-1 receptor; ACE2, Angiotensin-converting enzyme 2; Ang 1-7, Angiotensin (1-7); MasR, Mas Receptor. **(B)** The FDA-approved ACE-inhibitor drug Captopril inhibits *acn-1*, the only *C. elegans* ACE homolog, to control aging[85]. ACN-1, Angiotensin-converting enzyme-like non-peptidase. **(C)** The FDA-approved ACE inhibitor drug Lisinopril inhibits Ance, the *Drosophila* ACE homolog, to control aging[516]. Ance, ANgiotensin-converting enzyme. Blue, ACE and its homologs ACE2, Ance, and ACN-1; Red, ACE inhibitors (Captopril, Enalapril, Lisinopril) or ARBs (Losartan) which have been shown to influence aging.

In 2000, a second isoform of ACE was described in mammals, called ACE2[517]. ACE2 is a transmembrane protein that cleaves Ang I or Ang II into the heptapeptide angiotensin (1-7) (Ang(1-7)). Furthermore, the receptor for Ang(1-7) was discovered, called the Mas receptor

(MasR). Activation of the Mas receptor results in vasodilation (**Figure 1A**)[518]. The recent discovery that ACE2 appears to be the main entry point into cells for the SARS-CoV-2 coronavirus, the cause of the COVID-19 pandemic, has resulted in intense scrutiny[519]. Additionally, ACE2 has been proposed to influence aging, since inhibition accelerates age-related degenerative changes[520–522]. Other discoveries include the (pro)renin receptor [(P)RR], which binds and activates renin in tissues, and the Angiotensin II type 2 receptor (AGT2R) on vascular endothelial cells. AGT2R is a G-protein coupled receptor that initiates a signal transduction pathway resulting in vasodilation and reduced blood pressure. Thus, Ang II can increase blood pressure by acting through the AGT1R receptor and reduce blood pressure by acting through the AGT2R receptor, and the expression levels of the two receptors plays an important role in the overall response (**Figure 1A**).

The receptors for angiotensin peptides are expressed in a wide range of tissues, indicating they function in paracrine/autocrine systems controlled by local generation of peptide agonists (reviewed in [517,523,524]). The brain expresses the AGT1R and AGT2R receptors, which influence the autonomic nervous system, the hypothalamus-pituitary axis, vasopressin release, baroreflex sensitivity, and thirst and salt appetite. The overall effects of brain activation are to increase blood volume and blood pressure, but are also implicated in higher brain functions such as anxiety and stress[525,526]. In the kidney, local RAS signaling plays a role in kidney development and renal function in adults. In the heart, Ang II acts through the AGT1R to induce cardiac hypertrophy and fibrosis and through the AGT2R to cause the opposite effects. In the gastrointestinal system, the RAS regulates intestinal physiological functions including electrolyte homeostasis, digestion, peptide transport, glucose, sodium and water absorption, and gastrointestinal motility[527]. The RAS is important during pregnancy and acts locally in the

uteroplacental unit to mediate angiogenesis, trophoblastic invasion, and adequate placentation[528]. It is possible that the tissue specific functions of the RAS represent primordial functions and are the target of interventions that modulate aging.

A major breakthrough in the treatment of hypertension was the development of Captopril, the first ACE inhibitor compound, in 1975 (**Figure 2A**)[95]. Observations of the hypotensive effects of venom of the snake *Bothrops jararaca* made it clear that ACE was a critical regulator of blood pressure and a useful target for inhibition[95]. Rational drug design techniques allowed the creation of Captopril as a peptide-analogue targeting and inhibiting the active site of ACE, with later generations of ACE inhibitors, such as Enalapril (**Figure 2B**) or Lisinopril (**Figure 2C**), improving activity and bioavailability. Further research into the RAS led to the development of Angiotensin II receptor blockers (ARBs) such as Losartan (**Figure 2D**)[529] More recently, renin inhibitors such as Aliskiren were developed [530].

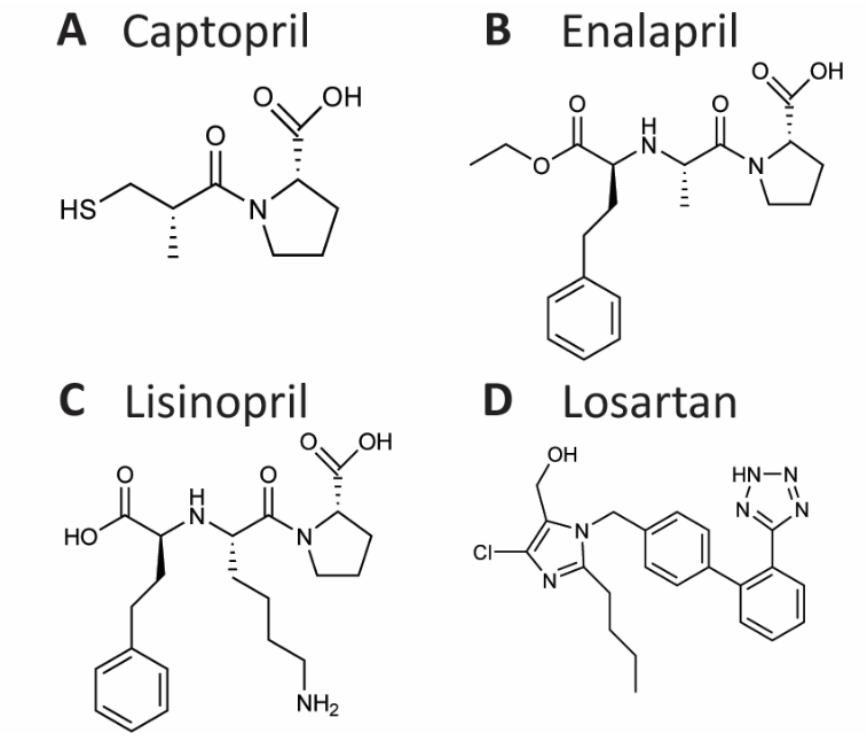

Figure 3: Chemical structure of the Angiotensin-converting enzyme inhibitors Captopril **(A)**, Enalapril **(B)**, and Lisinopril **(C)**, and of the Angiotensin II receptor blocker Losartan **(D)**. These drugs have been shown to control aging in *C. elegans*, *Drosophila*, and/or rodents.

The blood pressure regulation activity of the RAS is well characterized and has been studied in many mammalian model organisms (reviewed in [99,100,514,515]). However, components of the RAS have also been discovered in non-mammalian organisms which lack closed circulatory systems. ACE homologs have been identified in organisms throughout the Bilaterian clade, including the *C. elegans* homolog *acn-1* and the *Drosophila* homolog *Ance* (**Figure 1B,C**). Functional ACE homologs have also been identified in insects, crustaceans, annelids, and mollusks (reviewed in [531]). Based on its presence in such diverse phyla, it is likely that ACE first evolved in a common ancestor roughly 600 million years ago[532], prior to the evolution of the animal closed circulatory system[533]. These observations raise an intriguing question; what is the ancestral function of ACE? Insight into that function can help address the role of the RAS during aging.

Emerging evidence has identified important connections between the RAS and aging. Pharmacological or genetic inhibition of members of the RAS can extend lifespan and delay age-related degenerative changes in mice and rats (**Figure 3C, 4C**) (reviewed in [527,534–539]). The study of ACE and the RAS in the context of aging is complicated in mammalian systems due to their pleiotropic effects not only on aging but also vasoconstriction, renal, cardiovascular, and pulmonary health and function, and less understood functions in the brain (reviewed in [539]). In contrast, non-mammalian organisms lacking closed circulatory systems can be used to distinguish the aging effects of the RAS from the cardiovascular functions.

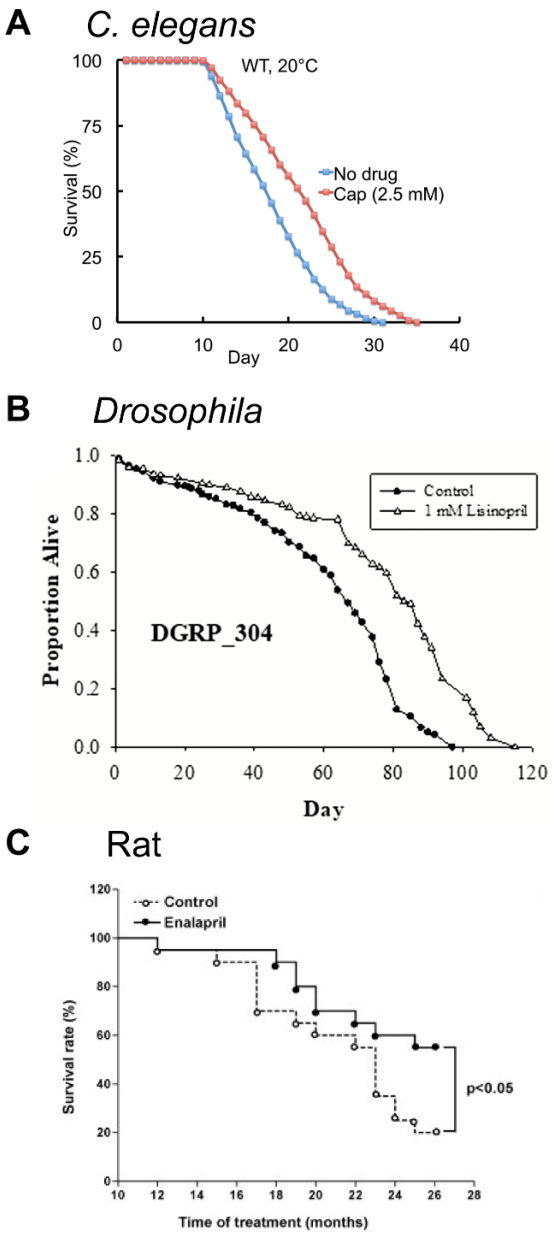

Figure 4: ACE inhibitors extend lifespan in model organisms. (A) The FDA-approved ACE inhibitor drug Captopril (Cap) extends adult lifespan in *C. elegans* by about 21%. Survival curves of wild-type (WT) hermaphrodites treated with 2.5 mM Captopril from the L4 stage onward at 20°C. Adapted from Kumar *et al.* (2016)[85]. **(B)** The FDA-approved ACE inhibitor drug Lisinopril extends lifespan in *Drosophila melanogaster*. Survival curve of populations of the Drosophila Genetic Reference Panel (DGRP, strain DGRP_304 is depicted) exposed to 1 mM Lisinopril. Adapted from Gabrawy *et al*. (2019) [516]. **(C)** The FDA-approved ACE-inhibitor drug Enalapril extends lifespan in adult rats. Survival curves of adult Wistar rats exposed to 10 mg/kg Enalapril in water for 26 months. Enalapril treatment reduced mortality by 45% in the 26 month period. Adapted from Santos *et al.* (2009)[540].

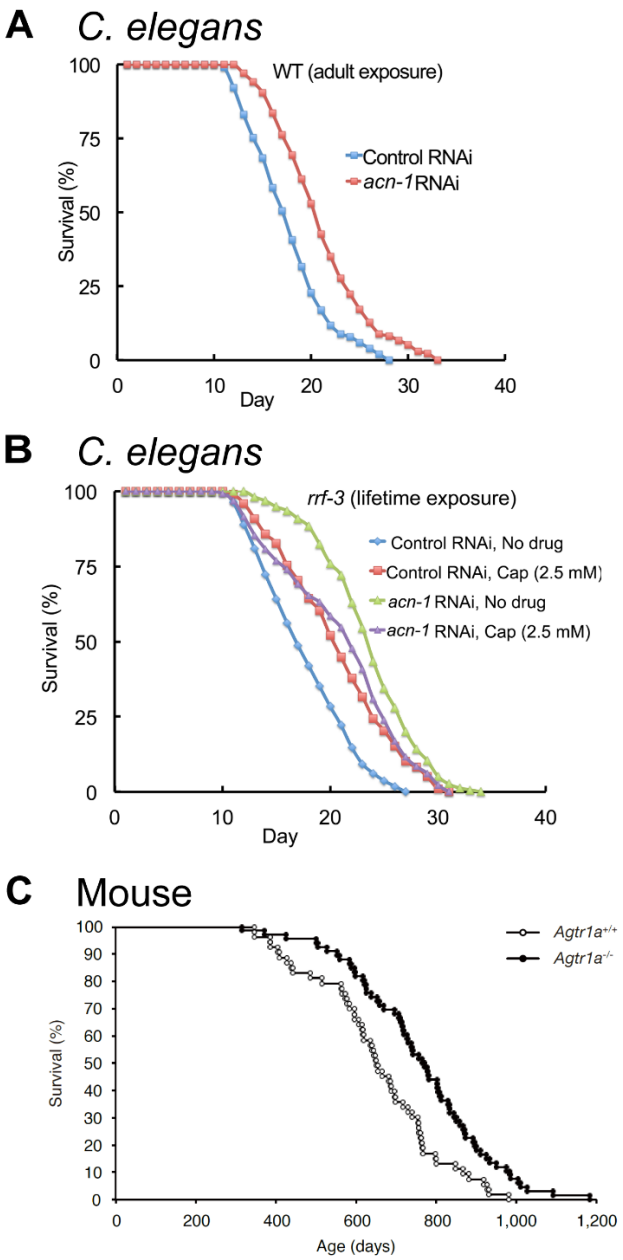

Figure 5: Reducing ACE expression extends lifespan in *C. elegans* and mice. (A) Reducing *acn-1* expression via RNA-interference (RNAi) extends adult lifespan in *C. elegans* by about 20%. Survival curves of wild-type (WT) hermaphrodites exposed to *acn-1* or control dsRNA-expressing bacteria from the L4 stage onward at 20°C. **(B)** Captopril and *acn-1* RNAi are not additive in extending the lifespan of adult *C. elegans*, suggesting that Captopril inhibits *acn-1* to control aging. Survival curves of RNAi-hypersensitive strain *rrf-3(pk1426)* exposed to *E. coli* bacteria expressing control or *acn-1* dsRNA from the embryonic stage and to 2.5 mM Captopril from L4 stage at 20°C. **(A,B)** Adapted from Kumar *et al.* (2016)[85]. **(C)** Knock-out of AGT1R extends adult lifespan in mice by about 17%. Survival curves of Agtr1a$^{-/-}$ and Agtr1a$^{+/+}$ mice [541] fed with a standard diet. Adapted from Yabumoto *et al.* (2015)[542].

5.3 Discussion

Captopril and the *acn-1* gene influence aging in *Caenorhabditis elegans*

The nematode ACE homolog *acn-1* was first identified by Brooks *et al.* (2003) as necessary for larval development and adult morphogenesis[102]. Green fluorescent protein (GFP)-tagged ACN-1 driven by an *acn-1* promoter was expressed in the embryo hypodermis, hypodermal seam cells and vulva of the L4 hermaphrodite, and the ray papillae in the L4 male tail. *acn-1* RNAi-mediated knockdown resulted in larval molting defects, characterized by a failure to shed the cuticle. Gonad injection of dsRNA resulted in larval arrest at L2 and an early mortality phenotype, indicating that it causes a strong reduction of function and that *acn-1* is necessary for larval survival; feeding of *acn-1* dsRNA-expressing bacteria allows many animals to survive the larval stage, indicating a less severe reduction of function, and animals display cuticle shedding defects in the L3/L4 and L4/adult molts. RNAi-mediated knockdown of *nhr-23* and *nhr-25* reduced expression of ACN-1, suggesting that these genes regulate *acn-1.* Loss of function of these two genes was previously reported to induce cuticle shedding defects similar to *acn-1* loss of function [543]. Indeed, a comprehensive RNAi screen by Frand *et al.* (2005) identified *acn-1*, along with *nhr-23* and *nhr-25*, as inducing molting defects[544]. Based on these results, *acn-1* appears to act in larval animals to regulate molting downstream of *nhr-23* and *nhr-25*.

Oskouian *et al.* (2005) replicated the finding of Brooks *et al.* (2003) that injection of worms with *acn-1* dsRNA resulted in arrest of larval development[102,545]. Kumar *et al*. (2016) did not observe significant larval arrest after *acn-1* RNAi feeding treatment[85]. The difference may be due to the method of administration (feeding in the case of Kumar *et al*. (2016), and injection into the gonad in the cases of Oskouian *et al*. (2005) and Brooks *et al*. (2003)[85,102,545]).

The heterochronic pathway controls the timing of molting and other development events by time-dependent expression of genes including several microRNAs. Knockdown of heterochronic pathway components disrupts crucial timing in cell fate decisions, leading to precocious or retarded cell fate phenotypes. Knockdown of *acn-1* suppresses the ectopic phenotypes associated with knockdown of the heterochronic pathway microRNA *let-7*, and *acn-1* expression is modulated throughout the L1 stage in a manner dependent on *lin-41* and *hbl-1,* both targets of *let-7*[103]. Thus, *acn-1* genetically interacts with several components of the heterochronic pathway. Ahn *et al.* (2006) found that *acn-1* transcription was downregulated in *tax-6(jh107)* mutants[546]. *tax-6* is the nematode homolog of the mammalian Calcineurin A subunit, and the *jh107* allele represents a constitutively active gain-of-function mutation. This suggests a role for *tax-6* in the regulation of *acn-1* protein expression[546]. Dubois *et al*. (2019) found that ACN-1 protein expression was affected by exposure to ionizing gamma radiation; protein expression was upregulated following chronic exposure, and down-regulated following acute exposure[547].

Based on sequence alignments, the predicted ACN-1 protein lacks several histidine residues that are ligands for the zinc cofactor necessary for the metallopeptidase activity of ACE, suggesting that ACN-1 protein lacks this enzyme activity[102]. Biochemical analyses of the catalytic activity of ACN-1 have not been performed, so it remains unknown if ACN-1 has the metallopeptidase activity observed in ACE. It has been speculated that ACN-1 may function by binding to and sequestering its substrate, but further research is needed to determine the biochemical function of ACN-1.

While *acn-1* function in larval animals is well established, Kumar *et al.* (2016) showed that *acn-1* RNAi treatment initiated after the L4 stage, when the animal has completed all of its larval molts, extends lifespan and delays age-related degenerative changes[85] (**Figure 4A, Table**

2). This suggests that *acn-1* functions in adults to control aging. Further research is required to better understand the function of *acn-1* in adult animals.

Kumar *et al.* (2016) performed a screen for FDA-approved medications that extend lifespan in *C. elegans*[85]. Captopril, an ACE inhibitor, extended lifespan in hermaphrodite worms by more than 30% (**Figure 3A; Table 1**); additionally, Captopril treatment delayed age-related degeneration in multiple systems, including body movement and pharyngeal pumping rate. Captopril treatment increased thermotolerance and oxidative stress resistance, phenotypes associated with extended longevity[85]. The lifespan extension phenotype appeared to be independent of several known longevity pathways, including the caloric restriction, mitochondrial dysfunction, sirtuin, and TOR signaling pathways.

Table 1: Pharmacological inhibition of the RAS system and effects on age-related phenotypes

Drug name[a]	**Animal**[b]	**Age-related phenotype(s)**[c]	**Dose/notes**[d]
Captopril (ACE inhibitor)	Worm	Lifespan ↑[85,548], pharyngeal pumping rate ↑[85,548], body movement rate ↑[85,548], thermotolerance ↑[85,548], oxidative stress resistance ↑[85,548], Lipid storage ↓[548]	2.5 mM in agar; hermaphrodites only
Lisinopril (ACE inhibitor)	Fly	Lifespan ↑[516], protein aggregation ↓[516], climbing speed ↑[549], endurance ↑[549], strength ↑[549], mitochondrial number ↑[550], starvation resistance ↓[550]	1 mM in feed; males only; effects are genotype-specific
Enalapril (ACE inhibitor)	Mouse	(1) Body weight ↑[551,552], mitochondrial number ↑[552], kidney mass ↑[552], glomerular number and size ↑[552], glomerulosclerosis ↓[552], serum potassium ↑[551], myocardiosclerosis ↓[551] (2) Frailty ↓, systolic blood pressure ↓[553]	(1) 5, 10, or 20 mg/L in water; females only (2) 30 mg/kg/day in feed; males and females
Enalapril (ACE inhibitor)	Rat	(1) Lifespan ↑[540], body weight ↓[540,554,555], caloric intake ↓[540], systolic blood pressure ↓[540,554–557], water intake ↑[554,555], heart weight ↓[554,555], cardiac health ↑ [554,555], renal health and function ↑[556,557], kidney degradation ↓[556,557], glomerular size	(1) 10 mg/kg/day in water; males only (2) 40 or 80 mg/kg/day by subcutaneous

		↓[556,557], proteinuria ↓[556–558], mitochondrial function ↑[556,557], glomerular size ↓[558] (2) Heart rate ↑[559], blood pressure ↓[559], body fat ↓[559], grip strength ↑[559], climbing of incline ↑[559] (3) Body weight ↓[560], fat mass ↓[560], grip strength ↑[560], food consumption ↓[560], movement ↑[560], tumor incidence ↓[560]	injection; males and females (3) 40 mg/kg/day in feed; males only
Losartan (Angiotensin II Type 1 receptor blocker)	Rat	(1) Systolic blood pressure ↓[555], water intake ↓[555], heart weight ↓[555], cardiac health ↑[555] (2) Systolic blood pressure ↓[554,556,557], renal health and function ↑[556,557], kidney degradation ↓[556–558], glomerular size ↓[556–558], proteinuria ↓[556–558], heart weight ↓[554], cardiac health ↑[554], mitochondrial number and function ↑[556,557] (3) Grip strength ↑[560]	(1) 10 mg/kg/day in water; males only (2) 30 mg/kg/day in water; males only (3) 30 mg/kg/day in feed; males only

[a] **Compound name** (protein target)

[b] Worm, *Caenorhabditis elegans;* Fly, *Drosophila melanogaster*; Mouse, *Mus musculus*; Rat, *Rattus norvegicus*

[c] Phenotypes display age-related change; arrow indicates direction of drug effect with respect to untreated age-matched cohort

[d] Drug dose; route of administration; sex of animals; notes

Table 2: Genetic interventions on the RAS system and effects on age-related phenotypes

Gene[a]	Intervention[b]	Animal[c]	Age-related phenotype(s)[d]	Notes[e]
acn-1	RNAi knockdown	Worm	Lifespan ↑[85], pharyngeal pumping rate ↑[85], body movement rate ↑[85], thermotolerance ↑[85], oxidative stress resistance ↑[85]	Hermaphrodites only
Ance	RNAi knockdown	Fly	Lifespan ↑[516]	Males only; effect is genotype-specific
Acer	RNAi knockdown	Fly	Lifespan ↓[561], heart rate ↓[561], heart failure rate ↑[561], end-systolic diameter ↑[561], end diastolic diameter ↑[561], fractional shortening ↓[561]	Males only; Tissue-specific RNAi knockdown in mesoderm and cardiac tissue
Acer	Chromosomal mutation (Null)	Fly	Lifespan ↓[562,563]	Females only

Agt1r	Chromosomal mutation (Null)	Mouse	Lifespan ↑[542,564], cardiac health and function ↑[564], mitochondrial number and function ↑[564], hair growth ↑[542], skin thickness ↑[542], fat layer thickness ↑[542], grip strength ↑[542], muscle repair ↑[542]	Males only
ACE2	Chromosomal mutation (Null)	Mouse	Grip strength ↓[520], running distance ↓[520], body weight ↓[520], maximal muscle force ↓[520]	Males only

[a] *Ance* is homologous to ACE; *Acer* is homologous to ACE2; *acn-1* is the only known ACE homolog in worms; Agt1r, Angiotensin II type-1 receptor; ACE2, Angiotensin-converting enzyme 2

[b] RNA-interference (RNAi) transiently reduces gene activity; chromosomal mutations appear to be null alleles

[c] Worm, *Caenorhabditis elegans;* Fly, *Drosophila melanogaster*; Mouse, *Mus musculus*

[d] Phenotypes display age-related change; arrow indicates direction of effect with respect to wild-type or untreated age-matched cohort for chromosomal mutation or RNAi-mediated knockdown, respectively

[e] RNAi affects either whole animal or specific tissues; sex of animal

Kucuktepe (2021) treated animals with Captopril and replicated the lifespan extension, delayed decline of pharyngeal pumping rate, increased thermotolerance, and increased oxidative stress resistance phenotypes reported by Kumar *et al.* (2016)[85,548]. Kucuktepe (2021) examined the effect of Captopril administration on lipid levels; triglyceride levels were significantly reduced based on oil red O-staining of L4-stage worms[548]. The primary effect was on intestinal lipid droplets, which were reduced in diameter. Biochemical analysis indicated a reduction in triglycerides and protein content after Captopril treatment.

Kumar *et al.* (2016) and Kucuktepe (2021) both demonstrated that the lifespan extension caused by Captopril treatment were abrogated by a *daf-16* loss-of-function mutation[85,548]. The DAF-16 transcription factor is the terminus of the insulin/insulin-like growth factor (IGF) signaling pathway, a well-characterized pathway that influences aging[565,566]. Kumar *et al.* (2016)

reported that DAF-16 does not display nuclear localization upon treatment with Captopril[85]. Furthermore, Kucuktepe (2021) observed that the body fat reduction caused by Captopril in wild-type animals was not displayed by *daf-16(lf)* mutants, suggesting that both lifespan extension and body fat reduction are DAF-16-dependent[548]. Further research is needed to determine the nature of the Captopril-DAF-16 interaction.

Kumar *et al*. (2016) examined interactions of the ACE inhibitor Captopril with the *acn-1* gene. RNAi-mediated inhibition of *acn-1* caused many phenotypes similar to Captopril administration, including lifespan extension (**Figure 4A**)[85]. Furthermore, RNAi-mediated knockdown of *acn-1* did not further enhance the lifespan extension caused by Captopril treatment (**Figure 4B**), suggesting that Captopril affects aging by inhibition of *acn-1*. By contrast to Kumar *et al.* (2016), Dalton *et al.* (2018) reported that treatment with *acn-1* RNAi decreased heat and oxidative stress resistance[85,567]. These results may be explained by differences in methodology, as the two studies differed in timing of temperature shift (larval day 1 or 2 in Dalton *et al*. (2018), and adult day 3 in Kumar *et al*. (2016)) and timing of *acn-1* RNAi administration (beginning at hatch for Dalton *et al*. (2018), and beginning at L4 for Kumar *et al*. (2016))[85,567].

The Greenwald group generated a compendium of *C. elegans* genes with homologs in humans, called 'Ortholist'[568,569]. Based on protein homology, nematode ACN-1 has homologs throughout the Bilaterian clade: in addition to humans, non-human primates, and rodents, ACE homologs are present in Zebrafish, *Xenopus*, *Drosophila*, and various other arthropods, suggesting that ACE-like proteins have been retained throughout many animal phyla for at least six hundred million years of evolutionary history. Moreover, this suggests that the evolution of the ACE protein predated the evolution of the animal circulatory system, implying that the

ancestral function of the ACE protein was unrelated to the regulation of blood pressure; this hypothesis is reinforced by the ACE protein's conservation in phyla which lack closed circulatory systems. This is further reinforced by the apparent lack of functional homologs to the primary substrate of mammalian ACE, Angiotensinogen, in worms or *Drosophila*, as well as the lack of functional analogs to mammalian Renin or the Angiotensinogen receptors in these model organisms. Thus, it is apparent that the ancestral function of ACE was unrelated to blood pressure regulation, and that this activity evolved later.

Lisinopril and *Ance* affect aging in *Drosophila melanogaster*

The fruit fly *Drosophila melanogaster* is a valuable model organism for studies of genetics, development, behavior, and aging, having been commonly used for over a century[570–573]. Low maintenance costs, rapid generation time, well-developed genetic techniques and relatively short lifespans make *Drosophila* one of the predominant model organisms for aging studies. Several studies have identified pathways that regulate aging including Dietary Restriction (DR), the Insulin/insulin-like growth factor (IGF) signaling pathway, and disruption of components of the mitochondrial electron transport chain (METC)[74,574,575]. *Drosophila* has been used to test anti-aging pharmacological interventions due the availability of high throughput screening techniques[576–580]. Compared to *C. elegans, Drosophila* has greater anatomical similarity to mammals[74,579].

The *Drosophila* genome encodes two primary homologs of ACE as well as several that are more diverged. *Ance* (ANgiotensin-Converting Enzyme) is most similar to mammalian ACE (**Figure 1C**); *Ance* is expressed throughout the lifespan and plays roles in development and fertility[581,582]. *Acer* (Angiotensin-Converting Enzyme-Related) is most similar to mammalian ACE2 and plays roles in heart morphogenesis[583]. Several other homologous genes, *Ance-2*

through *Ance-5*, likely resulted from gene duplication events; these genes do not have established functions and are not predicted to encode catalytically active proteins based on amino acid sequence[584]. *Ance* and *Acer*, in contrast to ACN-1, have highly conserved residues in the active site residues similar to mammalian ACE. These proteins have been demonstrated to be catalytically active, since they can cleave Ang I in purified extracts[584,585]. ACE inhibitors bind to and inhibit the enzymatic activity of *Acer* and *Ance*[585–587].

In agreement with results in worms, RNAi-mediated knockdown of *Ance*, the primary ACE homolog in *Drosophila*, extends lifespan[516] (**Table 2**). Lisinopril treatment fails to enhance this effect, suggesting that Lisinopril extends lifespan via inhibition of *Ance*[516]. In contrast, RNAi-mediated knockdown of the ACE2 homolog *Acer* reduces lifespan. Liao *et al.* (2013) used tissue-specific RNAi-mediated knockdown to reduce *Acer* activity in mesoderm and cardiac tissue, resulting in a reduction in lifespan, an increase in heart failure rate, a reduction in heart rate and the fractional shortening of the cardiac tissue, and an increase in systolic and diastolic diameter[561]. In agreement with this finding, Glover *et al.* (2019) observed that genetic knockout of *Acer* reduced lifespan when fed *ad libitum*, but that starvation abrogated this reduction[563] (**Table 2**).

Gabrawy *et al.* (2019) examined the effect of the ACE inhibitor Lisinopril (**Figure 2C**) on several strains of *Drosophila*[516]; in addition to extending lifespan (**Figure 3B**), Lisinopril increased physical performance in aged flies, as measured by climbing speed, strength, and endurance (**Table 1**). Lisinopril treatment reduced aberrant protein aggregation in the muscles of aged flies[516]. Lisinopril extended lifespan in three genetic backgrounds, although the degree of extension varied. However, physical performance and protein aggregation in aged flies varied in

the degree by which they were influenced by Lisinopril, suggesting that genotype can affect phenotypes caused by Lisinopril in a complex manner.

Ederer *et al.* (2018) reported a genotype-specific effect of Lisinopril on metabolism; Lisinopril lowered mitochondrial oxygen consumption in young flies, increased the number of mitochondria in aged flies, and reduced peroxide levels in young flies – however, each of these phenotypes occurred in strains with different genotypes[550]. Genotype-specific effects were also observed in thoracic metabolite concentrations upon treatment with Lisinopril.

Crocco *et al.* (2022) expanded on this work using genome-wide association studies (GWAS) on 126 *Drosophila* strains with different genotypes treated with Lisinopril; while the majority of strains displayed extended lifespan and reduced age-related physical decline, some strains displayed reduced lifespan or increased age-related decline[549]. GWAS implicated members of the WNT signaling pathway in the Lisinopril effect on climbing speed, and reducing the expression of some of these genes in skeletal muscle reduced Lisinopril's beneficial impact on climbing. However, the effect of the WNT signaling pathway on Lisinopril-induced lifespan extension or other aging phenotypes was not reported.

RAS inhibitors can increase lifespan in rodents

Rodents have long been the organism of choice for studying the RAS, given their historical use in drug discovery. Their use in the study of aging is more complicated because of their relatively long lifespan (~3 years) compared to worms and flies, making studies of the effects of drugs on lifespan more labor intensive and expensive.

The RAS has been a popular target of study for aging in mice and rats due to its well-studied effects on blood pressure. Several rodent models displaying spontaneous hypertension

are in common use; however, in comparison to the large body of evidence examining its effects on blood pressure regulation, relatively few studies have examined the effects of inhibition of the RAS on aging, normotensive rodents[588]. In aging hypertensive rodent models, inhibition of the RAS may increase survival rate due to alleviation of hypertension-associated morbidity; these effects cannot be distinguished from any beneficial effects on age-related degeneration itself. Therefore, the studies discussed below are only those that use normotensive rodents, that measure the effect of RAS inhibition in aged mice, and that use an untreated age-matched cohort as a control.

Genetic knockout of components of the RAS has been shown to influence aging in rodents. Benigni *et al.* (2009) showed that knockout of the Angiotensin II Type I Receptor (AGT1R) increased lifespan by 25% in mice, and a similar effect was reported by Yabumoto *et al.* (2015) (**Figure 4C; Table 2**)[542,564]. In addition to increased lifespan, *Agt1r*$^{-/-}$ mice displayed increased late-life cardiac health and mitochondrial function, as well as reduced frailty and healthier skin aging[542,564]. By contrast, knockout of ACE2 accelerates aging in mice[520–522], and knockout of ACE resulted in detrimental effects on health (**Table 2**)[589]; these data suggest that complete knockout of ACE is harmful, whereas complete knockout of AGT1R alone shows beneficial effects.

The effect of Enalapril on aging rodents is well-studied. Santos *et al.* (2009) showed that Enalapril treatment extends the lifespan of rats by 45% on either standard or high-fat diet (**Figure 1A, 3C; Table 1**)[540]. It has been noted that many age-related degenerative phenotypes displayed by the cardiovascular and renal system of normotensive mammals are similar to phenotypes observed in younger hypertensive mammals[590,591]. Thus, high blood pressure may accelerate aging of the cardiovascular system. Alternatively, high blood pressure may cause

pathologies that resemble age-related degeneration but are actually distinct. Treatment with anti-hypertensive medications in the absence of hypertension may have beneficial anti-aging properties[591,592]. Cardiovascular health declines with age[593], and treatment with Enalapril[554–560] or Losartan[554–558,560] improves many aspects of the health of aged rodents (**Figure 1A; Table 1**). Improvements were observed in cardiac[551,554,555] and renal health[552,556–558], reduced tumor incidence[560], reduced frailty[560], and reduced age-associated hypertension[553–557,559]. Enalapril, but not Losartan, reduced body weight in old age, suggesting that RAS inhibition of different targets may result in distinct phenotypes[551,552,554,555,560]. Body fat and food consumption were reduced, suggesting dietary restriction as a possible mechanism[559,560]. Others studies have implicated mitochondria by demonstrating an increase in mitochondrial number and function late in life and a reduction of reactive oxygen species[552,556,557].

Associations between a polymorphism in the ACE gene and longevity in humans

Human centenarians (>100 years of age) and supercentenarians (>110 years of age) are of interest for studies of aging due to their extreme longevity and extraordinarily healthy lives. In addition to extremely long lifespans, human centenarians exhibit fewer infectious diseases, lower inflammation and cancer rates, and reduced age-related comorbidities such as Alzheimer's Disease, cardiovascular disease, and hypertension[594–597]. Many studies, including several meta-analyses, investigate variants that are associated with the phenotype of extreme human longevity[598,599]. One candidate is the ACE polymorphism rs4340[599]. This polymorphism was discovered by Rigat *et al.* (1990) and is characterized by the presence or absence of a 287bp *Alu* repetitive element in intron 16[600]. The allele with the *Alu* sequence is defined as I (insertion), and the allele without the Alu sequence is defined as D (deletion)[600,601]. The D allele is most likely an ancestral version because the I allele insertion is absent from the genomes of non-human

primates[602,603]. The I and D alleles are not homogeneously distributed among the population[602,603]: the D allele is more frequent in Africa and the Middle East, whereas the I allele is more frequent in East Asia[603]. This polymorphism is likely to have a direct phenotypic consequence on the level of ACE in the plasma, since the level of ACE activity is increased in humans with the genotype D/D[601]. Cultured primary human endothelial cells with a I/I genotype exhibited lower Ang II levels and a higher cell viability compared to cells with the D/D genotype. D/D cells phenocopied I/I cells after addition of Captopril, indicating that the phenotype is caused by alterations in ACE activity[604].

Several studies investigated the association of the ACE I/D polymorphism with pathologies. The D allele is positively associated with hypertension, arteriosclerosis, cardiovascular disease, and diabetic microvascular disorders, and is negatively associated with Alzheimer's Disease[601]. By contrast, the I allele is associated with higher expression of ACE2, which has been shown to negatively affect health[605]. The positive association of the D allele with extreme longevity was investigated in over 32 studies[606]. Two meta-analysis included (1) 12 studies with a total of 1803 centenarians and 10,485 non-centenarian controls[607], and (2) 8 studies with 2043 individuals over 85 years of age and 8820 younger controls[599]. These studies identified a positive association between increased longevity and the presence of the D allele. The authors speculate that the D allele has a negative impact early in life and may grant a survival advantage in later life by effecting tissue repair and activating the immune system, thus representing a pleiotropic effect in favor of longevity[599]. It is important to note that studies with centenarians are cross-sectional rather than longitudinal, and the control group is younger individuals from a different birth cohort. In addition, associations might be caused by nearby polymorphisms that are linked to the D or I allele.

Currently available results suggest the possibility that ACE may have undefined functions in addition to its effect on blood pressure that may be responsible for the longevity effects. Humans treated with ACE inhibitors or ARBs display improvements in some measures of health and a reduction in all-cause mortality; however, no aging-focused study has been performed on normotensive humans treated with these drugs[608–611]. Interestingly, reduced mortality was reported in diabetic patients treated with ACE inhibitors but not in patients treated with the cholesterol-lowering medication Statin, suggesting that the effect of ACE inhibitors on human health is at least partially independent of its effect on cardiovascular health[610]. Future studies should address the mechanistic basis of ACE-associated longevity with a focus on determining to what degree this longevity is caused by a reduction in blood pressure.

5.4 Conclusions and perspectives

The large body of research performed on the RAS over the last several decades makes it clear that the RAS can significantly influence aging. However, several important questions at the intersection of the RAS and aging remain unanswered.

What is the function of the renin-angiotensin system in general, and the angiotensin-converting enzyme in particular, in non-vertebrate animals that lack closed circulatory systems? Treating hypertensive humans with medicines that reduce blood-pressure makes them live longer by alleviating the pathologies caused by high blood pressure, including strokes and heart disease. Thus, one model for how these same drugs extend lifespan is by reducing blood pressure. However, RAS inhibition extends lifespan in normotensive rodents. While this might indicate that lowering blood pressure below the normal level extends lifespan, it also hints that there is another mechanism. Furthermore, how does inhibition of ACE affect aging in animals that lack a closed circulatory system altogether? Clearly, in these animals, the effect cannot result from

regulation of blood pressure, so there must be an alternative mechanism. Although *Drosophila* has tissues that are analogous to the vertebrate cardiac and pulmonary systems, *C. elegans* lacks these systems altogether, yet ACE inhibitors extend lifespan in both of these organisms. We speculate that ACE has some ancestral function that mediates its effect on aging.

It is well-established that ACE is an essential enzyme in many organisms; knockout of ACE or its homologs in other species has severe negative effects on health in mammals, and is lethal in *Drosophila* and *C. elegans*[85,102,589,612,613]. ACE likely evolved in a hypothesized common ancestor of the Bilaterian clade; since that time functional ACE homologs have been conserved in such diverse species as insects[585,614–629], crustaceans[630–632], mollusks[633,634], annelids[635], nematodes[85,102,103,548], and vertebrates (reviewed in [636]). Metallopeptidase activity, predicted by the highly conserved histidine-rich HEXXH motif, is retained in all known organisms with an active ACE other than nematode ACN-1, indicating a high degree of evolutionary selective pressure to retain this motif. ACE inhibitors bind to and competitively inhibit this active site, and ACE inhibitors have been shown to function in non-vertebrate animals[615,617–619,621,622,624–627,629–632,635,637]. ACE has been shown to be involved in fertility in mice, *Drosophila* and other arthropods[582,615,617,618,620,621,624–626,629,631–633,637,638], being commonly expressed in the testis or ovaries, and effecting sperm motility or progeny production in many species. This is especially interesting considering the existence of a testis-specific isoform of ACE in mammals, called tACE; this isoform has been shown to regulate male fertility and sperm function[639]. ACE has also been implicated in ecdysis[103,615,617,622,637], being most strongly expressed during larval molts in several species. Thus, ACE plays many roles in many different organisms, but it is likely that its role as a blood pressure regulator was a later development, as this activity is not observed outside of vertebrates. It is likely that ACE evolved from earlier peptidyl dipeptidases and diverged to

serve many functions; one later development would be the maturation of blood pressure signaling peptides in a vertebrate ancestor, whose function was retained in modern vertebrates. It is likely, then, that any potential secondary effects on aging were retained in mammals as well, explaining the seemingly dual effects of ACE inhibitors on aging and blood pressure.

The *C. elegans* homolog of ACE does not conserve some amino acids necessary for catalytic function, leading to the model that it is not an active enzyme[102]. However, it has an essential function, as genetic knockout of *acn-1* is lethal; and it has been implicated as an essential regulator of molting and development, indicating an essential role for *acn-1* despite the predicted lack of metallopeptidase activity[85,102,103]. Kumar *et al.* (2016) demonstrated that Captopril treatment or knockdown of *acn-1* by RNAi still resulted in lifespan extension if administered after the final larval molt, once all known functions of *acn-1* on molting and development have presumably been completed[85]. What is the function of *acn-1* in adulthood, and why does inhibiting this function affect aging? It is possible that ACN-1 merely sequesters or is involved in the maturation of its substrate rather than acting through an enzymatic activity, or that it acts in concert with a second enzyme. Further research must be done to determine what, if any, substrate is associated with ACN-1.

The discovery of drugs which influence aging has traditionally been a strength of non-vertebrate model organisms; *C. elegans* in particular has been a fruitful ecosystem for repurposing well-studied human drugs into potential anti-aging treatments. Two of the most well-studied anti-aging compounds are the FDA-approved medications Metformin and Rapamycin. Metformin was first developed to treat type-2 diabetes, and Rapamycin is used as an immunosuppressant for organ transplants. Subsequent research in *C. elegans*[88,89,640] and *Drosophila*[641] demonstrated that these drugs control aging. Metformin has been shown to control

aging in nematodes and mice (reviewed in [642,643]). Additionally, the Targeting Research with MEtformin (TAME) project is currently testing the effect of Metformin on mortality in elderly humans[644]. The National Institute of Aging's Interventions Testing Program (ITP) has identified Rapamycin as a potent controller of aging, extending lifespan in both male and female mice by more than 10%[92,93]. Rapamycin has also been tested as a potential anti-aging therapy in non-human primates[645] and is currently being tested in canines[646]. Captopril was recently identified by the ITP as extending lifespan, making it the third FDA-approved drug with potential as an anti-aging therapy[94]. Captopril is an ideal candidate for future human studies due to its long history as a safe, effective blood pressure medication, but it has not yet been tested as an anti-aging therapy in normotensive humans. Future research in model organisms will lay the foundation for testing Captopril and other RAS inhibitors for use as an anti-aging therapy in humans.

Chapter 6: The ACE-inhibitor drug captopril inhibits ACN-1 to control dauer formation and aging

The work presented in Chapter 6 is a manuscript submitted for review to Development *with the following authors.*

It is available as a preprint on bioRxiv at https://doi.org/10.1101/2023.07.17.549402

Brian M. Egan[1], Franziska Pohl[1,2], Xavier Anderson[1,3], Shoshana C. Williams[1,4], Imienreluefe Gregory Adodo[1,5], Patrick Hunt[1], Zuoxu Wang[1], Chen-Hao Chiu[1], Andrea Scharf[1,6], Matthew Mosley[1], Sandeep Kumar[1], Daniel L. Schneider[1], Hideji Fujiwara[7], Fong-Fu Hsu[7], Kerry Kornfeld[1]

[1] Department of Developmental Biology, Washington University School of Medicine, St. Louis, MO, United States

[2] Department of Medicine, Washington University School of Medicine, St. Louis, MO, United States

[3] Department of Molecular Biosciences, Northwestern University, Evanston, IL, United States (present address)

[4] Department of Chemistry, Stanford University, Stanford, CA, United States (present address)

[5] Department of Internal Medicine, Morehouse School of Medicine, Atlanta, GA, United States (present address)

[6] Department of Biological Sciences, Missouri University of Science and Technology, Rolla, MO, United States

[7] Division of Endocrinology, Metabolism & Lipid Research, Washington University School of Medicine, St. Louis, MO, United States

I contributed to this article by designing and performing the majority of the experiments, analyzing the data, and writing the manuscript.

6.1 Abstract

The renin-angiotensin-aldosterone system (RAAS) plays a well-characterized role regulating blood pressure in mammals. Pharmacological and genetic manipulation of the RAAS has been shown to extend lifespan in *C. elegans*, *Drosophila*, and rodents, but its mechanism is not well defined. Here we investigate the angiotensin-converting enzyme (ACE) inhibitor drug captopril, which extends lifespan in worms and mice. To investigate the mechanism, we performed a forward genetic screen for captopril-hypersensitive mutants. We identified a missense mutation that causes a partial loss-of-function of the *daf-2* receptor tyrosine kinase gene, a powerful regulator of aging. The homologous mutation in the human insulin receptor causes Donohue syndrome, establishing these mutant worms as an invertebrate model of this disease. Captopril functions in *C. elegans* by inhibiting ACN-1, the worm homolog of ACE. Reducing the activity of *acn-1* via captopril or RNAi promoted dauer larvae formation, suggesting *acn-1* is a *daf* gene. Captopril-mediated lifespan extension was abrogated by *daf-16(lf)* and *daf-12(lf)* mutations. Our results indicate that captopril and *acn-1* control aging by modulating dauer formation pathways. We speculate that this represents a conserved mechanism of lifespan control.

6.2 Introduction

Aging is characterized by progressive degeneration of tissue structure and function that leads inexorably to death. A vital goal of aging research is to determine the mechanistic basis of age-related degeneration, since this information can help develop interventions that extend health span and lifespan. The renin-angiotensin-aldosterone system (RAAS) in mammals has been characterized extensively for its role in blood pressure regulation [97,99]. More recently, this pathway has been demonstrated to influence aging in a wide range of organisms; Egan *et al.*

(2022) recently reviewed emerging evidence that this pathway plays a conserved role in longevity control in worms, flies, and rodents [101]. However, the mechanism of longevity control has not been well defined in any animal, and this is now an important research objective.

Kumar *et al.* (2016) reported that captopril, an angiotensin-converting enzyme (ACE) inhibitor, extended *C. elegans* mean lifespan by ~23% and maximum lifespan by ~18% [85]. The first of what is now a large class of ACE inhibitors, captopril is an oligopeptide derivative developed in 1975 based on a peptide found in pit viper venom [509,95]. ACE inhibitors modulate the RAAS, a mechanism by which the body adapts to hypotension [513,100,514,97–99,647]. In response to a decline in blood pressure, the kidney releases renin, which cleaves angiotensinogen to angiotensin I. ACE converts angiotensin I to angiotensin II, and angiotensin II binds two transmembrane receptors – the primary effect is to stimulate aldosterone secretion and promote vasoconstriction to increase blood pressure. By blocking ACE and preventing the conversion of angiotensin I to angiotensin II, captopril lowers blood pressure (**Fig. 1A**).

Figure 1

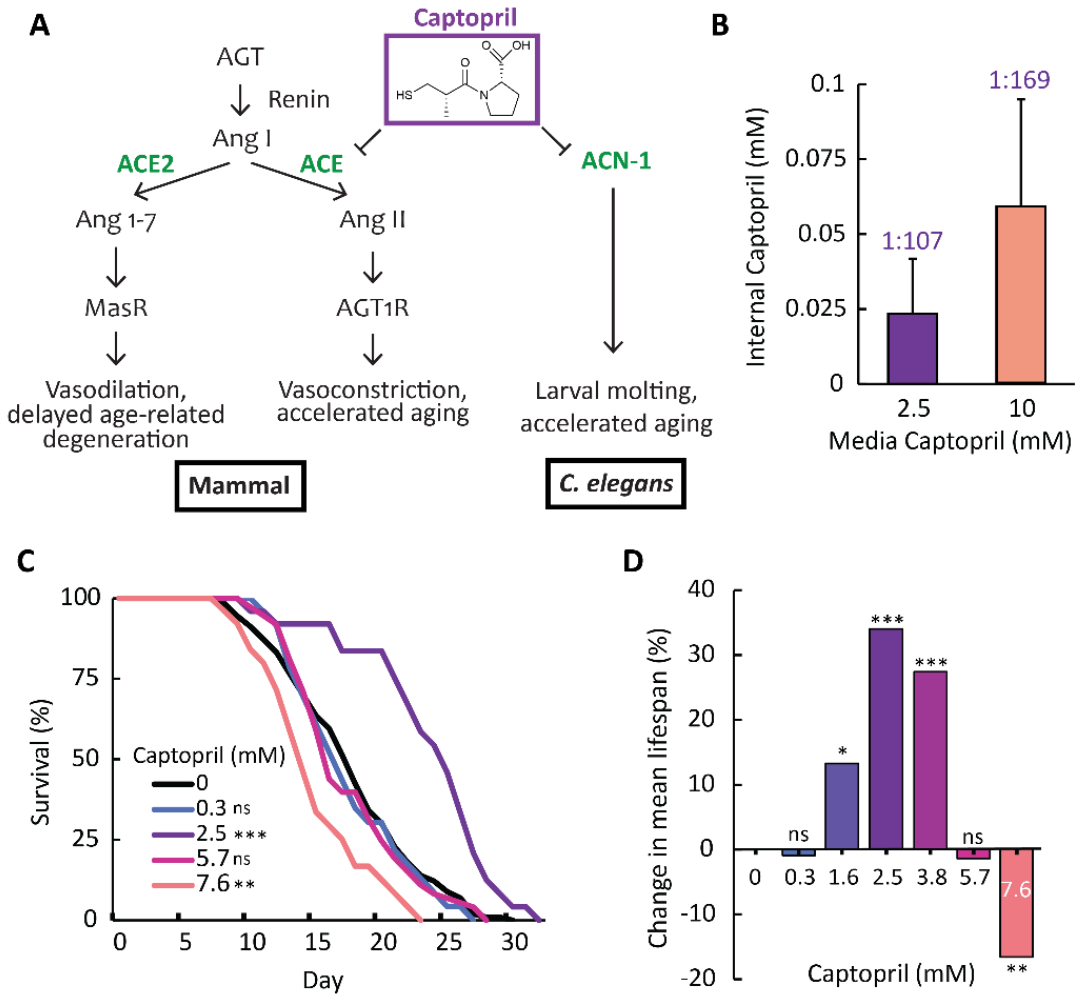

Figure 1: The ACE inhibitor captopril causes dose-dependent effects in *C. elegans*.

(A) Captopril inhibits ACE (Angiotensin-Converting Enzyme) in mammals and ACN-1 (ACE-like Non-metallopeptidase) in *C. elegans*. AGT, angiotensinogen; Ang I, angiotensin I; ACE2, angiotensin-converting enzyme 2; Ang 1-7, angiotensin 1-7; Ang II, angiotensin II; MasR, Mas receptor; AGT1R, angiotensin II type-I receptor. **(B)** The internal concentration of captopril in *C. elegans* was measured by high-performance liquid chromatography-mass spectroscopy (HPLC-MS). Media Captopril indicates the concentration in the agar medium used to culture worms; Internal Captopril indicates the concentration in whole-animal lysates. Numbers are the ratio of internal captopril to media captopril, an indication of the ability of the animals to exclude captopril. Bars represent average and s.d. n=4 biological replicates, Student's *t*-test. **(C,D)** Wild-type animals were cultured on NGM dishes seeded with *E. coli* bacteria and the indicated concentration of captopril in the medium. **(C)** Values indicate the fraction of the starting population that remains alive. **(D)** Bars represent the average change in mean lifespan compared to 0 mM control; positive values indicate lifespan extension, and negative values indicate lifespan reduction (see **Table S1** for statistics). ns, non-significant, $p \geq 0.05$; *, $p < 0.05$; **, $p < 0.01$; ***, $p < 0.001$.

In Drosophila, drugs that inhibit the ACE pathway and mutations in ACE pathway genes can both extend lifespan [550,516,648]. It has also been reported that the ACE inhibitor enalapril and the angiotensin II receptor antagonist losartan can extend the lifespan of normotensive mice and rats and delay age-related degeneration of tissue structure and function in the kidney, cardiovascular system, liver, and brain [649,552,551,555,650,557,651,559,652,554,556,558,540,560,535,553]. Based on findings in *C. elegans* [85], the Intervention Testing Program (ITP) of the National Institute on Aging tested captopril in normotensive mice; captopril significantly increased the median and maximum lifespan of female and male mice [94]. Genetic studies provide important support for these pharmacology studies, since disruption of the angiotensin II type I receptor (AGT_1R) promotes longevity in normotensive mice [564,653–656,542]. These results may be relevant to humans, since polymorphisms in the angiotensin II type I receptor gene are associated with extreme human longevity [600,657,607,599].

Isaac and colleagues reported in 2003 that *C. elegans acn-1* (ACE-like non-metallopeptidase) encodes the homolog of mammalian ACE [102]. To analyze the function of *acn-1*, Isaac and colleagues used *acn-1* RNAi [102]: larvae arrested at the L2 stage with unshed L1 cuticle, indicating a defect in molting. Delivering *acn-1* RNAi at later stages revealed cuticle defects in L3/L4 larvae and adults, indicating *acn-1* functions to promote molting at multiple stages of larval development. Furthermore, seam cells displayed fusion defects, indicating *acn-1* plays a role in establishing cell fates. Consistent with this analysis of molting, Ruvkun and colleagues identified *acn-1* in a genome wide RNAi screen for molting defects [544]. Analysis of ACN-1 transcriptional and translation reporters revealed that ACN-1 is expressed in hypodermal seam and excretory gland cells in embryos and larvae, as well as in the developing vulva and

male tail [102,544]. Slack and colleagues reported in 2017 that *acn-1* interacts with heterochronic pathways [103]. *acn-1* RNAi suppresses *let-7(lf)* lethality and seam cell defects and enhances the precocious phenotype of *hbl-1(lf)*. Loss of *apl-1* causes a similar phenotype, and loss of both *apl-1* and *acn-1* caused additive or synergistic defects. Reducing *acn-1* activity reduces expression of *apl-1*, suggesting *acn-1* functions upstream to control *apl-1* expression. These results are consistent with two reports of global analysis that identified *acn-1* among a set of genes with cyclic larval expression [658,659]. These studies led to the model that *acn-1* is a heterochronic gene that promotes larval seam cell fates by functioning downstream of *let-7* and upstream of *apl-1*.

To test the hypothesis that *acn-1* regulates lifespan, Kumar *et al.* (2016) used RNAi to reduce *acn-1* activity [85]. Wild-type animals cultured with *acn-1* RNAi starting at the embryonic stage displayed significantly extended lifespan [85]. Furthermore, *acn-1* functions in adults to extend lifespan, since animals cultured with RNAi bacteria starting at the L4 stage also display an extended lifespan; this indicates that, in addition to its regulation of molting and development in larvae, *acn-1* continues to be expressed in adults to control aging. *acn-1* RNAi delayed age-related declines of body movement and pharyngeal pumping and increased resistance to heat and oxidative stress, indicating *acn-1* activity accelerates aging and reduces stress resistance [85]. If captopril treatment and *acn-1* RNAi extend life span by a similar mechanism, then combining treatments is predicted to be non-additive. As predicted, captopril did not further extend the life span of animals treated with *acn-1* RNAi [85]. Based on these findings, Kumar *et al*. (2016) hypothesized that *acn-1* controls lifespan, and captopril extends lifespan by inhibiting ACN-1 activity (**Fig. 1A**) [85]. Captopril and other ACE inhibitors have been the topic of intense study in recent years as one of its targets, ACE2, is the cellular point-of-entry for the SARS-CoV-2 coronavirus responsible for the COVID-19 pandemic [660].

To investigate the mechanism of captopril in longevity control, we performed dose-response experiments and exploited this information to design a forward genetic screen for mutants that are hypersensitive to captopril. We identified *am326*, a novel missense allele of the *daf-2* gene, which encodes the *C. elegans* homolog of the insulin/IGF-1 receptor. The *daf-2(am326)* mutation results in an alanine to valine substitution at amino acid 261, a residue in the extracellular L1 ligand binding domain of the DAF-2 protein. This alanine residue is conserved in the human insulin receptor (INSR) at amino acid position 119 (or position 92 following the termination of the signal sequence), and human patients with the identical alanine to valine substitution suffer from Donohue syndrome (also known as "leprechaunism"), a disease characterized by growth restriction, morphological abnormalities, reduction of glucose homeostasis, and early death (<1 year of life) [661,662]. *daf-2* mutations cause an extended lifespan and a dauer constitutive (Daf-c) phenotype; mutant animals enter the dauer stage under conditions where wild type animals undergo reproductive development [663,70,48,64,566]. Our results indicate that captopril treatment and reducing the activity of *acn-1* by RNAi also cause a Daf-c phenotype, indicating that *acn-1* controls both dauer formation and adult longevity. The lifespan effects of captopril require the *daf-16* and *daf-12* genes, providing further evidence that *acn-1* interacts with the dauer pathway to promote longevity. Together, our results advance the understanding of the mechanism of action of the ACE pathway in longevity control.

6.3 Results

High dose captopril causes developmental arrest

Captopril is an established regulator of aging, since treatment can extend the lifespan of *C. elegans* and mice [85,101,94]. The optimal dose for extending longevity in *C. elegans*, 2.5 mM dissolved in nematode growth-medium (NGM), increased lifespan by more than 30% (**Fig.**

1C,D, Table S1) and delayed the age-related decline of pharyngeal pumping and body movement [85]. This dose also increases heat and oxidative stress resistance [85]. The longevity effect is dose-dependent; reducing the concentration to 0.3 mM or increasing the concentration to 5.7 mM abrogated the lifespan extension (Fig. 1C,D, Table S1). At even higher doses, captopril delayed larval development, reduced length of animals at adulthood, and reduced lifespan compared to untreated animals, indicating dose dependent toxicity (Fig. 1C,D, S1A,B, Table S1). When cultured on 16 mM captopril, most wild-type worms grew to adulthood and produced progeny by day 3 post-hatch (Fig. 2B, S1B). However, at a higher dose of 19 mM captopril, wild-type worms displayed high rates of lethality and were unable to reach adulthood (Fig. 2B).

Figure 2

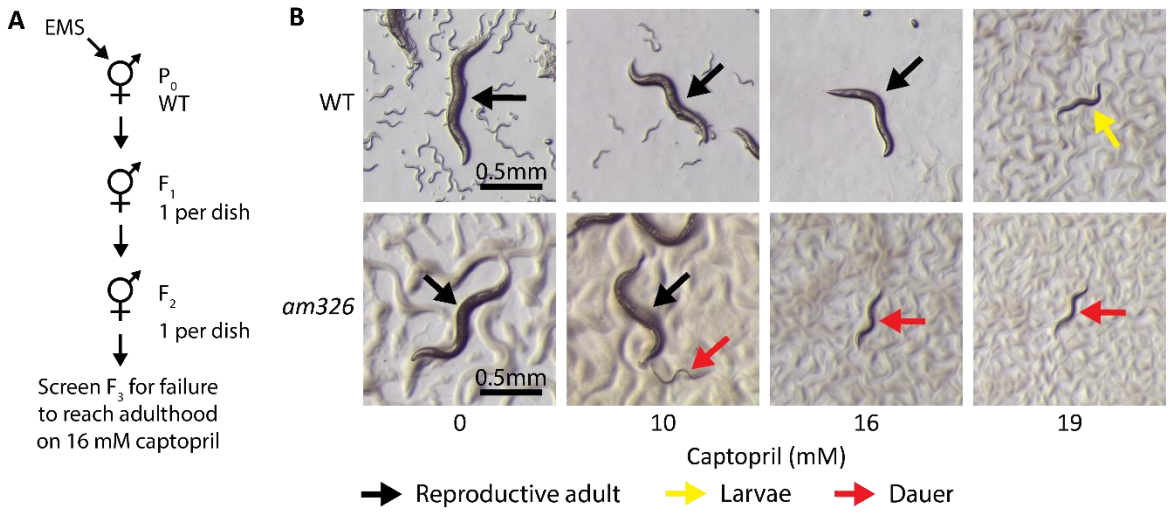

Figure 2: A forward genetic screen for mutants hypersensitive to high dose captopril.

(A) Diagram of a forward genetic screen for mutant animals that are hypersensitive to high-dose captopril. Wild-type L4 hermaphrodites were mutagenized with ethyl methanesulfonate (EMS), and clonal populations derived from individual F2 self-progeny were analyzed for failure to grow to adulthood on 16 mM captopril. **(B)** Brightfield images show WT and *am326* mutant animals cultured with the indicated concentration of captopril in the medium. WT animals mature to adulthood and produce progeny when cultured with 0, 10, and 16 mM captopril (black arrows) but display larval arrest when cultured with 19 mM captopril (yellow arrow). *am326*

mutant animals mature to adulthood and produce progeny when cultured with 0 and 10 mM captopril (black arrows), but develop as dauer larvae when cultured with 16 and 19 mM captopril (red arrow). Some *am326* animals enter dauer when cultured with 10 mM captopril. Scale bar=0.5 mm.

Determination of internal captopril concentration

C. elegans dwells in a chemically complex soil environment and is adept at excluding xenobiotic compounds. Thus, the concentration of a drug inside the worms is typically much lower than the concentration in its environment, often 2-4 orders of magnitude lower [664–666]. The concentration of captopril in the medium that is necessary for lifespan extension is well characterized, but the concentration inside the worms is unknown. To determine this value, we cultured a large population of animals with 2.5 and 10 mM captopril in the medium, collected a whole-worm lysate, and used High Performance Liquid Chromatography/Mass Spectroscopy (HPLC-MS) to measure the internal concentration of captopril. When the external concentration was 2.5 mM, the concentration in worm lysate was ~0.02 mM; this value is 107-fold lower than the external concentration, demonstrating that these animals are effective at excluding captopril (**Fig. 1B**). This value is less than one order of magnitude higher than the serum concentration in humans treated with captopril (~0.002-0.003 mM), indicating that the lifespan extending concentration in nematodes is similar to the therapeutic concentration in humans [667,668]. Increasing the external concentration to 10 mM resulted in an internal concentration of ~0.06 mM, 169-fold lower than the external concentration in the medium. Together the results indicate that the internal concentration of captopril is dose-dependent (**Fig. 1B**).

A forward-genetic screen for captopril-hypersensitive mutants

To investigate the mechanism of lifespan extension caused by captopril, we performed a genetic screen for mutants with an abnormal dose response to the drug. The aging-related

phenotypes caused by captopril, such as increased lifespan or delayed decline of body movement rate, are laborious to score and not suitable for such a genetic screen. Instead, we chose to screen for mutations that caused hypersensitivity to captopril larval arrest/lethality, since this phenotype can be readily scored. 16 mM captopril in the medium is the highest dose at which the majority of wild-type animals survive to adulthood and produce progeny (**Fig. 2B, S1B**); thus, we performed a clonal screen for populations of mutant animals that failed to survive and reproduce at this dose (**Fig. 2A**).

Wild-type L4 hermaphrodites were exposed to a chemical mutagen, 50 mM ethylmethansulfanate (EMS) as described in [3]. These P_0 animals were allowed to recover and reproduce, and their F_1 self-progeny were moved to individual dishes. F_2 progeny were moved to individual dishes and cultured until their F_3 progeny reached adulthood. Dishes containing large amounts of F_3 adults were treated with alkaline hypochlorite solution to yield eggs, and populations of F_4 eggs were cultured on dishes containing 16 mM captopril. After 4-5 days, these dishes were evaluated using a dissecting microscope for populations that lacked fertile adults.

To control for mutants that fail to thrive under non-specific stress conditions, we incorporated control dishes with a metal stress environment into the genetic screen. The same F4 population that was challenged with 16 mM captopril was also cultured on dishes containing high-dose manganese, high-dose zinc, or zinc deficiency caused by a zinc chelator (TPEN). If a mutant strain failed to reproduce in more than one stress condition, the mutant was discarded. After screening ~1,950 haploid mutant genomes, we identified one mutant strain that displayed specific hypersensitivity to captopril; we designated this mutation *am326* (**Fig. 2B**). This strain was backcrossed three times to the wild-type N2 strain, and the resulting strain (WU1939) was used for all future experiments.

am326, a mutation that causes hypersensitivity to captopril, also causes lifespan extension and promotes dauer development

When cultured with high-dose captopril, *am326* mutant animals failed to mature into adults and produced no progeny after 5 days (**Fig. 2B**). We noticed that these mutant animals formed dauer larvae, as determined by morphology observed with a dissecting microscope and survival following treatment with sodium dodecyl sulfate (SDS) [663,669–671,68]. Dauer is an alternative L3 larval stage that *C. elegans* can enter when conditions are not optimal for reproductive development [48,70,663]. These conditions include high population density, low resource availability, and elevated temperature [48,70,663]. Dauer animals are stress resistant and extremely long-lived [48,70,663,672]. *am326* mutants displayed high rates of dauer formation when cultured with 16 mM captopril; by contrast, wild-type animals did not form dauer larvae under these conditions (**Fig. 2B, 3A, Table S2**). Dauer formation was dose dependent; the percentage of dauer animals in a population increased as the captopril concentration increased (**Fig. 3A, Table S2**).

Figure 3

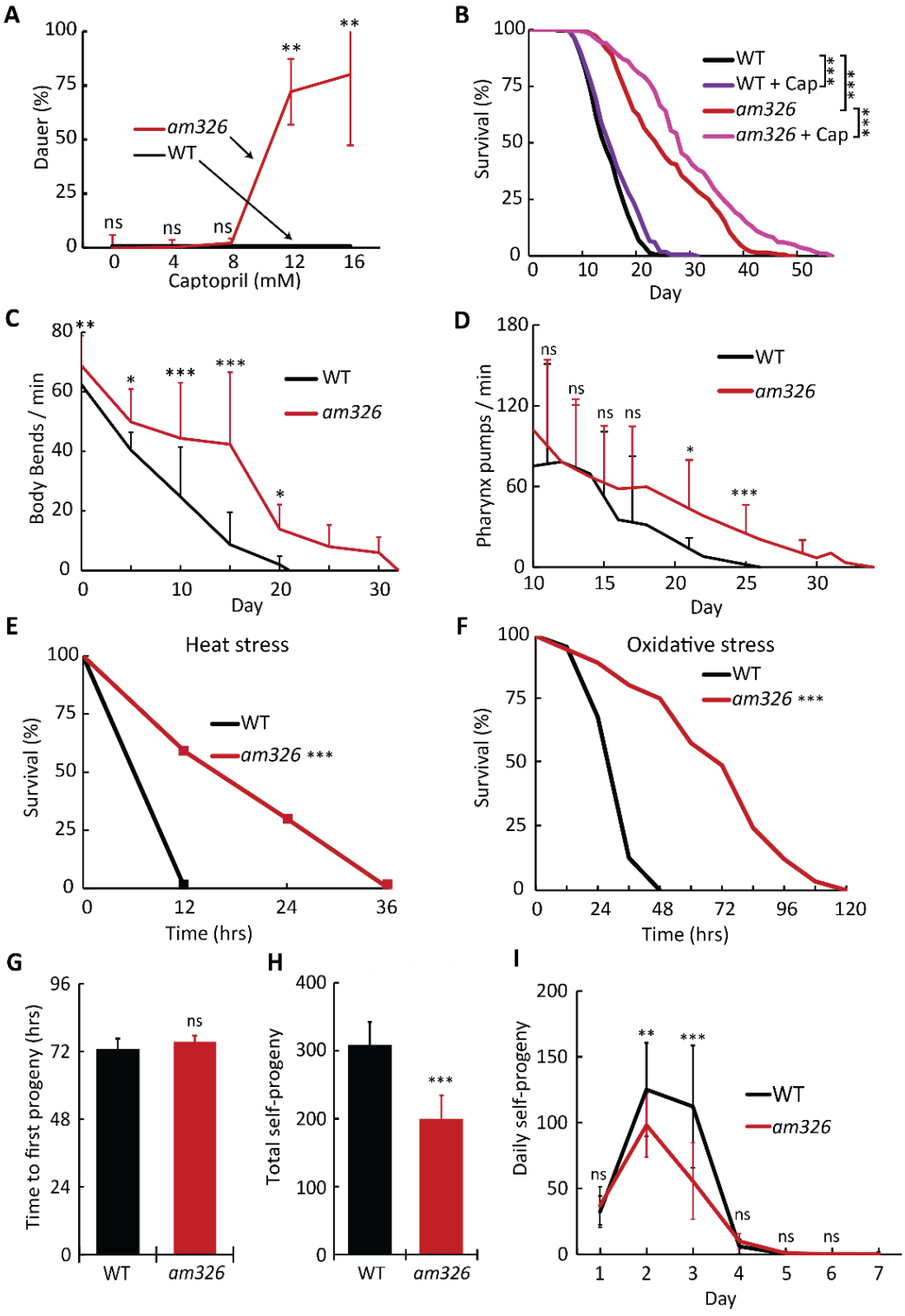
A
Dauer (%)
Captopril (mM)
am326
WT
ns
B
Survival (%)
Day
WT
WT + Cap
am326
am326 + Cap
C
Body Bends / min
Day
WT
am326
D
Pharynx pumps / min
Day
WT
am326
E
Heat stress
Survival (%)
Time (hrs)
WT
am326 ***
F
Oxidative stress
Survival (%)
Time (hrs)
WT
am326 ***
G
Time to first progeny (hrs)
WT
am326
H
Total self-progeny
WT
am326
I
Daily self-progeny
Day
WT
am326

Figure 3: Analysis of *am326* phenotypes.

(A) WT (black line) and *am326* mutant (red line) embryos were cultured on dishes containing the indicated concentration of captopril at 20°C. Values are the average percentage of animals in the dauer stage and s.d. (see **Table S2** for statistics). **(B)** WT and *am326* mutant animals were cultured with 0 or 2.5 mM captopril (+ Cap). Values indicate the fraction of the starting population that remains alive (see **Table S3** for statistics). **(C)** Movement of WT and *am326* mutant animals was measured by counting body turns in 15 s intervals using a dissecting microscope throughout adulthood. Values are body bends per minute and s.d. n=25-40 animals, one-way ANOVA with Tukey's post-hoc HSD. **(D)** Pharyngeal pumping rate of WT and *am326* mutant animals was measured in 15 s intervals using a dissecting microscope throughout adulthood. Values are average pharynx pumps per minute and s.d. n=27-30 animals, one-way ANOVA with Tukey's post-hoc HSD. **(E)** Thermotolerance was measured by culturing WT and *am326* mutant embryos at 20°C for 72 hrs (until ~adult day 0), shifting animals to 35°C, and measuring survival every 12 hrs. Values indicate the fraction of the starting population that remains alive (see **Table S3** for statistics). **(F)** Resistance to oxidative stress was measured by culturing WT and *am326* embryos on standard medium for 72 hrs (until ~adult day 0), transferring animals to medium containing 40 mM paraquat, and measuring survival every 12 hrs. In this experiment, animals that died from matricidal hatching were not censored because matricidal hatching was the primary cause of death for paraquat-treated animals. Values indicate the fraction of the starting population that remains alive (see **Table S3** for statistics). **(G)** Freshly laid eggs from WT and *am326* hermaphrodites were cultured for 65 hrs, then the resulting self-fertile adults were observed hourly to determine the time when they laid their first egg. Values are average time to first egg lay and s.d. n=15-16 animals, Student's *t*-test. **(H,I)** Total brood size and daily progeny production of self-fertile hermaphrodites were measured by counting the number of viable self-progeny produced by WT and *am326* hermaphrodites throughout their reproductive period. Values are average number of progeny and s.d. n=14 animals. H, Student's *t*-test; I, one-way ANOVA with Tukey's post-hoc HSD. ns, non-significant, $p \geq 0.05$; *, $p < 0.05$; **, $p < 0.01$; ***, $p < 0.001$.

To investigate the role of the *am326* mutation in aging, we measured age-related phenotypes. Homozygous *am326* mutant animals displayed an increased lifespan of 74.5% compared to wild type; captopril treatment further extends the lifespan of *am326* mutants, indicating the mutation does not abrogate the effect of the drug (**Fig. 3B, Table S3**). To analyze health span, we measured the age-related declines of body movement and pharynx pumping. Homozygous *am326* mutant animals displayed reduced age-related declines in body movement and pharyngeal pumping; these phenotypes are only apparent after mid-life (**Fig. 3C,D**). Some mutations that extend lifespan also increase stress resistance [673,674]. Homozygous *am326* mutant

animals displayed increased heat and oxidative stress resistance (**Fig. 3E,F, Table S3**). Some mutations that extend lifespan also delay development, reduce fecundity, and/or extend the reproductive period [15,199,675]. Homozygous *am326* mutants did not display delayed development compared to wild type, as determined by measuring the duration from hatching to egg-laying (**Fig. 3G**). Homozygous *am326* mutant hermaphrodites did display a 35% reduction in self-progeny number compared to wild type (**Fig. 3H**); however, these mutants did not display an extension of the reproductive period (**Fig. 3I**). Thus, the *am326* mutation causes a large magnitude lifespan extension, extension of neuromuscular health span, increased stress resistance, and a moderate reduction in brood size, but does not cause a delay in developmental or reproduction.

am326 is a previously uncharacterized missense mutation in the *daf-2* receptor-tyrosine kinase gene

To identify the molecular lesion in the *am326* strain, we utilized an EMS density mapping strategy [676]. We performed multiple independent backcrosses to the wild-type N2 strain using the temperature-dependent dauer formation phenotype to homozygose *am326/am326* animals. Using whole genome sequencing, we generated a list of 45 base pair variants that were present in all backcrossed *am326/am326* strains but were absent from wild type, indicating they were caused by the EMS mutagenesis and are strongly linked to *am326* (**Table S4**). 36 variants were clustered in a region of chromosome III between 2.5 and 5.6 Mbp, suggesting that one of the variants in this region was likely the causative mutation. The remaining 9 variants were dispersed on other chromosomes (**Fig. 4A, Table S4**). We predicted the effect of each variant on gene activity; variants outside coding regions (introns, 5' untranslated regions, intergenic regions, or non-coding RNA) were excluded. Eight variants affected exons, including one missense change in the *daf-2* gene. This mutation is a single nucleotide change (cytosine to

thymine) at position 782, resulting in an alanine (GCG) to valine (GTG) substitution. The lesion occurs in exon 7, which encodes the extracellular L1 ligand binding domain of the DAF-2

Figure 4

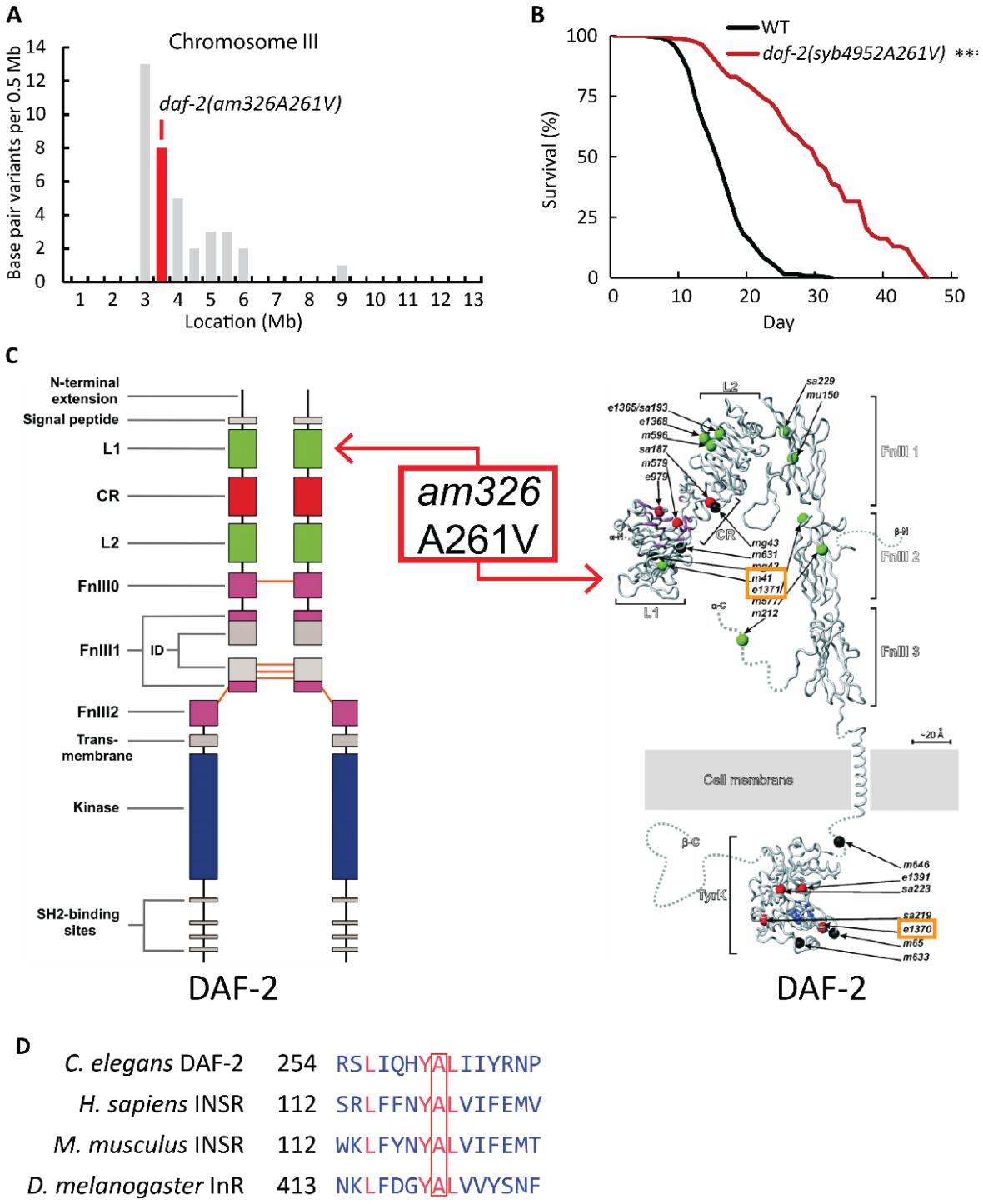

protein (**Fig. 4C**).

Figure 4: *am326* is an allele of *daf-2*.

(A) The x-axis represents the location on chromosome III in megabases (Mb). Bars indicate the number of base pair variants in the *am326* strain in 500,000 base pair bins. Red indicates the location of *am326*, an allele of *daf-2*, at position 3,015,386 bp (see **Table S4** for details). **(B)** WT and *daf-2(syb4952A261V)*, a CRISPR-generated mutant strain, were analyzed for survival. Values indicate the fraction of the starting population that remains alive. (***, $p<0.001$; see **Table S5** for statistics). **(C)** Left, a diagram of the predicted DAF-2 protein as a dimer with domains colored and labelled. The *am326* mutation causes an alanine to valine substitution at amino acid 261 that affects the L1 extracellular ligand-binding domain (L1BD); right, a structure of the DAF-2 protein showing the location of the alanine to valine substitution in the L1BD and the location of other amino acid substitutions caused by previously characterized mutations of *daf-2*. Orange boxes: *daf-2* mutations used in this study. Adapted from [67]. **(D)** Multiple sequence alignment of DAF-2 and homologs in humans, mice, and *Drosophila*. Conserved amino acids are red, and Alanine 261 is marked by the box. Alignment was performed using COBALT [677].

DAF-2 is a well-studied member of the insulin/IGF-1 signaling (IIS) pathway; numerous partial loss-of-function mutations in this gene have been shown to affect aging, development, and dauer entry [64,66,67]. We hypothesized that the missense mutation in *daf-2* is the cause of the *am326* mutant phenotype, since *daf-2* mutant animals have been previously demonstrated to cause phenotypes including Daf-c, extended lifespan, stress resistance, and reduced brood size [64,678,566] (reviewed in [66,67]). To test this hypothesis, we performed complementation assays. Male P_0 *am326* animals were crossed to hermaphrodite P_0 animals with *daf-2(lf)* mutations, as well as hermaphrodite P_0 animals with an *age-1(lf)* mutation as a control; *age-1(lf)* mutants also display temperature-dependent dauer formation [4,679,680]. Heterozygous F_1 larvae were temperature-shifted to 25°C for 48 hours and observed for dauer formation. **Table 1** shows that *am326* failed to complement *daf-2(lf)* mutations, but complemented an *age-1(lf)* mutation, indicating that the *am326* mutation is an allele of the *daf-2* gene.

Table 1: Complementation tests indicate that *am326* is an allele of *daf-2*

Genotype[a]	**Parental mating status[b]**	**Dauer (%) (25°C)[c]**	**N (n)[d]**
WT	Self	0	232 (3)

daf-2(am326)	Self	100	184 (3)
daf-2(syb4952)	Self	100	553 (6)
+/daf-2(am326)	Cross	0	255 (5)
daf-2(e1370)/daf-2(am326)	Cross	100	226 (5)
daf-2(e1368)/daf-2(am326)	Cross	100	77 (5)
daf-2(m41)/daf-2(am326)	Cross	84.7	72 (3)
age-1(hx546)/+ ; +/daf-2(am326)	Cross	0	49 (2)
+/daf-2(syb4952)	Cross	0	406 (5)
daf-2(am326)/daf-2(syb4952)	Cross	100	280 (4)
daf-2(e1370)/daf-2(syb4952)	Cross	99.6	225 (5)

[a] Animals were wild type (WT) or had the indicated alleles of *daf-2* and *age-1*. For cross progeny, the allele(s) contributed by the hermaphrodite are on the left, and allele(s) contributed by the male are on the right.

[b] Self: Self-fertile hermaphrodites generated homozygous progeny scored for dauer. Cross: males were mated to hermaphrodites, and F_1 cross-progeny were scored for dauer.

[c] The percentage of dauer larvae was determined by counting the number of dauer larvae and dividing by the total number of surviving animals. Animals were cultured at 25°C and analyzed 2-3 days after the embryo stage; dauer was defined using visual inspection and morphological criteria.

[d] N, total number of animals; n, number of independent trials.

DNA sequencing was used to confirm the presence of the *daf-2(am326A261V)* allele in the originally isolated *am326* mutant strain and in four serially backcrossed mutant strains (WU1975-WU1978); this allele was not present in the wild-type strain used for EMS mutagenesis, indicating a strong correlation between the *daf-2(am326A261V)* allele and the Daf-c phenotype. Because alanine and valine are similar amino acids, we wanted to rigorously confirm that this missense change causes the phenotype. CRISPR genome editing was used to insert this base change into the endogenous *daf-2* locus of a wild-type N2 strain. The resulting *daf-2(syb4952A261V)* mutant animals displayed a 100% penetrant Daf-c phenotype (**Table 1**). Furthermore, the *daf-2(syb4952)* allele failed to complement the *daf-2(am326)* and *daf-2(e1370)* mutations for the Daf-c phenotype, demonstrating that the A261V change caused a *daf-2* loss-of-function phenotype (**Table 1**)**.** As expected, the *daf-2(syb4952)* mutant animals displayed

temperature- and captopril-dependent dauer formation (**Table 1, S2**), and were long-lived (**Fig. 4B, Table S5**). DAF-2 is the nematode homolog of the mammalian insulin receptor (INSR); we performed amino acid sequence alignment to examine if this amino acid was conserved in homologous proteins. Alanine 261, as well as the adjacent amino acids, are present in the homologous position in human and mouse INSR and the *Drosophila* insulin receptor (InR), indicating that this region is highly conserved (**Fig. 4D**).

Captopril treatment influences dauer development

Some *daf-2* loss-of function mutations, such as *daf-2(e1370),* cause a temperature sensitive Daf-c phenotype [64,67]. To evaluate the temperature sensitivity of the *daf-2(am326)* phenotype, we cultured animals at 20, 22, and 25°C and measured the percentage of dauer larvae in the population. The percentage of dauer larvae increased significantly from 0% at 20°C to 16.8% at 22°C and 90% at 25°C (**Fig. 5A, Table S2**). To investigate the interaction with captopril treatment, we cultured animals with 0, 4, 8, 12 or 16 mM captopril at the three temperatures. At 20 and 22°C, captopril treatment caused a dose-dependent increase in dauer formation (**Fig. 5A, Table S2**). At 25°C, the lowest dose of captopril (4 mM) resulted in constitutive dauer formation; at 16 mM captopril, the percentage of animals that entered dauer was reduced as a result of some animals undergoing larval arrest prior to the L2 stage. Thus, the dauer formation promoting effect of captopril is dose dependent and additive with high temperature.

Figure 5

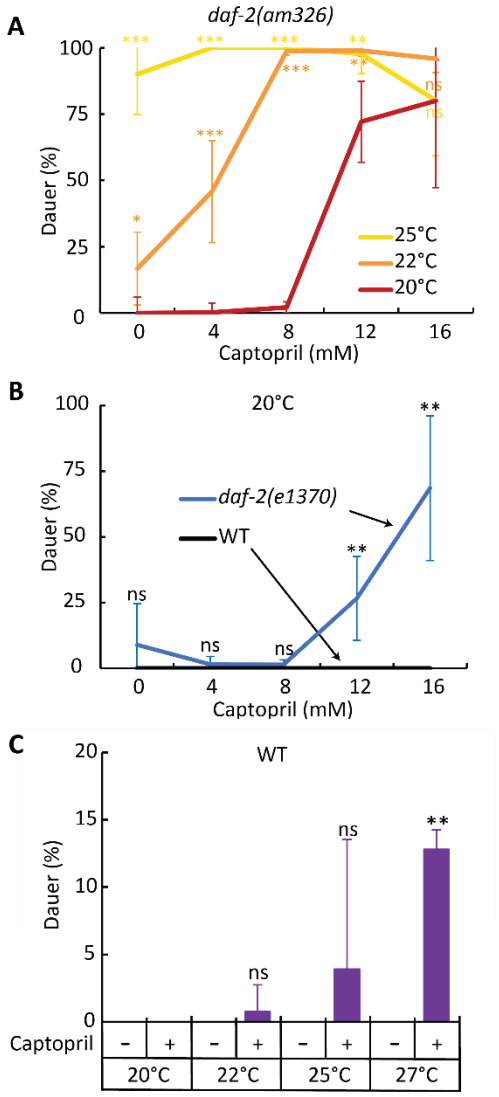

Figure 5: Captopril promotes dauer formation.

(A) *daf-2(am326)* embryos were cultured with the indicated concentration of captopril at 20°C (red), 22°C (orange) or 25°C (yellow). Values are the average percentage of animals in the dauer stage and s.d. At 22 and 25°C, animals treated with 16 mM captopril displayed less than 100% dauer because some animals arrested at developmental stages prior to L2. **(B)** WT (black line) and *daf-2(e1370)* mutant (blue line) embryos were cultured on dishes containing the indicated concentration of captopril at 20°C. Values are the average percentage of animals in the dauer stage and s.d. **(C)** WT embryos were cultured with either 0 (-) or 16 (+) mM captopril at the indicated temperatures. Values are the average percentage of animals in the dauer stage and s.d. (see **Table S2** for statistics on this figure). ns, non-significant, p≥0.05; *, p<0.05; **, p<0.01; ***, p<0.001.

To determine whether captopril-induced dauer formation was a specific effect of the *am326* allele or a general property of *daf-2(lf)* mutants, we measured the effect of captopril on *daf-2(e1370).* Captopril induced dauer formation in a dose-dependent manner, suggesting that this effect is not specific to *daf-2(am326)* (**Fig. 5B, Table S2**).

To evaluate the specificity of the captopril effect on dauer formation, we analyzed a different small molecule drug that extends lifespan and is toxic at high doses, the anticonvulsant ethosuximide [681,682]. Ethosuximide is an FDA-approved medication that was previously shown to extend lifespan in *C. elegans* at a similar concentration to captopril (2-4 mM). We exposed *daf-2(am326)* mutants to ethosuximide at concentrations up to 32 mM; no significant dose-dependent effect on dauer formation was observed at 20, 22, or 25°C (**Fig. S2A,B, Table S6**). These results suggest the dauer formation phenotype is a distinctive effect of captopril and not a general xenobiotic stress response.

To determine if the dauer promoting effects of captopril require a *daf-2* mutation or can also be observed in wild-type animals, we used high temperature to sensitive wild-type animals to dauer formation and examined the effect of captopril. We cultured wild-type animals at 20, 22, 25 and 27°C, since 27°C was previously shown to induce dauer in HID (high-temperature dauer induction) mutants [683]. At 22 and 25°C, 16 mM captopril treatment resulted in a small increase of dauer formation to 0.8% and 3.9%, respectively, that was not statistically significant with this sample size. At 27°C, 16 mM captopril significantly increased dauer formation to 12.8% (**Fig. 5C, Table S2**). Thus, the dauer promoting effect of captopril can be observed if animals are sensitized using a *daf-2* mutation or simply using high temperature in wild-type animals.

The *acn-1* gene promotes dauer formation

Based on our model that captopril functions by inhibiting the *acn-1* gene (**Fig. 1A**), we hypothesized that reducing the activity of *acn-1* would promote dauer formation. To test this hypothesis, we treated *daf-2(am326)* mutants with bacteria expressing *acn-1* dsRNA and measured dauer formation. *acn-1* RNAi failed to induce the dauer state in wild-type animals at either 20, 22, or 25°C (**Fig 6A, Table S7**); this result is consistent with our observation that captopril fails to significantly induce dauer formation under similar conditions. However, *acn-1* RNAi significantly increased the percentage of dauer stage animals in *am326* mutants from 13.8% to 31.5% at 22°C (**Fig. 6A, Table S7**). This finding suggests that reducing *acn-1* activity through RNAi or inhibition with captopril promotes dauer formation under the sensitized conditions created by the *daf-2(am326)* mutation.

Figure 6

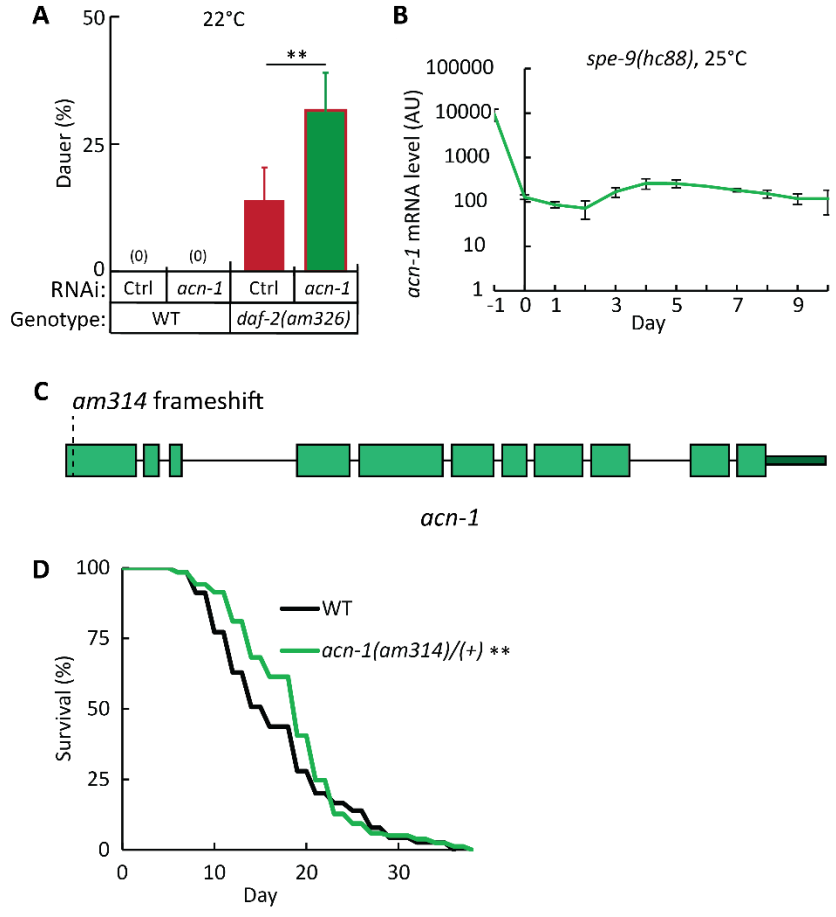

Figure 6: *acn-1* is expressed in larvae and adults and influences dauer formation and adult lifespan.

(A) WT and *daf-2(am326)* embryos were cultured at 22°C with *E. coli* HT115 expressing either *acn-1* dsRNA or a vector control. Values are the average percentage of dauer larvae and s.d. (see **Table S7** for statistics). **(B)** *spe-9(hc88)* arrested at the L1 stage were transferred to dishes with abundant *E. coli* and cultured at 25°C until the indicated day; total RNA was analyzed by RNAseq. Values are *acn-1* mRNA level in arbitrary units (AU) and s.d. Days -1 and 0 were larval stages, and Day 1 was defined as the first day of adulthood; at 25°C, Day 1 occurs approximately two days after arrested L1 animals were transferred to food. **(C)** Diagram of the *acn-1* gene showing the location of the *am314* frameshift mutation. Green boxes, exons; black lines, introns; dark green box, 3' UTR. **(D)** WT and animals heterozygous for *acn-1(am314)*, a CRISPR-generated mutation, were analyzed for survival. Values indicate the fraction of the starting population that remains alive (see **Table S5** for statistics). **, $p<0.01$.

To elucidate how reducing *acn-1* activity causes an extension of lifespan, we monitored *acn-1* expression daily beginning in larvae and extending until ~day 12 of adulthood. *acn-1* mRNA levels were measured by RNA-seq in a synchronized population of *spe-9(lf)* animals raised at 25°C to prevent progeny production. *acn-1* mRNA levels were high in larvae, consistent with previous reports (**Fig. 6B**) [102,544,545,103]**.** Interestingly, *acn-1* mRNA levels declined in young adults but then remained relatively constant throughout adulthood (**Fig. 6B**). These results suggest that *acn-1* is expressed in young and old adults, consistent with an activity in adults that controls aging.

We previously used RNAi to investigate *acn-1* function in adults. To extend this analysis, we used CRISPR/Cas9 genome editing to generate a chromosomal mutation, *acn-1(am314)*. This allele has a four base pair insertion that is predicted to cause an early frameshift mutation and a strong loss of function (**Fig. 6C**). Homozygous *acn-1(am314)* mutant animals are not viable, consistent with previous reports that the *acn-1* gene has an essential function in larval development [102,544,545,103]. To evaluate an effect on aging, we analyzed the lifespan of *acn-1(am314)/acn-1(+)* heterozygous animals, which are viable. *acn-1(am314)/acn-1(+)*

heterozygous mutants significantly extended mean lifespan by 15.1% compared to controls (**Fig. 6D, Table S5**). Thus, a partial reduction of *acn-1* activity caused a lifespan extension, indicating *acn-1* is necessary to accelerate adult lifespan. This result is consistent with results that *acn-1* RNAi, which also partially reduces gene activity, causes a lifespan extension [85].

The *acn-1* gene and captopril treatment interact with the *daf-16* and *daf-12* genes

daf-16 encodes a forkhead transcription factor that functions downstream of *daf-2* [684–686]. *daf-16(lf)* mutations cause a Daf-d phenotype and suppress both the Daf-c and lifespan-extension phenotypes caused by *daf-2(lf)* mutants [687]. To investigate the interaction with the new *daf-2(am326)* mutation, we constructed a double mutant with *daf-16(mu86),* a strong loss-of-function allele, and treated these animals with captopril. Whereas captopril treatment extended lifespan and promoted dauer formation in *daf-2(am326)* single mutants, captopril failed to extend lifespan or induce dauer formation in these double mutant animals (**Table S5**). Thus, *daf-16* is necessary for the lifespan extension and Daf-c phenotype caused by *daf-2(am326)* and/or captopril. Kumar *et al.* (2016) reported that captopril and *acn-1* RNAi do not cause a lifespan extension in *daf-16(lf)* mutants, indicating that the activity of *daf-16* is necessary for these lifespan extending treatments; here, we confirm the results from captopril treatment (**Fig. 7A, Table S5**) [85]. However, captopril treatment does not induce nuclear localization of DAF-16 [85]. To explore the mechanism of DAF-16 activity, we analyzed the expression of a *daf-16* target gene, *sod-3* [688–690], using RT-qPCR in adult day 1 animals. Captopril treatment did not increase *sod-3* expression levels (**Fig. S3A**), suggesting that captopril treatment does not activate DAF-16 transcriptional activity. To determine if the effect might be age specific, we analyzed young (adult day 1) and middle-aged (adult day 5) animals using a fluorescent *sod-3p::gfp* transcriptional reporter. Captopril treatment did not significantly increase *sod-3* expression at

either stage (**Fig. S3B**). Thus, captopril treatment does not cause nuclear localization of DAF-16 or the activation of the *sod-3* target gene, and yet *daf-16(lf)* mutations block the lifespan extension caused by the drug.

Figure 7

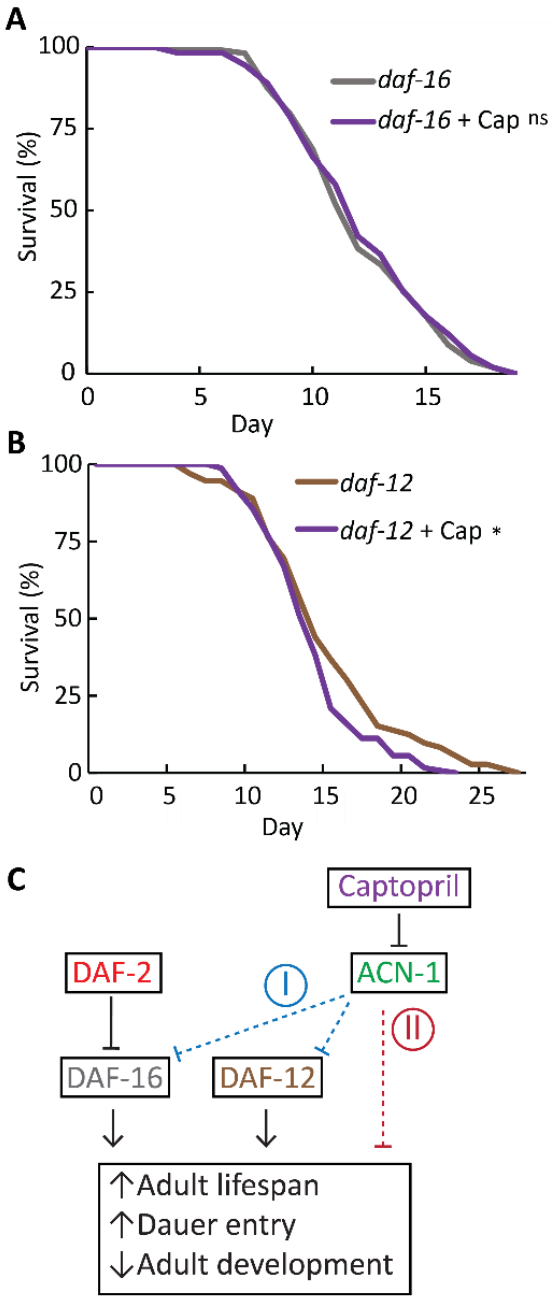

Figure 7: Captopril interacts with *daf-12* and *daf-16*.

(A,B) *daf-16(mu86) and daf-12(rh61rh411)* are both loss-of-function mutations. Mutant animals were cultured with 0 or 2.5 mM captopril (+ Cap). Values indicate the fraction of the starting population that remains alive. Captopril treatment caused a small yet significant reduction in mean lifespan in *daf-12* mutants and no significant change in *daf-16* mutants. ns, nonsignificant, $p \geq 0.05$; *, $p < 0.05$ (see **Table S5** for statistics). **(C)** A model for captopril/ACN-1-mediated control of aging and dauer formation. The DAF-2 receptor-tyrosine kinase inhibits the DAF-16 transcription factor (bar), thereby reducing lifespan, inhibiting dauer formation, and promoting larval development into reproductive adulthood. The DAF-12 transcription factor acts parallel to this pathway. ACN-1 functions to reduce adult lifespan, inhibit dauer formation, and promote larval development into reproductive adulthood; captopril functions by inhibiting ACN-1. We propose two models for ACN-1. I, blue: ACN-1 inhibits the activity of both the DAF-16 and DAF-12 transcription factors, reducing their ability to increase lifespan, promote dauer formation, and inhibit reproductive development. II, red: ACN-1 acts parallel to DAF-16 and DAF-12 to affect these phenotypes independently.

The *daf-12* gene encodes a nuclear hormone receptor that functions in parallel to DAF-16 to promote dauer formation and transcription of longevity-inducing genes [687,691–693]. *daf-12(lf)* mutations reduce lifespan and cause a Daf-d phenotype, similar to *daf-16(lf)* mutations [669,671,694–696,691,693]. To investigate the interaction with captopril, we treated *daf-12(rh61rh411)* mutants with the drug. Captopril treatment did not extend the lifespan of *daf-12(rh61rh411)* mutants, indicating *daf-12* is necessary for captopril-induced lifespan extension (**Fig. 7B, Table S5**). Thus, the activity of both *daf-16* and *daf-12* are necessary for the lifespan extension caused by captopril, linking two genes involved in dauer formation with the lifespan extension effects of captopril.

6.4 Discussion

The *C. elegans* DAF-2(A261V) mutant protein corresponds to the human INSR(A119V) mutant protein that causes Donohue syndrome

An important avenue of research in the field of aging is the identification and characterization of genes which control aging. Insulin signaling controls aging across species – reducing the activity of IIS pathway components in *C. elegans, Drosophila,* and mice extends

lifespan and delays age-related degeneration [64,697–700,165,701]. In humans, this relationship is more complex, as reduction of insulin signaling is most often associated with diabetes and reduced lifespan. However, humans with exceptional longevity often display reduced insulin resistance [702], and altered insulin signaling in the brain has been associated with age-related neurodegenerative diseases such as Alzheimer's Disease [703,704], pointing to a complex role of insulin signaling in human aging. The discovery and characterization of mutations affecting IIS pathway components represents an important avenue for furthering our understanding of aging.

In addition to aging, this pathway also regulates entry into the dauer state. Using an unbiased forward genetic screen, we identified a novel *daf-2* mutant and used it to characterize a previously unobserved interaction between captopril treatment, *acn-1* inhibition, and the dauer state. Much work has been done to categorize the numerous *daf-2* mutants based on their common phenotypes [66,67]; these include extended lifespan, ectopic dauer formation, thermotolerance, and a reduction in the percentage of unfertilized oocytes compared to wild type. Subsets of *daf-2* mutants display additional phenotypes, including larval arrest, gonad abnormalities, reduced motility, and reduced fecundity. Our results suggest *daf-2(am326)* is a class II allele, based on constitutive dauer larvae formation at 22 and 25°C, extended lifespan, thermotolerance, and reduced brood size. Although *daf-2(am326)* mutants display a reduced brood size, these animals are relatively healthy in other respects. We did not observe a delay in development, reduced motility, larval arrest, gonad abnormalities, or elevated matricidal hatching. Thus, *daf-2(am326)* lacks many negative pleiotropies common to other *daf-2(lf)* mutants, and represents a useful reagent for future research on aging and insulin signaling.

The *daf-2(am326)* mutant phenotype results from an alanine to valine substitution at amino acid position 261. This residue is located in the extracellular L1 ligand binding domain of

the DAF-2 protein, where a variety of ligands bind to and activate the kinase activity of DAF-2 [566,705,706]. Several other point mutations in this region have been shown to affect DAF-2 function, including *pe1230, gv51,* and *e979*, suggesting that relatively minor changes in protein primary structure in this region can result in large changes to protein function [707,67,708,709]. This alanine residue is conserved in the human insulin receptor (INSR) at amino acid position 119 [662]. Interestingly, the precise molecular lesion observed in *daf-2(am326)* has been associated with human patients that suffer from Donohue syndrome, a disease characterized by growth restriction, morphological abnormalities, reduction of glucose homeostasis, and early death (<1 year of life) [662]. Our results contribute two valuable insights regarding this A to V mutation that may be relevant to the human condition: (1) this mutation is recessive; (2) this mutation causes a strong loss of function in an intact animal. Consistent with these conclusions, cell culture experiments revealed that the A119V substitution severely reduces the ligand binding activity of the human INSR [662]. Previous work by Krause and colleagues has established *C. elegans* as a useful model for human insulin receptoropathies, though the INSR A119V mutation has not previously been examined in an animal model [709]. Thus, *daf-2(am326)* represents a unique opportunity to model a human INSR receptor pathology in the experimentally powerful *C. elegans* system.

Identification of *acn-1* as a regulator of dauer formation

The identification of compounds that delay aging is critical for the field of gerontology, and model organisms such as *C. elegans* are extremely useful for screening large numbers of potential compounds. While many compounds have been found to extend lifespan in *C. elegans,* only a few have been shown to extend lifespan in mammalian model organisms, and none have been identified in humans (reviewed in [12,13,710]). Pharmacological and genetic inhibition of the

RAAS pathway can extend lifespan in *C. elegans, Drosophila melanogaster*, and rodents [101]. However, the mechanism has not yet been well defined. Given the well-established function of the RAAS in mammalian blood pressure regulation, an appealing explanation is that RAAS inhibition extends lifespan by lowering blood pressure, thereby reducing mortality related to hypertension. However, ACE inhibitors extend lifespan even in normotensive rodents [540]. Furthermore, this hypothesis fails to explain the effect in *Drosophila* or *C. elegans*, animals which lack closed circulatory systems, suggesting that this is not a general model. It appears that the ACE protein evolved prior to the evolution of the closed circulatory system, implying that ACE has an ancestral function unrelated to blood pressure regulation [533,711]. The observation that ACE inhibition extends lifespan in multiple species suggests that this ancestral function may control aging. Our results indicate that ACE modulates insulin/IGF-1 signaling pathways to control aging and development.

Previous studies indicate *acn-1* as a critical regulator of molting, development, and aging [85,102,103], and here we demonstrate a previously uncharacterized activity: control of dauer entry. Our results are consistent with two models (**Fig. 7C**). In **Model I**, ACN-1 acts upstream in a linear genetic pathway to inhibit DAF-16 and DAF-12; the mechanism of regulation is likely indirect. Inhibition of ACN-1 by captopril or RNAi promotes the activity of DAF-16 and DAF-12, thereby increasing lifespan and dauer formation. In **Model II**, ACN-1 functions in a parallel genetic pathway to DAF-16 and DAF-12 to reduce lifespan and promote reproductive development. While our results are consistent with either model, it is notable that *acn-1* RNAi and/or captopril treatment did not cause DAF-16 nuclear localization [85] or activation of the *sod-3* target gene which favors Model II.

During early development, *C. elegans* must measure a spectrum of external signals (food availability, population, temperature, etc.) and integrate that input into a binary output: either dauer or non-dauer. Here, we provide evidence that ACN-1 is acting as a member of the dauer decision machinery. The dauer stage is a diapause mechanism that promotes survival during long-term stresses and resource deprivation – situations that are common in the wild. Dauer animals are able to survive in conditions that are fatal to non-dauers; however, dauers are sterile, and cannot transition back into reproductive development until conditions improve. Thus, improper entry into the dauer state under conditions which would otherwise permit reproduction represents a severe malus to the animal's fitness. Complex regulatory mechanisms have evolved to provide accurate information on environmental conditions, allowing worms to make developmental decisions that maximize fitness outcomes. The insulin/IGF-1 signaling pathway is involved in interpreting external signals and implementing changes in gene expression. The receptor-tyrosine kinase DAF-2 interacts with a variety of extracellular substrates which, under dauer-inducing conditions, result in a series of phosphorylation events that serve to inhibit the DAF-16/FOXO transcription factor. In *daf-2(lf)* mutants, DAF-16 is activated, promoting dauer formation and the expression of stress-resistance and longevity-inducing genes, such as *sod-3* [688–690]. ACN-1 may function in a similar fashion to integrate or modulate external signals into developmental decision-making.

To date, few compounds have been identified that induce dauer formation in *C. elegans*. Ascarosides, a structurally diverse group of small molecule signaling pheromones, are excreted under conditions of high population density [712,713]. Dafachronic acids, a group of endogenously produced steroid hormones, bind to and remove the co-repressor from the DAF-12 nuclear hormone receptor [691,714]. In addition to these endogenously produced compounds, the small

molecule dafadine induces the dauer state by inhibiting DAF-9, a key effector of dafachronic acid synthesis and DAF-12-dependent dauer entry [715]. Captopril represents a newly discovered addition to the list of compounds that induce dauer, and our results suggest that the mechanism may be through modulation of the *daf* pathway. Captopril is the only one of these compounds that is known to be biologically active in humans, and whose effects on aging are conserved across species. Numerous genetic interventions have been discovered that ectopically induce or inhibit dauer formation, but these suffer from an inability to effectively titrate their effects. In this study, we have demonstrated the effectiveness of captopril in inducing dauer formation in a concentration-dependent manner. Captopril may prove useful as a tool for future screens of dauer-regulating genes.

Numerous compounds have been discovered that extend lifespan in *C. elegans*, but few have been further shown control to aging other organisms. In searching for compounds that delay aging in humans, the ideal candidate would be a compound which reproducibly controls aging in a broad range of species; this would drastically simplify mechanistic studies of aging. Recent reports show that captopril significantly extends lifespan in genetically heterologous mice [94]. Based on this evidence and our increasing understanding of the mechanism of action of captopril in worms, we propose that captopril represents a promising candidate for future anti-aging studies in humans.

6.5 Materials and Methods

General methods and strains

Caenorhabditis elegans were cultured as described by [3]. Unless otherwise noted, strains were maintained at 20°C on Petri dishes containing nematode growth medium (NGM) and

seeded with 200 µL *E. coli* OP50 bacteria. Nematode strains are listed below. CGC, *Caenorhabditis* Genetics Center at University of Minnesota. Strains WU1975-WU1978 were created by independently backcrossing WU1939 to wild type N2 (Bristol).

Genotype	**Source**	**Strain**
C. elegans: wild type	CGC	N2 (Bristol)
C. elegans: daf-2(am326) III	This study; 3X backcross	WU1939
C. elegans: daf-2(am326) III	This study; 4X independent backcross	WU1975
C. elegans: daf-2(am326) III	This study; 4X independent backcross	WU1976
C. elegans: daf-2(am326) III	This study; 4X independent backcross	WU1977
C. elegans: daf-2(am326) III	This study; 4X independent backcross	WU1978
C. elegans: daf-2(am326) III;daf-16(mu86) I	This study	WU2008
C. elegans: daf-2(syb4952) III	This study; SUNY Biotech	PHX4952
C. elegans: daf-2(e1370) III	CGC	CB1370
C. elegans: daf-2(e1370) III;daf-16(mu86) I	CGC	DR1309
C. elegans: daf-2(e1368) III	CGC	DR1572
C. elegans: daf-2(e1371) III	CGC	DR1568
C. elegans: daf-2(m41) III	CGC	DR1564
C. elegans: daf-16(mu86) I	CGC	CF1038
C. elegans: age-1(hx546) II	CGC	TJ401
C. elegans: acn-1(am314) X	This study	WU1746
C. elegans: daf-12(rh61rh411) X	CGC	AA86
C. elegans: muIs84 [(pAD76) sod-3p::GFP + rol-6(su1006)]	CGC	CF1553
C. elegans: spe-9(hc88) I	CGC	BA671

Captopril and ethosuximide culture conditions

Captopril (*N*-[(S)-3-Mercapto-2-methylpropionyl]-L-proline, C4042, Sigma-Aldrich, Burlington, MA) was stored as a powder, dissolved in water at 75 mg/mL, and filter sterilized. Captopril-infused NGM dishes were prepared as previously described [85]: captopril was added to liquid agar at ~50°C immediately prior to dispensing into dishes. Captopril-infused dishes were

stored at 4°C for up to one month. For captopril dose-response experiments, embryos were placed onto *E. coli* seeded captopril dishes and observed after 72 hrs. Adult and larval animals were scored based on morphological characteristics using a dissecting microscope.

Ethosuximide (2-Ethyl-2-methylsuccinimide, E7138, Sigma-Aldrich, Burlington, MA) was similarly stored and prepared (based on methods previously described in [681,682]).

Measurement of internal captopril concentration

High Performance Liquid Chromatography/Mass Spectroscopy (HPLC-MS) was performed on whole-animal lysate. 20-30 wild-type adult hermaphrodites were cultured on medium containing 2.5 mM or 10 mM captopril and allowed to lay eggs for 2 hrs; the adults were removed, and the eggs were cultured at 20°C for 72 hrs. To remove captopril that is outside the animals, we washed animals off dishes using 1 mL water, pelleted animals by centrifugation, and removed the supernatant. Three successive wash steps were performed, and then the worms were incubated in 1 mL water on the benchtop for one hour to allow excess captopril in the intestinal lumen to be secreted. A sample of this liquid was retained for analysis, and three further wash steps were performed. The size of the worm pellet was estimated to be 2.5 µL based on the criteria and technique established in Evason *et al.* (2005) [681]. The animals were lysed with Proteinase K (S-1000-1, EZ Bioresearch, St. Louis, MO), resuspended into a final volume of 100 µL, centrifuged at high speed to pellet debris, and the supernatant was submitted for HPLC-MS.

100 ng of deuterated phenylalanine d_8 (Cayman Chemical, Ann Arbor, MI) was spiked in 100 µL of the extract as the internal standard for quantification. At the same time, 4-point calibration samples (0.05 ng/100 µL, 0.5 ng/100 µL, 10 ng/100 µL, and 100 ng/100 µL) containing 100 ng of phenylalanine d_8 for absolute quantification. HPLC-MS equipped with a

Shimadzu autosampler (20X), Shimadzu HPLC (20A, Columbia, MD), and an Applied Biosystem Sciex API-4500 Qtrap mass spectrometer (Foster City, CA) were utilized for analysis operating in positive ion multiple reaction monitoring (MRM) mode. The transitions of Q1/Q3 ions for Captopril and phenylalanine d_8 detections were set at 218.1/116.1 and 174.1/128.1, respectively. HPLC solvent (A: 10 mM ammonium acetate in 7:3 water/ACN; B: 10 mM ammonium acetate in 1:1 isopropanol/methanol) gradient was 75% B to 30% in 4 min with a flow rate at 1 mL/min. A HILIC LC column (Waters Atlantis 2 x 100 mm, 3 μm, Milford, MA) was used. The Sciex data system (Analyst 1.52 v) was used for instrument control and data analysis (quantification). Each sample was injected twice to get the average data. Data were analyzed using Student's *t*-test.

Lifespan Determination

50-60 hermaphrodites at the L4 larval stage were removed from gravid populations cultured in standard conditions onto new dishes unless otherwise noted. Beginning one day later ("Day 1"), animals were observed for spontaneous movement; if no movement was observed, they were gently stimulated with a piece of platinum wire. If no stimulated movement was observed, animals were considered dead and removed from the dish. Worms which died by matricidal hatching, extrusion of the gonad, or desiccation on the sides of the dish were censored from that day onward. Worms were moved to new dishes daily during the reproductive period, or as needed thereafter. Measurement continued until all worms expired. Statistical analyses were performed using Kaplan-Meier survival function and log-rank (Mantel-Cox) test [129,498].

Measurement of body movement and pharyngeal pumping

20-30 hermaphrodites at the L4 stage were removed from gravid populations cultured in standard conditions. Animals were evaluated daily, beginning one day later ("Day 1"). Body movement was measured by depositing a worm on a dish and immediately counting the number of sinusoidal movements completed in a 15 s span; one "body movement" was defined as the movement of the head from its left-most position to its right-most position (or vice-versa) while the animal moved either forward or backward. Pharynx pumping was counted in 15 s increments per animal. Animals were transferred to a new dish during the reproductive period or as needed thereafter. Assays were continued until all animals had expired. Living animals that displayed no body movement or pharyngeal pumping were counted as "0" for the given phenotype, while dead animals were censored. Data were analyzed using one-way ANOVA with Tukey post-hoc HSD.

Measurement of heat and oxidative stress resistance

To measure resistance to acute heat stress, we transferred 20-30 adult hermaphrodites to standard NGM dishes for one hour. Synchronized eggs laid during this hour were moved to new dishes, 30 per dish. The eggs were cultured at 20°C for 72 hrs, shifted to 35°C, and scored as alive or dead every 12 hrs until all expired. To measure resistance to oxidative stress, we prepared NGM dishes as above and added paraquat (*N,N'*-dimethyl-4,4'-bipyridium dichloride, 36541, Sigma-Aldrich, Burlington MA) to the molten agar to a final concentration of 40 mM. Eggs obtained as described above were cultured at 20°C for 72 hrs, and then worms were transferred to paraquat-containing medium. Animals were scored as alive or dead every 12 hrs until all expired. We observed that matricidal hatching was the most common cause of death in animals exposed to paraquat; therefore, animals that died from matricidal hatching were not

censored from the data analysis. Statistical analyses were performed using Kaplan-Meier survival function and log-rank (Mantel-Cox) test [129,498].

Determination of dauer formation

30-50 embryos were picked from mixed stage populations cultured in standard conditions, placed on new dishes, and maintained at 20°C or shifted to 22, 25, or 27°C. After 2-3 days, dauer larvae were counted. The morphological criteria used to define dauer were: dark coloration, elongated and radially constricted body, lack of pharyngeal pumping, and presence of oral plug [663,669,671,68]. Animals were observed until all had formed dauer, reached adulthood, or expired. The average percentage of dauer animals in a population was calculated by dividing the number of dauer larvae by the total number of animals. Data were analyzed using one-way ANOVA with Tukey post-hoc HSD.

Measurement of developmental rate and fecundity

To determine the percentage of embryos that can reach adulthood within 72 hrs, we allowed wild-type hermaphrodites to lay eggs on a standard NGM dish for one hour. Approximately 30 eggs were picked onto several dishes containing 0, 4, 8, 12, or 16 mM captopril and cultured at 20°C for 72 hrs. Animals were scored as larva or adult using a dissecting microscope based on morphological criteria characteristic of late-stage larvae (size, presence of developing vulva, etc.) or adults (fully formed gonad with embryos, etc.).

To determine the time to first progeny, we placed 20-30 adults on a fresh dish for one hour. 20-30 of these synchronized eggs were picked onto individual dishes and cultured at 20°C for 65 hrs. Animals were then observed each hour to determine if they laid an egg(s). The time

when unhatched embryos were first observed was defined as the time to first progeny, which is equivalent to the duration necessary to complete the life cycle.

To measure total and daily progeny production, 20-30 L4 hermaphrodites ("P_0") were transferred individually to fresh dishes and cultured with standard conditions. P_0 animals were transferred to new dishes every 24 hrs; dishes containing eggs were cultured for 2-3 days to facilitate progeny identification, and the number of F_1 progeny was counted. The experiment ended when self-fertile P_0 hermaphrodites did not produce progeny for two consecutive days. Time to first progeny and total progeny were analyzed using Student's *t*-test; daily progeny production was analyzed using one-way ANOVA and Tukey post-hoc HSD.

Determination of worm length

30-40 embryos were picked onto dishes with medium containing 16 mM captopril and cultured for 72 hrs. Animals were washed into Eppendorf tubes using 1 mL M9 and collected by centrifugation. After aspirating the supernatant, three further wash steps were performed using 1 mL M9 to remove excess bacteria. The animals were pipetted onto standard NGM dishes lacking a bacterial lawn. Excess liquid was allowed to dry, and the animals were allowed to crawl away from each other. Photographs of individual worms were obtained using a Leica Microsystems IC80 HD microscope and then converted to greyscale using Fiji (ImageJ, 1.53f51). Determination of length was performed using the WormSizer plugin [716], and data were analyzed using Student's *t*-test.

A forward genetic screen for captopril hypersensitive mutants

To perform the chemical mutagenesis, we cultured large numbers of wild-type L4 hermaphrodites on dishes, washed the animals into 15 mL conical tubes using M9 buffer,

pelleted animals by centrifugation at 2000 rpm for 3 min, and aspirated excess liquid to yield a volume of 4 mL. EMS (Ethyl methansulfanate, M0880, Sigma-Adrich, Burlington, MA) was added to a final concentration of 50 mM, and animals were gently agitated on a shaker for 4 hrs at 20°C. To remove the EMS, we performed four wash steps: animals were pelleted, the supernatant was aspirated, and the animals were resuspended in 10 mL M9 buffer. Animals were transferred to NGM dishes seeded with *E. coli* OP50 and allowed to recover and lay eggs. F_1 self-progeny embryos were picked onto individual dishes; one F_2 self-progeny from each F_1 hermaphrodite was picked onto an individual dish and cultured until a gravid population had formed. The F_{3+} embryos were extracted using alkaline hypochlorite treatment and divided equally between dishes that were untreated, or contained 16 mM captopril, 50 µM zinc chloride (229997, Sigma-Aldrich, Burlington, MA), 10 µM TPEN (N,N,N',N'-*tetrakis*-(2-Pyridylmethyl)ethylenediamine, 616394, Sigma-Aldrich, Burlington, MA), or 500 µM manganese (II) chloride (M8054, Sigma-Aldrich, Burlington, MA); dishes were seeded with 200 µL of 5X concentrated *E. coli* OP50 bacteria. Animals were allowed to grow for 3-5 days. If a strain failed to reach adulthood and produce progeny when cultured with 16 mM captopril, but did reach adulthood and produce progeny in all other stressful condition, then it was pursued.

Whole-genome sequencing of *daf-2(am326)* mutants

The *am326* mutation was identified with whole-genome sequencing (WGS) using an EMS density mapping strategy (described in [676]). Using the temperature-dependent dauer phenotype to score *am326* mutant animals, we performed three successive outcrosses to N2, generating WU1939. Next, four parallel populations of WU1939 were established, and each was serially outcrossed to N2 four times. These strains, WU1975, WU1976, WU1977, and WU1978,

each contained homozygous mutations at the *am326* locus and had been outcrossed a total of 7 times.

To collect chromosomal DNA from these strains, we cultured mixed-stage populations on 6-8 dishes. When all bacteria had been consumed, the animals were collected with 1mL M9 buffer into 15 mL conical tubes, centrifuged at 2000 rpm for 5 min, and excess liquid aspirated. Four successive wash steps were performed with M9 to remove excess bacteria, and the worm pellet was snap-frozen using liquid nitrogen. Four further freeze-thaw cycles were performed to lyse the worms, and the lysate was treated with Proteinase K in a 55°C water bath for 3 hrs. To remove excess worm debris, we centrifuged the lysate at 2000 rpm for 10 min and removed the supernatant from the pellet. Chromosomal DNA was extracted using the DNeasy Blood and Tissue Kit (69504, Qiagen, Venlo, Netherlands). 4 µg of DNA per sample were submitted to the Washington University Genome Technology Access Center (GTAC) for whole genome sequencing. Libraries were constructed using the KAPA Hyper PCR-free Kit (KR0961, KAPA Biosystems, Wilmington, MA) and sequencing was performed using a NovaSeq S4 XP (Illumina, San Diego, CA) at a coverage depth of ~30X.

Analysis of whole-genome sequencing data

Analysis of whole-genome sequencing data was performed using an EMS-density mapping approach described in [676,717]. First, we aligned the reads to the WS220.64/ce10 *C. elegans* reference genome originally derived by the Genome Institute at Washington University (WUSTL) and the Sanger Institute. Reads were aligned using the bowtie2 read-alignment tool [718]. Analysis of differences between strains was performed using the MiModD v.0.1.9 toolkit (https://sourceforge.net/projects/mimodd/). Loci in the mutant strains that differed from the N2 strain were examined. Based on the logic that the *am326* mutation must be present in all

backcrossed strains but absent in the N2 strain, we disregarded mutations present in some – but not all – backcrossed strains. We disregarded mutations present in the N2 strain (likely due to genetic drift causing differences between our lab N2 strain and the WS220.64 reference genome). This resulted in a list of 56 variants. Eleven variants, small insertions or deletions ("indels") in repetitive regions, were disregarded as likely sequencing errors, since EMS mutagenesis typically creates base pair changes rather than indels. Each mutation was manually analyzed using the UCSC Genome Browser (UCSC Genomics Institute, Santa Cruz, CA) to determine the genomic region affected. See **Table S4** for detailed information on these variants. Multiple sequence alignment with human and mouse INSR and *Drosophila* InR was performed using COBALT (constraint-based multiple alignment tool) with *C. elegans* DAF-2 as the reference sequence [677].

Complementation assays

Adult male *daf-2(am326)* or *daf-2(syb4952)* animals were mated to hermaphrodites of a different genotype at 20°C (**Table 1**). F_1 embryo cross-progeny were shifted to 25°C and examined for dauer formation based on morphological characteristics, as described above.

Time-series RNA-seq

Heat-sensitive sterile *spe-9(hc88)* mutant animals were synchronized by alkaline hypochlorite treatment and allowed to hatch overnight in S Basal medium. Arrested L1 larvae were transferred to 10 cm NGM dishes seeded with 200 µL *E. coli* OP50 at a density of ~1000 animals per dish and cultured at 25°C. One dish was harvested every 24 hrs by washing with M9 buffer, after which worms were lysed with TRIzol reagent (15596026, Invitrogen, Waltham, MA) and repeatedly freeze/thawed in liquid nitrogen. Total RNA was obtained by phenol chloroform

extraction and purified according to the RNeasy Micro kit protocol (74004, Qiagen, Venlo, Netherlands). RNA quality was assessed using a 4200 TapeStation system (Agilent, Santa Clara, CA). Library preparation and sequencing were carried out by Novogene Co., Ltd. (Beijing, China).

RNAi

RNA interference was performed as described in [163]. *E. coli* HT115 bacteria expressing either a control plasmid (L4440) or a plasmid encoding *acn-1* dsRNA were obtained from the Ahringer library [162]. NGM dishes containing 50 µg/mL ampicillin (A-301-25, Gold Biotechnology, St. Louis, MO) and 1 mM IPTG (isopropyl-β-D-thiogalactoside, I2481-C50, Gold Biotechnology, St. Louis, MO) were poured and allowed to cool on the benchtop overnight. RNAi bacteria were grown overnight at 37°C in LB media supplemented with 50 µg/mL ampicillin; this starter culture was diluted 1:100 into LB media supplemented with 50 µg/mL ampicillin and grown for 6 hrs at 37°C. 200 µL was seeded onto the NGM RNAi dishes. Dishes were allowed to dry on the benchtop at room temperature overnight, then stored at 4°C. Embryos were transferred to RNAi dishes and cultured at 20, 22, or 25°C until they either reached adulthood or formed dauer larvae.

CRISPR-mediated generation of the *am314* mutation in the *acn-1* locus

CRISPR-mediated modification of the *acn-1* locus was performed using the Co-CRISPR methodology described in [295,719]. Our goal was to introduce a frameshift into the first exon of the endogenous *acn-1* locus, thus eliminating ACN-1 activity. The following mixture was injected into the gonads of P_0 wild-type hermaphrodites: 50 ng/µL Cas9-expressing PDD162 (gift from Mike Nonet); 20 ng/µL *dpy-10* guide plasmid pMN3153; 500 nM *dpy-10(cn64)* ssDNA repair

template AFZF827; *acn-1* guide plasmids (pANS1, 40 ng/µL each); 600 nM ssDNA repair template (pANS2). We selected F_1 progeny displaying the *Rol* phenotype. *acn-1(am314)* WU1746 was derived using pyrosequencing to select heterozygous F_2 progeny. Lifespan assays were performed by picking L4 hermaphrodites from this population as described above. To confirm the genotype of the animals that were analyzed, we performed pyrosequencing on the dead animals, and censored animals that did not display the *acn-1(am314)/acn-1(+)* genotype.

Determination of *sod-3* gene expression levels by RT-qPCR

To measure relative gene expression, we collected whole-worm RNA, transcribed RNA into cDNA, and analyzed gene expression levels using real-time quantitative polymerase chain reaction (RT-qPCR). To isolate whole worm RNA, we picked approximately 400-500 unhatched embryos from dishes cultured in standard conditions onto 10 cm NGM dishes, which contained either 0 or 2.5 mM captopril and were seeded with 2 mL of *E. coli* OP50 bacteria. Worms were cultured at 20°C for 72 hrs and collected by washing four times with M9. Worms were compacted by centrifugation at 2000 rpm for 5 min, and excess liquid was removed via aspiration. Tubes containing the worms were frozen in liquid nitrogen and stored at -80°C. Worms were lysed by four successive freeze-thaw cycles in liquid nitrogen. 500 µL Trizol and 100 µL chloroform were added to the lysed worm solution. The mixture was vortexed and then centrifuged at 12,000 g for 15 min at 4°C. The clear supernatant layer was extracted and mixed with 500 µL isopropanol, vortexed, and centrifuged at 12,000 g for 15 min at 4°C. The RNA pellet was washed with 1 mL of 70% ethanol and centrifuged as before. Excess ethanol was aspirated, and the pellet was dried in a 60°C heat block. The pellet was resuspended in 50 µL nuclease-free water, and the RNA concentration was measured by UV spectroscopy (NanoDrop One Microvolume UV-Vis Spectrophotometer, ND-ONE-W, Thermo Fisher Scientific, Waltham,

MA). Reverse transcription was performed using the iScript cDNA Synthesis Kit (1708891, Bio-Rad, Hercules, CA) using 1 µg RNA (50 ng/µL). RT-qPCR was performed using iTaq Universal SYBR Green Supermix (1725121, Bio-Rad, Hercules, CA) using 200 ng of cDNA. Relative fold-change was calculated using the comparative C_T method [720]; *sod-3* mRNA level was normalized using the *ama-1* control gene, and data were analyzed using Student's *t*-test.

Determination of *sod-3* expression using a fluorescent reporter strain

Transgenic animals containing the *sod-3p::gfp* construct were cultured from the egg stage in medium containing 0 or 2.5 mM captopril for 3 days (adult day 1) or 7 days (adult day 5). To perform fluorescence microscopy, we prepared 3% agar slides, added a drop of levamisol (3 mM) (PHR1798, Sigma-Aldrich, Burlington, MA) to the agar, and added ~10 worms per slide. As necessary, animals were oriented using an eye lash. Excess levamisol was removed, and a cover slide was applied and sealed with 3% agar. Brightfield and fluorescence images of animals were acquired using a Leica DMi8 using the same settings for control and drug treated animals in each experiment. Fluorescence intensity of each worm was measured using Fiji (ImageJ, 1.53f51). The experiments were repeated at least three times independently, and data were analyzed using Student's *t*-test.

Chapter 7: Low sodium chloride concentration extends lifespan in *C. elegans*

This work was done in partnership with Franziska Pohl and with the assistance of Chen-Hao Chiu and Micklaus Garcia. A manuscript is currently in preparation.

7.1 Abstract

Aging in the nematode *C. elegans* is controlled, in part, by the interplay of genetic programs with external environmental conditions. A worm's survival is dependent on its ability to sense and respond to environmental stresses such as temperature, pH, infectious microorganisms, and osmolarity. Worms have evolved complex mechanisms that allow them to sense the concentration of external osmolytes and regulate the production of internal osmolytes in order to maintain osmotic homeostasis. In the laboratory, worms are grown on Petri dishes containing nematode growth medium (NGM), an agar medium seeded with *E. coli* OP50 bacteria and supplemented with approximately 50 mM sodium chloride (NaCl). This medium has remained the standard for nematode culture for nearly fifty years. However, research into worm aging has revealed that these 'standard' conditions are often suboptimal for survival. Here, we show that removal of supplemental salt from NGM significantly extends worm lifespan, with no apparent deleterious effects. We hypothesize that standard formulations of NGM induce mild osmotic stress, an effect which only becomes apparent as the animal ages and its ability to respond to osmotic stress is reduced. These results provide important insight into the interaction between osmotic stress and aging, and suggest that future aging research should be performed with a more critical eye toward nematode culture conditions.

7.2 Introduction

Animals have evolved mechanisms to sense and regulate osmolarity in response to variable environments or diets [721]. The analysis of osmoregulation in *C. elegans* has focused on how worms maintain homeostasis by sensing and responding to high osmolarity [104]. Osmoregulatory organs include the hypodermis, intestine, and excretory cell. Osmolarity is sensed by amphid neurons in the head, including ASH and ASE [722,723], and worms avoid high osmolarity - a behavior called osmotic avoidance. Notably, mutations in genes necessary for osmotic avoidance, such as *osm-3*, also cause a lifespan extension [724,725].

In order to characterize the interaction between longevity and osmoregulation in worms, we varied the level of NaCl (sodium chloride, salt) in the nematode growth medium (NGM); NGM normally contains 50 mM supplemental salt in addition to an undefined level of sodium contributed by components such as agarose and peptone. Surprisingly, worms cultured on NGM with 0 mM supplemental salt displayed a significantly extended mean lifespan of ~25% compared to animals cultured on 50 mM supplemental salt dishes. Thus, supplemental NaCl in the NGM medium decreases lifespan. These results identify a new dietary manipulation that can extend worm lifespan.

It has long been known that the conditions under which nematodes are cultured in the laboratory differ greatly from their natural environment, and that laboratory conditions are not necessarily optimal for survival. In the wild, worms spend most of their lifespan in the dauer stage, only emerging if environmental conditions permit [337]. Wild nematodes experience rapid and extreme changes in their chemical and microbiological environment, and experience high rates of extrinsic death [338,726]. Conversely, in the laboratory, animals are cultured at a constant 20°C and provided with ample food in the form of *E. coli* OP50 bacteria [3]; “domesticated”

worms rarely experience extreme stress and spend most of their lifespan as adults. These culture conditions are not necessarily optimized for long-term survival, though, as reducing temperature to 15°C can extend lifespan, as can culture on alternative non-pathogenic bacterial food sources [48,113,145,146,727]. Early research into *C. elegans* was primarily focused on physiological and neurological development, and thus these culture conditions have not been optimized to maximize worm lifespan. Here, we identify sodium chloride concentration as an additional factor in nematode culture that negatively affects aging.

We attempted to characterize the mechanism of lifespan extension by examining the role of the osmotic stress response. When confronted with high osmolarity, worms synthesize and accumulate high levels of the organic osmolyte glycerol, a small polyol that is protective against osmotic stress [106,728,729]. Transcriptional induction of *gpdh-1* (glycerol-3-phosphate dehydrogenase-1) is responsible for glycerol synthesis during hypertonic stress. Induction of *gpdh-1* occurs rapidly, within the first hour of exposure, and is specific to osmotic stress, since it does not occur during heat, oxidative or endoplasmic reticulum stress [728]. Thus, *gpdh-1* transcript levels are a useful marker of the response to high osmolarity, which we use to characterize the role of the osmotic stress response in aging under different supplemental salt conditions.

7.3 Results

Previous work has shown that nematode survival can be reduced by increasing the concentration of supplemental sodium chloride (NaCl, hereafter referred to as 'salt') in the NGM agar above the standard dose of 50 mM [106]. In attempting to replicate these results, we measured worm lifespan at a standard supplemental salt dose of 50 mM, at an elevated dose of 200 mM, and, as a negative control, at a depleted dose of 0 mM (**Figure 1A, Table 1**). We observed that worm survival was reduced at a dose of 200 mM compared to 50 mM control. Serendipitously,

we also observed that removing supplemental salt extended lifespan by ~25% compared to 50 mM. This result was surprising, and to our knowledge has not been reported by other groups.

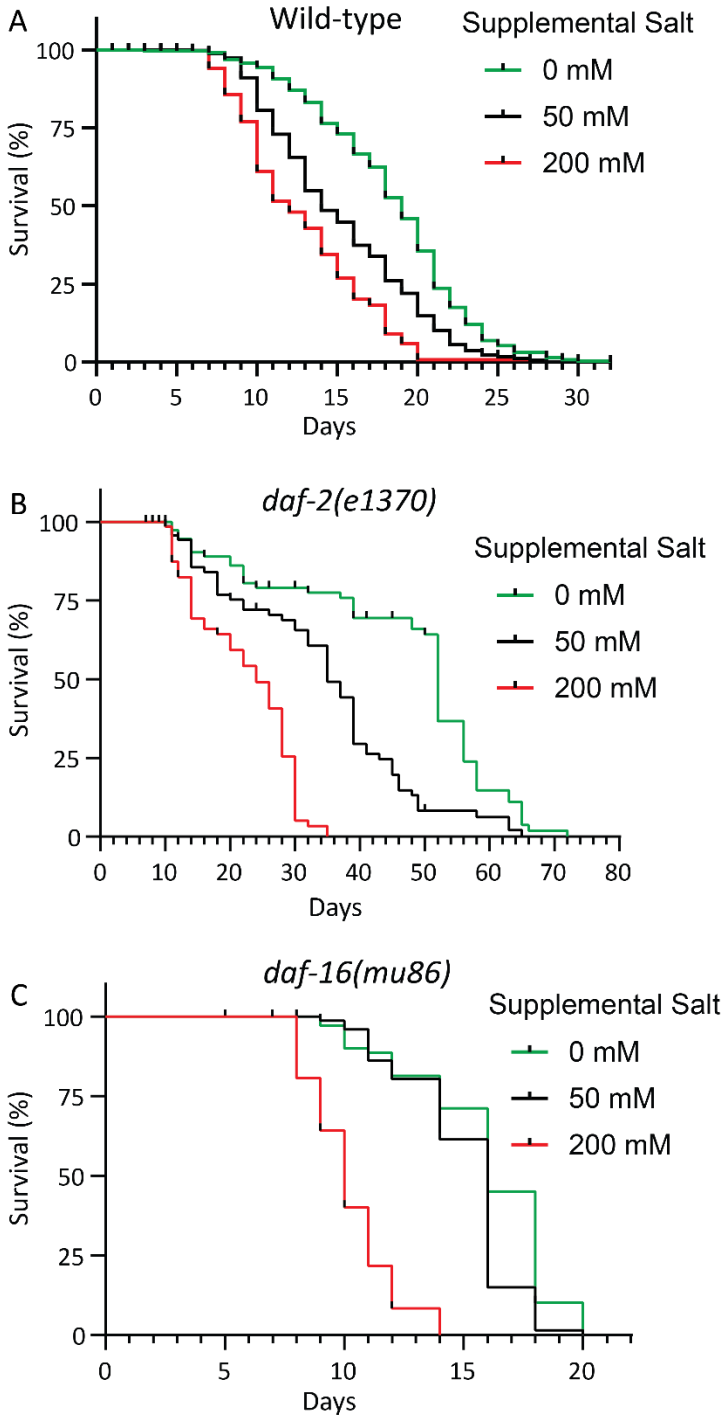

Figure 1. Removal of supplemental salt extends lifespan in wild-type and *daf-2(lf)* animals, but not in *daf-16(lf)* animals.

Animals were raised from embryo on dishes containing nematode growth medium (NGM) supplemented with the indicated concentration of NaCl (salt). Formulations of NGM used in standard nematode culture conditions contain 50 mM supplemental salt, here used as an untreated control. **(A)** Wild-type worm lifespan is dependent on salt concentration, and removal of supplemental salt from the media extends lifespan compared to the standard (50 mM) concentration. **(B,C)** Lifespan is dependent on salt concentration in *daf-2(e1370)* mutants **(B)**, but not in *daf-16(mu86)* mutants **(C)**. See **Table 1** for details and statistics.

Table S1: Effect of supplemental salt concentration on lifespan in wild type, *daf-2(e1370)*, and *daf-16(mu86)*.

Genotype[a]	Supplemental salt (mM)[b]	Mean lifespan (days ± s.e.)[c]	% Change[d]	N (n)[e]
Wild type	0	17.2 ± 0.3	24.6 ***	363 (10)
	50	13.8 ± 0.3		484 (13)
	200	11.2 ± 0.3	-18.8 ***	278 (8)
daf-2(e1370)	0	42.6 ± 2.2	31.9 ***	75 (3)
	50	32.3 ± 1.7		75 (3)
	200	21.6 ± 1.0	-33.1 ***	76 (3)
daf-16(mu86)	0	17.0 ± 0.5	4.3 **	75 (3)
	50	16.3 ± 0.4		75 (3)
	200	10.9 ± 0.2	-33.1 ***	75 (3)

[a] Animals were wild type or had the indicated alleles of *daf-2* or *daf-16*.

[b] Embryos were cultured on nematode growth medium (NGM) supplemented with the indicated concentration of salt (sodium chloride, NaCl) at 20°C. Measurement of mean lifespan began on the first day of adulthood.

[c] Mean lifespan and standard error (s.e.) determined by Kaplan-Meier survival function.

[d] Percent change in mean lifespan. Animals are compared to same-genotype 50 mM controls, as this concentration of supplemental salt represents that found in the standard formulation of NGM. Negative values indicate reduction of mean lifespan, and positive values indicate extension of mean lifespan. ns, non-significant, $p \geq 0.05$; **, $p < 0.01$; ***, $p < 0.001$ by log-rank (Mantel-Cox) test.

[e] N, total number of animals; n, number of independent trials.

Our next steps focused on understanding how reducing supplemental salt concentration extended lifespan. We attempted to understand the role genotype plays in this interaction. Different nematode culture conditions, such as temperature, can differentially impact lifespan in

long- or short-lived mutants [730,731]. We examined the effect of supplemental salt on lifespan in long-lived *daf-2(lf)* and short-lived *daf-16(lf)* mutant backgrounds (**Figure 1B,C**). 200 mM supplemental salt significantly reduced lifespan in both backgrounds. Removing supplemental salt significantly extended lifespan in *daf-2(e1370)* mutant animals compared to 50 mM control, indicating that this effect further extends lifespan in long-lived mutants (**Figure 1B**). Removing salt significantly extended lifespan in short-lived *daf-16(mu86)* mutant animals, though to a lesser degree than in other genetic backgrounds (4.3%) (**Figure 1C**). *daf-16* encodes the DAF-16/FOXO transcription factor that is the terminus of the age-regulating insulin/IGF-1 signaling pathway [65]. DAF-16 controls transcription of stress-resistance and longevity-promoting genes [65]; this suggests that the mechanism of lifespan extension by salt removal may be partially DAF-16-dependent, though more data is required to support this conclusion.

Interventions which extend worm lifespan often reduce age-related degenerative phenotypes as well [5,15]. To this end, we measured how animal body movement and pharyngeal pumping rate was affected by salt concentration. At doses of 200 mM, both body movement and pharyngeal pumping were reduced in rate compared to 50 mM control; animals grown on high doses of supplemental salt experienced rapid decline in pharyngeal pumping rate with age (**Figure 2A,B**). Removing supplemental salt reduced age-related decline in body movement rate late in life (**Figure 2A**). Conversely, removing supplemental salt failed to reduce age-related decline in pharyngeal pumping rate (**Figure 2B**). For more information on potential future directions regarding age-related degenerative phenotypes and supplemental salt removal, please refer to **Chapter 8.6**.

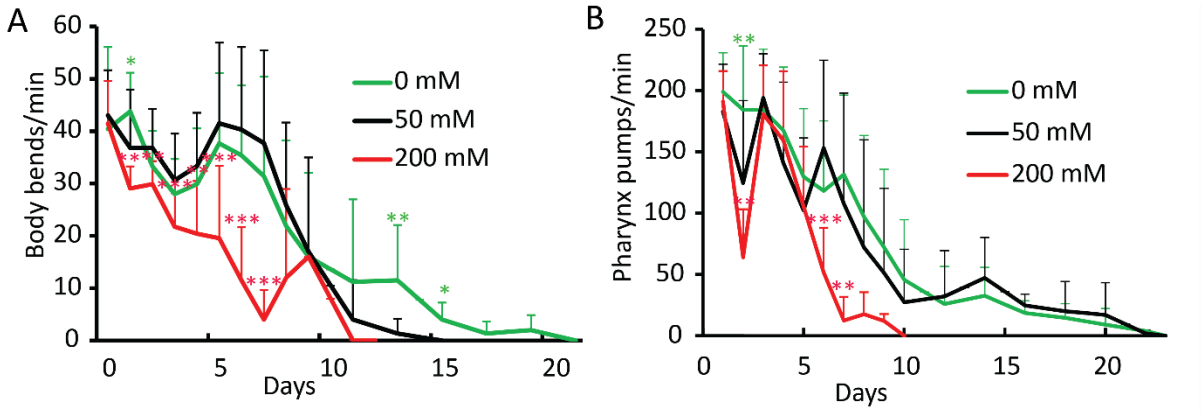

Figure 2. Measuring the effect of salt concentration on body movement and pharyngeal pumping rate.

(A) Mean body movement rate and standard deviation was measured by counting the number of sinusoidal body bends per minute of wild-type animals. Animals cultured on NGM supplemented with 200 mM salt experienced reduced body movement rate, compared to 50 mM control, but animals cultured on 0 mM did not experience a significant change in body movement rate compared to control. N=19-20 animals. **(B)** Mean pharyngeal pumping rate and standard deviation was similarly measured; wild-type animals cultured on 200 mM supplemental salt experienced a reduced number of pharynx pumps per minute compared to 50 mM control, while animals raised on 0 mM experienced no change compared to control. N=19-20 animals. Relationships were non-significant unless otherwise noted. *, $p<0.05$; **, $p<0.01$; ***, $p<0.001$. Data were analyzed using two-way ANOVA with post-hoc Tukey HSD.

We devised two hypotheses to explain why removing salt extended lifespan. First, that removing a necessary nutrient extended lifespan by inducing a dietary restriction (DR) phenotype; second, that the addition of 50 mM supplemental salt induced a mild osmotic stress that reduced lifespan, and that removing this stress extended lifespan.

To test the first hypothesis, we measured development rate and fecundity. DR in worms is associated with extended development time and reduced reproductive capacity as a result of nutrient depletion [5,48,193]. We measured developmental rate in worms raised from embryo on NGM dishes containing 0, 50, or 200 mM supplemental salt (**Figure 3A**). An elevated supplemental salt concentration of 200 mM significantly extended the developmental period compared to 50 mM supplemental salt control. However, reducing supplemental salt to 0 mM

did not significantly impact development rate, suggesting that DR does not play a role under these conditions.

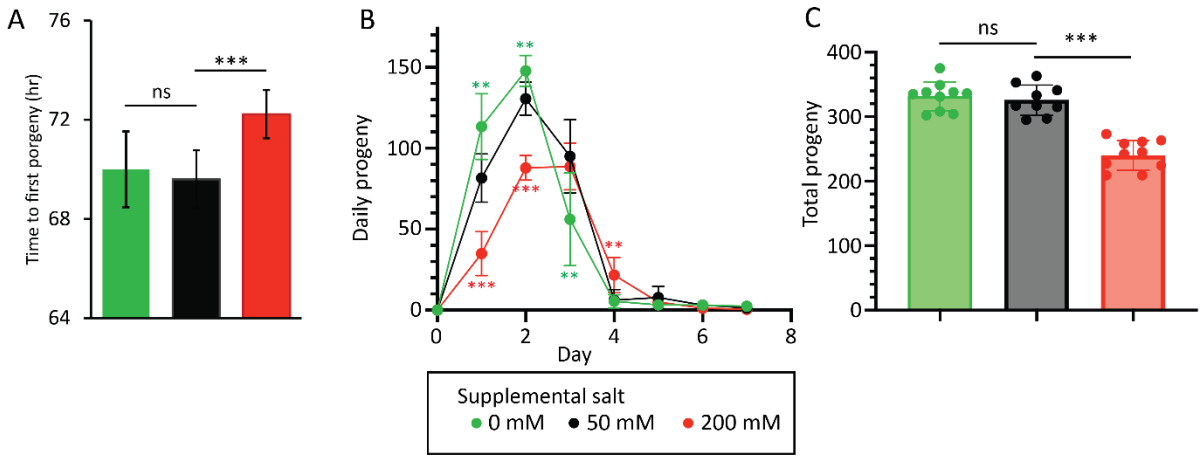

Figure 3. Removal of supplemental salt does not reduce rate of development or reproduction.

(A) The effect of supplemental salt on development rate was determined by measuring the mean number of hours and standard deviation that expired from when a wild-type animal was laid as an egg to when it had reached adulthood and laid its first egg ("time to first progeny"). Animals were maintained on NGM dishes supplemented with 0, 50, or 200 mM salt for the duration of the experiment. Animals which failed to reach adulthood or expired prior to laying its first egg were censored from the experiment. Eggs were synchronized via timed egg lay and were observed hourly beginning ~66 hours later. Experiment continued until all animals had reproduced or expired. N=7-10 animals. **(B,C)** Average daily and total progeny production and standard deviation were measured by counting the number of progeny produced daily throughout an animals reproductive span compared to 50 mM control. Animals were moved to new plates daily, and progeny were counted 2-3 days later. Animals were raised on NGM dishes supplemented with 0, 50, or 200 mM salt for the duration of the experiment. The measurement continued until each animal failed to produce progeny for at least two consecutive days. Animals which expired prior the end of their reproductive span were censored from the day of their death onward. N=9-10 animals. Data were analyzed using two-way ANOVA with Dunnett's multiple comparisons test. Relationships were non-significant unless otherwise indicated. ns, non-significant, $p \geq 0.05$; **, $p < 0.01$; ***, $p < 0.001$

Next, we measured the effect of supplemental salt concentration on reproductive span. Animals grown on 200 mM supplemental salt had reduced fecundity, as measured by both reduced total number of eggs laid (**Figure 3B**) and by daily progeny production (**Figure 3C**)

compared to 50 mM control. Growing animals on 0 mM supplemental salt caused slightly earlier progeny production compared to animals grown on 50 mM; 0 mM animals produce more progeny early in adulthood (Day 1-2), and fewer progeny late in adulthood (Day 3-4) (**Figure 3B**), though the total number of progeny produced remained unchanged (**Figure 3A**). These results are inconsistent with a DR phenotype, which usually results in delayed and/or reduced progeny production. We interpret these results as indicating that animals grown on 0 mM supplemental salt are not nutrient deficient, and that their extended lifespan is not the result of DR.

We next tested our second hypothesis, that the standard formulation of NGM containing 50 mM supplemental salt confers mild osmotic stress, and that removal of this salt results in reduced stress and increased survival. We measured activation of the *gpdh-1* glycerol-3-phosphate dehydrogenase gene, which mediates production of the osmolyte glycerol and is upregulated in response to osmotic stress [106,728,729]. The fluorescent transcriptional reporter strains OG119 and VP198 express green fluorescent protein (GFP) under the control of the *gpdh-1* promoter, and thus fluorescent intensity can be used to as a proxy measurement for *gpdh-1* transcriptional activation [728,729]. We measured activation of *gpdh-1p::GFP* throughout adult lifespan in animals raised from embryo in 0, 50, or 200 mM supplemental salt conditions (**Figure 4A-E**). As expected, animals raised on 200 mM supplemental salt experienced elevated *gpdh-1* transcriptional reporter activation early in life compared to 50 mM control (**Figure 4A-D**). This elevation disappeared by Day 3-5; by Day 11, mean fluorescent intensity continued to increase compared to control throughout the remainder of the adult lifespan. We interpret this result to indicate that animals experiencing high levels of osmotic stress upregulate *gpdh-1* to reestablish osmotic homeostasis. Once equilibrium has been reached, *gpdh-1* expression is

reduced to baseline levels. Late in life, as the animals' ability to maintain tissue structure and osmotic homeostasis is reduced due to aging, they again upregulate *gpdh-1* activity in response to this stress.

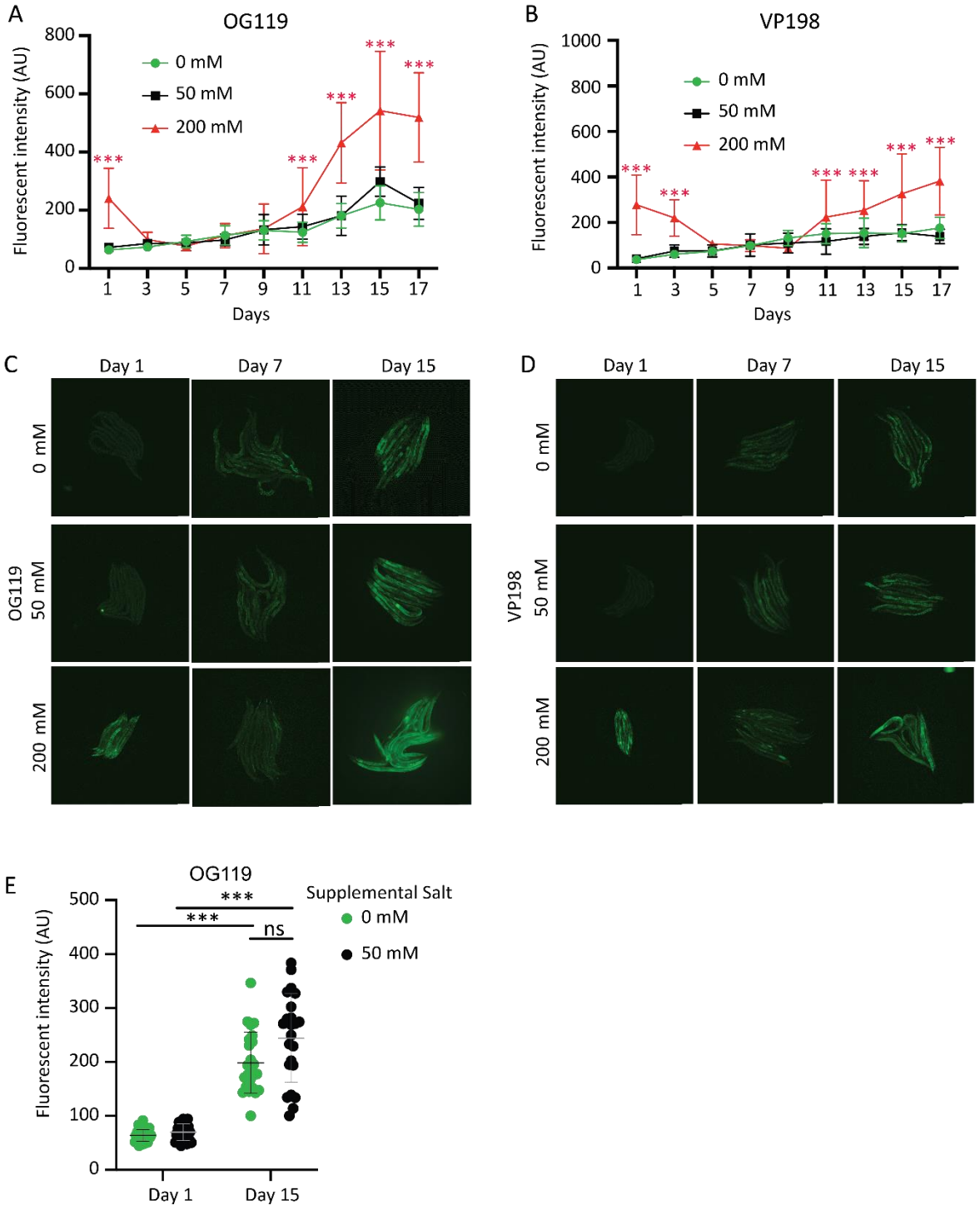

Figure 4. Expression of *gpdh-1* osmotic stress response gene increases in aged worms in all supplemental salt conditions.

The expression of *gpdh-1* was measured using two different techniques, **(A-E)** and expression of fluorescent reporters, and **(F)** RT-qPCR. **(A,B)** A GFP fluorescent transcriptional reporter was used to measure time- and salt-dependent increase *gpdh-1* transcriptional activation. OG119 **(A)** or VP198 **(B)** animals were grown on NGM dishes supplemental with the indicated concentration of salt. 5-10 animals were picked from the population daily, fluorescent intensity was measured, and the animals were then discarded. On Day 1, fluorescent intensity was elevated in animals grown on 200 mM supplemental salt compared to those grown on 0 or 50 mM. This increase disappears by Day 3-5; beginning on Day 9-11, fluorescent intensity continues to increase throughout the remainder of the lifespan. Animals grown on 0 or 50 mM supplemental salt show a gradual time-dependent increase in fluorescent intensity; however, animals grown in these conditions do not display significantly different fluorescent intensity compared to each other. N=6-15 animals per day, n=4 experiments. **(C,D)** Representative images show activation of fluorescent reporter throughout lifespan. **(E)** Representation of fluorescent intensity data of OG119 animals grown on 0 or 50 mM supplemental salt in early (Day 1) or late (Day 15) adulthood. Fluorescent intensity is increased late in life, is not significantly different between salt conditions. Data were analyzed using two-way ANOVA with Bonferroni's multiple comparisons test. Relationships were non-significant unless otherwise indicated. ns, non-significant, $p \geq 0.05$; *, p **, $p < 0.01$; ***, $p < 0.001$.

Fluorescent reporter intensity was elevated in animals cultured on 0 and 50 mM supplemental salt in aged (Day 15) compared to young (Day 1) animals (**Figure 4A,B,E**); however, there was no significant difference in fluorescent intensity between the two salt conditions at any age. These results are inconsistent with our hypothesis that lifespan extension in animals cultured on 0 mM supplemental salt results from osmotic stress, but neither do these results completely disprove the hypothesis. For further information of future research with respect to activation of the osmotic stress response in 0 and 50 mM conditions, see **Chapter 8.6**.

7.4 Conclusions

Here, we report a previously unobserved interaction between salt concentration and aging, and discuss the implications for future studies on nematode aging. In the wild, *C. elegans* live primarily in soil, feeding on bacteria found on rotting plant material. These animals exist in a

world of ever-changing environmental conditions, and are forced to deal with extremes of temperature, pH, osmolarity, oxidation, and infection with a variety of bacteria, fungi, and viruses. The extreme conditions of their natural environment are reflected in the nematode life cycle: wild *C. elegans* spend most of their lives in the stress-resistant dauer state, exiting it only to reproduce when conditions are favorable [337]. In the laboratory, however, nematodes exist in stable temperature and environmental conditions, ample resource availability, and co-culture with the only mildly pathogenic *E. coli* OP50.

It has long been understood, then, that the conditions under which we grow worms in the laboratory may not resemble the environmental conditions that they would most commonly experience in the wild. Indeed, laboratory culture conditions are sometimes selected arbitrarily without regard for what best represents the worms' 'natural' environment. Culturing worms on agar medium and feeding with *E. coli* was historically chosen for the sake of convenience, as these reagents were commonly available to most investigators when research into *C. elegans* first became common in the 1970's [3,726]. *E. coli* may not be the most optimal food source; though it is relatively nonpathogenic in young animals, it is pathogenic in older animals, and may be a major cause of death in aged worms [113,212]. Even the standard culture temperature of 20°C does not represent the optimal conditions for survival; it is well known that worms grown at 15°C live longer than those grown at higher temperatures, but this effect is considered to be "lifespan extension" simply because 20°C has been arbitrarily assigned as the standard culture temperature.

Thus, careful examination of *C. elegans* culture conditions is absolutely critical in order to fully understand how changing those conditions can affect lifespan. In **Chapter 3**, I describe such a situation regarding the commonly studied dietary restriction mutant *eat-2* [63]. *eat-2(lf)*

mutants have reduced pharyngeal pumping rate and were long used as models for DR due to their lowered food intake [49]. Our laboratory was able to demonstrate that lifespan extension in *eat-2(lf)* was not caused solely by reduced food intake, but rather by induction of food avoidance behavior and activation of the innate immune system; *eat-2(lf)* mutant lifespan extension was abrogated under nonpathogenic conditions.

Here, we observe a similar effect with salt concentration. NaCl is a necessary nutrient for both the worms themselves as well as their bacterial food source. Nevertheless, it has been demonstrated that excess salt can have detrimental effects on worm lifespan [106]. Here, we demonstrate that this detrimental effect is present even at 'standard' dose of 50 mM NaCl, the concentration commonly used in standard NGM formulations [3]. Worms grown on lower-salt conditions experience increased survival compared to those grown at the 'standard' dose.

Based on our early results that reduced supplemental salt extended lifespan, we generated two hypotheses; first, that removal of a dietary nutrient extended lifespan by DR, and second, that 50 mM supplemental salt was mildly stressful, and that removing this stress enhanced survival. We were able to exclude the first hypothesis as a likely explanation based on a lack of developmental delay or reduced fecundity, phenotypes common in DR conditions [5,48,193]. Our current results regarding the second hypothesis are unable to completely rule out lowered osmotic stress as a mechanism for lifespan extension. Expression of the *gpdh-1* osmotic stress response gene appears to increase late in life in worms raised on 0 and 50 mM supplemental salt, which we hypothesize results from aging-induced reductions in stress resistance and degradation of tissue structure. However, animals raised on 0 mM supplemental salt do not appear to experience reduced osmotic stress as measured by *gpdh-1* activation. However, our current reagents do not allow us to completely rule out this hypothesis. Future research will be focused

on detailed examination of nematode osmotic stress response pathways to determine their degree of activation in different salt conditions, and to see if these pathways are altered by removing supplemental salt. For further discussion of future experiments, please see **Chapter 8.6**.

7.5 Materials and Methods

Nematode strains and culture conditions

Nematodes were cultured as described in [3]; culture temperature was maintained at 20°C unless otherwise noted. Standard recipes for Nematode Growth Medium (NGM) were modified to examine the effect of altering salt concentration; standard formulations add supplemental NaCl ("salt") to a final concentration of 51.3 mM prior to autoclaving. For the purpose of these experiments, we considered 50 mM supplemental salt to be the "standard" dose. For concentrations higher than 50 mM, additional salt was added to reach the desired final concentration. For dishes containing 0 mM supplemental salt, no salt was added to the medium. NGM was prepared as previously described, seeded with 200 µL *E. coli* OP50 bacteria, allowed to dry on the benchtop overnight, and stored at 4°C for up to one month.

Genotype	**Strain**	**Source**
Wild type	N2 Bristol	CGC
daf-16(mu86) I	CF1038	CGC
daf-2(e1370) III	CB1370	CGC
kbIs5 [gpdh-1p::GFP + rol-6(su1006)]	VP198	CGC, [728]
drIs4 [gpdh-1p::GFP + col-12p::DsRed] IV	OG119	CGC, [729]

Survival analysis

To measure mean lifespan, nematodes were raised from embryo on NGM agar dishes containing 0, 50, or 200 mM supplemental salt and seeded with 200 µL *E. coli* OP50. Measurement of survival began on the first day of adulthood, ~72 hours after the animals were laid as embryos.

Animals were moved to new plates daily throughout the reproductive period and every 2-3 days thereafter. Animals which died due to matricidal hatching, gonad extrusion, or desiccation on the edge of the dish were considered to be alive on the day prior to their death, and were censored from the experiment for each day thereafter. Animals were determined to be dead by observation and gentle manipulation with a sterile platinum wire; if no spontaneous or induced movement was observed, they were counted as dead. Experiments continued until all animals had died or been censored. Mean lifespan and standard error were determined using Kaplan-Meier survival analysis and log-rank (Mantel-Cox) test [129,498].

Measurement of body movement and pharyngeal pumping rate

Animals were observed daily throughout their adult lifespan for body movement and pharyngeal pumping rate. Body movement was measured by picking animals individually onto NGM dishes containing 0, 50, or 200 mM supplemental salt. The number of sinusoidal body movements was measured over a 15 s interval, and that number was multiplied by four to determine the movement rate per minute. One movement was defined as the movement of the animal's head from its left-most position to its right-most position or *vice versa*, while the animal was moving either forward or backward. Pharyngeal pumping rate was measured by counting the number of pharynx pumps in a 15 s interval and multiplying this number by 4 to determine the number of pharynx pumps per minute.

Measurement of reproductive span, development rate, and total progeny

Duration of the reproductive span, development rate, and total number of progeny was measured in wild-type animals grown on NGM dishes containing 0, 50, or 200 mM supplemental salt. A synchronized egg lay was performed by placing 10-20 P_0 adult hermaphrodites onto dishes,

allowing them to lay eggs for one hour, then removing the adults and transferring one F_1 egg per dish onto ~20 dishes per salt concentration. Beginning ~68 hours later, each F1 was examined hourly for the presence of eggs laid on the dish. The number of hours for each animal to be laid as an egg, grow into an adult, and produce its first egg was defined as the time to first progeny.

Every 24 hours, the F_1 adults were transferred to new dishes, and the dishes containing the progeny laid over the previous day were retained. 2-3 days later the F_2 progeny were counted and discarded. This procedure continued until each F_1 had ceased egg laying for at least two consecutive days. Mean progeny number and standard deviation was determined by summing the total number of eggs laid by each F_1 animal throughout its reproductive span.

Determination of *gpdh-1* transcriptional reporter activity

Transgenic animals VP198 and OG119, both containing the *gpdh-1p::gfp* construct, were cultured from the egg stage in medium containing 0, 50, or 200 mM supplemental salt for 3 days, until they had reached adulthood. Every day thereafter, 5-10 animals were picked onto agar slides for observation; the remaining animals were transferred to new dishes. This process continued until day 17 of adulthood. To perform fluorescence microscopy, we prepared 3% agar slides, added a drop of levamisol (3 mM) (PHR1798, Sigma-Aldrich, Burlington, MA) to the agar, and added ~5-10 worms per slide. As necessary, animals were oriented using an eye lash. Excess levamisol was removed, and a cover slide was applied and sealed with 3% agar. Brightfield and fluorescence images of animals were acquired using a Leica DMi8 using the same settings for control and drug treated animals in each experiment. Fluorescence intensity of each worm was measured using Fiji (ImageJ, 1.53f51).

Chapter 8: Conclusions and future directions

8.1 Analysis of lifespan extension in *phm-2(lf)* and *eat-2(lf)* mutants

As described in **Chapter 3**, our current model for lifespan extension in *phm-2(lf)* and *eat-2(lf)* mutants is as follows: 1) disruption of pharyngeal structure and function results in incomplete grinding of the bacterial food source; 2) colonization of the intestinal lumen by live bacteria; 3) upregulation of antimicrobial peptides and other components of the innate immune system; 4) bacterial food avoidance behavior, reduction in caloric intake, and lifespan extension by dietary restriction [63]. Steps 1, 2, and 4 have been rigorously proven, but the precise role of the innate immune system remains unexplored. The innate immune system is composed of dozens or hundreds of genes which are upregulated in response to bacterial, fungal, or viral infection, and which serve to promote survival under pathogenic conditions. Several components of the innate immune system, including *clec-7, clec-60, clec-82,* and *lys*-5 are upregulated in *phm-2(lf)* and *eat-2(lf)* mutants fed live *E. coli* OP50 bacteria [63]. However, preliminary research suggests they are not necessary for lifespan extension, as knockdown of individual genes does not reduce survival; neither are they sufficient for lifespan extension, as overexpression of *clec-60* fails to extend lifespan on its own.

It is likely that the survival-promoting effects of innate immune activation are distributed among a large number of genes, such that reducing the activity of one will result in the others 'taking up the slack', and that overexpressing one is insufficient to promote survival on its own. Alternatively, not all innate immune system components that are upregulated under these conditions have been identified; it is possible that there is a singular component that is indispensable for this process which has not yet been discovered.

Thus, given its size and complexity, it is unlikely that complete knockout of the innate immune system is possible. Instead, future research should focus on determining which components are most indispensable for control of aging in *phm-2(lf)* and *eat-2(lf)* mutants. I propose using RNAseq on *phm-2(lf)* and *eat-2(lf)* mutants grown on live *E. coli* OP50 and on UV-killed *E. coli* OP50. By identifying a subset of genes that are most highly expressed in pathogenic conditions compared to nonpathogenic conditions, we will be able to measure the activation of all relevant innate immune system genes simultaneously.

It is likely that the genes which are most required for lifespan extension would be the most highly upregulated in pathogenic conditions. A reverse-genetic screen using either RNAi or knockout mutants could then be used to determine the effect of each gene's knockout on *phm-2(lf)* and *eat-2(lf)* mutant survival. I would predict that genes which are the most highly upregulated will be the most indispensable for survival under these conditions, and that their knockdown will reduce lifespan extension. Determination of which, if any, components of the innate immune system are necessary for this lifespan extension phenotype would increase our understanding of its mechanism.

Lifespan extension in *phm-2(lf)* and *eat-2(lf)* mutants results from a combination of dietary restriction and innate immune activation, and thus far it has been difficult to isolate these factors to identify which is most responsible for lifespan extension. The two are causally linked, as animals raised on small lawns of pathogenic *E. coli* OP50 exhibit both food avoidance (and thus DR) and innate immune activation. If the animals are prevented from avoiding the food via culture on large lawns spread over the surface of the agar dish, however, the pathogenic activity of the *E. coli* bacteria results in reduced survival by infection.

A method to disentangle these factors would be to raise the animals on large lawns consisting of a titrated mixture of both *E. coli* OP50 and the non-pathogenic bacteria *Comamonas*. By serially reducing the ratio of *E. coli* to *Comamonas* in this mixture and then measuring the resulting activation of previously identified innate immune genes via RT-qPCR, we could find a dietary composition that results in a modest activation of the innate immune system without the consequent reduction in food intake. As these animals would be fed *ad libitum* on non-pathogenic *Comamonas*, I would expect many of the phenotypes associated with DR to be abrogated, including small body size, extended reproductive period, delayed development, and reduced progeny production. Conversely, those phenotypes which primarily result from innate immune activation should not be affected. By measuring lifespan, we would be able to determine the degree to which DR and innate immune activation influence survival. If lifespan extension is abrogated, that would indicate that lifespan extension in *phm-2(lf)* and *eat-2(lf)* mutants primarily results from DR; conversely, if lifespan extension remains unchanged compared to animals grown on small lawns of *E. coli* alone, then that would indicate that lifespan extension primarily results from innate immune activation. An intermediate lifespan would indicate that the phenotype is multicausal.

8.2 Analysis of antimicrobial activity of the Amyloid Beta peptide

In **Chapter 4**, I discovered that expression of the human amyloid beta peptide increases survival and reduces matricidal hatching under pathogenic conditions in hypersensitive *phm-2(am117)* animals. While initial results are compelling, this research is in its early state, and future directions should focus on characterizing the Aß peptide and its effects on survival. The simple and tractable worm model system allows us the opportunity to functionally characterize the Aß peptide with respect to its antimicrobial activity.

To do this, I propose to further characterize the range of pathogens on which Aß acts. In *C. elegans*, Aß has been shown to increase wild-type survival on the highly pathogenic fungus *C. albicans* and the bacteria *S. typhimurium* [482]; our hypersensitive model allows further research into mild pathogens, broadening the range of potential targets. Previous research has shown that Aß inhibits microbial proliferation in vivo [477]; using our model, we will measure the effect of Aß expression on survival following co-culture with *S. aureus, E. faecalis, S. pneumoniae*, etc. in an *in-vivo* system. We predict that Aß expression will significantly increase survival on these pathogens.

Previous research in nematodes has focused on the antibacterial and antifungal properties of Aß. In humans, AD development is most often correlated with activation of latent viruses within the brain, most commonly those of genus *Herpesviridae*, and Aß aggregates are associated with viral particles, suggesting a causal link [481,481,496,497,732,733]. I propose to further characterize Aß antiviral activity by measuring infection by the Orsay virus, one of the only known viruses that infects wild *C. elegans* [734]. These experiments will be performed in an *rde-1(lf)* virus-hypersensitive background. Control animals and animals expressing Aß will be exposed to the Orsay virus; the degree of viral infection will be determined using RT-qPCR to measure relative viral genome copy number. I predict that viral genome copy number will be reduced in animals expressing Aß compared to control.

Further research is required to come to a mechanistic understanding of how Aß functions in an antimicrobial fashion. Initial research in nematodes has shown that Aß preferentially aggregates around fungal and bacterial pathogens [477,482]; we hypothesize that the native function of the Aß antimicrobial peptide is to bind to and aggregate around infectious microorganisms and viruses, preventing cellular entry and allowing their uptake and degradation by the immune

system. I propose further characterizing this activity by performing structure-function analysis on the Aß peptide. The peptide will be serially modified by site-directed mutagenesis of 3-5 amino acid regions of the 42 amino acid peptide. We hypothesize that the antimicrobial activity of the Aß peptide is directly proportional to its aggregation capacity. Aggregation in transgenic worms expressing Aß in the muscle cells can be measured by two methods: first, raising animals at an elevated temperature of 25°C induces Aß aggregation in the muscles, which results in paralysis; the degree of paralysis is correlated with the degree of aggregation. Second, dyes such as Thioflavin T may be used to microscopically observe aggregates directly. We predict that mutations in Aß which reduce its aggregation will also reduce its antimicrobial activity, as measured by rescue of survival on pathogenic bacteria. Thus, we will perform site-directed mutagenesis on the Aß peptide and measure the resulting effect on aggregation and survival on pathogenic bacteria. I predict that mutations which inhibit aggregation capacity will also reduce antimicrobial activity and survival.

8.3 Functional analysis of *daf-2(am326A261V)*

In **Chapter 6**, I describe the discovery and characterization of a novel partial loss-of-function allele of the *daf-2* receptor tyrosine kinase gene, called *daf-2(am326).* This allele was discovered in a screen for mutants that are hypersensitive to captopril [71]. Like other alleles of *daf-2*, *daf-2(am326)* animals are long-lived, stress resistant, and exhibit ectopic dauer entry. Other alleles of *daf-2* often display negative pleiotropies such as delayed development, altered reproductive span, and elevated rates of embryonic or larval death [66,67]. In contrast, *daf-2(am326)* lacks many of these pleiotropies, making it a useful reagent for future studies of *daf-2*.

DAF-2 is homologous to the human insulin receptor (INSR), and previous research has utilized DAF-2 as a model for human insulin receptoropathies [709]. The *daf-2(am326)* mutant

phenotype results from an alanine to valine substitution at amino acid position 261. This substitution occurs in the L1 ligand binding domain, the extracellular region that is targeted by a variety of insulin-like ligands to activate the kinase activity of DAF-2. The A261V substitution represents a relatively minor change in primary structure, as both alanine and valine are small non-polar amino acids. As this relatively small change results in large changes in protein function, we can hypothesize that this substitution affects a region of the protein which is critical for DAF-2 functionality, likely the site of ligand binding. Further research into this may prove difficult, as DAF-2 binds a variety of insulin-like ligands, not all of which have been identified. Furthermore, little research has been done on DAF-2 with respect to structure-function analysis, complicating future research into the structural consequences of the *daf-2(am326)* substitution.

Future research should instead focus on using *daf-2(am326)* as a model for human insulin receptor syndromes. DAF-2 alanine 261 is conserved in the human INSR, corresponding to alanine 119. Interestingly, the precise molecular lesion responsible for the *daf-2(am326)* phenotype, A261V, corresponds to a previously characterized A119V substitution in humans. This mutation causes Donohue syndrome, an insulin receptor disease that results in craniofacial abnormalities, severe insulin resistance, developmental delays, and early death [661,662]. In cell culture, the A119V substitution results in drastically decreased activation of INSR [662]; this result strongly suggests that the homologous mutation in worms similarly results in impaired insulin binding and reduced DAF-2 kinase activity.

One potential avenue of research would be to examine the effect of the *daf-2(am326A261V)* mutation of the ligand binding activity of DAF-2. *daf-2(am326A261V)* is one of the only known alleles of DAF-2 whose homologous mutation in human INSR has been experimentally demonstrated to reduce ligand binding activity [662,709]. This allele could be used as

tool to study the effect of reduced binding of DAF-2 ligands, such as *daf-28, ins-1, ins-18,* etc., and to match this reduction in activity to a phenotypic effect [705].

8.4 Functional analysis of ACN-1

In **Chapters 5 and 6**, I discuss current research into the renin-angiotensin-aldosterone system and its effects on aging. This research centers around the role of ACN-1, the nematode homolog of the angiotensin-converting enzyme (ACE), in controlling aging and developmental decision making. In mammals, the structure and function of the ACE protein is well-characterized: manipulation and cleavage of the Angiotensin I substrate is effected by the highly-conserved, histidine-rich, penta-residue motif HEXXH [735,736]. These histidine residues bind zinc cofactors that are critical for the metallopeptidase activity of the ACE protein [735,736]. This active site is also the site of action of ACE-inhibitor drugs like captopril, which function as competitive inhibitors [95,509]. These residues are highly conserved in mammalian ACE, *Drosophila* Ance and Acer, and the ACE homologs of a variety of other species including mollusks, crustaceans, annelids, etc. (reviewed in [101]). This suggests that these residues appeared in the ancestral ACE-like protein prior to the divergence of these species more than 500 million years ago [532]. Thus, the HEXXH motif is critical to the functionality of almost all known ACE homologs and has survived genetic drift for long periods of evolutionary time.

The HEXXH motif is not present in *C. elegans* ACN-1, being replaced by the structurally unrelated amino acids SLLVQ [102]. This amino acid motif is also present in the related *Caenorhabditis* species *C. japonica, C. breneri,* and *C. briggsae,* suggesting that the SLLVQ motif appeared in a common *Caenorhabditis* ancestor (genome accessed via www.wormbase.org). ACN-1 appears to lack an active site: to date, no enzymatic activity has been ascribed to ACN-1, proteolytic or otherwise, and no substrate has been identified. However,

it is clear that ACN-1 retains some activity: genetic knockout of *acn-1* is embryonic lethal, and it is actively expressed in both larvae and adults, indicating that this gene remains both functional and essential for life [71,85]. Furthermore, inhibition of ACN-1 via either RNAi-mediated knockdown or treatment with captopril displays a wide variety of phenotypes, including extended lifespan, reduced age-related degeneration, elevated stress resistance, and ectopic dauer entry [71,85]. Thus, ACN-1 is functional, actively expressed, and performs vital functions necessary for the survival of the organism. The fact that inhibition via captopril phenocopies RNAi-mediated knockdown is especially interesting: since captopril binds to and inhibits ACE-like proteins at the active site, this would suggest that the active site of ACN-1 remains functional, despite an apparent lack of critical residues.

Future research on *acn-1* should focus on the characterization of its native function. As genetic knockout of *acn-1* is lethal due to inability to complete early larval molts, *acn-1* functionality can be assessed by observing rates of larval lethality. One way to accomplish this would be to determine the function of the ACN-1 active site via site-directed mutagenesis and examination of the resulting phenotypes. Due to the apparent site-specific inhibitory effect of captopril, I would predict that mutagenesis of the SLLVQ into structurally distinct amino acids would abrogate ACN-1 activity and induce high rates of larval lethality. Conversely, rescue could be accomplished by introduction of mammalian HEXXH residues into ACN-1. If, instead, these residues are dispensable for the activity of ACN-1, I would not predict mutagenesis at this site to have any phenotypic effect. This experiment would determine whether the predicted active site was functional, and whether it functioned in the same way as the mammalian motif.

An alternative hypothesis is that ACN-1 has evolved to utilize a different active site. In mammalian ACE, two active sites are present: the well-studied C-domain active site, which is the

site of Angiotensin I peptidase activity; and the N-domain active site, which hydrolyzes a structurally distinct peptide to control hematopoietic stem cell differentiation [737–739]. Though ACE-inhibitor compounds like captopril bind to both active sites with comparable affinity [736], their anti-hypertensive activity arises from competitive inhibition of the C-domain active site alone. ACN-1 contains only one region that is homologous to the ACE active sites, but ACN-1 features two domains which are not present in mammalian ACE. These are ~100 amino acid extensions of both the N- and C-terminus [102]. These regions contain several sites predicted to function in post-translational modification of the protein. To determine if these regions are necessary for ACN-1-mediated control of aging, I propose to selectively knockout these regions individually and in combination, and assay the resulting effect on larval and adult survival.

In other species, captopril directly binds to the active site of ACE and competitively inhibits its metallopeptidase activity [740,741]. Captopril was originally designed as a chemical mimetic of a peptide found in the venom of the Brazilian pit viper *Bothrops jararaca* [95,509]. Thus, captopril and other ACE inhibitors function via specific inhibition of the ACE active site. Because of this, it is highly likely that captopril inhibits ACN-1 in the same manner: by directly binding to and inhibiting its active site. However, no direct evidence that captopril directly inhibits ACN-1 has yet been found. The evidence linking captopril-mediated control of aging to ACN-1 inhibition is twofold: 1) that captopril treatment phenocopies *acn-1* RNAi, and 2) that epistasis experiments show that captopril fails to further extend the lifespan *acn-1* RNAi-treated worms, suggesting that they function via a shared mechanism.

Direct proof of the captopril-ACN-1 interaction would require both evidence that captopril binds to ACN-1 and evidence that captopril binding affects ACN-1 activity. X-Ray

crystallography of ACN-1 in complex with captopril could prove the binding model, and additionally would show whether or not captopril binds to the ACE-like active site.

Though not direct proof, evidence of other ACE-inhibitor compounds controlling aging would further reinforce the ACN-1 inhibition hypothesis – it is unlikely that two structurally distinct drugs would cause the same phenotypes by anything other than a shared mechanism. Most ACE-inhibitors are pro-drugs, and it is unlikely that worms would metabolize them in the same way that mammals do. Lisinopril is a non-pro-drug ACE-inhibitor that has been shown to control aging in *Drosophila*, and it would be useful to determine if lisinopril also extends lifespan in *C. elegans* [516,550]. This may be difficult, as captopril extends lifespan only in a very narrow range of concentrations (~1-4mM), necessitating a large range of lisinopril doses to be tested for lifespan extension [71].

Future research on ACN-1 is hampered by the lack of known substrates. ACN-1 lacks histidine residues that bind zinc cofactors which are mechanistically required to cleave the Ang I substrate. However, this is supposition based only on observations of the protein's primary structure in comparison to mammalian ACE; a lack of metallopeptidase activity in ACN-1 has not been observed experimentally. Experimental determination of ACN-1 cleavage activity could be accomplished by generating ACN-1 protein *in vitro* via expression in cell culture. Measurement of Ang I can be accomplished by a number of reagents which utilize colorimetrically measured synthetic substrates. If Ang I cleavage is observed, this would fundamentally alter our understanding of the mechanism of ACN-1, and would suggest that ACN-1 mediates its effect on aging via proteolytic cleavage of an Ang I-like substrate. If no cleavage activity is observed, alternative hypotheses should be considered.

One alternative hypothesis is that ACN-1 simply binds to and traffics or sequesters its substrate. In this case, direct evidence of ACN-1 substrate binding would need to be observed. It is likely that an ACN-1 substrate would be structurally similar to Ang I. Isolation of the substrate could be accomplished by a variety of techniques, such as co-immunoprecipitation or affinity binding assay; identification of the substrate could be accomplished using techniques such as HPLC or protein NMR. These techniques could be used to identify any or all substrates that bind to ACN-1

8.5 Characterization of DAF-12 and DAF-16 activity in ACN-1-mediated lifespan extension

The DAF-16 transcription factor and the DAF-12 nuclear hormone receptor are critical regulators of molting, development, dauer entry, and aging. DAF-16 acts at the terminus of the IIS pathway to mediate the transcription of stress-resistance and pro-longevity genes. *daf-16* is necessary for the lifespan extension effect observed from knockout of IIS pathway members such as *daf-2* and *age-1.* The DAF-12 nuclear hormone receptor acts as the terminus of the transforming growth factor ß (TGFß)-like signal transduction pathway, and acts parallel to DAF-16 to downregulate genes involved in reproductive growth and upregulate genes involved in survival and dauer entry. Both genes are necessary for entry into the dauer state and delayed aging; loss-of-function mutations in *daf-16* and *daf-12* block dauer entry and reduce lifespan.

Epistasis experiments have revealed that *acn-1*-mediated control of aging requires both DAF-16 and DAF-12, but the precise mechanism for this interaction is unknown [71]. DAF-16 nuclear localization is controlled by AKT-1/2-mediated phosphorylation. Within the nucleus, DAF-16 bind to a variety of downstream targets, and promotes their transcription. However, treatment with captopril does not drive DAF-16 nuclear localization and does not promote the

transcription of the *sod-3* superoxide dismutase, a canonical target of DAF-16 [71,85]. The DAF-12 nuclear hormone receptor binds to dafachronic acid steroid hormones, activating its transcriptional activity and promoting the expression of genes which control reproduction, development, and longevity in response to environmental cues [695,696,742–745]. The nature of the DAF-12/ACN-1 interaction is poorly understood. Future research should seek to answer the following questions:

1. Is DAF-16 transcriptional activity controlled by ACN-1? It is possible that ACN-1 mediates its effects on lifespan through DAF-16 by some mechanism that does not involve activation of canonical targets. Captopril treatment does not increase expression of the canonical DAF-16 target *sod*-3, but other targets have not been examined. An RT-qPCR screen focusing on known targets of DAF-16 could establish whether or not treatment with captopril influences the transcriptional activity of DAF-16.
2. Is DAF-16 necessary for phenotypes associated with *acn-1* knockdown other than lifespan? *daf-16(lf)* mutations also block captopril-mediated dauer entry, but this is likely to result from the general Daf-d phenotype associated with *daf-16*. It is unclear if DAF-16 is necessary for phenotypes such as high-captopril induced larval arrest or captopril-associated molting defects.
3. What is the precise nature of the DAF-16/ACN-1 interaction? Canonical activation of DAF-16 occurs via nuclear localization and activation of downstream transcriptional targets. It is likely that ACN-1 does not directly inhibit DAF-16, but rather is part of a pathway that influences its activation, or acts in a parallel pathway. ACN-1 may serve to inhibit the expression or activity of DAF-16 target genes. RNAseq can be used to

determine a broad range of transcriptional changes that result from captopril administration or *acn-1* RNAi-mediated knockdown. Examining this list for DAF-16 targets could provide information on the interaction of these two pathways.

4. Further characterization of the DAF-12/ACN-1 interaction. Does *daf-12(lf)* block ACN-1-induced dauer entry and larval arrest? Does *daf-12(lf)* block lifespan extension in animals exposed to *acn-1* RNAi?

8.6 Understanding the role of salt concentration in worm aging

In **Chapter 7**, I discuss the discovery that reducing supplemental salt concentration to 0 mM in NGM agar extends lifespan compared to the standard formulation of 50 mM. Currently, we have not identified a mechanism to explain this observation. Two hypotheses present themselves: first, that the removal of NaCl, a necessary dietary nutrient both for the worms themselves as well as the *E. coli* OP50 bacterial food source, induces a DR phenotype and subsequent lifespan extension. Second, that 50 mM supplemental salt induces mild osmotic stress in the animals that only becomes apparent later in life as tissue structure and function degrade, and that removal of this stress increases survival.

We addressed the first hypothesis by measuring development and fecundity; animals grown on 0 mM supplemental salt did not display extended development rate, reduced progeny, or extended reproductive span, phenotypes that would be expected under DR conditions. To further address this hypothesis, we plan to measure the effect of removing supplemental salt in an *eat-2(lf)* mutant background; *eat-2* mutants are commonly used as models of dietary restriction. If salt removal further extends lifespan in *eat-2(lf)* animals, this would indicate that the two operate via distinct mechanisms, allowing us to confidently exclude DR as a causative mechanism.

We plan to further address the second hypothesis, that 50 mM supplemental salt conditions induce a mild osmotic stress, by detailed examination of the worm osmotic stress response pathways. Currently, we have used both RT-qPCR and fluorescent transcriptional reporters to measure the expression of *gpdh-1*, a gene necessary for the production of glycerol, an alternative organic osmolyte [106,728,729]. *gpdh-1* is upregulated under conditions of osmotic stress, and can be used as a proxy to measure this phenotype. We hypothesized that *gpdh-1* expression would increase later in life, as the animals' tissue structure and ability to maintain homeostasis were reduced. We did observe an age-dependent increase, but this increase was not significantly different between animals grown in 0 and 50 mM supplemental salt conditions. If our hypothesis that 50 mM represented a stressful condition compared to 0 mM were true, we would expect that aged animals would significantly upregulate *gpdh-1* in 50 mM conditions compared to 0 mM conditions.

However, further research is needed to fully exclude this hypothesis. We plan to further examine mechanism for osmotic stress response in aged animals to detect if there is a difference in animals grown in 0 or 50 mM supplemental salt conditions. Mutations in *osr-1, osm-7,* and *osm-11* elevate internal concentrations of glycerol and confer resistance to hyperosmotic stress [746,747]. Our hypothesis is that 50 mM supplemental salt reduces survival via mild osmotic stress; thus, we predict that the lifespan of *osr-1(lf)*, *osm-7(lf),* and *osm-11(lf)* mutants will be extended in 50 mM supplemental salt conditions, and will be unchanged compared to 0 mM supplemental salt conditions.

Further research is needed to characterize the effect of salt removal on aging in more detail. Removal of supplemental salt did not reduce age-related decline in pharyngeal pumping rate, and reduced decline in body movement rate only late in life. However, we have anecdotally

observed that, while movement speed may not increase in 0 mM supplemental salt conditions, the percentage of animals exhibiting spontaneous movement is increased. We will quantify this observation by measuring the percentage of animals exhibiting different movement modalities, as described in [117]. We expect that removal of supplemental salt will increase the percentage of animals exhibiting Class A (vigorous, spontaneous) movement compared to animals cultured on 50 mM supplemental salt.

Finally, we will characterize the effect of salt removal on other age-related phenotypes, including heat and oxidative stress resistance. We will also characterize its effect in other mutant backgrounds, such as *isp-1,* a long-lived mitochondrial dysfunction mutant [72]; *che-1*, which encodes a transcription factor necessary for chemosensory neuron formation [748]; *che-3*, a long-lived mutant which is necessary for salt sensation and chemotaxis [749]; and *gpdh-1*, which is necessary for formation of the organic osmolyte glycerol in response to osmotic stress [106,728,729]. This will allow us to better understand the genetic pathways involved in this method of lifespan extension.

References

1. Nielsen, J. *et al.* Eye lens radiocarbon reveals centuries of longevity in the Greenland shark (Somniosus microcephalus). *Science* **353**, 702–704 (2016).

2. Carey, J. R. Longevity minimalists: life table studies of two species of northern Michigan adult mayflies. *Exp. Gerontol.* **37**, 567–570 (2002).

3. Brenner, S. The genetics of Caenorhabditis elegans. *Genetics* **77**, 71–94 (1974).

4. Friedman, D. B. & Johnson, T. E. A mutation in the age-1 gene in Caenorhabditis elegans lengthens life and reduces hermaphrodite fertility. *Genetics* **118**, 75–86 (1988).

5. Collins, J. J., Huang, C., Hughes, S. & Kornfeld, K. The measurement and analysis of age-related changes in Caenorhabditis elegans. *WormBook* 1–21 (2007) doi:10.1895/wormbook.1.137.1.

6. Markaki, M. & Tavernarakis, N. Modeling human diseases in Caenorhabditis elegans. *Biotechnol. J.* **5**, 1261–1276 (2010).

7. C. elegans Sequencing Consortium. Genome sequence of the nematode C. elegans: a platform for investigating biology. *Science* **282**, 2012–2018 (1998).

8. Moerman, D. G. & Barstead, R. J. Towards a mutation in every gene in Caenorhabditis elegans. *Brief. Funct. Genomics* **7**, 195–204 (2008).

9. Fire, A. *et al.* Potent and specific genetic interference by double-stranded RNA in Caenorhabditis elegans. *Nat. 1998 3916669* **391**, 806–811 (1998).

10. Friedland, A. E. *et al.* Heritable genome editing in C. elegans via a CRISPR-Cas9 system. *Nat. Methods* **10**, 741–743 (2013).

11. Carretero, M., Gomez-Amaro, R. L. & Petrascheck, M. Pharmacological classes that extend lifespan of Caenorhabditis elegans. (2015) doi:10.3389/fgene.2015.00077.

12. Collins, J. J., Evason, K. & Kornfeld, K. Pharmacology of delayed aging and extended lifespan of Caenorhabditis elegans. *Exp. Gerontol.* **41**, 1032–1039 (2006).

13. Lucanic, M., Lithgow, G. J. & Alavez, S. Pharmacological lifespan extension of invertebrates. *Ageing Res. Rev.* **12**, 445–458 (2013).

14. Johnson, T. E. Aging can be genetically dissected into component processes using long-lived lines of Caenorhabditis elegans. *Proc. Natl. Acad. Sci. U. S. A.* **84**, 3777–3781 (1987).

15. Huang, C., Xiong, C. & Kornfeld, K. Measurements of age-related changes of physiological processes that predict lifespan of Caenorhabditis elegans. *Proc. Natl. Acad. Sci. U. S. A.* **101**, 8084–8089 (2004).

16. Whitehead, J. C. *et al.* A Clinical Frailty Index in Aging Mice: Comparisons With Frailty Index Data in Humans. *J. Gerontol. Ser. A* **69**, 621–632 (2014).

17. Bisset, E. S. & Howlett, S. E. The biology of frailty in humans and animals: Understanding frailty and promoting translation. *AGING Med.* **2**, 27–34 (2019).

18. Scharf, A., Pohl, F., Egan, B. M., Kocsisova, Z. & Kornfeld, K. Reproductive Aging in Caenorhabditis elegans: From Molecules to Ecology. *Front. Cell Dev. Biol.* **9**, (2021).

19. Speakman, J. R. Correlations between physiology and lifespan – two widely ignored problems with comparative studies. *Aging Cell* **4**, 167–175 (2005).

20. Speakman, J. R. Body size, energy metabolism and lifespan. *J. Exp. Biol.* **208**, 1717–1730 (2005).

21. Von Neumann, J. On the theory of games of strategy. *Contrib. Theory Games* **4**, 13–42 (1959).

22. Smith, J. M. Evolution and the theory of games. *Am. Sci.* **64**, 41–45 (1976).

23. Cohen, A. A. Female post-reproductive lifespan: A general mammalian trait. *Biol. Rev. Camb. Philos. Soc.* **79**, 733–750 (2004).

24. Lahdenperä, M., Mar, K. U. & Lummaa, V. Reproductive cessation and post-reproductive lifespan in Asian elephants and pre-industrial humans. *Front. Zool.* **11**, 1–14 (2014).

25. Medawar, P. An unsolved problem of biology. (1952).

26. Williams, G. C. Pleiotropy, Natural Selection, and the Evolution of Senescence. *Evolution* **11**, 398–411 (1957).

27. Williams, P. D., Day, T., Fletcher, Q. & Rowe, L. The shaping of senescence in the wild. *Trends Ecol. Evol.* **21**, 458–463 (2006).

28. Promislow, D. E. L. Senescence in Natural Populations of Mammals: A Comparative Study. *Evolution* **45**, 1869–1887 (1991).

29. Nussey, D. H., Froy, H., Lemaitre, J. F., Gaillard, J. M. & Austad, S. N. Senescence in natural populations of animals: Widespread evidence and its implications for bio-gerontology. *Ageing Res. Rev.* **12**, 214–225 (2013).

30. Wilder, S. M., Rypstra, A. L. & Elgar, M. A. The Importance of Ecological and Phylogenetic Conditions for the Occurrence and Frequency of Sexual Cannibalism. *Annu. Rev. Ecol. Evol. Syst.* **40**, 21–39 (2009).

31. Hughes, S. E., Evason, K., Xiong, C. & Kornfeld, K. Genetic and pharmacological factors that influence reproductive aging in nematodes. *PLoS Genet.* **3**, e25 (2007).

32. Kraus, C., Pavard, S. & Promislow, D. E. L. The Size–Life Span Trade-Off Decomposed: Why Large Dogs Die Young. *Am. Nat.* **181**, 492–505 (2013).

33. Sebastiani, P. & Perls, T. The Genetics of Extreme Longevity: Lessons from the New England Centenarian Study. *Front. Genet.* **3**, (2012).

34. McGue, M., Vaupel, J. W., Holm, N. & Harvald, B. Longevity Is Moderately Heritable in a Sample of Danish Twins Born 1870–1880. *J. Gerontol.* **48**, B237–B244 (1993).

35. Karasik, D., Demissie, S., Cupples, L. A. & Kiel, D. P. Disentangling the Genetic Determinants of Human Aging: Biological Age as an Alternative to the Use of Survival Measures. *J. Gerontol. Ser. A* **60**, 574–587 (2005).

36. Gudmundsson, H. *et al.* Inheritance of human longevity in Iceland. *Eur. J. Hum. Genet.* **8**, 743–749 (2000).

37. Morris, B. J., Willcox, B. J. & Donlon, T. A. Genetic and epigenetic regulation of human aging and longevity. *Biochim. Biophys. Acta BBA - Mol. Basis Dis.* **1865**, 1718–1744 (2019).

38. Burtner, C. R. & Kennedy, B. K. Progeria syndromes and ageing: what is the connection? *Nat. Rev. Mol. Cell Biol.* **11**, 567–578 (2010).

39. Kennedy, B. K. The genetics of ageing: insight from genome-wide approaches in invertebrate model organisms. *J. Intern. Med.* **263**, 142–152 (2008).

40. Stanfel, M. N., Shamieh, L. S., Kaeberlein, M. & Kennedy, B. K. The TOR pathway comes of age. *Biochim. Biophys. Acta* **1790**, 1067–1074 (2009).

41. Cantó, C. & Auwerx, J. Caloric restriction, SIRT1 and longevity. *Trends Endocrinol. Metab. TEM* **20**, 325–331 (2009).

42. Blüher, M., Kahn, B. B. & Kahn, C. R. Extended longevity in mice lacking the insulin receptor in adipose tissue. *Science* **299**, 572–574 (2003).

43. Liang, H. *et al.* Genetic mouse models of extended lifespan. *Exp. Gerontol.* **38**, 1353–1364 (2003).

44. McCay, C. M., Crowell, M. F. & Maynard, L. A. The effect of retarded growth upon the length of life span and upon the ultimate body size. 1935. *Nutr. Burbank Los Angel. Cty. Calif* **5**, 155–171; discussion 172 (1935).

45. Fabrizio, P. & Longo, V. D. The chronological life span of Saccharomyces cerevisiae. *Aging Cell* **2**, 73–81 (2003).

46. Burger, J. M. S., Buechel, S. D. & Kawecki, T. J. Dietary restriction affects lifespan but not cognitive aging in Drosophila melanogaster. *Aging Cell* **9**, 327–335 (2010).

47. Bross, T. G., Rogina, B. & Helfand, S. L. Behavioral, physical, and demographic changes in Drosophila populations through dietary restriction. *Aging Cell* **4**, 309–317 (2005).

48. Klass, M. R. Aging in the nematode Caenorhabditis elegans: Major biological and environmental factors influencing life span. *Mech. Ageing Dev.* **6**, 413–429 (1977).

49. Lakowski, B. & Hekimi, S. The genetics of caloric restriction in Caenorhabditis elegans. *Proc. Natl. Acad. Sci. U. S. A.* **95**, 13091–13096 (1998).

50. Weindruch, R. Effect of caloric restriction on age-associated cancers. *Exp. Gerontol.* **27**, 575–581 (1992).

51. Lawler, D. F. *et al.* Diet restriction and ageing in the dog: major observations over two decades. *Br. J. Nutr.* **99**, 793–805 (2008).

52. Speakman, J. R. & Mitchell, S. E. Caloric restriction. *Mol. Aspects Med.* **32**, 159–221 (2011).

53. Cypser, J. R., Tedesco, P. & Johnson, T. E. Hormesis and aging in Caenorhabditis elegans. *Exp. Gerontol.* **41**, 935–939 (2006).

54. Minois, N. Longevity and aging: beneficial effects ofexposure to mild stress. *Biogerontology* **1**, 15–29 (2000).

55. Johnson, T. E., Lithgow, G. J. & Murakami, S. Hypothesis: Interventions That Increase the Response to Stress Offer the Potential for Effective Life Prolongation and Increased Health. *J. Gerontol. Ser. A* **51A**, B392–B395 (1996).

56. Kaeberlein, T. L. *et al.* Lifespan extension in Caenorhabditis elegans by complete removal of food. *Aging Cell* **5**, 487–494 (2006).

57. Sharp, Z. D. Aging and TOR: interwoven in the fabric of life. *Cell. Mol. Life Sci.* **68**, 587–597 (2011).

58. Morselli, E. *et al.* Caloric restriction and resveratrol promote longevity through the Sirtuin-1-dependent induction of autophagy. *Cell Death Dis.* **1**, e10–e10 (2010).

59. Hosono, R., Nishimoto, S. & Kuno, S. Alterations of life span in the nematode Caenorhabditis elegans under monoxenic culture conditions. *Exp. Gerontol.* **24**, 251–264 (1989).

60. Greer, E. L. *et al.* An AMPK-FOXO Pathway Mediates Longevity Induced by a Novel Method of Dietary Restriction in C. elegans. *Curr. Biol.* **17**, 1646–1656 (2007).

61. Lee, G. D. *et al.* Dietary deprivation extends lifespan in Caenorhabditis elegans. *Aging Cell* **5**, 515–524 (2006).

62. McKay, J. P., Raizen, D. M., Gottschalk, A., Schafer, W. R. & Avery, L. eat-2 and eat-18 are Required for Nicotinic Neurotransmission in the Caenorhabditis elegans Pharynx. *Genetics* **166**, 161–169 (2004).

63. Kumar, S. *et al.* Lifespan Extension in C. elegans Caused by Bacterial Colonization of the Intestine and Subsequent Activation of an Innate Immune Response. *Dev. Cell* **49**, 100-117.e6 (2019).

64. Kenyon, C., Chang, J., Gensch, E., Rudner, A. & Tabtiang, R. A C. elegans mutant that lives twice as long as wild type. *Nature* **366**, 461–464 (1993).

65. Murphy, C. T. & Hu, P. J. Insulin/insulin-like growth factor signaling in C. elegans. *WormBook Online Rev. C Elegans Biol.* 1–43 (2013) doi:10.1895/wormbook.1.164.1.

66. Gems, D. *et al.* Two Pleiotropic Classes of daf-2 Mutation Affect Larval Arrest, Adult Behavior, Reproduction and Longevity in Caenorhabditis elegans. *Genetics* **150**, 129–155 (1998).

67. Patel, D. S. *et al.* Clustering of Genetically Defined Allele Classes in the Caenorhabditis elegans DAF-2 Insulin/IGF-1 Receptor. *Genetics* **178**, 931–946 (2008).

68. Hu, P. J. Dauer. in *WormBook: The Online Review of C. elegans Biology* (WormBook, 2018).

69. Gerisch, B. & Antebi, A. Hormonal signals produced by DAF-9/cytochrome P450 regulate C. elegans dauer diapause in response to environmental cues. *Development* **131**, 1765–1776 (2004).

70. Klass, M. & Hirsh, D. Non-ageing developmental variant of Caenorhabditis elegans. *Nature* **260**, 523–525 (1976).

71. Egan, B. M. *et al.* The ACE-inhibitor drug captopril inhibits ACN-1 to control dauer formation and aging. *bioRxiv* **2023**, 2023.07.17.549402 (2023).

72. Feng, J., Bussière, F. & Hekimi, S. Mitochondrial Electron Transport Is a Key Determinant of Life Span in Caenorhabditis elegans. *Dev. Cell* **1**, 633–644 (2001).

73. Rea, S. L., Ventura, N. & Johnson, T. E. Relationship Between Mitochondrial Electron Transport Chain Dysfunction, Development, and Life Extension in Caenorhabditis elegans. *PLOS Biol.* **5**, e259 (2007).

74. Copeland, J. M. *et al.* Extension of Drosophila Life Span by RNAi of the Mitochondrial Respiratory Chain. *Curr. Biol.* **19**, 1591–1598 (2009).

75. Dell'agnello, C. *et al.* Increased longevity and refractoriness to Ca(2+)-dependent neurodegeneration in Surf1 knockout mice. *Hum. Mol. Genet.* **16**, 431–444 (2007).

76. Lee, S. S. *et al.* A systematic RNAi screen identifies a critical role for mitochondria in C. elegans longevity. *Nat. Genet.* **33**, 40–48 (2003).

77. Liu, X. *et al.* Evolutionary conservation of the clk-1-dependent mechanism of longevity: loss of mclk1 increases cellular fitness and lifespan in mice. *Genes Dev.* **19**, 2424–2434 (2005).

78. Ziegler, D. V., Wiley, C. D. & Velarde, M. C. Mitochondrial effectors of cellular senescence: beyond the free radical theory of aging. *Aging Cell* **14**, 1–7 (2015).

79. Van Raamsdonk, J. M. & Hekimi, S. Superoxide dismutase is dispensable for normal animal lifespan. *Proc. Natl. Acad. Sci. U. S. A.* **109**, 5785–5790 (2012).

80. Kauppila, J. H. K. & Stewart, J. B. Mitochondrial DNA: Radically free of free-radical driven mutations. *Biochim. Biophys. Acta BBA - Bioenerg.* **1847**, 1354–1361 (2015).

81. Hansen, M. *et al.* Lifespan extension by conditions that inhibit translation in Caenorhabditis elegans. *Aging Cell* **6**, 95–110 (2007).

82. Pan, K. Z. *et al.* Inhibition of mRNA translation extends lifespan in Caenorhabditis elegans. *Aging Cell* **6**, 111–119 (2007).

83. Syntichaki, P., Troulinaki, K. & Tavernarakis, N. Protein Synthesis Is a Novel Determinant of Aging in Caenorhabditis elegans. *Ann. N. Y. Acad. Sci.* **1119**, 289–295 (2007).

84. Blackwell, T. K., Sewell, A. K., Wu, Z. & Han, M. TOR Signaling in Caenorhabditis elegans Development, Metabolism, and Aging. *Genetics* **213**, 329–360 (2019).

85. Kumar, S., Dietrich, N. & Kornfeld, K. Angiotensin Converting Enzyme (ACE) Inhibitor Extends Caenorhabditis elegans Life Span. *PLOS Genet.* **12**, e1005866 (2016).

86. Honda, Y., Tanaka, M. & Honda, S. Trehalose extends longevity in the nematode Caenorhabditis elegans. *Aging Cell* **9**, 558–569 (2010).

87. Barzilai, N., Crandall, J. P., Kritchevsky, S. B. & Espeland, M. A. Metformin as a Tool to Target Aging. *Cell Metab.* **23**, 1060–1065 (2016).

88. Cabreiro, F. *et al.* Metformin retards aging in C. elegans by altering microbial folate and methionine metabolism. *Cell* **153**, 228–239 (2013).

89. Onken, B. & Driscoll, M. Metformin induces a dietary restriction-like state and the oxidative stress response to extend C. elegans healthspan via AMPK, LKB1, and SKN-1. *PLoS ONE* **5**, (2010).

90. Anisimov, V. N. *et al.* Metformin slows down aging and extends life span of female SHR mice. *Cell Cycle* **7**, 2769–2773 (2008).

91. Ehninger, D., Neff, F. & Xie, K. Longevity, aging and rapamycin. *Cell. Mol. Life Sci.* **71**, 4325–4346 (2014).

92. Harrison, D. E. *et al.* Rapamycin fed late in life extends lifespan in genetically heterogeneous mice. *Nature* **460**, 392 (2009).

93. Miller, R. A. *et al.* Rapamycin, But Not Resveratrol or Simvastatin, Extends Life Span of Genetically Heterogeneous Mice. *J. Gerontol. Ser. A* **66A**, 191–201 (2011).

94. Strong, R. *et al.* Lifespan benefits for the combination of rapamycin plus acarbose and for captopril in genetically heterogeneous mice. *Aging Cell* **21**, e13724 (2022).

95. Cushman, D. W. & Ondetti, M. A. History of the Design of Captopril and Related Inhibitors of Angiotensin Converting Enzyme. *Hypertension* **17**, 589–592 (1991).

96. Ibrahim, M. M. RAS inhibition in hypertension. *J. Hum. Hypertens.* **20**, 101–108 (2006).

97. Basso, N. & Terragno, N. A. History About the Discovery of the Renin-Angiotensin System. *Hypertension* **38**, 1246–1249 (2001).

98. Fyhrquist, F. & Saijonmaa, O. Renin-angiotensin system revisited. *J. Intern. Med.* **264**, 224–236 (2008).

99. Igic, R. A short history of the renin-angiotensin system. *Acta Medica Salin.* **38**, 8–12 (2009).

100. Peach, M. J. Renin angiotensin system: Biochemistry and mechanisms of action. *Physiol. Rev.* **57**, 313–370 (1977).

101. Egan, B. M., Scharf, A., Pohl, F. & Kornfeld, K. Control of aging by the renin–angiotensin system: a review of C. elegans, Drosophila, and mammals. *Front. Pharmacol.* **13**, 938650 (2022).

102. Brooks, D. R., Appleford, P. J., Murray, L. & Isaac, R. E. An Essential Role in Molting and Morphogenesis of Caenorhabditis elegans for ACN-1, a Novel Member of the Angiotensin-converting Enzyme Family That Lacks a Metallopeptidase Active Site. *J. Biol. Chem.* **278**, 52340–52346 (2003).

103. Metheetrairut, C., Ahuja, Y. & Slack, F. J. acn-1, a C. elegans homologue of ACE, genetically interacts with the let-7 microRNA and other heterochronic genes. *Cell Cycle* **16**, 1800–1809 (2017).

104. Choe, K. P. Physiological and molecular mechanisms of salt and water homeostasis in the nematode Caenorhabditis elegans. *Am. J. Physiol. - Regul. Integr. Comp. Physiol.* **305**, (2013).

105. Choe, K. P. & Strange, K. Molecular and genetic characterization of osmosensing and signal transduction in the nematode Caenorhabditis elegans. *FEBS J.* **274**, 5782–5789 (2007).

106. Lamitina, S. T., Morrison, R., Moeckel, G. W. & Strange, K. Adaptation of the nematode Caenorhabditis elegans to extreme osmotic stress. *Am. J. Physiol. - Cell Physiol.* **286**, (2004).

107. Jemielity, S., Chapuisat, M., Parker, J. D. & Keller, L. Long live the queen: Studying aging in social insects. *Age* **27**, 241–248 (2005).

108. Angeles-Albores, D. *et al.* The Caenorhabditis elegans Female State: Decoupling the Transcriptomic Effects of Aging and Sperm-Status. *G3 Genes Genomes Genet.* **7**, 2969–2977 (2017).

109. Balaban, R. S., Nemoto, S. & Finkel, T. Mitochondria, Oxidants, and Aging. *Cell* **120**, 483–495 (2005).

110. de la Guardia, Y. *et al.* Run-on of germline apoptosis promotes gonad senescence in C. elegans. *Oncotarget* **7**, 39082–39096 (2016).

111. Ezcurra, M. *et al.* C. elegans Eats Its Own Intestine to Make Yolk Leading to Multiple Senescent Pathologies. *Curr. Biol.* **28**, 2544–2556 (2018).

112. Baker, G. T. & Sprott, R. L. Biomarkers of aging. *Exp. Gerontol.* **23**, 223–239 (1988).

113. Garigan, D. *et al.* Genetic analysis of tissue aging in Caenorhabditis elegans: A role for heat-shock factor and bacterial proliferation. *Genetics* **161**, 1101–1112 (2002).

114. Gerstbrein, B., Stamatas, G., Kollias, N. & Driscoll, M. In vivo spectrofluorimetry reveals endogenous biomarkers that report healthspan and dietary restriction in Caenorhabditis elegans. *Aging Cell* **4**, 127–137 (2005).

115. Pincus, Z. & Slack, F. J. Developmental biomarkers of aging in Caenorhabditis elegans. *Dev. Dyn.* **239**, 1306–1314 (2010).

116. Petrascheck, M. & Miller, D. L. Computational Analysis of Lifespan Experiment Reproducibility. *Front. Genet.* **8**, 92 (2017).

117. Herndon, L. A. *et al.* Stochastic and genetic factors influence tissue-specific decline in ageing C. elegans. *Nature* **419**, 808–814 (2002).

118. Chow, D. K., Glenn, C. F., Johnston, J. L., Goldberg, I. G. & Wolkow, C. A. Sarcopenia in the Caenorhabditis elegans pharynx correlates with muscle contraction rate over lifespan. *Exp. Gerontol.* **41**, 252–260 (2006).

119. Newell Stamper, B. L. *et al.* Movement decline across lifespan of Caenorhabditis elegans mutants in the insulin/insulin-like signaling pathway. *Aging Cell* **17**, e12704 (2018).

120. Bansal, A., Zhu, L. J., Yen, K. & Tissenbaum, H. A. Uncoupling lifespan and healthspan in caenorhabditis elegans longevity mutants. *Proc. Natl. Acad. Sci. U. S. A.* **112**, E277–E286 (2015).

121. Bolanowski, M. A., Jacobson, L. A. & Russell, R. L. Quantitative measures of aging in the nematode caenorhabditis elegans: II. Lysosomal hydrolases as markers of senescence. *Mech. Ageing Dev.* **21**, 295–319 (1983).

122. Wang, M. C., Oakley, H. D., Carr, C. E., Sowa, J. N. & Ruvkun, G. Gene Pathways That Delay Caenorhabditis elegans Reproductive Senescence. *PLoS Genet.* **10**, e1004752 (2014).

123. Stroustrup, N. *et al.* The Caenorhabditis elegans Lifespan Machine. *Nat. Methods* **10**, 665–670 (2013).

124. Solis, G. M. & Petrascheck, M. Measuring Caenorhabditis elegans life span in 96 well microtiter plates. *J. Vis. Exp.* **49**, e2496 (2011).

125. Hulme, S. E. *et al.* Lifespan-on-a-chip: microfluidic chambers for performing lifelong observation of C. elegans. *Lab Chip* **10**, 589–597 (2010).

126. Zhang, W. B. *et al.* Extended Twilight among Isogenic C. elegans Causes a Disproportionate Scaling between Lifespan and Health. *Cell Syst.* **3**, 333–345 (2016).

127. Churgin, M. A. *et al.* Longitudinal imaging of Caenorhabditis elegans in a microfabricated device reveals variation in behavioral decline during aging. *eLife* **6**, e26652 (2017).

128. Kamili, F. & Lu, H. Recent Advances and Trends in Microfluidic Platforms for C. elegans Biological Assays. *Annu. Rev. Anal. Chem.* **11**, 245–264 (2018).

129. Kaplan, E. L. & Meier, P. Nonparametric Estimation from Incomplete Observations. *J. Am. Stat. Assoc.* **53**, 457–481 (1958).

130. Pletcher, S. D., Khazaeli, A. A. & Curtsinger, J. W. Why Do Life Spans Differ? Partitioning Mean Longevity Differences in Terms of Age-Specific Mortality Parameters. *J. Gerontol. Ser. Biol. Sci. Med. Sci.* **55**, B381–B389 (2000).

131. Stroustrup, N. *et al.* The temporal scaling of Caenorhabditis elegans ageing. *Nature* **530**, 103–107 (2016).

132. Shaw, W. M., Luo, S., Landis, J., Ashraf, J. & Murphy, C. T. The C. elegans TGF-β Dauer Pathway Regulates Longevity via Insulin Signaling. *Curr. Biol.* **17**, 1635–1645 (2007).

133. Pickett, C. L. & Kornfeld, K. Age-related degeneration of the egg-laying system promotes matricidal hatching in Caenorhabditis elegans. *Aging Cell* **12**, 544–553 (2013).

134. Leiser, S. F. *et al.* Age-associated vulval integrity is an important marker of nematode healthspan. *AGE* **38**, 419–431 (2016).

135. Angelo, G. & Van Gilst, M. R. Starvation protects germline stem cells and extends reproductive longevity in C. elegans. *Science* **326**, 954–958 (2009).

136. Fletcher, M. & Kim, D. H. Age-Dependent Neuroendocrine Signaling from Sensory Neurons Modulates the Effect of Dietary Restriction on Longevity of Caenorhabditis elegans. *PLOS Genet.* **13**, 1–15 (2017).

137. Yang, J. S. *et al.* OASIS: Online application for the survival analysis of lifespan assays performed in aging research. *PLoS ONE* **6**, e23525 (2011).

138. Han, S. K. *et al.* OASIS 2: online application for survival analysis 2 with features for the analysis of maximal lifespan and healthspan in aging research. *Oncotarget* **7**, 56147–56152 (2016).

139. Stiernagle, T. Maintenance of C. elegans. *WormBook* 1–11 (2006) doi:10.1895/wormbook.1.101.1.

140. Gershon, D. Studies on Aging in Nematodes I: The Nematode as a Model Organism for Aging Research. *Exp. Gerontol.* **5**, 13–19 (1970).

141. Aitlhadj, L. & Stürzenbaum, S. R. The use of FUdR can cause prolonged longevity in mutant nematodes. *Mech. Ageing Dev.* **131**, 364–365 (2010).

142. van Raamsdonk, J. M. & Hekimi, S. FUdR causes a twofold increase in the lifespan of the mitochondrial mutant gas-1. *Mech. Ageing Dev.* **132**, 519–521 (2011).

143. Amrit, F. R. G., Ratnappan, R., Keith, S. A. & Ghazi, A. The C. elegans lifespan assay toolkit. *Methods* **68**, 465–475 (2014).

144. Anderson, E. N. *et al.* C. elegans lifespan extension by osmotic stress requires FUdR, base excision repair, FOXO, and sirtuins. *Mech. Ageing Dev.* **154**, 30–42 (2016).

145. Gems, D. & Riddle, D. L. Genetic, behavioral and environmental determinants of male longevity in Caenorhabditis elegans. *Genetics* **154**, 1597–1610 (2000).

146. Brooks, K. K., Liang, B. & Watts, J. L. The Influence of Bacterial Diet on Fat Storage in C. elegans. *PLOS ONE* **4**, e7545 (2009).

147. Soukas, A. A., Kane, E. A., Carr, C. E., Melo, J. A. & Ruvkun, G. Rictor/TORC2 regulates fat metabolism, feeding, growth, and life span in Caenorhabditis elegans. *Genes Dev.* **23**, 496–511 (2009).

148. Maier, W., Adilov, B., Regenass, M. & Alcedo, J. A Neuromedin U Receptor Acts with the Sensory System to Modulate Food Type-Dependent Effects on C. elegans Lifespan. *PLOS Biol.* **8**, e1000376 (2010).

149. Sowa, J. N., Mutlu, A. S., Xia, F. & Wang, M. C. Olfaction Modulates Reproductive Plasticity through Neuroendocrine Signaling in Caenorhabditis elegans. *Curr. Biol.* **25**, 2284–2289 (2015).

150. Garsin, D. A. *et al.* Long-Lived C. elegans daf-2 Mutants Are Resistant to Bacterial Pathogens. *Science* **300**, 1921–1921 (2003).

151. Ikeda, T., Yasui, C., Hoshino, K., Arikawa, K. & Nishikawa, Y. Influence of Lactic Acid Bacteria on Longevity of Caenorhabditis elegans and Host Defense against Salmonella enterica Serovar Enteritidis. *Appl. Environ. Microbiol.* **73**, 6404–6409 (2007).

152. Sánchez-Blanco, A. & Kim, S. K. Variable pathogenicity determines individual lifespan in Caenorhabditis elegans. *PLoS Genet.* **7**, e1002047 (2011).

153. Sánchez-Blanco, A. *et al.* Dietary and microbiome factors determine longevity in Caenorhabditis elegans. *Aging* **8**, 1513–1539 (2016).

154. Kato, M., Hamazaki, Y., Sun, S., Nishikawa, Y. & Kage-Nakadai, E. Clostridium butyricum MIYAIRI 588 Increases the Lifespan and Multiple-Stress Resistance of Caenorhabditis elegans. *Nutrients* **10**, 1921 (2018).

155. Tan, M.-W., Mahajan-Miklos, S. & Ausubel, F. M. Killing of Caenorhabditis elegans by Pseudomonas aeruginosa used to model mammalian bacterial pathogenesis. *Proc. Natl. Acad. Sci.* **96**, 715–720 (1999).

156. Labrousse, A., Chauvet, S., Couillault, C., Léopold Kurz, C. & Ewbank, J. J. Caenorhabditis elegans is a model host for Salmonella typhimurium. *Curr. Biol.* **10**, 1543–1545 (2000).

157. Sifri, C. D., Begun, J., Ausubel, F. M. & Calderwood, S. B. Caenorhabditis elegans as a Model Host for Staphylococcus aureus Pathogenesis. *Infect. Immun.* **71**, 2208–2217 (2003).

158. Macneil, L. T., Watson, E., Arda, H. E., Zhu, L. J. & Walhout, A. J. M. Diet-Induced Developmental Acceleration Independent of TOR and Insulin in C. elegans. *Cell* **153**, 240–252 (2013).

159. Kauffman, A. L., Ashraf, J. M., Orces-Zimmerman, M. R., Landis, J. N. & Murphy, C. T. Insulin signaling and dietary restriction differentially influence the decline of learning and memory with age. *PLoS Biol.* **8**, e1000372 (2010).

160. Avery, L. & Shtonda, B. B. Food transport in the C. elegans pharynx. *J. Exp. Biol.* **206**, 2441–2457 (2003).

161. Timmons, L. & Fire, A. Specific interference by ingested dsRNA. *Nature* **395**, 854 (1998).

162. Kamath, R. S., Martinez-Campos, M., Zipperlen, P., Fraser, A. G. & Ahringer, J. Effectiveness of specific RNA-mediated interference through ingested double-stranded RNA in Caenorhabditis elegans. *Genome Biol.* **2**, research0002.1 (2000).

163. Kamath, R. S. *et al.* Systematic functional analysis of the Caenorhabditis elegans genome using RNAi. *Nature* **421**, 231–237 (2003).

164. Xiao, R. *et al.* RNAi Interrogation of Dietary Modulation of Development, Metabolism, Behavior, and Aging in C. elegans. *Cell Rep.* **11**, 1123–33 (2015).

165. Kenyon, C. J. The genetics of ageing. *Nature* **464**, 504–512 (2010).

166. Son, H. G., Altintas, O., Eun, J. E. K., Kwon, S. & Lee, S.-J. V. Age-dependent changes and biomarkers of aging in Caenorhabditis elegans. *Aging Cell* **18**, e12853 (2019).

167. Epstein, J., Himmelhoch, S. & Gershon, D. Studies on ageing in nematodes III. Electronmicroscopical studies on age-associated cellular damage. *Mech. Ageing Dev.* **1**, 245–255 (1972).

168. Croll, N. A., Smith, J. M. & Zuckerman, B. M. The aging process of the nematode Caenorhabditis elegans in bacterial and axenic culture. *Exp. Aging Res.* **3**, 175–189 (1977).

169. Walker, G. A. *et al.* Heat shock protein accumulation is upregulated in a long-lived mutant of Caenorhabditis elegans. *J. Gerontol. - Ser. Biol. Sci. Med. Sci.* **56**, B281–B287 (2001).

170. Labbadia, J. & Morimoto, R. I. Repression of the Heat Shock Response Is a Programmed Event at the Onset of Reproduction. *Mol. Cell* **59**, 639–650 (2015).

171. Darr, D. & Fridovich, I. Adaptation to oxidative stress in young, but not in mature or old, Caenorhabditis elegans. *Free Radic. Biol. Med.* **18**, 195–201 (1995).

172. Klass, M., Nguyen, P. N. & Dechavigny, A. Age-correlated changes in the DNA template in the nematode Caenorhabditis elegans. *Mech. Ageing Dev.* **22**, 253–263 (1983).

173. Meyer, J. N. *et al.* Decline of nucleotide excision repair capacity in aging Caenorhabditis elegans. *Genome Biol.* **8**, 1–17 (2007).

174. Maures, T. J. *et al.* Males shorten the life span of C. elegans hermaphrodites via secreted compounds. *Science* **343**, 541–544 (2014).

175. Youngman, M. J., Rogers, Z. N. & Kim, D. H. A decline in p38 MAPK signaling underlies immunosenescence in Caenorhabditis elegans. *PLoS Genet.* **7**, e1002082 (2011).

176. Hosono, R., Sato, Y., Aizawa, S.-I. & Mitsui, Y. Age-dependent changes in mobility and separation of the nematode Caenorhabditis elegans. *Exp. Gerontol.* **15**, 285–289 (1980).

177. Bolanowski, M. A., Russell, R. L. & Jacobson, L. A. Quantitative measures of aging in the nematode Caenorhabditis elegans. I. Population and longitudinal studies of two behavioral parameters. *Mech. Ageing Dev.* **15**, 279–295 (1981).

178. Hsu, A.-L. L., Feng, Z., Hsieh, M.-Y. & Xu, X. Z. S. Identification by machine vision of the rate of motor activity decline as a lifespan predictor in C. elegans. *Neurobiol. Aging* **30**, 1498–503 (2009).

179. Restif, C. *et al.* CeleST: Computer Vision Software for Quantitative Analysis of C. elegans Swim Behavior Reveals Novel Features of Locomotion. *PLoS Comput. Biol.* **10**, e1003702 (2014).

180. Hahm, J.-H. *et al.* C. elegans maximum velocity correlates with healthspan and is maintained in worms with an insulin receptor mutation. *Nat. Commun.* **6**, 8919 (2015).

181. Beck, C. D. O. & Rankin, C. H. Effects of aging on habituation in the nematode Caenorhabditis elegans. *Behav. Processes* **28**, 145–163 (1993).

182. Murakami, H., Bessinger, K., Hellmann, J. & Murakami, S. Aging-dependent and -independent modulation of associative learning behavior by insulin/insulin-like growth factor-1 signal in Caenorhabditis elegans. *J Neurosci* **25**, 10894–10904 (2005).

183. Hosono, R. Age dependent changes in the behavior of Caenorhabditis elegans on attraction to Escherichia coli. *Exp. Gerontol.* **13**, 31–36 (1978).

184. Russell, J. C. *et al.* Electrophysiological Measures of Aging Pharynx Function in C. elegans Reveal Enhanced Organ Functionality in Older, Long-lived Mutants. *J. Gerontol. Ser. A* **74**, 1173–1179 (2019).

185. Thomas, J. H. Genetic analysis of defecation in Caenorhabditis elegans. *Genetics* **124**, 855–872 (1990).

186. Felkai, S. *et al.* CLK-1 controls respiration, behavior and aging in the nematode Caenorhabditis elegans. *EMBO J.* **18**, 1783–92 (1999).

187. Glenn, C. F. *et al.* Behavioral Deficits During Early Stages of Aging in Caenorhabditis elegans Result From Locomotory Deficits Possibly Linked to Muscle Frailty. *J. Gerontol. A. Biol. Sci. Med. Sci.* **59**, 1251–1260 (2004).

188. Pan, C.-L., Peng, C.-Y., Chen, C.-H. & McIntire, S. Genetic analysis of age-dependent defects of the Caenorhabditis elegans touch receptor neurons. *Proc. Natl. Acad. Sci.* **108**, 9274–9279 (2011).

189. Tank, E. M. H., Rodgers, K. E. & Kenyon, C. Spontaneous Age-Related Neurite Branching in Caenorhabditis elegans. *J. Neurosci.* **31**, 9279–9288 (2011).

190. Toth, M. L. *et al.* Neurite Sprouting and Synapse Deterioration in the Aging Caenorhabditis elegans Nervous System. *J. Neurosci.* **32**, 8778–8790 (2012).

191. Morsci, N. S., Hall, D. H., Driscoll, M. & Sheng, Z.-H. Age-Related Phasic Patterns of Mitochondrial Maintenance in Adult Caenorhabditis elegans Neurons. *J. Neurosci.* **36**, 1373–1385 (2016).

192. Liu, J. *et al.* Functional aging in the nervous system contributes to age-dependent motor activity decline in C. elegans. *Cell Metab.* **18**, 392–402 (2013).

193. Szewczyk, N. J. *et al.* Delayed development and lifespan extension as features of metabolic lifestyle alteration in C. elegans under dietary restriction. *J. Exp. Biol.* **209**, 4129–4139 (2006).

194. Muschiol, D., Schroeder, F. & Traunspurger, W. Life cycle and population growth rate of Caenorhabditis elegans studied by a new method. *BMC Ecol.* **9**, 1–13 (2009).

195. Mendenhall, A. R. *et al.* Genetic dissection of late-life fertility in Caenorhabditis elegans. *J. Gerontol. - Ser. Biol. Sci. Med. Sci.* **66**, 842–854 (2011).

196. Andux, S. & Ellis, R. E. Apoptosis maintains oocyte quality in aging Caenorhabditis elegans females. *PLoS Genet.* **4**, e1000295 (2008).

197. Golden, T. R. *et al.* Dramatic age-related changes in nuclear and genome copy number in the nematode Caenorhabditis elegans. *Aging Cell* **6**, 179–188 (2007).

198. Luo, S., Kleemann, G. A., Ashraf, J. M., Shaw, W. M. & Murphy, C. T. TGF-β and Insulin Signaling Regulate Reproductive Aging via Oocyte and Germline Quality Maintenance. *Cell* **143**, 299–312 (2010).

199. Hughes, S. E., Huang, C. & Kornfeld, K. Identification of mutations that delay somatic or reproductive aging of Caenorhabditis elegans. *Genetics* **189**, 341–356 (2011).

200. Riesen, M. *et al.* MDL-1, a growth- and tumor-suppressor, slows aging and prevents germline hyperplasia and hypertrophy in C. elegans. *Aging* **6**, 98–117 (2014).

201. Wang, H. *et al.* A parthenogenetic quasi-program causes teratoma-like tumors during aging in wild-type C. elegans. *Npj Aging Mech. Dis.* **4**, 6 (2018).

202. Kocsisova, Z., Kornfeld, K. & Schedl, T. Rapid population-wide declines in stem cell number and activity during reproductive aging in C. elegans. *Development* **146**, dev173195 (2019).

203. Schisa, J. A., Pitt, J. N. & Priess, J. R. Analysis of RNA associated with P granules in germ cells of C. elegans adults. *Development* **128**, 1287–1298 (2001).

204. Jaramillo-Lambert, A., Ellefson, M., Villeneuve, A. M. & Engebrecht, J. A. Differential timing of S phases, X chromosome replication, and meiotic prophase in the C. elegans germ line. *Dev. Biol.* **308**, 206–221 (2007).

205. Crittenden, S. L., Leonhard, K. A., Byrd, D. T. & Kimble, J. Cellular analyses of the mitotic region in the Caenorhabditis elegans adult germ line. *Mol. Biol. Cell* **17**, 3051–3061 (2006).

206. Killian, D. J. & Hubbard, E. J. A. Caenorhabditis elegans germline patterning requires coordinated development of the somatic gonadal sheath and the germ line. *Dev. Biol.* **279**, 322–335 (2005).

207. Shi, C. & Murphy, C. T. Mating induces shrinking and death in Caenorhabditis mothers. *Science* **343**, 536–540 (2014).

208. Qin, Z. & Hubbard, E. J. A. Non-autonomous DAF-16/FOXO activity antagonizes age-related loss of C. elegans germline stem/progenitor cells. *Nat. Commun.* **6**, 7107 (2015).

209. Roy, D. *et al.* Cell cycle features of C. elegans germline stem/progenitor cells vary temporally and spatially. *Dev. Biol.* **409**, 261–271 (2016).

210. Narbonne, P., Maddox, P. S. & Labbé, J. C. DAF-18/PTEN locally antagonizes insulin signalling to couple germline stem cell proliferation to oocyte needs in C. elegans. *Development* **142**, 4230–4241 (2015).

211. Shamir, L., Wolkow, C. A. & Goldberg, I. G. Quantitative measurement of aging using image texture entropy. *Bioinformatics* **25**, 3060–3063 (2009).

212. Zhao, Y. *et al.* Two forms of death in ageing Caenorhabditis elegans. *Nat. Commun.* **8**, 15458 (2017).

213. McGee, M. D. *et al.* Loss of intestinal nuclei and intestinal integrity in aging C. elegans. *Aging Cell* **10**, 699–710 (2011).

214. Yasuda, K. *et al.* Age-related changes of mitochondrial structure and function in Caenorhabditis elegans. *Mech. Ageing Dev.* **127**, 763–770 (2006).

215. Gruber, J. *et al.* Mitochondrial Changes in Ageing Caenorhabditis elegans – What Do We Learn from Superoxide Dismutase Knockouts? *PLoS ONE* **6**, e19444 (2011).

216. Regmi, S. G., Rolland, S. G. & Conradt, B. Age-dependent changes in mitochondrial morphology and volume are not predictors of lifespan. *Aging* **6**, 118–130 (2014).

217. Haithcock, E. *et al.* Age-related changes of nuclear architecture in Caenorhabditis elegans. *Proc. Natl. Acad. Sci.* **102**, 16690–16695 (2005).

218. Rousakis, A. *et al.* Diverse Functions of mRNA Metabolism Factors in Stress Defense and Aging of Caenorhabditis elegans. *PLoS ONE* **9**, e103365 (2014).

219. Tserevelakis, G. J. *et al.* Label-free imaging of lipid depositions in C. elegans using third-harmonic generation microscopy. *PLoS ONE* **9**, e84431 (2014).

220. Mari, M. *et al.* Imaging ectopic fat deposition in Caenorhabditis elegans muscles using nonlinear microscopy. *Microsc. Res. Tech.* **78**, 523–528 (2015).

221. Palikaras, K. *et al.* Ectopic fat deposition contributes to age-associated pathology in Caenorhabditis elegans. *J. Lipid Res.* **58**, 72–80 (2017).

222. Chang, J. T., Kumsta, C., Hellman, A. B., Adams, L. M. & Hansen, M. Spatiotemporal regulation of autophagy during Caenorhabditis elegans aging. *eLife* **6**, 1–23 (2017).

223. Pu, M. *et al.* Trimethylation of Lys36 on H3 restricts gene expression change during aging and impacts life span. *Genes Dev.* **29**, 718–731 (2015).

224. Pu, M., Wang, M., Wang, W., Velayudhan, S. S. & Lee, S. S. Unique patterns of trimethylation of histone H3 lysine 4 are prone to changes during aging in Caenorhabditis elegans somatic cells. *PLoS Genet.* **14**, e1007466 (2018).

225. Fabian, T. J. & Johnson, T. E. Identification genes that are differentially expressed during aging in Caenorhabditis elegans. *J. Gerontol. A. Biol. Sci. Med. Sci.* **50**, B245-53 (1995).

226. Lund, J. *et al.* Transcriptional Profile of Aging in C. elegans are part of an insulin-related signaling pathway are in. *Curr. Biol.* **12**, 1566–1573 (2002).

227. Kato, M., Chen, X., Inukai, S., Zhao, H. & Slack, F. J. Age-associated changes in expression of small, noncoding RNAs, including microRNAs, in C. elegans. *RNA* **17**, 1804–1820 (2011).

228. Rangaraju, S. *et al.* Suppression of transcriptional drift extends C. Elegans lifespan by postponing the onset of mortality. *eLife* **4**, e08833 (2015).

229. Hastings, J. *et al.* Multi-Omics and Genome-Scale Modeling Reveal a Metabolic Shift During C. elegans Aging. *Front. Mol. Biosci.* **6**, 1–18 (2019).

230. Golden, T. R. & Melov, S. Gene expression changes associated with aging in C. elegans. *WormBook* 1–12 (2007) doi:10.1895/wormbook.1.127.2.

231. Heintz, C. *et al.* Splicing factor 1 modulates dietary restriction and TORC1 pathway longevity in C. elegans. *Nature* **541**, 102–106 (2017).

232. Ibáñez-Ventoso, C. *et al.* Modulated microRNA expression during adult lifespan in Caenorhabditis elegans. *Aging Cell* **5**, 235–246 (2006).

233. Pincus, Z., Smith-Vikos, T. & Slack, F. J. MicroRNA predictors of longevity in Caenorhabditis elegans. *PLoS Genet.* **7**, e1002306 (2011).

234. Cortés-López, M. *et al.* Global accumulation of circRNAs during aging in Caenorhabditis elegans. *BMC Genomics* **19**, 1–12 (2018).

235. Adachi, H., Fujiwara, Y. & Ishii, N. Effects of Oxygen on Protein Carbonyl and Aging in Caenorhabditis elegans Mutants With Long (age-1) and Short (mev-1) Life Spans. *J. Gerontol. Biol. Sci.* **53**, 24–244 (1998).

236. Goudeau, J. & Aguilaniu, H. Carbonylated proteins are eliminated during reproduction in C. elegans. *Aging Cell* **9**, 991–1003 (2010).

237. Walther, D. M. *et al.* Widespread proteome remodeling and aggregation in aging C. elegans. *Cell* **161**, 919–932 (2015).

238. Narayan, V. *et al.* Deep Proteome Analysis Identifies Age-Related Processes in C. elegans. *Cell Syst.* **3**, 144–159 (2016).

239. Ben-Zvi, A., Miller, E. A. & Morimoto, R. I. Collapse of proteostasis represents an early molecular event in Caenorhabditis elegans aging. *Proc. Natl. Acad. Sci.* **106**, 14914–14919 (2009).

240. David, D. C. *et al.* Widespread protein aggregation as an inherent part of aging in C. elegans. *PLoS Biol.* **8**, 47–48 (2010).

241. Taylor, R. C. & Dillin, A. Aging as an event of proteostasis collapse. *Cold Spring Harb. Perspect. Biol.* **3**, a004440 (2011).

242. Shemesh, N., Shai, N. & Ben-Zvi, A. Germline stem cell arrest inhibits the collapse of somatic proteostasis early in Caenorhabditis elegans adulthood. *Aging Cell* **12**, 814–822 (2013).

243. Taylor, R. C. & Dillin, A. XBP-1 Is a Cell-Nonautonomous Regulator of Stress Resistance and Longevity. *Cell* **153**, 1435–1447 (2013).

244. Vanfleteren, J. R., Braeckman, B. P., Roelens, I. & De Vreese, A. Age-specific Modulation of Light Production Potential, and Alkaline Phosphatase and Protein Tyrosine Kinase Activities in Various Age Mutants of Caenorhabditis elegans. *J. Gerontol. A. Biol. Sci. Med. Sci.* **53**, B380–B390 (1998).

245. Yuan, Y. *et al.* Reciprocal changes in phosphoenolpyruvate carboxykinase and pyruvate kinase with age are a determinant of aging in Caenorhabditis elegans. *J. Biol. Chem.* **291**, 1307–1319 (2016).

246. Davis, B. 0, Anderson, G. L. & Dusenbery, D. B. Total Luminescence Spectroscopy of Fluorescence Changes during Aging in Caenorhabditis elegans? *Biochemistry* **21**, 4089–4095 (1982).

247. Hosokawa, H. *et al.* Rapid accumulation of fluorescent material with aging in an oxygen-sensitive mutant mev-1 of Caenorhabditis elegans. *Mech. Ageing Dev.* **74**, 161–170 (1994).

248. Coburn, C. *et al.* Anthranilate Fluorescence Marks a Calcium-Propagated Necrotic Wave That Promotes Organismal Death in C. elegans. *PLOS Biol.* **11**, e1001613 (2013).

249. Pincus, Z., Mazer, T. C. & Slack, F. J. Autofluorescence as a measure of senescence in C. elegans: look to red, not blue or green. *Aging* **8**, 889–898 (2016).

250. Van Voorhies, W. A. & Ward, S. Genetic and environmental conditions that increase longevity in Caenorhabditis elegans decrease metabolic rate. *Proc. Natl. Acad. Sci. U. S. A.* **96**, 11399–403 (1999).

251. Braeckman, B. P. *et al.* No reduction of energy metabolism in Clk mutants. *Mech. Ageing Dev.* **123**, 1447–1456 (2002).

252. Braeckman, B. P., Houthoofd, K., De Vreese, A. & Vanfleteren, J. R. Assaying metabolic activity in ageing Caenorhabditis elegans. *Mech. Ageing Dev.* **123**, 105–119 (2002).

253. Braeckman, B. P., Houthoofd, K. & Vanfleteren, J. R. Assessing metabolic activity in aging Caenorhabditis elegans: concepts and controversies. *Aging Cell* **1**, 82–88 (2002).

254. Brys, K., Castelein, N., Matthijssens, F., Vanfleteren, J. R. & Braeckman, B. P. Disruption of insulin signalling preserves bioenergetic competence of mitochondria in ageing Caenorhabditis elegans. *BMC Biol.* **8**, 1–15 (2010).

255. Pontoizeau, C. *et al.* Metabolomics analysis uncovers that dietary restriction buffers metabolic changes associated with aging in Caenorhabditis elegans. *J Proteome Res* **13**, 2910–2919 (2014).

256. Copes, N. *et al.* Metabolome and proteome changes with aging in Caenorhabditis elegans. *Exp. Gerontol.* **72**, 67–84 (2015).

257. Davies, S. K., Bundy, J. G. & Leroi, A. M. Metabolic youth in middle age: Predicting aging in Caenorhabditis elegans using metabolomics. *J. Proteome Res.* **14**, 4603–4609 (2015).

258. Gao, A. W. *et al.* A sensitive mass spectrometry platform identifies metabolic changes of life history traits in C. elegans. *Sci. Rep.* **7**, 2408 (2017).

259. Wan, Q.-L. *et al.* Metabolomic signature associated with reproduction-regulated aging in Caenorhabditis elegans. *Aging* **9**, 47 (2017).

260. Yanase, S., Suda, H., Yasuda, K. & Ishii, N. Impaired p53/CEP-1 is associated with lifespan extension through an age-related imbalance in the energy metabolism of C. elegans. *Genes Cells* **22**, 1004–1010 (2017).

261. Klang, I. M. *et al.* Iron promotes protein insolubility and aging in C. elegans. *Aging* **6**, 975–991 (2014).

262. Chatterjee, I. *et al.* Dramatic fertility decline in aging C. elegans males is associated with mating execution deficits rather than diminished sperm quality. *Exp. Gerontol.* **48**, 1156–1166 (2013).

263. Shi, C., Runnels, A. M. & Murphy, C. T. Mating and male pheromone kill Caenorhabditis males through distinct mechanisms. *eLife* **6**, e23493 (2017).

264. Pickett, C. L., Dietrich, N., Chen, J., Xiong, C. & Kornfeld, K. Mated progeny production is a biomarker of aging in Caenorhabditis elegans. *G3 Genes Genomes Genet.* **3**, 2219–2232 (2013).

265. Wolkow, C. A. Identifying factors that promote functional aging in Caenorhabditis elegans. *Exp. Gerontol.* **41**, 1001–1006 (2006).

266. Johnston, J., Iser, W. B., Chow, D. K., Goldberg, I. G. & Wolkow, C. A. Quantitative image analysis reveals distinct structural transitions during aging in Caenorhabditis elegans tissues. *PLoS One* **3**, e2821 (2008).

267. Hess, M., Gomariz, A., Goksel, O. & Ewald, C. Y. In-Vivo Quantitative Image Analysis of Age-Related Morphological Changes of C. elegans Neurons Reveals a Correlation between Neurite Bending and Novel Neurite Outgrowths. *eNeuro* **6**, (2019).

268. Dambroise, E. *et al.* Two phases of aging separated by the Smurf transition as a public path to death. *Sci. Rep.* **6**, 23523 (2016).

269. Tiku, V. *et al.* Small nucleoli are a cellular hallmark of longevity. *Nat. Commun.* **8**, 16083 (2017).

270. Lucanic, M. *et al.* Impact of genetic background and experimental reproducibility on identifying chemical compounds with robust longevity effects. *Nat. Commun.* **8**, 14256 (2017).

271. Portal-Celhay, C., Bradley, E. R. & Blaser, M. J. Control of intestinal bacterial proliferation in regulation of lifespan in Caenorhabditis elegans. *BMC Microbiol.* **12**, 1–17 (2012).

272. Podshivalova, K., Kerr, R. A. & Kenyon, C. How a Mutation that Slows Aging Can Also Disproportionately Extend End-of-Life Decrepitude. *Cell Rep.* **19**, 441–450 (2017).

273. Kurz, C. L. & Ewbank, J. J. Caenorhabditis elegans: an emerging genetic model for the study of innate immunity. *Nat. Rev. Genet.* **4**, 380–390 (2003).

274. Kim, D. H. Bacteria and the Aging and Longevity of Caenorhabditis elegans. *Annu. Rev. Genet.* **47**, 233–246 (2013).

275. Laws, T. R., Harding, S. V., Smith, M. P., Atkins, T. P. & Titball, R. W. Age influences resistance of Caenorhabditis elegans to killing by pathogenic bacteria. *FEMS Microbiol. Lett.* **234**, 281–287 (2006).

276. Burns, D. M. F., Harper, J. M. & Lynne, A. M. Age Does Not Affect the Induction of Mortality by the Foodborne Pathogen Salmonella enterica in Caenorhabditis elegans. *Adv. Microbiol.* **7**, 689–695 (2017).

277. Timbers, T. A., Giles, A. C., Ardiel, E. L., Kerr, R. A. & Rankin, C. H. Intensity discrimination deficits cause habituation changes in middle-aged Caenorhabditis elegans. *Neurobiol. Aging* **34**, 621–631 (2013).

278. Avery, L. & Thomas, J. H. Feeding and defecation. *C Elegans II* **33**, 679–716 (1997).

279. Li, G. *et al.* Genetic and pharmacological interventions in the aging motor nervous system slow motor aging and extend life span in *C. elegans*. *Sci. Adv.* **5**, eaau5041 (2019).

280. Byerly, L., Cassada, R. C. & Russell, R. L. The life cycle of the nematode Caenorhabditis elegans: I. Wild-type growth and reproduction. *Dev. Biol.* **51**, 23–33 (1976).

281. McCarter, J., Bartlett, B., Dang, T. & Schedl, T. On the control of oocyte meiotic maturation and ovulation in Caenorhabditis elegans. *Dev. Biol.* **205**, 111–128 (1999).

282. Ward, S. & Carrel, J. S. Fertilization and sperm competition in the nematode Caenorhabditis elegans. *Dev. Biol.* **73**, 304–321 (1979).

283. Hodgkin, J. & Barnes, T. M. More is not better: brood size and population growth in a self-fertilizing nematode. *Proc. R. Soc. Lond. B Biol. Sci.* **246**, 19–24 (1991).

284. Hibshman, J. D., Hung, A. & Baugh, L. R. Maternal Diet and Insulin-Like Signaling Control Intergenerational Plasticity of Progeny Size and Starvation Resistance. *PLOS Genet.* **12**, e1006396 (2016).

285. Hughes, S. E. Characterization of Reproductive Aging in Caenorhabditis elegans. (Washington University in St. Louis, 2005).

286. Pazdernik, N. & Schedl, T. Introduction to Germ Cell Development in Caenorhabditis elegans. in *Advances in experimental medicine and biology* vol. 757 1–16 (2013).

287. Gumienny, T. L., Lambie, E., Hartwieg, E., Horvitz, H. R. & Hengartner, M. O. Genetic control of programmed cell death in the Caenorhabditis elegans hermaphrodite germline. *Development* **126**, 1011–1022 (1999).

288. Wolke, U., Jezuit, E. A. & Priess, J. R. Actin-dependent cytoplasmic streaming in C. elegans oogenesis. *Development* **134**, 2227–2236 (2007).

289. Agarwal, I. *et al.* HOP-1 presenilin deficiency causes a late-onset notch signaling phenotype that affects adult germline function in caenorhabditis elegans. *Genetics* **208**, 745–762 (2018).

290. Hansen, D., Hubbard, E. J. A. & Schedl, T. Multi-pathway control of the proliferation versus meiotic development decision in the Caenorhabditis elegans germline. *Dev. Biol.* **268**, 342–357 (2004).

291. Fox, P. M. *et al.* Cyclin e and CDK-2 regulate proliferative cell fate and cell cycle progression in the C. elegans germline. *Development* **138**, 2223–2234 (2011).

292. Korta, D. Z., Tuck, S. & Hubbard, E. J. A. S6K links cell fate, cell cycle and nutrient response in C. elegans germline stem/progenitor cells. *Development* **139**, 859–870 (2012).

293. Fox, P. M. & Schedl, T. Analysis of germline stem cell differentiation following loss of GLP-1 notch activity in Caenorhabditis elegans. *Genetics* **201**, 167–184 (2015).

294. Seidel, H. S. & Kimble, J. Cell-cycle quiescence maintains Caenorhabditis elegans germline stem cells independent of GLP-1/Notch. *eLife* **4**, e10832 (2015).

295. Kocsisova, Z., Kornfeld, K. & Schedl, T. Cell cycle accumulation of the proliferating cell nuclear antigen PCN-1 transitions from continuous in the adult germline to intermittent in the early embryo of C. elegans. *BMC Dev. Biol.* **18**, 1–9 (2018).

296. Kocsisova, Z., Mohammad, A., Kornfeld, K. & Schedl, T. Cell cycle analysis in the C. elegans germline with the thymidine analog edu. *J. Vis. Exp.* **140**, e58339 (2018).

297. Byrd, D. T., Knobel, K., Affeldt, K., Crittenden, S. L. & Kimble, J. A DTC niche plexus surrounds the germline stem cell pool in Caenorhabditis elegans. *PLoS ONE* **9**, e88372 (2014).

298. Kershner, A. M., Shin, H., Hansen, T. J. & Kimble, J. Discovery of two GLP-1/Notch target genes that account for the role of GLP-1/Notch signaling in stem cell maintenance. *Proc. Natl. Acad. Sci. U. S. A.* **111**, 3739–3744 (2014).

299. Lee, C. H. *et al.* C. elegans GLP-1/Notch activates transcription in a probability gradient across the germline stem cell pool. *eLife* **5**, 269–282 (2016).

300. Shin, H. *et al.* SYGL-1 and LST-1 link niche signaling to PUF RNA repression for stem cell maintenance in Caenorhabditis elegans. *PLoS Genet.* **13**, e1007121 (2017).

301. Leiser, S. F., Begun, A. & Kaeberlein, M. HIF-1 modulates longevity and healthspan in a temperature-dependent manner. *Aging Cell* **10**, 318–326 (2011).

302. Chen, D., Thomas, E. L. & Kapahi, P. HIF-1 modulates dietary restriction-mediated lifespan extension via IRE-1 in Caenorhabditis elegans. *PLoS Genet* **5**, e1000486 (2009).

303. Zhang, M. *et al.* Role of CBP and SATB-1 in aging, dietary restriction, and insulin-like signaling. *PLoS Biol* **7**, e1000245 (2009).

304. Simpson, V. J., Johnson, T. E. & Hammen, R. F. Caenorhabditis elegans DNA does not contain 5-methylcytosine at any time during development or aging. *Nucleic Acids Res.* **14**, 6711–6719 (1986).

305. Melov, S., Lithgow, G. J., Fischer, D. R., Tedesco, P. M. & Johnson, T. E. Increased frequency of deletions in the mitochondrial genome with age of *Caenorhabditis elegans*. *Nucleic Acids Res.* **23**, 1419–1425 (1995).

306. Fabian, T. J. & Johnson, T. E. Total RNA, rRNA and poly(A)+ RNA abundances during aging in Caenorhabditis elegans. *Mech. Ageing Dev.* **83**, 155–170 (1995).

307. Cherkasova, V., Ayyadevara, S., Egilmez, N. & Reis, R. S. Diverse Caenorhabditis elegans genes that are upregulated in dauer larvae also show elevated transcript levels in long-lived, aged, or starved adults. *J. Mol. Biol.* **300**, 433–448 (2000).

308. Hill, A. A., Hunter, C. P., Tsung, B. T., Tucker-Kellogg, G. & Brown, E. L. Genomic Analysis of Gene Expression in C. elegans. *Science* **290**, 809–812 (2000).

309. Golden, T. R. & Melov, S. Microarray analysis of gene expression with age in individual nematodes. *Aging Cell* **3**, 111–124 (2004).

310. Roux, A. E. *et al.* The complete cell atlas of an aging multicellular organism. *bioRxiv* **2022–06**, (2022).

311. Reis-Rodrigues, P. *et al.* Proteomic analysis of age-dependent changes in protein solubility identifies genes that modulate lifespan. *Aging Cell* **11**, 120–127 (2012).

312. Porta, E. A. Pigments in Aging: An Overview. *Ann. N. Y. Acad. Sci.* **959**, 57–65 (2006).

313. Jung, T., Bader, N. & Grune, T. Lipofuscin: Formation, distribution, and metabolic consequences. *Ann. N. Y. Acad. Sci.* **1119**, 97–111 (2007).

314. Hoffman, J. M., Lyu, Y., Pletcher, S. D. & Promislow, D. E. L. Proteomics and metabolomics in ageing research: from biomarkers to systems biology. *Essays Biochem.* **61**, 379–388 (2017).

315. Meier, R., Ruttkies, C., Treutler, H. & Neumann, S. Bioinformatics can boost metabolomics research. *J. Biotechnol.* **261**, 137–141 (2017).

316. Fabian, T. J. & Johnson, T. E. Production of Age-synchronous Mass Cultures of Caenorhabditis elegans. *J. Gerontol.* **49**, B145–B156 (1994).

317. Golden, T. R., Hubbard, A., Dando, C., Herren, M. A. & Melov, S. Age-related behaviors have distinct transcriptional profiles in *Caenorhabditis elegans*. *Aging Cell* **7**, 850–865 (2008).

318. Howlett, S. E. Assessment of Frailty in Animal Models. *Interdiscip. Top. Gerontol. Geriatr.* **41**, 15–25 (2015).

319. López-Otín, C., Blasco, M. A., Partridge, L., Serrano, M. & Kroemer, G. The hallmarks of aging. *Cell* **153**, 1194–1217 (2013).

320. Cook, D. E. *et al.* The genetic basis of natural variation in Caenorhabditis elegans telomere length. *Genetics* **204**, 371–383 (2016).

321. Campisi, J. *et al.* From discoveries in ageing research to therapeutics for healthy ageing. *Nature* **571**, 183–192 (2019).

322. Harman, D. Aging: a theory based on free radical and radiation chemistry. *J. Gerontol.* **11**, 298–300 (1956).

323. Harman, D. Free radical theory of aging. *Mutat. Res.* **275**, 257–266 (1992).

324. Ishii, N., Tsuda, M., Yasuda, K., Yanase, S. & Suzuki, K. A mutation in succinate dehydrogenase cytochrome. *Nat. Lett.* **394**, 694–697 (1998).

325. Kayser, E. B., Morgan, P. G., Hoppel, C. L. & Sedensky, M. M. Mitochondrial Expression and Function of GAS-1 in Caenorhabditis elegans. *J. Biol. Chem.* **276**, 20551–20558 (2001).

326. Wang, Y. & Hekimi, S. Mitochondrial dysfunction and longevity in animals: untangling the knot. *Science* **350**, 1204–1207 (2015).

327. Yang, W. & Hekimi, S. A mitochondrial superoxide signal triggers increased longevity in Caenorhabditis elegans. *PLoS Biol.* **8**, e1000556 (2010).

328. Gems, D. & McElwee, J. J. Broad spectrum detoxification: The major longevity assurance process regulated by insulin/IGF-1 signaling? *Mech. Ageing Dev.* **126**, 381–387 (2005).

329. Scharf, A., Piechulek, A. & Von Mikecz, A. Effect of nanoparticles on the biochemical and behavioral aging phenotype of the nematode Caenorhabditis elegans. *ACS Nano* **7**, 10695–10703 (2013).

330. Labbadia, J. *et al.* Mitochondrial Stress Restores the Heat Shock Response and Prevents Proteostasis Collapse during Aging. *Cell Rep.* **21**, 1481–1494 (2017).

331. Blagosklonny, M. V. Aging and Immortality: Quasi-Programmed Senescence and Its Pharmacologic Inhibition. *Cell Cycle* **5**, 2087–2102 (2006).

332. Gems, D. & de la Guardia, Y. Alternative Perspectives on Aging in *Caenorhabditis elegans*: Reactive Oxygen Species or Hyperfunction? *Antioxid. Redox Signal.* **19**, 321–329 (2013).

333. Darwin, E. *The Temple of Nature; Or, the Origin of Society: a Poem, with philosophical Notes. The Poetical Works: Containing The Botanic Garden, in Two Parts, and the Temple of Nature* (M. & J. Conrad & Co., 1804).

334. Darwin, C. *Notebook B: Transmutation of Species*. vol. CUL-DAR121 (1837).

335. Robertson, O. H. Prolongation of the life span of konkanee salmon (Oncorhynchus nerka kennerlyi) by castration before beginning of gonad development. *Proc. Natl. Acad. Sci.* **47**, 609–621 (1961).

336. Law, R. Optimal Life Histories Under Age-Specific Predation. *Am. Nat.* **114**, 399–417 (1979).

337. Barrière, A. & Félix, M. A. High local genetic diversity and low outcrossing rate in Caenorhabditis elegans natural populations. *Curr. Biol.* **15**, 1176–1184 (2005).

338. Van Voorhies, W. A., Fuchs, J. & Thomas, S. The longevity of Caenorhabditis elegans in soil. *Biol. Lett.* **1**, 247–249 (2005).

339. Wilhelm, T. *et al.* Neuronal inhibition of the autophagy nucleation complex extends life span in post-reproductive C. elegans. *Genes Dev.* **31**, 1561–1572 (2017).

340. Anderson, J. L., Reynolds, R. M., Morran, L. T., Tolman-Thompson, J. & Phillips, P. C. Experimental evolution reveals antagonistic pleiotropy in reproductive timing but not life

span in caenorhabditis elegans. *J. Gerontol. - Ser. Biol. Sci. Med. Sci.* **66 A**, 1300–1308 (2011).

341. Jenkins, N. L., Mccoll, G. & Lithgow, G. J. Fitness cost of extended lifespan in Caenorhabditis elegans. *Proc. R. Soc. Lond. B Biol. Sci.* **271**, 2523–2526 (2004).

342. Van Voorhies, W. A., Curtsinger, J. W. & Rose, M. R. Do longevity mutants always show trade-offs? *Exp. Gerontol.* **41**, 1055–1058 (2006).

343. Blagosklonny, M. V. Paradoxes of Aging. *Cell Cycle* **6**, 2997–3003 (2007).

344. Kirkwood, T. B. L. Evolution of ageing. *Nature* **270**, 301–304 (1977).

345. Watson, J. D. & Crick, F. H. C. The Structure of DNA. *Cold Spring Harb. Symp. Quant. Biol.* **18**, 123–131 (1953).

346. Scharf, A. *et al.* A laboratory and simulation platform to integrate individual life history traits and population dynamics. *Nat. Comput. Sci.* **2**, 90–101 (2022).

347. Taylor, P. H., Cinquin, A. & Cinquin, O. Quantification of in vivo progenitor mutation accrual with ultra-low error rate and minimal input DNA using SIP-HAVA-seq. *Genome Res.* 1600–1611 (2016) doi:10.1101/gr.200501.115.

348. Rogina, B., Reenan, R. A., Nilsen, S. P. & Helfand, S. L. Extended life-span conferred by cotransporter gene mutations in Drosophila. *Science* **290**, 2137–2140 (2000).

349. Cournil, A. & Kirkwood, T. If you would live long, choose your parents well. *Trends Genet.* **17**, 233–235 (2001).

350. Luckinbill, L. S. & Clare, M. J. Selection for life span in Drosophila melanogaster. *Heredity* **55**, 9–18 (1985).

351. Rose, M. R. Laboratory Evolution of Postponed Senescence in Drosophila melanogaster. *Evolution* **38**, 1004–1010 (1984).

352. Kirkwood, T. B. L. & Melov, S. On the programmed/non-programmed nature of ageing within the life history. *Curr. Biol.* **21**, R701–R707 (2011).

353. Stewart, E. J., Madden, R., Paul, G. & Taddei, F. Aging and death in an organism that reproduces by morphologically symmetric division. *PLoS Biol.* **3**, e45 (2005).

354. Steinkraus, K. A. *et al.* Dietary restriction suppresses proteotoxicity and enhances longevity by an hsf-1-dependent mechanism in Caenorhabditis elegans. *Aging Cell* **7**, 394–404 (2008).

355. Robertson, O. H. & Wexler, B. C. Histological changes in the organs and tissues of senile castrated kokanee salmon (Oncorhynchus nerka kennerlyi). *Gen. Comp. Endocrinol.* **2**, 458–472 (1962).

356. Walker, G., Houthoofd, K., Vanfleteren, J. R. & Gems, D. Dietary restriction in C. elegans: From rate-of-living effects to nutrient sensing pathways. *Mech. Ageing Dev.* **126**, 929–937 (2005).

357. Kirkwood, T. B. & Holliday, R. The evolution of ageing and longevity. *Proc. R. Soc. Lond. B Biol. Sci.* **205**, 531–46 (1979).

358. Kirkwood, T. B. L. & Austad, S. N. Why do we age? *Nature* **408**, 233–238 (2000).

359. Bonduriansky, R. & Brassil, C. E. Rapid and costly ageing in wild male flies. *Nature* **420**, 377 (2002).

360. Brenner, S. The genetics of Caenorhabditis elegans. *Genetics* **77**, 71–94 (1974).

361. Klass, M. R. Aging in the nematode Caenorhabditis elegans: Major biological and environmental factors influencing life span. *Mech. Ageing Dev.* **6**, 413–429 (1977).

362. Johnson, T. E. & Wood, W. B. Genetic analysis of life-span in Caenorhabditis elegans. *Proc. Natl. Acad. Sci. U. S. A.* **79**, 6603–7 (1982).

363. McCay, C. M., Crowell, M. F. & Maynard, L. A. The effect of retarded growth upon the length of life span and upon the ultimate body size. *J. Nutr.* **5**, 63-79. DOI: (1935).

364. Kapahi, P. *et al.* With TOR, less is more: A key role for the conserved nutrient-sensing TOR pathway in aging. *Cell Metabolism* vol. 11 453–465 Preprint at https://doi.org/10.1016/j.cmet.2010.05.001 (2010).

365. Kenyon, C. J. The genetics of ageing. *Nature* vol. 464 504–512 Preprint at https://doi.org/10.1038/nature08980 (2010).

366. Guarente, L. & Kenyon, C. Genetic pathways that regulate ageing in model organisms. *Nature* **408**, 255–62 (2000).

367. Lee, S. S. *et al.* A systematic RNAi screen identifies a critical role for mitochondria in C. elegans longevity. *Nat. Genet.* **33**, 40–48 (2003).

368. Hansen, M., Hsu, A. L., Dillin, A. & Kenyon, C. New genes tied to endocrine, metabolic, and dietary regulation of lifespan from a Caenorhabditis elegans genomic RNAi screen. *PLoS Genet.* **1**, 0119–0128 (2005).

369. Lakowski, B. & Hekimi, S. Determination of Life-Span in Caenorhabditis elegans by Four Clock Genes. *Sci. New Ser.* **272**, 1010–1013 (1996).

370. Hughes, S. E., Huang, C. & Kornfeld, K. Identification of mutations that delay somatic or reproductive aging of Caenorhabditis elegans. *Genetics* **189**, 341–356 (2011).

371. Lakowski, B. & Hekimi, S. The genetics of caloric restriction in Caenorhabditis elegans. *Proc. Natl. Acad. Sci.* **95**, 13091–13096 (1998).

372. Avery, L. The genetics of feeding in Caenorhabditis elegans. *Genetics* **133**, 897–917 (1993).

373. Labrousse, a, Chauvet, S., Couillault, C., Kurz, C. L. & Ewbank, J. J. Caenorhabditis elegans is a model host for Salmonella typhimurium. *Curr. Biol. CB* **10**, 1543–5 (2000).

374. Smith, M. P. *et al.* A liquid-based method for the assessment of bacterial pathogenicity using the nematode Caenorhabditis elegans. *FEMS Microbiol. Lett.* **210**, 181–185 (2002).

375. Darby, C., Hsu, J. W., Ghori, N. & Falkow, S. Caenorhabditis elegans: Plague bacteria biofilm blocks food intake. *Nature* **417**, 243–244 (2002).

376. Portal-Celhay, C., Bradley, E. R. & Blaser, M. J. Control of intestinal bacterial proliferation in regulation of lifespan in Caenorhabditis elegans. *BMC Microbiol.* **12**, (2012).

377. Collins, J. J., Huang, C., Hughes, S. & Kornfeld, K. The measurement and analysis of age-related changes in Caenorhabditis elegans. *WormBook Online Rev. C Elegans Biol.* 1–21 (2008) doi:10.1895/wormbook.1.137.1.

378. Huang, C., Xiong, C. & Kornfeld, K. Measurements of age-related changes of physiological processes that predict lifespan of Caenorhabditis elegans. *Proc. Natl. Acad. Sci.* **101**, 8084–8089 (2004).

379. Zhang, Y., Lu, H. & Bargmann, C. I. Pathogenic bacteria induce aversive olfactory learning in Caenorhabditis elegans. *Nature* **438**, 179–184 (2005).

380. Melo, J. A. & Ruvkun, G. Inactivation of conserved C. elegans genes engages pathogen- and xenobiotic-associated defenses. *Cell* **149**, 452–466 (2012).

381. Perkins, L. A., Hedgecock, E. M., Thomson, J. N. & Culotti, J. G. Mutant sensory cilia in the nematode Caenorhabditis elegans. *Dev. Biol.* **117**, 456–487 (1986).

382. Starich, T. A. *et al.* Mutations affecting in chemosensory neurons of Caenorhabditis elegans. *Genetics* **139**, 171–188 (1995).

383. Lithgow, G. J., White, T. M., Melov, S. & Johnson, T. E. Thermotolerance and extended life-span conferred by single-gene mutations and induced by thermal stress. *Proc. Natl. Acad. Sci.* **92**, 7540–7544 (1995).

384. Johnson, T. E. *et al.* Gerontogenes mediate health and longevity in nematodes through increasing resistance to environmental toxins and stressors. in *Experimental Gerontology* vol. 35 687–694 (2000).

385. Friedman, D. B. & Johnson, T. E. A mutation in the age-1 gene in Caenorhabditis elegans lengthens life and reduces hermaphrodite fertility. *Genetics* **118**, 75–86 (1988).

386. Kenyon, C., Chang, J., Gensch, E., Rudner, A. & Tabtiang, R. A C. elegans mutant that lives twice as long as wild type. *Nature* **366**, 461–464 (1993).

387. Morris, J. Z., Tissenbaum, H. A. & Ruvkun, G. A phosphatidylinositol-3-OH kinase family member regulating longevity and diapause in Caenorhabditis elegans. *Nature* **382**, 536–539 (1996).

388. Kimura, K. D., Tissenbaum, H. A., Liu, Y. & Ruvkun, G. Daf-2, an insulin receptor-like gene that regulates longevity and diapause in Caenorhabditis elegans. *Science* **277**, 942–946 (1997).

389. Lin, K., Dorman, J. B., Rodan, A. & Kenyon, C. daf-16: An HNF-3/forkhead family member that can function to double the life-span of Caenorhabditis elegans. *Science* **278**, 1319–1322 (1997).

390. Ogg, S. *et al.* The fork head transcription factor DAF-16 transduces insulin-like metabolic and longevity signals in C. elegans. *Nature* **389**, 994–999 (1997).

391. Malone, E. A. & Thomas, J. H. A screen for nonconditional dauer-constitutive mutations in Caenorhabditis elegans. *Genetics* **136**, 879–886 (1994).

392. Feng, J., Bussière, F. & Hekimi, S. Mitochondrial electron transport is a key determinant of life span in Caenorhabditis elegans. *Dev. Cell* **1**, 633–644 (2001).

393. Apfeld, J., O'Connor, G., McDonagh, T., DiStefano, P. S. & Curtis, R. The AMP-activated protein kinase AAK-2 links energy levels and insulin-like signals to lifespan in C. elegans. *Genes Dev.* **18**, 3004–3009 (2004).

394. Curtis, R., O'Connor, G. & DiStefano, P. S. Aging networks in Caenorhabditis elegans: AMP-activated protein kinase (aak-2) links multiple aging and metabolism pathways. *Aging Cell* **5**, 119–126 (2006).

395. McKay, J. P., Raizen, D. M., Gottschalk, A., Schafer, W. R. & Avery, L. eat-2 and eat-18 are Required for Nicotinic Neurotransmission in the Caenorhabditis elegans Pharynx. *Genetics* **166**, 161–169 (2004).

396. Schreiber, M. A., Pierce-Shimomura, J. T., Chan, S., Parry, D. & McIntire, S. L. Manipulation of behavioral decline in Caenorhabditis elegans with the Rag GTPase raga-1. *PLoS Genet.* (2010) doi:10.1371/journal.pgen.1000972.

397. Wullschleger, S., Loewith, R. & Hall, M. N. TOR signaling in growth and metabolism. *Cell* vol. 124 471–484 Preprint at https://doi.org/10.1016/j.cell.2006.01.016 (2006).

398. Hansen, M. *et al.* Lifespan extension by conditions that inhibit translation in Caenorhabditis elegans. *Aging Cell* **6**, 95–110 (2007).

399. Vellai, T. *et al.* Genetics: Influence of TOR kinase on lifespan in C. elegans. *Nature* **426**, 620–620 (2003).

400. Pan, K. Z. *et al.* Inhibition of mRNA translation extends lifespan in Caenorhabditis elegans. *Aging Cell* **6**, 111–119 (2007).

401. Selman, C. *et al.* Ribosomal protein S6 kinase 1 signaling regulates mammalian life span. *Science* **326**, 140–4 (2009).

402. Panowski, S. H., Wolff, S., Aguilaniu, H., Durieux, J. & Dillin, A. PHA-4/Foxa mediates diet-restriction-induced longevity of C. elegans. *Nature* **447**, 550–555 (2007).

403. Hansen, M. *et al.* A role for autophagy in the extension of lifespan by dietary restriction in C. elegans. *PLoS Genet.* **4**, (2008).

404. Hillier, L. D. W. *et al.* Whole-genome sequencing and variant discovery in C. elegans. *Nat. Methods* **5**, 183–188 (2008).

405. Garee, J. P. & Oesterreich, S. SAFB1's multiple functions in biological control-lots still to be done! *J. Cell. Biochem.* **109**, 312–9 (2010).

406. Doncaster, C. C. Nematode feeding mechanisms. 1. observations on rhabditis and pelodera. *Nematologica* **8**, 313–320 (1962).

407. Avery, L. Motor neuron M3 controls pharyngeal muscle relaxation timing in Caenorhabditis elegans. *J. Exp. Biol.* **175**, 283–97 (1993).

408. Irazoqui, J. E. *et al.* Distinct pathogenesis and host responses during infection of C. elegans by P. aeruginosa and S. aureus. *PLoS Pathog.* **6**, 1–24 (2010).

409. Sifri, C. D., Begun, J., Ausubel, F. M. & Calderwood, S. B. Caenorhabditis elegans as a model host for Staphylococcus aureus pathogenesis. *Infect. Immun.* **71**, 2208–2217 (2003).

410. Settembre, C. *et al.* TFEB links autophagy to lysosomal biogenesis. *Science* **332**, 1429–1433 (2011).

411. Lapierre, L. R. *et al.* The TFEB orthologue HLH-30 regulates autophagy and modulates longevity in Caenorhabditis elegans. *Nat. Commun.* **4**, (2013).

412. Visvikis, O. *et al.* Innate host defense requires TFEB-mediated transcription of cytoprotective and antimicrobial genes. *Immunity* **40**, 896–909 (2014).

413. Pradel, E. *et al.* Detection and avoidance of a natural product from the pathogenic bacterium Serratia marcescens by Caenorhabditis elegans. *Proc. Natl. Acad. Sci. U. S. A.* **104**, 2295–300 (2007).

414. Pujol, N. *et al.* A reverse genetic analysis of components of the Toll signaling pathway in Caenorhabditis elegans. *Curr. Biol.* **11**, 809–821 (2001).

415. Kim, D. H. *et al.* A conserved p38 MAP kinase pathway in Caenorhabditis elegans innate immunity. *Science* **297**, 623–6 (2002).

416. Troemel, E. R. *et al.* p38 MAPK regulates expression of immune response genes and contributes to longevity in C. elegans. *PLoS Genet.* **2**, 1725–1739 (2006).

417. Reddy, K. C., Andersen, E. C., Kruglyak, L. & Kim, D. H. A polymorphism in npr-1 is a behavioral determinant of pathogen susceptibility in C. elegans. *Science* **323**, 382–384 (2009).

418. Kao, C. Y. *et al.* Global functional analyses of cellular responses to pore-forming toxins. *PLoS Pathog.* **7**, (2011).

419. Schulenburg, H. & Ewbank, J. J. The genetics of pathogen avoidance in Caenorhabditis elegans. *Molecular Microbiology* vol. 66 563–570 Preprint at https://doi.org/10.1111/j.1365-2958.2007.05946.x (2007).

420. Félix, M. A. & Duveau, F. Population dynamics and habitat sharing of natural populations of Caenorhabditis elegans and C. briggsae. *BMC Biol.* **10**, (2012).

421. Garigan, D. *et al.* Genetic analysis of tissue aging in Caenorhabditis elegans: A role for heat-shock factor and bacterial proliferation. *Genetics* **161**, 1101–1112 (2002).

422. Peña, F. G. *et al.* Comparison of alternate scoring of variables on the performance of the frailty index. *BMC Geriatr.* **14**, (2014).

423. Rockwood, K. *et al.* A global clinical measure of fitness and frailty in elderly people. *Cmaj* vol. 173 489–495 http://ovidsp.ovid.com/ovidweb.cgi?T=JS&PAGE=reference&D=psyc4&NEWS=N&AN=2005-10427-001 (2005).

424. Bansal, A., Zhu, L. J., Yen, K. & Tissenbaum, H. A. Uncoupling lifespan and healthspan in *Caenorhabditis elegans* longevity mutants. *Proc. Natl. Acad. Sci.* **112**, E277–E286 (2015).

425. Te Velde, E. R. & Pearson, P. L. The variability of female reproductive ageing. *Human Reproduction Update* vol. 8 141–154 Preprint at https://doi.org/10.1093/humupd/8.2.141 (2002).

426. Hartge, P. Genetics of reproductive lifespan. *Nature Genetics* vol. 41 637–638 Preprint at https://doi.org/10.1038/ng0609-637 (2009).

427. Hughes, S. E., Evason, K., Xiong, C. & Kornfeld, K. Genetic and pharmacological factors that influence reproductive aging in nematodes. *PLoS Genet.* **3**, 0254–0265 (2007).

428. Luo, S., Shaw, W. M., Ashraf, J. & Murphy, C. T. TGF-ß Sma/Mab signaling mutations uncouple reproductive aging from somatic aging. *PLoS Genet.* **5**, (2009).

429. Wang, M. C., Oakley, H. D., Carr, C. E., Sowa, J. N. & Ruvkun, G. Gene Pathways That Delay Caenorhabditis elegans Reproductive Senescence. *PLoS Genet.* **10**, (2014).

430. Kumar, S., Kocsisova, Z. & Kornfeld, K. Keep on Laying Eggs Mama, RNAi My Reproductive Aging Blues Away. *PLoS Genet.* **10**, (2014).

431. Weighardt, F. *et al.* A novel hnRNP protein (HAP/SAF-B) enters a subset of hnRNP complexes and relocates in nuclear granules in response to heat shock. *J. Cell Sci.* **112 (Pt 1**, 1465–1476 (1999).

432. Townson, S. M., Kang, K., Lee, A. V. & Oesterreich, S. Structure-function analysis of the estrogen receptor α corepressor scaffold attachment factor-B1: Identification of a potent transcriptional repression domain. *J. Biol. Chem.* **279**, 26074–26081 (2004).

433. Oesterreich, S. *et al.* Tamoxifen-bound estrogen receptor (ER) strongly interacts with the nuclear matrix protein HET/SAF-B, a novel inhibitor of ER-mediated transactivation. *Mol. Endocrinol. Baltim. Md* **14**, 369–81 (2000).

434. Oesterreich, S. Scaffold Attachment Factors SAFB1 and SAFB2: Innocent Bystanders or Critical Players in Breast Tumorigenesis? *Journal of Cellular Biochemistry* vol. 90 653–661 Preprint at https://doi.org/10.1002/jcb.10685 (2003).

435. Aravind, L. & Koonin, E. V. SAP - A putative DNA-binding motif involved in chromosomal organization. *Trends in Biochemical Sciences* vol. 25 112–114 Preprint at https://doi.org/10.1016/S0968-0004(99)01537-6 (2000).

436. Köthe, M. *et al.* Killing of Caenorhabditis elegans by Burkholderia cepacia is controlled by the cep quorum-sensing system. *Cell. Microbiol.* **5**, 343–351 (2003).

437. Gems, D. & Riddle, D. L. Genetic, behavioral and environmental determinants of male longevity in Caenorhabditis elegans. *Genetics* **154**, 1597–1610 (2000).

438. Garsin, D. A. *et al.* Long-lived C. elegans daf-2 Mutants are resistant to bacterial pathogens. *Science* **300**, 1921 (2003).

439. Powell, J. R., Kim, D. H. & Ausubel, F. M. The G protein-coupled receptor FSHR-1 is required for the Caenorhabditis elegans innate immune response. *Proc. Natl. Acad. Sci. U. S. A.* **106**, 2782–2787 (2009).

440. Tenor, J. L. & Aballay, A. A conserved Toll-like receptor is required for Caenorhabditis elegans innate immunity. *EMBO Rep.* **9**, 103–109 (2008).

441. Endo, T. *et al.* Neurochemistry and neuropharmacology of emesis - The role of serotonin. *Toxicology* **153**, 189–201 (2000).

442. Szø, J. Y., Victor, M., Loer, C., Shi, Y. & Ruvkun, G. Food and metabolic signalling defects in a Caenorhabditis elegans serotonin-synthesis mutant. *Nature* **403**, 560–564 (2000).

443. Greer, E. L. *et al.* An AMPK-FOXO Pathway Mediates Longevity Induced by a Novel Method of Dietary Restriction in C. elegans. *Curr. Biol.* **17**, 1646–1656 (2007).

444. Greer, E. L. & Brunet, A. Different dietary restriction regimens extend lifespan by both independent and overlapping genetic pathways in C. elegans. *Aging Cell* **8**, 113–127 (2009).

445. Kauffman, A. L., Ashraf, J. M., orces-Zimmerman, M. R., Landis, J. N. & Murphy, C. T. Insulin signaling and dietary restriction differentially influence the decline of learning and memory with age. *PLoS Biol.* **8**, (2010).

446. Kamath, R. S. *et al.* Systematic functional analysis of the Caenorhabditis elegans genome using RNAi. *Nature* **421**, 231–237 (2003).

447. Kamath, R. S., Martinez-Campos, M., Zipperlen, P., Fraser, A. G. & Ahringer, J. Effectiveness of specific RNA-mediated interference through ingested double-stranded RNA in Caenorhabditis elegans. *Genome Biol.* **2**, RESEARCH0002 (2001).

448. Mello, C. C., Kramer, J. M., Stinchcomb, D. & Ambros, V. Efficient gene transfer in C.elegans: extrachromosomal maintenance and integration of transforming sequences. *EMBO J.* **10**, 3959–70 (1991).

449. Kumar, S., Dietrich, N. & Kornfeld, K. Angiotensin Converting Enzyme (ACE) Inhibitor Extends Caenorhabditis elegans Life Span. *PLoS Genet.* **12**, 1–28 (2016).

450. McColl, G. *et al.* Insulin-like signaling determines survival during stress via posttranscriptional mechanisms in C. elegans. *Cell Metab.* **12**, 260–272 (2010).

451. Moore, B. T., Jordan, J. M. & Baugh, L. R. WormSizer: High-throughput Analysis of Nematode Size and Shape. *PLoS ONE* **8**, (2013).

452. Powell, J. R. & Ausubel, F. M. Models of Caenorhabditis elegans infection by bacterial and fungal pathogens. *Methods Mol. Biol. Clifton NJ* **415**, 403–427 (2008).

453. Estes, K. a, Dunbar, T. L., Powell, J. R., Ausubel, F. M. & Troemel, E. R. bZIP transcription factor zip-2 mediates an early response to Pseudomonas aeruginosa infection in Caenorhabditis elegans. *Proc. Natl. Acad. Sci. U. S. A.* **107**, 2153–2158 (2010).

454. Kiyama, Y., Miyahara, K. & Ohshima, Y. Active uptake of artificial particles in the nematode Caenorhabditis elegans. *J. Exp. Biol.* **215**, 1178–1183 (2012).

455. Collins, J. J., Evason, K., Pickett, C. L., Schneider, D. L. & Kornfeld, K. The anticonvulsant ethosuximide disrupts sensory function to extend C. elegans lifespan. *PLoS Genet.* **4**, (2008).

456. Davis, D. E. *et al.* The cation diffusion facilitator gene cdf-2 mediates zinc metabolism in Caenorhabditis elegans. *Genetics* **182**, 1015–1033 (2009).

457. Schmittgen, T. D. & Livak, K. J. Analyzing real-time PCR data by the comparative CT method. *Nat. Protoc.* **3**, 1101–1108 (2008).

458. Yang, J. S. *et al.* OASIS: Online application for the survival analysis of lifespan assays performed in aging research. *PLoS ONE* **6**, (2011).

459. Prince, M., Comas-Herrera, A., Knapp, M., Guerchet, M. & Karagiannidou, M. World Alzheimer report 2016: improving healthcare for people living with dementia: coverage, quality and costs now and in the future. http://www.alz.co.uk/ (2016).

460. Tanzi, R. E. & Bertram, L. Twenty years of the Alzheimer's disease amyloid hypothesis: a genetic perspective. *Cell* **120**, 545–555 (2005).

461. O'Brien, R. J. & Wong, P. C. Amyloid Precursor Protein Processing and Alzheimer's Disease. *Annu. Rev. Neurosci.* **34**, 185–204 (2011).

462. Glenner, G. G. Amyloid beta protein and the basis for Alzheimer's disease. *Prog. Clin. Biol. Res.* **317**, 857–868 (1989).

463. Glenner, G. G. & Wong, C. W. Alzheimer's disease: Initial report of the purification and characterization of a novel cerebrovascular amyloid protein. *Biochem. Biophys. Res. Commun.* **120**, 885–890 (1984).

464. Masters, C. L. *et al.* Amyloid plaque core protein in Alzheimer disease and Down syndrome. *Proc. Natl. Acad. Sci.* **82**, 4245–4249 (1985).

465. Saido, T. C. *et al.* Dominant and differential deposition of distinct β-amyloid peptide species, AβN3(pE), in senile plaques. *Neuron* **14**, 457–466 (1995).

466. Mori, H., Takio, K., Ogawara, M. & Selkoe, D. J. Mass spectrometry of purified amyloid beta protein in Alzheimer's disease. *J. Biol. Chem.* **267**, 17082–17086 (1992).

467. Jarrett, J. T., Berger, E. P. & Lansbury, P. T. The carboxy terminus of the beta amyloid protein is critical for the seeding of amyloid formation: implications for the pathogenesis of Alzheimer's disease. *Biochemistry* **32**, 4693–4697 (1993).

468. Goate, A. *et al.* Segregation of a missense mutation in the amyloid precursor protein gene with familial Alzheimer's disease. *Nature* **349**, 704–706 (1991).

469. Levy, E. *et al.* Mutation of the Alzheimer's Disease Amyloid Gene in Hereditary Cerebral Hemorrhage, Dutch Type. *Science* **248**, 1124–1126 (1990).

470. Cummings, J. L., Morstorf, T. & Zhong, K. Alzheimer's disease drug-development pipeline: few candidates, frequent failures. *Alzheimers Res. Ther.* **6**, 37 (2014).

471. Panza, F., Lozupone, M., Logroscino, G. & Imbimbo, B. P. A critical appraisal of amyloid-β-targeting therapies for Alzheimer disease. *Nat. Rev. Neurol.* **15**, 73–88 (2019).

472. Jeremic, D., Jiménez-Díaz, L. & Navarro-López, J. D. Past, present and future of therapeutic strategies against amyloid-β peptides in Alzheimer's disease: a systematic review. *Ageing Res. Rev.* **72**, 101496 (2021).

473. Hardy, J. & Allsop, D. Amyloid deposition as the central event in the aetiology of Alzheimer's disease. *Trends Pharmacol. Sci.* **12**, 383–388 (1991).

474. Itzhaki, R. F. *et al.* Microbes and Alzheimer's disease. *J. Alzheimers Dis.* **51**, 979–984 (2016).

475. Moir, R. D., Lathe, R. & Tanzi, R. E. The antimicrobial protection hypothesis of Alzheimer's disease. *Alzheimers Dement.* **14**, 1602–1614 (2018).

476. Vojtechova, I., Machacek, T., Kristofikova, Z., Stuchlik, A. & Petrasek, T. Infectious origin of Alzheimer's disease: Amyloid beta as a component of brain antimicrobial immunity. *PLOS Pathog.* **18**, e1010929 (2022).

477. Soscia, S. J. *et al.* The Alzheimer's Disease-Associated Amyloid β-Protein Is an Antimicrobial Peptide. *PLoS ONE* **5**, e9505 (2010).

478. Fülöp, T. *et al.* Targeting Infectious Agents as a Therapeutic Strategy in Alzheimer's Disease. *CNS Drugs* **34**, 673–695 (2020).

479. Iqbal, U. H., Zeng, E. & Pasinetti, G. M. The Use of Antimicrobial and Antiviral Drugs in Alzheimer's Disease. *Int. J. Mol. Sci.* **21**, 4920 (2020).

480. Dominy, S. S. *et al.* Porphyromonas gingivalis in Alzheimer's disease brains: Evidence for disease causation and treatment with small-molecule inhibitors. *Sci. Adv.* **5**, eaau3333 (2019).

481. Wozniak, M. A., Mee, A. P. & Itzhaki, R. F. Herpes simplex virus type 1 DNA is located within Alzheimer's disease amyloid plaques. *J. Pathol.* **217**, 131–138 (2009).

482. Kumar, D. K. V. *et al.* Amyloid-β peptide protects against microbial infection in mouse and worm models of Alzheimer's disease. *Sci. Transl. Med.* **8**, 340ra72 (2016).

483. Readhead, B. *et al.* Multiscale Analysis of Independent Alzheimer's Cohorts Finds Disruption of Molecular, Genetic, and Clinical Networks by Human Herpesvirus. *Neuron* **99**, 64-82.e7 (2018).

484. Miklossy, J. Alzheimer's disease - a neurospirochetosis. Analysis of the evidence following Koch's and Hill's criteria. *J. Neuroinflammation* **8**, 90 (2011).

485. Carter, C. J. Genetic, Transcriptome, Proteomic, and Epidemiological Evidence for Blood-Brain Barrier Disruption and Polymicrobial Brain Invasion as Determinant Factors in Alzheimer's Disease. *J. Alzheimers Dis. Rep.* **1**, 125–157 (2017).

486. Miklossy, J. Bacterial Amyloid and DNA are Important Constituents of Senile Plaques: Further Evidence of the Spirochetal and Biofilm Nature of Senile Plaques. *J. Alzheimers Dis.* **53**, 1459–1473 (2016).

487. Lövheim, H., Gilthorpe, J., Adolfsson, R., Nilsson, L.-G. & Elgh, F. Reactivated herpes simplex infection increases the risk of Alzheimer's disease. *Alzheimers Dement.* **11**, 593–599 (2015).

488. Mcgeer, P., Mcgeer, E., Rogers, J. & Sibley, J. Anti-inflammatory drugs and Alzheimer disease. *The Lancet* **335**, 1037 (1990).

489. Schnier, C., Janbek, J., Lathe, R. & Haas, J. Reduced dementia incidence after varicella zoster vaccination in Wales 2013–2020. *Alzheimers Dement. Transl. Res. Clin. Interv.* **8**, e12293 (2022).

490. Lehrer, S. & Rheinstein, P. H. Herpes Zoster Vaccination Reduces Risk of Dementia. *In Vivo* **35**, 3271–3275 (2021).

491. Tzeng, N. S. *et al.* Anti-herpetic Medications and Reduced Risk of Dementia in Patients with Herpes Simplex Virus Infections—a Nationwide, Population-Based Cohort Study in Taiwan. *Neurotherapeutics* **15**, 417–429 (2018).

492. McColl, G. *et al.* Utility of an improved model of amyloid-beta (Aβ1-42) toxicity in Caenorhabditis elegans for drug screening for Alzheimer's disease. *Mol. Neurodegener.* **7**, 57 (2012).

493. Fay, D. S., Fluet, A., Johnson, C. J. & Link, C. D. In vivo aggregation of beta-amyloid peptide variants. *J. Neurochem.* **71**, 1616–1625 (1998).

494. McColl, G. *et al.* The Caenorhabditis elegans Aβ1–42 Model of Alzheimer Disease Predominantly Expresses Aβ3–42*. *J. Biol. Chem.* **284**, 22697–22702 (2009).

495. Sergeant, N. *et al.* Truncated beta-amyloid peptide species in pre-clinical Alzheimer's disease as new targets for the vaccination approach. *J. Neurochem.* **85**, 1581–1591 (2003).

496. Cairns, D. M., Itzhaki, R. F. & Kaplan, D. L. Potential Involvement of Varicella Zoster Virus in Alzheimer's Disease via Reactivation of Quiescent Herpes Simplex Virus Type 1. *J. Alzheimers Dis.* **88**, 1189–1200 (2022).

497. Devanand, D. P. Viral Hypothesis and Antiviral Treatment in Alzheimer's Disease. *Curr. Neurol. Neurosci. Rep.* **18**, 55 (2018).

498. Mantel, N. Evaluation of survival data and two new rank order statistics arising in its consideration. *Cancer Chemother. Rep.* **50**, 163–170 (1966).

499. Vijg, J. & Campisi, J. Puzzles, promises and a cure for ageing. *Nat. 2008 4547208* **454**, 1065–1071 (2008).

500. Guarente, L. & Kenyon, C. Genetic pathways that regulate ageing in model organisms. *Nature* **408**, 255–262 (2000).

501. Kaeberlein, M. *et al.* Regulation of yeast replicative life span by TOR and Sch9 response to nutrients. *Science* **310**, 1193–1196 (2005).

502. Powers, R. W., Kaeberlein, M., Caldwell, S. D., Kennedy, B. K. & Fields, S. Extension of chronological life span in yeast by decreased TOR pathway signaling. *Genes Dev.* **20**, 174–184 (2006).

503. The C. elegans Sequencing Consortium. Genome sequence of the nematode C. elegans: A platform for investigating biology. *Science* **282**, 2012–2018 (1998).

504. Sulston, J. E. & Horvitz, H. R. Post-embryonic cell lineages of the nematode, Caenorhabditis elegans. *Dev. Biol.* **56**, 110–156 (1977).

505. Chalfie, M., Tu, Y., Euskirchen, G., Ward, W. W. & Prasher, D. C. Green Fluorescent Protein as a Marker for Gene Expression. *Science* **263**, 802–805 (1994).

506. Kenyon, C. A Conserved Regulatory System for Aging. *Cell* **105**, 165–168 (2001).

507. Carroll, P. M., Dougherty, B., Ross-Macdonald, P., Browman, K. & FitzGerald, K. Model systems in drug discovery: chemical genetics meets genomics. *Pharmacol. Ther.* **99**, 183–220 (2003).

508. Jones, A. K., Buckingham, S. D. & Sattelle, D. B. Chemistry-to-gene screens in Caenorhabditis elegans. *Nat. Rev. Drug Discov. 2005 44* **4**, 321–330 (2005).

509. Ondetti, M. A., Rubin, B. & Cushman, D. W. Design of Specific Inhibitors of Angiotensin-Converting Enzyme: New Class of Orally Active Antihypertensive Agents. *Science* **4288**, 441–444 (1977).

510. Mills, K. T., Stefanescu, A. & He, J. The global epidemiology of hypertension. *Nat. Rev. Nephrol.* **16**, 223–237 (2020).

511. Forouzanfar, M. H. *et al.* Global Burden of Hypertension and Systolic Blood Pressure of at Least 110 to 115 mm Hg, 1990-2015. *JAMA* **317**, 165–182 (2017).

512. Singh, G. M. *et al.* The age associations of blood pressure, cholesterol, and glucose: Analysis of health examination surveys from international populations. *Circulation* **125**, 2204–2211 (2012).

513. Skeggs, L. T., Kahn, J. R. & Shumway, N. P. The preparation and function of the hypertensin-converting enzyme. *J. Exp. Med.* **103**, 295 (1956).

514. Reid, I. A., Morris, B. J. & Ganong, W. F. THE RENIN-ANGIOTENSIN SYSTEM. *Ann Rev Physiol* **40**, 377–410 (1978).

515. Santos, R. A. S. *et al.* The renin-angiotensin system: Going beyond the classical paradigms. *Am. J. Physiol. - Heart Circ. Physiol.* **316**, H958–H970 (2019).

516. Gabrawy, M. M. *et al.* Lisinopril Preserves Physical Resilience and Extends Life Span in a Genotype-Specific Manner in Drosophila melanogaster. *J. Gerontol.* **74**, 1844–1852 (2019).

517. Bader, M. Tissue Renin-Angiotensin-Aldosterone Systems: Targets for Pharmacological Therapy. *Annu. Rev. Pharmacol. Toxicol.* **50**, 439–465 (2010).

518. Santos, R. A. S. *et al.* Angiotensin-(1-7) is an endogenous ligand for the G protein-coupled receptor Mas. *Proc. Natl. Acad. Sci. U. S. A.* **100**, 8258–8263 (2003).

519. Wrapp, D. *et al.* Cryo-EM structure of the 2019-nCoV spike in the prefusion conformation. (2019).

520. Takeshita, H. *et al.* Angiotensin-converting enzyme 2 deficiency accelerates and angiotensin 1-7 restores age-related muscle weakness in mice. *J. Cachexia Sarcopenia Muscle* **9**, 975–986 (2018).

521. Takeshita, H. *et al.* Different effects of the deletion of angiotensin converting enzyme 2 and chronic activation of the renin-angiotensin system on muscle weakness in middle-aged mice. *Hypertens. Res.* **43**, 296–304 (2020).

522. Nozato, S. *et al.* Angiotensin 1-7 alleviates aging-associated muscle weakness and bone loss, but is not associated with accelerated aging in ACE2-knockout mice. *Clin. Sci.* **133**, 2005–2018 (2019).

523. Lavoie, J. L. & Sigmund, C. D. Minireview: Overview of the Renin-Angiotensin System—An Endocrine and Paracrine System. *Endocrinology* **144**, 2179–2183 (2003).

524. Nehme, A., Zouein, F. A., Zayeri, Z. D. & Zibara, K. An Update on the Tissue Renin Angiotensin System and Its Role in Physiology and Pathology. *J. Cardiovasc. Dev. Dis. 2019 Vol 6 Page 14* **6**, 14 (2019).

525. Balthazar, L., Lages, Y. V. M., Romano, V. C., Landeira-Fernandez, J. & Krahe, T. E. The association between the renin-angiotensin system and the hypothalamic-pituitary-adrenal axis in anxiety disorders: A systematic review of animal studies. *Psychoneuroendocrinology* **132**, 105354 (2021).

526. Abiodun, O. A. & Ola, M. S. Role of brain renin angiotensin system in neurodegeneration: An update. *Saudi J. Biol. Sci.* **27**, 905–912 (2020).

527. Jaworska, K., Koper, M. & Ufnal, M. Gut microbiota and renin-angiotensin system: A complex interplay at local and systemic levels. *Am. J. Physiol. - Gastrointest. Liver Physiol.* **321**, G355–G366 (2021).

528. Leal, C. R. V. *et al.* Renin-angiotensin system in normal pregnancy and in preeclampsia: A comprehensive review. *Pregnancy Hypertens.* **28**, 15–20 (2022).

529. Duncia, J. V. *et al.* The Discovery of Potent Nonpeptide Angiotensin II Receptor Antagonists: A New Class of Potent Hypertensives. *J Med Chem* **33**, 183–201 (1990).

530. Jensen, C., Herold, P. & Brunner, H. R. Aliskiren: the first renin inhibitor for clinical treatment. *Nat. Rev. Drug Discov.* **7**, 399–410 (2008).

531. Fournier, D., Luft, F. C., Bader, M., Ganten, D. & Andrade-Navarro, M. A. Emergence and evolution of the renin-angiotensin-aldosterone system. *J. Mol. Med.* **90**, 495–508 (2021).

532. Dos Reis, M. *et al.* Uncertainty in the Timing of Origin of Animals and the Limits of Precision in Molecular Timescales. *Curr. Biol.* **25**, 2939–2950 (2015).

533. Simões-Costa, M. S. *et al.* The evolutionary origin of cardiac chambers. *Dev. Biol.* **277**, 1–15 (2005).

534. Mogi, M. Effect of renin–angiotensin system on senescence. *Geriatr. Gerontol. Int.* **20**, 520–525 (2020).

535. de Cavanagh, E. M. V., Inserra, F. & Ferder, L. Angiotensin II blockade: A strategy to slow ageing by protecting mitochondria? *Cardiovasc. Res.* **89**, 31–40 (2011).

536. Basso, N. *et al.* Protective effect of the inhibition of the renin-angiotensin system on aging. *Regul. Pept.* **128**, 247–252 (2005).

537. Kamo, T., Akazawa, H., Suzuki, J. ichi & Komuro, I. Roles of renin-angiotensin system and Wnt pathway in aging-related phenotypes. *Inflamm. Regen.* **36**, (2016).

538. S.A. Capettini, L. *et al.* Role of Renin-Angiotensin System in Inflammation, Immunity and Aging. *Curr. Pharm. Des.* **18**, 963–970 (2012).

539. Le, D., Brown, L., Malik, K. & Murakami, S. Two Opposing Functions of Angiotensin-Converting Enzyme (ACE) That Links Hypertension, Dementia, and Aging. *Int. J. Mol. Sci. 2021 Vol 22 Page 13178* **22**, 13178 (2021).

540. Santos, E. L. *et al.* Long term treatment with ACE inhibitor enalapril decreases body weight gain and increases life span in rats. *Biochem. Pharmacol.* **78**, 951–958 (2009).

541. Sugaya, T. *et al.* Angiotensin II type 1a receptor-deficient mice with hypotension and hyperreninemia. *J. Biol. Chem.* **270**, 18719–18722 (1995).

542. Yabumoto, C. *et al.* Angiotensin II receptor blockade promotes repair of skeletal muscle through down-regulation of aging-promoting C1q expression. *Sci. Rep.* **5**, 14453 (2015).

543. Gissendanner, C. R. & Sluder, A. E. nhr-25, the Caenorhabditis elegans ortholog of ftz-f1, is required for epidermal and somatic gonad development. *Dev. Biol.* **221**, 259–272 (2000).

544. Frand, A. R., Russel, S. & Ruvkun, G. Functional genomic analysis of c. elegans molting. *PLoS Biol.* **3**, e312 (2005).

545. Oskouian, B. *et al.* Regulation of sphingosine-1-phosphate lyase gene expression by members of the GATA family of transcription factors. *J. Biol. Chem.* **280**, 18403–18410 (2005).

546. Ahn, D. H., Singaravelu, G., Lee, S., Ahnn, J. & Shim, Y. H. Functional and phenotypic relevance of differentially expressed proteins in calcineurin mutants of Caenorhabditis elegans. *PROTEOMICS* **6**, 1340–1350 (2006).

547. Dubois, C. *et al.* Differential modification of the C. elegans proteome in response to acute and chronic gamma radiation: Link with reproduction decline. *Sci. Total Environ.* **676**, 767–781 (2019).

548. Kucuktepe, S. The Anti-Obesity Effects of the Angiotensin-Converting Enzyme (ACE) Inhibitor Captopril – Metabolomics and Transcriptomics Studies. (La Trobe University, 2021). doi:10.26181/60879586931A0.

549. Crocco, P. *et al.* Genome-Wide Analysis in Drosophila Reveals the Genetic Basis of Variation in Age-Specific Physical Performance and Response to ACE Inhibition. *Genes* **13**, (2022).

550. Ederer, K. A. *et al.* Age-and genotype-specific effects of the angiotensin-converting enzyme inhibitor lisinopril on mitochondrial and metabolic parameters in drosophila melanogaster. *Int. J. Mol. Sci.* **19**, 3351 (2018).

551. Inserra, F., Romano, L., Ercole, L., De Cavanagh, E. M. V. & Ferder, L. Cardiovascular changes by long-term inhibition of the renin-angiotensin system in aging. *Hypertension* **25**, 437–442 (1995).

552. Ferder, L. *et al.* Decreased Glomeruloscierosis in Aging by Angiotensin-Converting Enzyme Inhibitor. *J. Am. Soc. Nephrol.* **5**, 1147–1152 (1994).

553. Keller, K., Kane, A., Heinze-Milne, S., Grandy, S. A. & Howlett, S. E. Chronic treatment with the ace inhibitor enalapril attenuates the development of frailty and differentially modifies pro- and anti-inflammatory cytokines in aging male and female c57bl/6 mice. *J. Gerontol.* **74**, 1149–1157 (2019).

554. Basso, N. *et al.* Protective effect of long-term angiotensin II inhibition. *Am. J. Physiol. - Heart Circ. Physiol.* **293**, 1351–1358 (2007).

555. González Bosc, L., Kurnjek, M. L., Müller, A. & Basso, N. Effect of chronic angiotensin II inhibition on the cardiovascular system of the normal rat. *Am. J. Hypertens.* **13**, 1301–1307 (2000).

556. de Cavanagh, E. M. V., Flores, I., Ferder, M., Inserra, F. & Ferder, L. Renin-angiotensin system inhibitors protect against age-related changes in rat liver mitochondrial DNA content and gene expression. *Exp. Gerontol.* **43**, 919–928 (2008).

557. de Cavanagh, E. M. V. *et al.* Enalapril and losartan attenuate mitochondrial dysfunction in aged rats. *FASEB J.* **17**, 1096–1098 (2003).

558. Inserra, F. *et al.* Changes seen in the aging kidney and the effect of blocking the renin—angiotensin system. *Ther. Adv. Cardiovasc. Dis.* **3**, 341–346 (2009).

559. Carter, C. S. *et al.* Angiotensin-Converting Enzyme Inhibition, Body Composition, and Physical Performance in Aged Rats. *J. Gerontol. Ser. A* **59**, 416–423 (2004).

560. Carter, C. S. *et al.* Differential effects of enalapril and losartan on body composition and indices of muscle quality in aged male Fischer 344 × Brown Norway rats. *AGE* **33**, 167–183 (2011).

561. Liao, F.-T., Chang, C.-Y., Su, M.-T. & Kuo, W.-C. Necessity of angiotensin-converting enzyme-related gene for cardiac functions and longevity of Drosophila melanogaster assessed by optical coherence tomography. *J. Biomed. Opt.* **19**, 1 (2013).

562. Carhan, A., Tang, K., Shirras, C. A., Shirras, A. D. & Isaac, R. E. Loss of angiotensin-converting enzyme-related (ACER) peptidase disrupts night-time sleep in adult Drosophila melanogaster. *J. Exp. Biol.* **214**, 680–686 (2011).

563. Glover, Z. *et al.* Loss of angiotensin-converting enzyme-related (ACER) peptidase disrupts behavioural and metabolic responses to diet in Drosophila melanogaster. *J. Exp. Biol.* **222**, (2019).

564. Benigni, A. *et al.* Disruption of the Ang II type 1 receptor promotes longevity in mice. *J. Clin. Invest.* **119**, 524–530 (2009).

565. Tissenbaum, H. A. & Ruvkun, G. An insulin-like signaling pathway affects both longevity and reproduction in Caenorhabditis elegans. *Genetics* **148**, 703–717 (1998).

566. Kimura, K. D., Tissenbaum, H. A., Liu, Y. & Ruvkun, G. Daf-2, an insulin receptor-like gene that regulates longevity and diapause in Caenorhabditis elegans. *Science* **277**, 942–946 (1997).

567. Dalton, H. M. & Curran, S. P. Hypodermal responses to protein synthesis inhibition induce systemic developmental arrest and AMPK-dependent survival in Caenorhabditis elegans. *PLOS Genet.* **14**, e1007520 (2018).

568. Shaye, D. D. & Greenwald, I. OrthoList: A Compendium of C. elegans Genes with Human Orthologs. *PLOS ONE* **6**, e20085 (2011).

569. Kim, W., Underwood, R. S., Greenwald, I. & Shaye, D. D. OrthoList 2: A New Comparative Genomic Analysis of Human and Caenorhabditis elegans Genes. *Genetics* **210**, 445–461 (2018).

570. Castle, W. E. Inbreeding, Cross-Breeding and Sterility in Drosophila. *Science* **23**, 153–153 (1906).

571. Dunn, L. C. Old and new in genetics. *Bull. N. Y. Acad. Med.* **40**, 325 (1964).

572. Morgan, T. H. Sex Limited Inheritance in Drosophila. *Science* **32**, 120–122 (1910).

573. Roberts, D. B. Drosophila melanogaster: the model organism. *Entomol. Exp. Appl.* **121**, 93–103 (2006).

574. Altintas, O., Park, S. & Lee, S. J. V. The role of insulin/IGF-1 signaling in the longevity of model invertebrates, C. elegans and D. melanogaster. *BMB Rep.* **49**, 81 (2016).

575. Broughton, S. J. *et al.* Longer lifespan, altered metabolism, and stress resistance in Drosophila from ablation of cells making insulin-like ligands. *Proc. Natl. Acad. Sci. U. S. A.* **102**, 3105–3110 (2005).

576. Giacomotto, J. & Ségalat, L. High-throughput screening and small animal models, where are we? *Br. J. Pharmacol.* **160**, 204–216 (2010).

577. Jafari, M. Drosophila melanogaster as a model system for the evaluation of anti-aging compounds. *Fly (Austin)* **4**, 253–257 (2010).

578. Lee, S. H. & Min, K. J. Drosophila melanogaster as a model system in the study of pharmacological interventions in aging. *Transl. Med. Aging* **3**, 98–103 (2019).

579. Pandey, U. B. & Nichols, C. D. Human Disease Models in Drosophila melanogaster and the Role of the Fly in Therapeutic Drug Discovery. *Pharmacol. Rev.* **63**, 411–436 (2011).

580. Willoughby, L. F. *et al.* An in vivo large-scale chemical screening platform using Drosophila for anti-cancer drug discovery. *DMM Dis. Models Mech.* **6**, 521–529 (2013).

581. Houard, X. *et al.* The Drosophila melanogaster-related angiotensin-I-converting enzymes Acer and Ance Distinct enzymic characteristics and alternative expression during pupal development. *Eur J Biochem* **257**, 599606 (1998).

582. Hurst, D., Rylett, C. M., Isaac, R. E. & Shirras, A. D. The drosophila angiotensin-converting enzyme homologue Ance is required for spermiogenesis. *Dev. Biol.* **254**, 238–247 (2003).

583. Crackower, M. A. *et al.* Angiotensin-converting enzyme 2 is an essential regulator of heart function. *Nat. 2002 4176891* **417**, 822–828 (2002).

584. Coates, D. *et al.* Functional Conservation of the Active Sites of Human and Drosophila Angiotensin I-Converting Enzyme†. *Biochemistry* **39**, 8963–8969 (2000).

585. Cornell, M. J. *et al.* Cloning and expression of an evolutionary conserved single-domain angiotensin converting enzyme from Drosophila melanogaster. *J. Biol. Chem.* **270**, 13613–13619 (1995).

586. Akif, M. *et al.* High-Resolution Crystal Structures of Drosophila melanogaster Angiotensin-Converting Enzyme in Complex with Novel Inhibitors and Antihypertensive Drugs. *J. Mol. Biol.* **400**, 502–517 (2010).

587. Lee, S. H., Gomes, S. M., Boulianne, G. L., Ghalayini, J. & Iliadi, K. G. Angiotensin Converting Enzyme Inhibitors and Angiotensin Receptor Blockers Rescue Memory Defects in Drosophila-Expressing Alzheimer's Disease-Related Transgenes Independently of the Canonical Renin Angiotensin System. *eNeuro* **7**, (2020).

588. Jama, H. A. *et al.* Rodent models of hypertension. *Br. J. Pharmacol.* **179**, 918–937 (2022).

589. Esther Jr, C. R. *et al.* Mice lacking angiotensin-converting enzyme have low blood pressure, renal pathology, and reduced male fertility. *Lab. Investig. J. Tech. Methods Pathol.* **74**, 953–965 (1996).

590. F, P. *et al.* Paradoxical role of angiotensin II type 2 receptors in resistance arteries of old rats. *Hypertens. Dallas Tex 1979* **50**, 96–102 (2007).

591. Benetos, A., Laurent, S., Hoeks, A. P., Boutouyrie, P. H. & Safar, M. E. Arterial alterations with aging and high blood pressure. A noninvasive study of carotid and femoral arteries. *Arterioscler. Thromb. J. Vasc. Biol.* **13**, 90–97 (1993).

592. Assayag, P. *et al.* Senescent Heart Compared With Pressure Overload–Induced Hypertrophy. *Hypertension* **29**, 15–21 (1997).

593. Miller, A. J. & Arnold, A. C. The renin-angiotensin system and cardiovascular autonomic control in aging. *Peptides* **150**, 170733 (2022).

594. Willcox, D. C. *et al.* Life at the extreme limit: Phenotypic characteristics of supercentenarians in Okinawa. *J. Gerontol. - Ser. Biol. Sci. Med. Sci.* **63**, 1201–1208 (2008).

595. Hirata, T. *et al.* Associations of cardiovascular biomarkers and plasma albumin with exceptional survival to the highest ages. *Nat. Commun.* **11**, (2020).

596. Sato, Y. *et al.* Novel bile acid biosynthetic pathways are enriched in the microbiome of centenarians. *Nat. 2021 5997885* **599**, 458–464 (2021).

597. Andersen, S. L., Sebastiani, P., Dworkis, D. A., Feldman, L. & Perls, T. T. Health Span Approximates Life Span Among Many Supercentenarians: Compression of Morbidity at the Approximate Limit of Life Span. *J. Gerontol. Ser. A* **67A**, 395–405 (2012).

598. Sebastiani, P. *et al.* Meta-analysis of genetic variants associated with human exceptional longevity. *Aging* **5**, 653–661 (2013).

599. Revelas, M. *et al.* Review and meta-analysis of genetic polymorphisms associated with exceptional human longevity. *Mech. Ageing Dev.* **175**, 24–34 (2018).

600. Rigat, B. *et al.* An insertion/deletion polymorphism in the angiotensin I-converting enzyme gene accounting for half the variance of serum enzyme levels. *J. Clin. Invest.* **86**, 1343–1346 (1990).

601. Sayed-Tabatabaei, F. A., Oostra, B. A., Isaacs, A., Van Duijn, C. M. & Witteman, J. C. M. ACE polymorphisms. *Circ. Res.* **98**, 1123–1133 (2006).

602. Batzer, M. A. *et al.* African origin of human-specific polymorphic Alu insertions. *Proc. Natl. Acad. Sci. U. S. A.* **91**, 12288–12292 (1994).

603. Li, X., Sun, X., Li, J. & Xue, F. Worldwide spatial genetic structure of angiotensin-converting enzyme gene: a new evolutionary ecological evidence for the thrifty genotype hypothesis. *Eur. J. Hum. Genet.* **19**, 1002–1008 (2011).

604. Hamdi, H. K. & Castellon, R. A genetic variant of ACE increases cell survival: a new paradigm for biology and disease. *Biochem. Biophys. Res. Commun.* **318**, 187–191 (2004).

605. Delanghe J.R., Speekaert, M.M., Buyzere, M. L. The host's angiotensin-converting enzyme polymorphism may explain epidemiological findings in COVID-19 infections. *Clincica Chim. Acta* 192–193 (2020) doi:10.1016/j.cca.2020.03.031.

606. LongevityMap: Genetic association studies of longevity. https://genomics.senescence.info/longevity/search.php?search=ACE.

607. Garatachea, N., Marín, P. J. & Lucia, A. The ACE DD genotype and D-allele are associated with exceptional longevity: A meta-analysis. *Ageing Res. Rev.* **12**, 1079–1087 (2013).

608. Kwang Chae, Y. *et al.* Cancer Investigation Reduced Risk of Breast Cancer Recurrence in Patients Using ACE Inhibitors, ARBs, and/or Statins CAUSATION AND PREVENTION Reduced Risk of Breast Cancer Recurrence in Patients Using ACE Inhibitors, ARBs, and/or Statins. *Cancer Invest.* **29**, 585–593 (2011).

609. Zoja, C. *et al.* Adding a statin to a combination of ACE inhibitor and ARB normalizes proteinuria in experimental diabetes, which translates into full renoprotection. *Am. J. Physiol. - Ren. Physiol.* **299**, 1203–1211 (2010).

610. Faglia, E. *et al.* Effectiveness of combined therapy with angiotensin-converting enzyme inhibitors and statins in reducing mortality in diabetic patients with critical limb ischemia: An observational study. *Diabetes Res. Clin. Pract.* **103**, 292–297 (2014).

611. Abdel-Zaher, A. O., Elkoussi, A. E. A., Abudahab, L. H., Elbakry, M. H. & Elsayed, E. A. E. Effect of simvastatin on the antihypertensive activity of losartan in hypertensive hypercholesterolemic animals and patients: Role of nitric oxide, oxidative stress, and high-sensitivity C-reactive protein. *Fundam. Clin. Pharmacol.* **28**, 237–248 (2014).

612. Tatei, K., Cai, H., Ip, Y. T. & Levine, M. Race: a drosophila homologue of the angiotensin converting enzyme. *Mech. Dev.* **51**, 157–168 (1995).

613. Nichols, H. J., Zecherle, L. & Arbuckle, K. Patterns of philopatry and longevity contribute to the evolution of post-reproductive lifespan in mammals. *Biol. Lett.* **12**, (2016).

614. Burnham, S., Smith, J. A., Lee, A. J., Isaac, R. E. & Shirras, A. D. The angiotensin-converting enzyme (ACE) gene family of Anopheles gambiae. *BMC Genomics* **6**, 1–13 (2005).

615. Ekbote, U., Looker, M. & Isaac, R. E. ACE inhibitors reduce fecundity in the mosquito, Anopheles stephensi. *Comp. Biochem. Physiol. B Biochem. Mol. Biol.* **134**, 593–598 (2003).

616. Abu Hasan, Z. I. *et al.* The toxicity of angiotensin converting enzyme inhibitors to larvae of the disease vectors Aedes aegypti and Anopheles gambiae. *Sci. Rep. 2017 71* **7**, 1–10 (2017).

617. Ekbote, U. V., Weaver, R. J. & Isaac, R. E. Angiotensin I-converting enzyme (ACE) activity of the tomato moth, Lacanobia oleracea: Changes in levels of activity during development and after copulation suggest roles during metamorphosis and reproduction. *Insect Biochem. Mol. Biol.* **33**, 989–998 (2003).

618. Wijffels, G. *et al.* Cloning and characterisation of angiotensin-converting enzyme from the dipteran species, Haematobia irritans exigua, and its expression in the maturing male reproductive system. *Eur. J. Biochem.* **237**, 414–423 (1996).

619. Lamango, N. S. & Isaac, R. E. Identification and properties of a peptidyl dipeptidase in the housefly, Musca domestica, that resembles mammalian angiotensin-converting enzyme. *Biochem. J.* **299 (Pt 3)**, 651–657 (1994).

620. Loeb, M. J., De Loof, A., Schoofs, L. & Isaac, E. Angiotensin ii and angiotensin-converting enzyme as candidate compounds modulating the effects of testis ecdysiotropin in testes of the gypsy moth, Lymantria dispar. *Gen. Comp. Endocrinol.* **112**, 232–239 (1998).

621. Nagaoka, S., Kawasaki, S., Kawasaki, H. & Kamei, K. The angiotensin converting enzyme (ACE) inhibitor, captopril disrupts the motility activation of sperm from the silkworm, Bombyx mori. *J. Insect Physiol.* **103**, 18–28 (2017).

622. Lemeire, E., Vanholme, B., Van Leeuwen, T., Van Camp, J. & Smagghe, G. Angiotensin-converting enzyme in Spodoptera littoralis: Molecular characterization, expression and activity profile during development. *Insect Biochem. Mol. Biol.* **38**, 166–175 (2008).

623. Wang, W. *et al.* Angiotensin-converting enzymes modulate aphid-plant interactions. *Sci. Rep.* **5**, (2015).

624. Nathalie, M. *et al.* Isolation of angiotensin converting enzyme from testes of Locusta migratoria (Orthoptera). (2003) doi:10.14411/eje.2003.070.

625. Vandingenen, A. *et al.* Presence of angiotensin converting enzyme (ACE) interactive factors in ovaries of the grey fleshfly Neobellieria bullata. *Comp. Biochem. Physiol. B Biochem. Mol. Biol.* **132**, 27–35 (2002).

626. Wijffels, G., Gough, J., Muharsini, S., Donaldson, A. & Eisemann, C. Expression of angiotensin-converting enzyme-related carboxydipeptidases in the larvae of four species of fly. *Insect Biochem. Mol. Biol.* **27**, 451–460 (1997).

627. Vandingenen, A. *et al.* Captopril, a specific inhibitor of angiotensin converting enzyme, enhances both trypsin and vitellogenin titers in the grey fleshfly Neobellieria bullata. *Arch. Insect Biochem. Physiol.* **47**, 161–167 (2001).

628. Wang, X. *et al.* Immune function of an angiotensin-converting enzyme against Rice stripe virus infection in a vector insect. *Virology* **533**, 137–144 (2019).

629. Isaac, R. E., Ekbote, U., Coates, D. & Shirras, A. D. Insect angiotensin-converting enzyme: A processing enzyme with broad substrate specificity and a role in reproduction. *Ann. N. Y. Acad. Sci.* **897**, 342–347 (1999).

630. Smiley, J. W. & Doig, M. T. Distribution and characterization of angiotensin-converting enzyme-like activity in tissues of the blue crab Callinectes sapidus. *Comp Biochem Physiol* **108**, 491–496 (1994).

631. Sook Chung, J. & Webster, S. G. Angiotensin-converting enzyme-like activity in crab gills and its putative role in degradation of crustacean hyperglycemic hormone. *Arch. Insect Biochem. Physiol.* **68**, 171–180 (2008).

632. Kamech, N. *et al.* Evidence for an angiotensin-converting enzyme (ACE) polymorphism in the crayfish Astacus leptodactylus. *Peptides* **28**, 1368–1374 (2007).

633. Riviere, G., Fellous, A., Franco, A., Bernay, B. & Favrel, P. A crucial role in fertility for the oyster angiotensin-converting enzyme orthologue CgACE. *PLoS ONE* **6**, (2011).

634. Laurent, V., Stefano, G. & Salzet, M. Presence and biochemical properties of a molluscan invertebrate angiotensin-converting enzyme. *Regul. Pept.* **69**, 53–61 (1997).

635. Rivière, G. *et al.* Characterization of the first non-insect invertebrate functional angiotensin-converting enzyme (ACE): leech TtACE resembles the N-domain of mammalian ACE. *Biochem. J.* **382**, 565–573 (2004).

636. Lv, Y. *et al.* A Genomic Survey of Angiotensin-Converting Enzymes Provides Novel Insights into Their Molecular Evolution in Vertebrates. *Molecules* **23**, 2923 (2018).

637. Vercruysse, L. *et al.* The angiotensin converting enzyme inhibitor captopril reduces oviposition and ecdysteroid levels in Lepidoptera. *Arch. Insect Biochem. Physiol.* **57**, 123–132 (2004).

638. Ramaraj, P., Kessler, S. P., Colmenares, C. & Sen, G. C. Selective Restoration of Male Fertility in Mice Lacking Angiotensin-converting Enzymes by Sperm-specific Expression of the Testicular Isozyme. *J Clin Invest* **102**, 371–378 (1998).

639. Hagaman, J. R. *et al.* Angiotensin-converting enzyme and male fertility. *Proc. Natl. Acad. Sci. U. S. A.* **95**, 2552–2557 (1998).

640. Robida-Stubbs, S. *et al.* TOR Signaling and Rapamycin Influence Longevity by Regulating SKN-1/Nrf and DAF-16/FoxO. *Cell Metab.* **15**, 713–724 (2012).

641. Bjedov, I. *et al.* Mechanisms of Life Span Extension by Rapamycin in the Fruit Fly Drosophila melanogaster. *Cell Metab.* **11**, 35–46 (2010).

642. Hu, D. *et al.* Metformin: A Potential Candidate for Targeting Aging Mechanisms. *Aging Dis.* **12**, 480 (2021).

643. Glossmann, H. H. & Lutz, O. M. D. Metformin and Aging: A Review. *Gerontology* **65**, 581–590 (2019).

644. Justice, J. N. *et al.* A framework for selection of blood-based biomarkers for geroscience-guided clinical trials: report from the TAME Biomarkers Workgroup. *GeroScience* **40**, 419–436 (2018).

645. Ross, C. N. *et al.* Metabolic Consequences of Long-Term Rapamycin Exposure on Common Marmoset Monkeys (Callithrix Jacchus) Repository Citation. *Aging* **7**, 964 (2015).

646. Kaeberlein, M., Creevy, K. E. & Promislow, D. E. L. The dog aging project: translational geroscience in companion animals. *Mamm. Genome* **27**, 279–288 (2016).

647. Zehnder, J., Katzung, S. M. & Trevor, A. *Basic and clinical pharmacology*. (McGraw-Hill Medical, New York, 2009).

648. Gabrawy, M. M. *et al.* Genome-Wide Analysis in Drosophila Reveals the Genetic Basis of Variation in Age-Specific Physical Performance and Response to ACE Inhibition. *Genes* **13**, 143 (2022).

649. Ferder, L., Inserra, F., Romano, L., Ercole, L. & Pszenny, V. Effects of angiotensin-converting enzyme inhibition on mitochondrial number in the aging mouse. *Am. J. Physiol. - Cell Physiol.* **265**, C15–C18 (1993).

650. Ferder, L. F., Inserra, F. & Basso, N. Advances in our understanding of aging: role of the renin–angiotensin system. *Curr. Opin. Pharmacol.* **2**, 189–194 (2002).

651. Inserra, F. Effects of renin–angiotensin system blockade in the aging kidney. *Exp. Gerontol.* **38**, 237–244 (2003).

652. Basso, N. *et al.* Protective effect of the inhibition of the renin–angiotensin system on aging. *Regul. Pept.* **128**, 247–252 (2005).

653. Mattson, M. P. & Maudsley, S. Live Longer sans the AT1A Receptor. *Cell Metab.* **9**, 403–405 (2009).

654. Nishiyama, A., Matsusaka, T. & Miyata, T. Angiotensin II type 1A receptor deficiency and longevity. *Nephrol. Dial. Transplant.* **24**, 3280–3281 (2009).

655. Benigni, A., Cassis, P. & Remuzzi, G. Angiotensin II revisited: new roles in inflammation, immunology and aging. *EMBO Mol. Med.* **2**, 247–257 (2010).

656. Cassis, P., Conti, S., Remuzzi, G. & Benigni, A. Angiotensin receptors as determinants of life span. *Pflugers Arch.* **459**, 325–332 (2010).

657. Benigni, A. *et al.* Variations of the angiotensin II type 1 receptor gene are associated with extreme human longevity. *AGE* **35**, 993–1005 (2013).

658. Kim, D. H., Grün, D. & Van Oudenaarden, A. Dampening of expression oscillations by synchronous regulation of a microRNA and its target. *Nat. Genet.* **45**, 1337–1344 (2013).

659. Hendriks, G. J., Gaidatzis, D., Aeschimann, F. & Großhans, H. Extensive Oscillatory Gene Expression during C. elegans Larval Development. *Mol. Cell* **53**, 380–392 (2014).

660. Wrapp, D. *et al.* Cryo-EM structure of the 2019-nCoV spike in the prefusion conformation. *Science* **367**, 1260–1263 (2020).

661. Donohue, W. L. Dysendocrinism. *J. Pediatr.* **32**, 739–748 (1948).

662. Longo, N. *et al.* Genotype–phenotype correlation in inherited severe insulin resistance. *Hum. Mol. Genet.* **11**, 1465–1475 (2002).

663. Cassada, R. C. & Russell, R. L. The dauerlarva, a post-embryonic developmental variant of the nematode Caenorhabditis elegans. *Dev. Biol.* **46**, 326–342 (1975).

664. Lindblom, T. H. & Dodd, A. K. Xenobiotic detoxification in the nematode Caenorhabditis elegans. *J. Exp. Zoolog. A Comp. Exp. Biol.* **305A**, 720–730 (2006).

665. Burns, A. R. *et al.* A predictive model for drug bioaccumulation and bioactivity in Caenorhabditis elegans. *Nat. Chem. Biol.* **6**, 549–557 (2010).

666. Xiong, H., Pears, C. & Woollard, A. An enhanced C. elegans based platform for toxicity assessment. *Sci. Rep.* **7**, 9839 (2017).

667. Bahmaei, M., Khosravi, A., Zamiri, C., Massoumi, A. & Mahmoudian, M. Determination of captopril in human serum by high performance liquid chromatography using solid-phase extraction. *J. Pharm. Biomed. Anal.* **15**, 1181–1186 (1997).

668. Huang, T. *et al.* Simultaneous determination of captopril and hydrochlorothiazide in human plasma by reverse-phase HPLC from linear gradient elution. *J. Pharm. Biomed. Anal.* **41**, 644–648 (2006).

669. Riddle, D. L., Swanson, M. M. & Albert, P. S. Interacting genes in nematode dauer larva formation. *Nature* **290**, 668–671 (1981).

670. Swanson, M. M. & Riddle, D. L. Critical periods in the development of the Caenorhabditis elegans dauer larva. *Dev. Biol.* **84**, 27–40 (1981).

671. Vowels, J. J. & Thomas, J. H. Genetic Analysis of Chemosensory Control of Dauer Formation in Caenorhabditis Elegans. *Genetics* **130**, 105–123 (1992).

672. Larsen, P. L. Aging and resistance to oxidative damage in Caenorhabditis elegans. *Proc. Natl. Acad. Sci.* **90**, 8905–8909 (1993).

673. Lithgow, G. J., White, T. M., Melov, S. & Johnson, T. E. Thermotolerance and extended life-span conferred by single-gene mutations and induced by thermal stress. *Proc. Natl. Acad. Sci. U. S. A.* **92**, 7540–7544 (1995).

674. Johnson, T. E. *et al.* Gerontogenes mediate health and longevity in nematodes through increasing resistance to environmental toxins and stressors. *Exp. Gerontol.* **35**, 687–694 (2000).

675. Luo, S. & Murphy, C. T. Caenorhabditis elegans reproductive aging: Regulation and underlying mechanisms. *Genesis* **49**, 53–65 (2011).

676. Zuryn, S., Le Gras, S., Jamet, K. & Jarriault, S. A Strategy for Direct Mapping and Identification of Mutations by Whole-Genome Sequencing. *Genetics* **186**, 427–430 (2010).

677. Papadopoulos, J. S. & Agarwala, R. COBALT: constraint-based alignment tool for multiple protein sequences. *Bioinformatics* **23**, 1073–1079 (2007).

678. Dorman, J. B., Albinder, B., Shroyer, T. & Kenyon, C. The age-1 and daf-2 genes function in a common pathway to control the lifespan of Caenorhabditis elegans. *Genetics* **141**, 1399–1406 (1995).

679. Friedman, D. B. & Johnson, T. E. Three Mutants That Extend Both Mean and Maximum Life Span of the Nematode, Caenorhabditis Elegans, Define the Age-1 Gene. *J. Gerontol.* **43**, B102–B109 (1988).

680. Klass, M. R. A method for the isolation of longevity mutants in the nematode Caenorhabditis elegans and initial results. *Mech. Ageing Dev.* **22**, 279–286 (1983).

681. Evason, K., Huang, C., Yamben, I., Covey, D. F. & Kornfeld, K. Anticonvulsant medications extend worm life-span. *Science* **307**, 258–262 (2005).

682. Collins, J. J., Evason, K., Pickett, C. L., Schneider, D. L. & Kornfeld, K. The anticonvulsant ethosuximide disrupts sensory function to extend C. elegans lifespan. *PLoS Genet.* **4**, e1000230 (2008).

683. Ailion, M. & Thomas, J. H. Isolation and characterization of high-temperature-induced dauer formation mutants in Caenorhabditis elegans. *Genetics* **165**, 127–144 (2003).

684. Larsen, P. L., Albert, P. S. & Riddle, D. L. Genes that regulate both development and longevity in Caenorhabditis elegans. *Genetics* **139**, 1567–1583 (1995).

685. Lin, K., Dorman, J. B., Rodan, A. & Kenyon, C. daf-16: An HNF-3/forkhead family member that can function to double the life-span of Caenorhabditis elegans. *Science* **278**, 1319–1322 (1997).

686. Ogg, S. *et al.* The fork head transcription factor DAF-16 transduces insulin-like metabolic and longevity signals in C. elegans. *Nature* **389**, 994–999 (1997).

687. Gottlieb, S. & Ruvkun, G. daf-2, daf-16 and daf-23: Genetically interacting genes controlling dauer formation in Caenorhabditis elegans. *Genetics* **137**, 107–120 (1994).

688. Honda, Y. & Honda, S. The daf-2 gene network for longevity regulates oxidative stress resistance and Mn-superoxide dismutase gene expression in Caenorhabditis elegans. *FASEB J.* **13**, 1385–1393 (1999).

689. Yanase, S., Yasuda, K. & Ishii, N. Adaptive responses to oxidative damage in three mutants of Caenorhabditis elegans (age-1, mev-1 and daf-16) that affect life span. *Mech. Ageing Dev.* **123**, 1579–1587 (2002).

690. Landis, J. N. & Murphy, C. T. Integration of diverse inputs in the regulation of Caenorhabditis elegans DAF-16/FOXO. *Dev. Dyn.* **239**, 1405–1412 (2010).

691. Ludewig, A. H. *et al.* A novel nuclear receptor/coregulator complex controls C. elegans lipid metabolism, larval development, and aging. *Genes Dev.* **18**, 2120–2133 (2004).

692. Shostak, Y., Gilst, M. R. V., Antebi, A. & Yamamoto, K. R. Identification of C. elegans DAF-12-binding sites, response elements, and target genes. *Genes Dev.* **18**, 2529–2544 (2004).

693. Fisher, A. L. & Lithgow, G. J. The nuclear hormone receptor DAF-12 has opposing effects on Caenorhabditis elegans lifespan and regulates genes repressed in multiple long-lived worms. *Aging Cell* **5**, 127–138 (2006).

694. Thomas, J. H., Birnby, D. A. & Vowels, J. J. Evidence for parallel processing of sensory information controlling dauer formation in Caenorhabditis elegans. *Genetics* **134**, 1105–1117 (1993).

695. Antebi, A., Culotti, J. G. & Hedgecock, E. M. daf-12 regulates developmental age and the dauer alternative in Caenorhabditis elegans. *Development* **125**, 1191–1205 (1998).

696. Antebi, A., Yeh, W.-H., Tait, D., Hedgecock, E. M. & Riddle, D. L. daf-12 encodes a nuclear receptor that regulates the dauer diapause and developmental age in C. elegans. *Genes Dev.* **14**, 1512–1527 (2000).

697. Clancy, D. J. *et al.* Extension of life-span by loss of CHICO, a Drosophila insulin receptor substrate protein. *Science* **292**, 104–106 (2001).

698. Tatar, M. *et al.* A Mutant Drosophila Insulin Receptor Homolog That Extends Life-Span and Impairs Neuroendocrine Function. *Science* **292**, 107–110 (2001).

699. Taguchi, A. & White, M. F. Insulin-Like Signaling, Nutrient Homeostasis, and Life Span. *Annu. Rev. Physiol.* **70**, 191–212 (2008).

700. Bartke, A. Insulin and aging. *Cell Cycle* **7**, 3338–3343 (2008).

701. Kannan, K. & Fridell, Y.-W. Functional implications of Drosophila insulin-like peptides in metabolism, aging, and dietary restriction. *Front. Physiol.* **4**, 288 (2013).

702. Bonafè, M. *et al.* Polymorphic variants of insulin-like growth factor I (IGF-I) receptor and phosphoinositide 3-kinase genes affect IGF-I plasma levels and human longevity: cues for an evolutionarily conserved mechanism of life span control. *J. Clin. Endocrinol. Metab.* **88**, 3299–3304 (2003).

703. Watson, G. S. & Craft, S. The Role of Insulin Resistance in the Pathogenesis of Alzheimer's Disease. *CNS Drugs* **17**, 27–45 (2003).

704. Cole, G. M. & Frautschy, S. A. The role of insulin and neurotrophic factor signaling in brain aging and Alzheimer's Disease. *Exp. Gerontol.* **42**, 10–21 (2007).

705. Pierce, S. B. *et al.* Regulation of DAF-2 receptor signaling by human insulin and ins-1, a member of the unusually large and diverse C. elegans insulin gene family. *Genes Dev.* **15**, 672–686 (2001).

706. Kimura, K. D., Riddle, D. L. & Ruvkun, G. The C. elegans DAF-2 Insulin-Like Receptor is Abundantly Expressed in the Nervous System and Regulated by Nutritional Status. *Cold Spring Harb. Symp. Quant. Biol.* **76**, 113–120 (2011).

707. Lewis, J. A. & Hodgkin, J. A. Specific neuroanatomical changes in chemosensory mutants of the nematode Caenorhabditis elegans. *J. Comp. Neurol.* **172**, 489–510 (1977).

708. Ohno, H. *et al.* Role of synaptic phosphatidylinositol 3-kinase in a behavioral learning response in C. elegans. *Science* **345**, 313–317 (2014).

709. Bulger, D. A. *et al.* Caenorhabditis elegans DAF-2 as a Model for Human Insulin Receptoropathies. *G3 Genes Genomes Genet.* **7**, 257–268 (2017).

710. Partridge, L., Fuentealba, M. & Kennedy, B. K. The quest to slow ageing through drug discovery. *Nat. Rev. Drug Discov.* **19**, 513–532 (2020).

711. Burggren, W. W. & Reiber, C. Evolution of cardiovascular systems and their endothelial linings. in *Endothelial Biomedicine* 29–49 (Cambridge University Press, 2007).

712. Golden, J. W. & Riddle, D. L. The Caenorhabditis elegans dauer larva: Developmental effects of pheromone, food, and temperature. *Dev. Biol.* **102**, 368–378 (1984).

713. Ludewig, A. H. & Schroeder, F. C. Ascaroside signaling in C. elegans. in *WormBook: The Online Review of C. elegans Biology* (WormBook, 2018).

714. Motola, D. L. *et al.* Identification of Ligands for DAF-12 that Govern Dauer Formation and Reproduction in C. elegans. *Cell* **124**, 1209–1223 (2006).

715. Luciani, G. M. *et al.* Dafadine inhibits DAF-9 to promote dauer formation and longevity of Caenorhabditis elegans. *Nat. Chem. Biol.* **7**, 891–893 (2011).

716. Moore, B. T., Jordan, J. M. & Baugh, L. R. WormSizer: High-throughput Analysis of Nematode Size and Shape. *PLoS ONE* **8**, e57142 (2013).

717. Zuryn, S. & Jarriault, S. Deep sequencing strategies for mapping and identifying mutations from genetic screens. *Worm* **2**, e25081 (2013).

718. Langmead, B. & Salzberg, S. L. Fast gapped-read alignment with Bowtie 2. *Nat. Methods* **9**, 357–359 (2012).

719. Arribere, J. A. *et al.* Efficient marker-free recovery of custom genetic modifications with CRISPR/Cas9 in Caenorhabditis elegans. *Genetics* **198**, 837–846 (2014).

720. Schmittgen, T. D. & Livak, K. J. Analyzing real-time PCR data by the comparative CT method. *Nat. Protoc.* **3**, 1101–1108 (2008).

721. Bourque, C. W. Central mechanisms of osmosensation and systemic osmoregulation. *Nat. Rev. Neurosci. 2008 97* **9**, 519–531 (2008).

722. Suzuki, H. *et al.* Functional asymmetry in Caenorhabditis elegans taste neurons and its computational role in chemotaxis. *Nature* **454**, 114–117 (2008).

723. Thiele, T. R., Faumont, S. & Lockery, S. R. The Neural Network for Chemotaxis to Tastants in Caenorhabditis elegans Is Specialized for Temporal Differentiation. *J. Neurosci.* **29**, 11904–11911 (2009).

724. Apfeld, J. & Kenyon, C. Regulation of lifespan by sensory perception in Caenorhabditis elegans. *Nat. 1999 4026763* **402**, 804–809 (1999).

725. Alcedo, J. & Kenyon, C. Regulation of C. elegans Longevity by Specific Gustatory and Olfactory Neurons. *Neuron* **41**, 45–55 (2004).

726. Félix, M.-A. & Braendle, C. The natural history of Caenorhabditis elegans. *Curr. Biol.* **20**, R965–R969 (2010).

727. Hosono, R., Mitsui, Y., Sato, Y., Aizawa, S. & Miwa, J. Life span of the wild and mutant nematode Caenorhabditis elegans: Effects of Sex, Sterilization, and Temperature. *Exp. Gerontol.* **17**, 163–172 (1982).

728. Lamitina, T., Huang, C. G. & Strange, K. Genome-wide RNAi screening identifies protein damage as a regulator of osmoprotective gene expression. *Proc. Natl. Acad. Sci. U. S. A.* **103**, 12173–12178 (2006).

729. Urso, S. J., Comly, M., Hanover, J. A. & Lamitina, T. The O-GlcNAc transferase OGT is a conserved and essential regulator of the cellular and organismal response to hypertonic stress. *PLOS Genet.* **16**, e1008821 (2020).

730. Savory, F. R., Sait, S. M. & Hope, I. A. DAF-16 and Δ9 Desaturase Genes Promote Cold Tolerance in Long-Lived Caenorhabditis elegans age-1 Mutants. *PLoS ONE* **6**, e24550 (2011).

731. Lithgow, G. J., White, T. M., Hinerfeld, D. A. & Johnson, T. E. Thermotolerance of a long-lived mutant of Caenorhabditis elegans. *J. Gerontol.* **49**, B270-276 (1994).

732. Eimer, W. A. *et al.* Alzheimer's Disease-Associated β-Amyloid Is Rapidly Seeded by Herpesviridae to Protect against Brain Infection. *Neuron* **99**, 56-63.e3 (2018).

733. Itzhaki, R. F. Corroboration of a major role for herpes simplex virus type 1 in Alzheimer's disease. *Front. Aging Neurosci.* **10**, (2018).

734. Félix, M.-A. *et al.* Natural and Experimental Infection of Caenorhabditis Nematodes by Novel Viruses Related to Nodaviruses. *PLOS Biol.* **9**, e1000586 (2011).

735. Soubrier, F. *et al.* Two putative active centers in human angiotensin I-converting enzyme revealed by molecular cloning. *Proc. Natl. Acad. Sci. U. S. A.* **85**, 9386–9390 (1988).

736. Wei, L., Clauser, E., Alhenc-Gelas, F. & Corvol, P. The two homologous domains of human angiotensin I-converting enzyme interact differently with competitive inhibitors. *J. Biol. Chem.* **267**, 13398–13405 (1992).

737. Junot, C. *et al.* RXP 407, a Selective Inhibitor of the N-Domain of Angiotensin I-Converting Enzyme, Blocks in Vivo the Degradation of Hemoregulatory Peptide Acetyl-Ser-Asp-Lys-Pro with No Effect on Angiotensin I Hydrolysis. *J. Pharmacol. Exp. Ther.* **297**, 606–611 (2001).

738. Robinson, S., Lenfant, M., Wdzieczak-Bakala, J., Melville, J. & Riches, A. The mechanism of action of the tetrapeptide acetyl-N-Ser-Asp-Lys-Pro (AcSDKP) in the control of haematopoietic stem cell proliferation. *Cell Prolif.* **25**, 623–632 (1992).

739. Rieger, K. J. *et al.* Involvement of human plasma angiotensin I-converting enzyme in the degradation of the haemoregulatory peptide *N* -acetyl-seryl-aspartyl-lysyl-proline. *Biochem. J.* **296**, 373–378 (1993).

740. Natesh, R., Schwager, S. L. U., Sturrock, E. D. & Acharya, K. R. Crystal structure of the human angiotensin-converting enzyme–lisinopril complex. *Nat. 2003 4216922* **421**, 551–554 (2003).

741. Brew, K. Structure of human ACE gives new insights into inhibitor binding and design. *Trends Pharmacol. Sci.* **24**, 391–394 (2003).

742. Hochbaum, D. *et al.* DAF-12 Regulates a Connected Network of Genes to Ensure Robust Developmental Decisions. *PLOS Genet.* **7**, e1002179 (2011).

743. Fisher, A. L. & Lithgow, G. J. The nuclear hormone receptor DAF-12 has opposing effects on Caenorhabditis elegans lifespan and regulates genes repressed in multiple long-lived worms. *Aging Cell* **5**, 127–138 (2006).

744. Antebi, A. Steroid Regulation of C. elegans Diapause, Developmental Timing, and Longevity. *Curr. Top. Dev. Biol.* **105**, 181–212 (2013).

745. Snow, M. I. & Larsen, P. L. Structure and expression of daf-12: a nuclear hormone receptor with three isoforms that are involved in development and aging in Caenorhabditis elegans. *Biochim. Biophys. Acta BBA - Gene Struct. Expr.* **1494**, 104–116 (2000).

746. Wheeler, J. M. & Thomas, J. H. Identification of a novel gene family involved in osmotic stress response in Caenorhabditis elegans. *Genetics* **174**, 1327–1336 (2006).

747. Solomon, A. *et al.* Caenorhabditis elegans OSR-1 regulates behavioral and physiological responses to hyperosmotic environments. *Genetics* **167**, 161–170 (2004).

748. Uchida, O., Nakano, H., Koga, M. & Ohshima, Y. The C. elegans che-1 gene encodes a zinc finger transcription factor required for specification of the ASE chemosensory neurons. *Development* **130**, 1215–1224 (2003).

749. Wicks, S. R., de Vries, C. J., van Luenen, H. G. A. M. & Plasterk, R. H. A. CHE-3, a Cytosolic Dynein Heavy Chain, Is Required for Sensory Cilia Structure and Function in Caenorhabditis elegans. *Dev. Biol.* **221**, 295–307 (2000).

Appendix

Appendix 1: List of Publications

Egan, B. M., Pohl, F., Anderson, X., Williams, S. C., Adodo, I. G., Hunt, P., Wang, Z., Chiu, C.-H., Scharf, A., Mosley, M., Kumar, S., Schneider, D. L., Fujiwara, H., Hsu, F.- F., Kornfeld, K. (2023). The ACE-inhibitor drug captopril inhibits ACN-1 to control dauer formation and aging. *bioRxiv* 2023.07.17.549402.

Kocsisova, Z.*, **Egan, B. M.***, Scharf, A., Anderson, X., Pohl, F. How to measure, analyze, and interpret age-related changes in *Caenorhabditis elegans*: lessons for mechanistic and evolutionary theories of aging. (Submitted for review) *, authors contributed equally.

Kocsisova, Z., Bagatelas, E., Santiago-Borges, J., Lei, H. C., **Egan, B. M.**, Schneider, D. L., Schedl, T., Kornfeld, K. (2023). Notch signaling in germ line stem cells controls reproductive aging in *C. elegans*. *PNaS*. (Accepted for publication).

Egan, B. M., Scharf, A., Pohl, F., & Kornfeld, K. (2022). Control of aging by the renin–angiotensin system: A review of *C. elegans*, *Drosophila*, and mammals. *Frontiers in Pharmacology*, *13*, 938650.

Murphy, J. T., Liu, H., Ma, X., Shaver, A., **Egan, B. M.**, Oh, C., Boyko, A., Mazer, T., Ang, S., Khopkar, R. and Javaheri, A., Kumar, S., Jiang, X., Ory, D., Mani, K., Matkovich, S. J., Kornfeld, K., Diwan, A. (2019). Simple nutrients bypass the requirement for HLH-30 in coupling lysosomal nutrient sensing to survival. *PLoS biology*, *17*(5), p.e3000245.

Kumar, S., **Egan, B. M.**, Kocsisova, Z., Schneider, D. L., Murphy, J. T., Diwan, A., & Kornfeld, K. (2019). Lifespan extension in *C. elegans* caused by bacterial colonization of the intestine and subsequent activation of an innate immune response. *Developmental cell*, *49*(1), 100-117.

Appendix 2: Supplemental data for Chapter 3

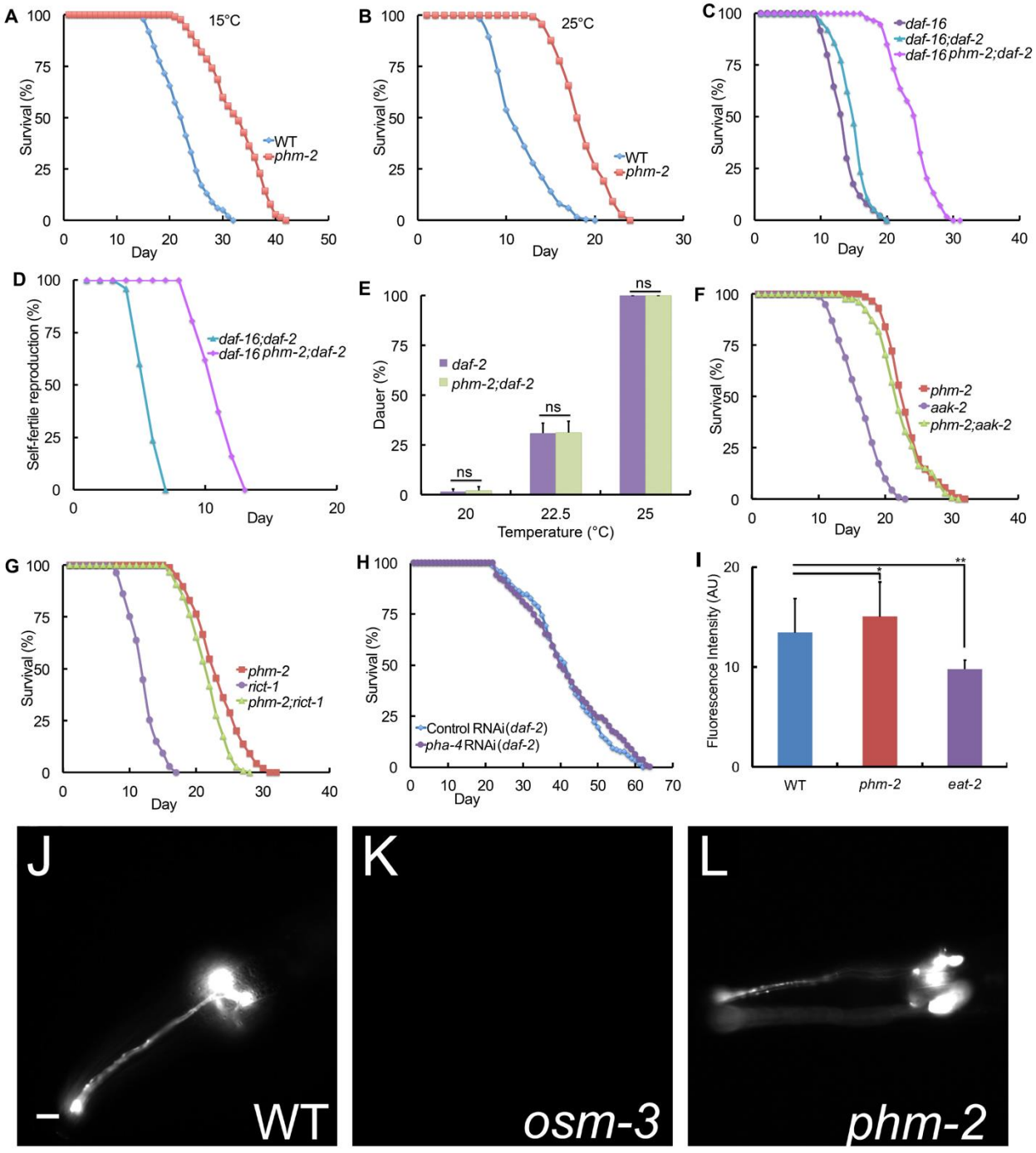

Figure S1. The *phm-2(lf)* extended lifespan phenotype was observed at multiple temperatures and in multiple genetic backgrounds

Animals were cultured on NGM dishes with live *E. coli* OP50 bacteria. **(A-B)** Survival curves of wild-type (blue) and *phm-2(am117)* (red) animals cultured at 15°C and 25°C. See **Table S1** for summary statistics of lifespan assays, number of animals and number of independent experiments.

(C-D) Survival and self-fertile reproduction curves at 20°C for the FOXO transcription factor gene *daf-16(mu86)*, *daf-16(mgDf47); daf-2(e1370)* and *daf-16(mu86) phm-2(am117); daf-2(e1370)* mutant animals. The *phm-2* extended lifespan and reproductive span phenotypes were not suppressed by *daf-16(lf)* (For panel D, n=8-9 animals).

(E) The percent of animals that form dauer larvae at three temperatures was determined for the insulin/IGF-1 receptor gene *daf-2(e1370)* and *phm-2(am117); daf-2(e1370)* animals. *phm-2(lf)* did not significantly affect the temperature sensitive Daf-c phenotype of *daf-2* mutants (Three biological replicates with N>100 animals each; n.s., not significant, $P > 0.05$ by Student's *t*-test). **(F-G)** Survival curves at 20°C for *phm-2(am117)*, the AMP kinase gene *aak-2(ok524), phm-2(am117)*; *aak-2(ok524),* the target of rapamycin complex 2 gene *rict-1(mg360)*, and *phm-2(am117)*; *rict-1(mg360)*. See **Table S1** for summary statistics of lifespan assays, number of animals and number of independent experiments.

(H) *daf-2(e1370)* mutant animals were cultured on *pha-4* RNAi bacteria or control RNAi bacteria. See **Table S4** for summary statistics of lifespan assays, number of animals and number of independent experiments.

(I) Quantification of whole animal fluorescence for wild type, *phm-2(am117)* and *eat-2(ad1116)* adult animals cultured with green fluorescent microspheres for 10 minutes. Values in arbitrary units (AU) are the average (+/-S.D.) of five biological replicates (N=35-61 animals per replicate). Tukey post hoc HSD; *, $P < 0.05$; **, $P < 0.01$.

(J-L) Wild-type, *phm-2(am117)* and *osm-3(p802)* animals were incubated with dye DiO that allows visualization of amphid neurons that project to the outside of the body. Representative fluorescence microscope images show the head region. WT and *phm-2(am117)* animals displayed strong DiO staining in amphid neuron axons and their cell bodies in the pharyngeal region. *osm-3(p802)* animals, which have defective amphid neuron morphology, did not display staining (the Dyf phenotype). Scale bar = 10 μm.

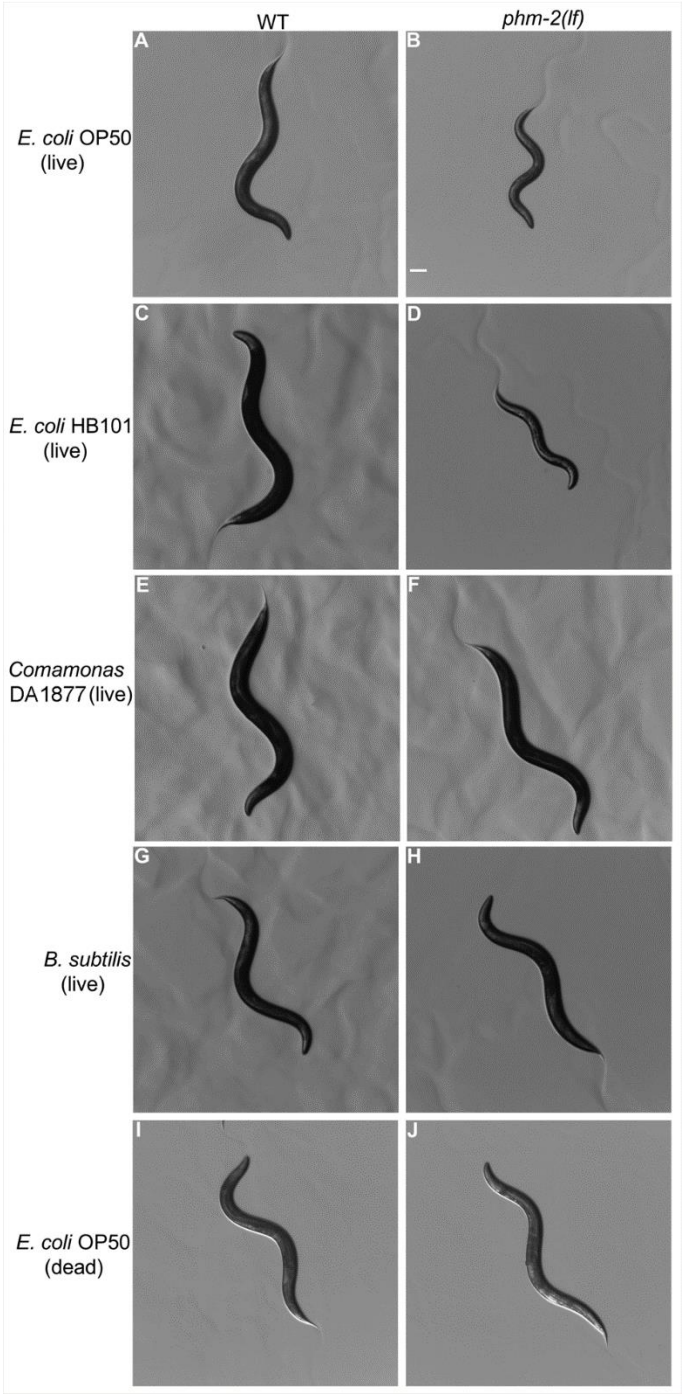

Figure S2. Diet affected the scrawny body morphology phenotype of *phm-2(lf)* mutants

Eggs from wild-type (left column) or *phm-2(am117*) (right column) hermaphrodites were cultured with the bacterial food sources labeled in each row. Bright field images of representative live animals were captured using a dissecting microscope with identical magnification on day four after the L4 stage. Live *E. coli* OP50, *E. coli* HB101, *Comamonas* DA1877*,* and *Bacillus subtilis* proliferated on the dish, whereas dead *E. coli* OP50 was treated with UV light. Scale bar = 100 μm.

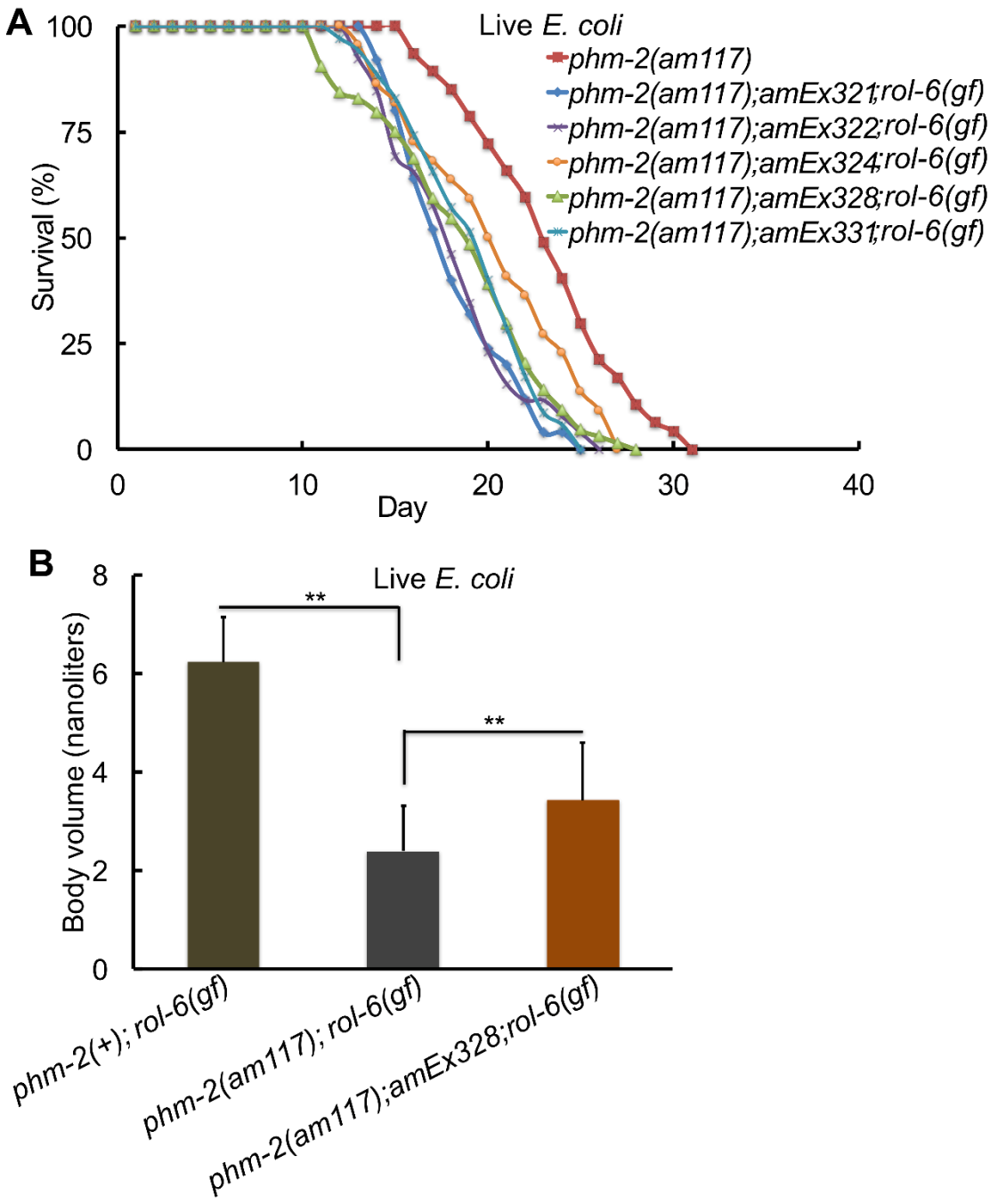

Figure S3. The wild-type F32B4.4a cDNA partially rescued the *phm-2(am117)* extended lifespan and scrawny body morphology phenotypes

(A) Transgenic animals contained the chromosomal mutation *phm-2(am117)* and an extrachromosomal array composed of plasmid pSK2 with the upstream *phm-2* promoter driving the F32B4.4a cDNA and the plasmid pRF4 that causes a dominant Rol phenotype used to identify transgenic animals. Five independently-derived transgenic strains were analyzed, named

amEx321, *amEx322*, *amEx324*, *amEx328*, and *amEx331*. Lifespan assays were initiated with L4 stage transgenic animals that displayed the Rol phenotype, and animals were cultured on NGM dishes with live *E. coli* OP50. All five transgenic strains displayed shorter mean (14-23%) and maximum (12-22%) lifespans than *phm-2(am117)* mutant animals. See **Table S1** for summary statistics of lifespan assays and number of animals analyzed.

(B) Bars represent the average volume of individual worms (+/-S.D) four days after the L4 stage determined by analyzing dissecting microscope images with the WormSizer algorithm. To control for the effects of the dominant Rol marker used to make transgenic strains, we used the integrated insertion sequence allele *acIs101* [F35E12.5p::GFP + *rol-6(su1006)*] to generate *acIs101; phm-2(am117)* animals that displayed the Rol and scrawny body morphology phenotypes. Transgenic *phm-2(am117); amEx328* animals displayed a significantly higher (42%) volume compared *acIs101; phm-2(am117)* animals when cultured on NGM dishes with live *E. coli* OP50 (n=30-43 animals analyzed: Tukey post hoc HSD; **, $P < 0.01$).

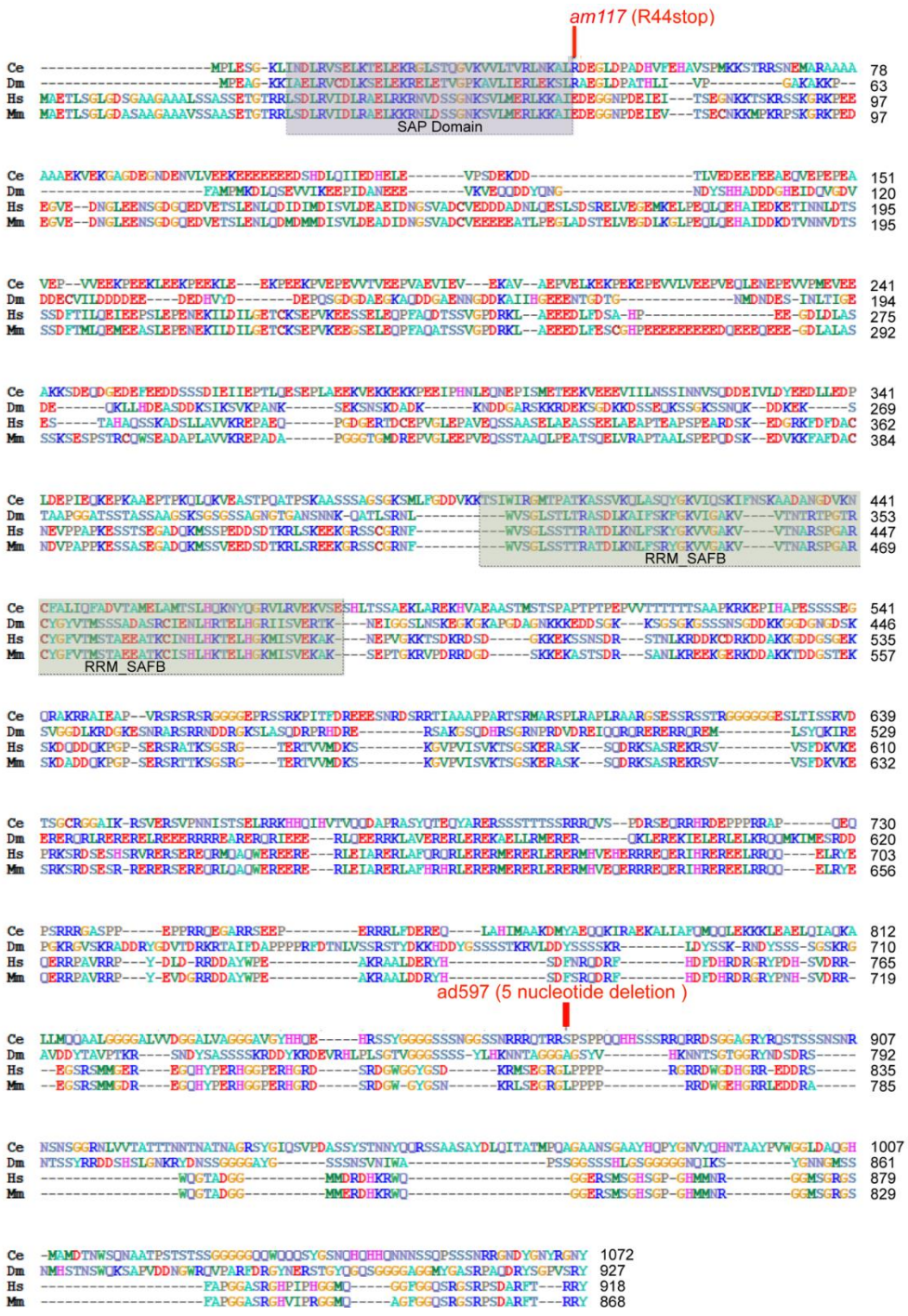

Figure S4. Alignment of PHM-2 protein with insect and mammalian SAFB proteins

The predicted *C. elegans* (Ce) PHM-2 (F32B4.4a) protein is aligned with homologous Scaffold attachment factor B (SAF-B) proteins from the insect *Drosophila melanogaster* (Dm) and the mammals *Homo sapiens* (Hs) and *Mus musculus* (Mm). The *am117* nonsense mutation (red line) and the *ad597* deletion mutation (red line) are marked. Two highly conserved domains are highlighted: the SAP domain (purple) is a putative DNA binding domain and the RRM_SAF domain (green) is a putative RNA recognition motif[432,435].

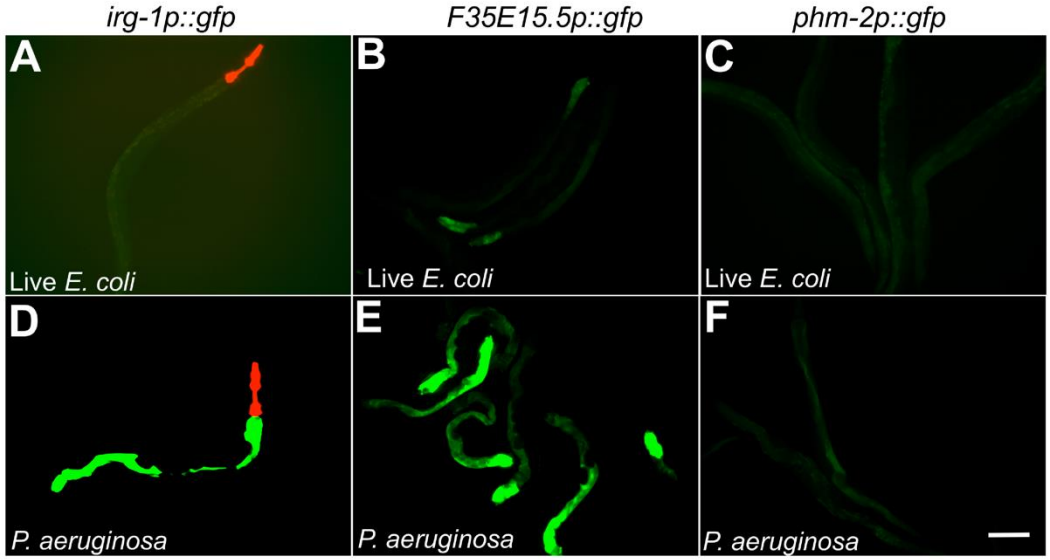

G

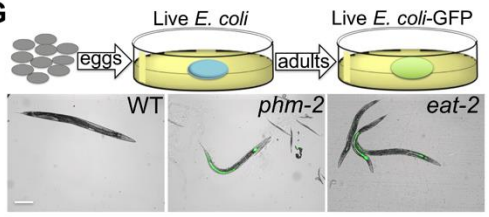

H

Genotype	RNAi	% GFP positive animals ± SD	N (n)
WT	control	1±1	164 (5)
WT	*pha-4*	3±3 ^{ns}	188 (5)
phm-2	control	91±5	122 (5)
phm-2	*pha-4*	88±5 ^{ns}	117 (5)

I

Genotype	% GFP positive animals ± SD	N (n)
WT	4±4	116 (5)
rsks-1(ok1255)	4±5 ^{ns}	105 (5)
phm-2(am117)	95±3	108 (5)
phm-2;rsks-1	100±0 ^{ns}	93 (5)

J

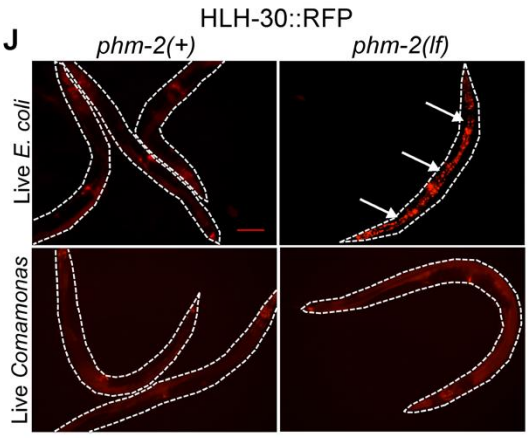

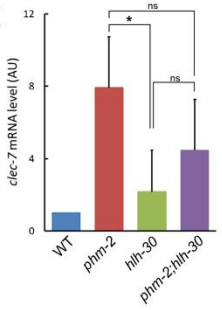

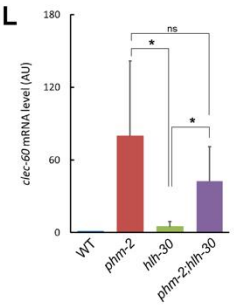

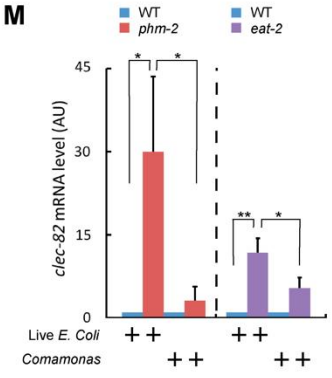

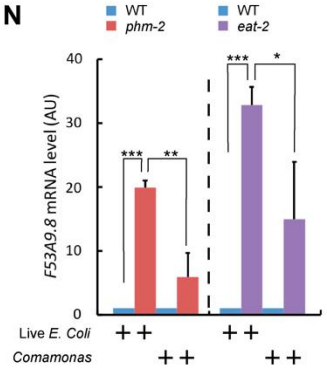

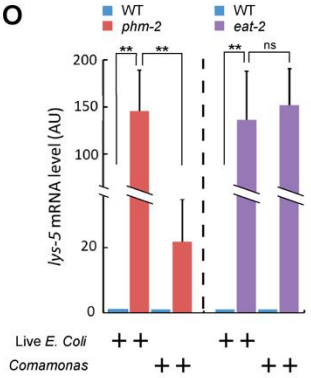

Figure S5. Transcriptional regulation of innate immune genes and HLH-30 nuclear localization

Fluorescence photomicrographs show transgenic animals cultured with live *E. coli* OP50 **(A-C)** or *P. aeruginosa* strain PA14 **(D-F)** for 24 hours. Images were captured at the same time with the same camera exposure. Each of the three transgenic strains contained a promoter driving GFP. *irg-1* (left, *irg-1p::GFP)* and *F35E15.5* (middle, *F35E15.5p::GFP)* are established innate immune response genes, and both strains displayed increased GFP fluorescence when cultured on *P. aeruginosa* compared to live *E. coli.* Animals expressing *phm-2* (right, *phm-2p::GFP)* did not display increased GFP fluorescence when cultured on *P. aeruginosa* compared to live *E. coli*. Red fluorescence in the left panels is a marker that is expressed in the pharynx and used to identify transgenic animals. Scale bar = 100 μm.

(G) Schematic of method (upper), and representative bright field photographs (lower). Green fluorescent animals were not observed in wild-type but were observed in *phm-2(am117)* and *eat-2(ad465)* mutants.

(H-I) Quantification of number of fluorescent animals; adult animals were cultured with green fluorescent *E. coli* for 24 hours. N(n) indicates total number of animals and number of independent trials. **(H)** Wild-type or *phm-2(am117)* hermaphrodites were cultured on *pha-4* RNAi bacteria or control RNAi bacteria until adulthood, then transferred to RNAi plates seeded with a 1:3 mixture of GFP expressing *E. coli* OP50 and RNAi bacteria. WT with *pha-4* RNAi was compared to WT with control, and *phm-2* with *pha-4* RNAi was compared to *phm-2* with control. **(I)** Wild-type, *phm-2(am117)*, *rsks-1(ok1255), and phm-2; rsks-1* adult animals were cultured with green fluorescent *E. coli* for 24 hours. ANOVA; ns, $P > 0.05$; *rsks-1(ok1255)* animals were compared to WT, and *phm-2; rsks-1* animals were compared to *phm-2(am117)*.

(J) Representative fluorescence micrographs of animals that were *phm-2(+)* or *phm-2(am117),* that express HLH-30::RFP, and were cultured on live *E. coli* OP50 or live *Comamonas.* n≥100 animals. Scale bar = 100 μm. Only *phm-2(lf)* animals cultured on live *E. coli* displayed nuclear localized fluorescence (White arrows).

(K-O) Bars represent mRNA levels (+/-S.D) for *clec-7*, *clec-60, clec-82, F53A9.8,* and *lys-5* pathogen response genes determined by qPCR in wild-type, *phm-2(am117), eat-2(ad465), hlh-30(tm1978),* and *phm-2(am117); hlh-30(tm1978)* animals cultured on live *E. coli* OP50 (**M-O** as indicated and **K-L**) or live *Comamonas* bacteria (**M-O** as indicated). Values in arbitrary units (AU) are the average of three to five biological replicates. ANOVA; *, **, $P < 0.05$, $P < 0.005$; ns, not significant, $P > 0.05$.

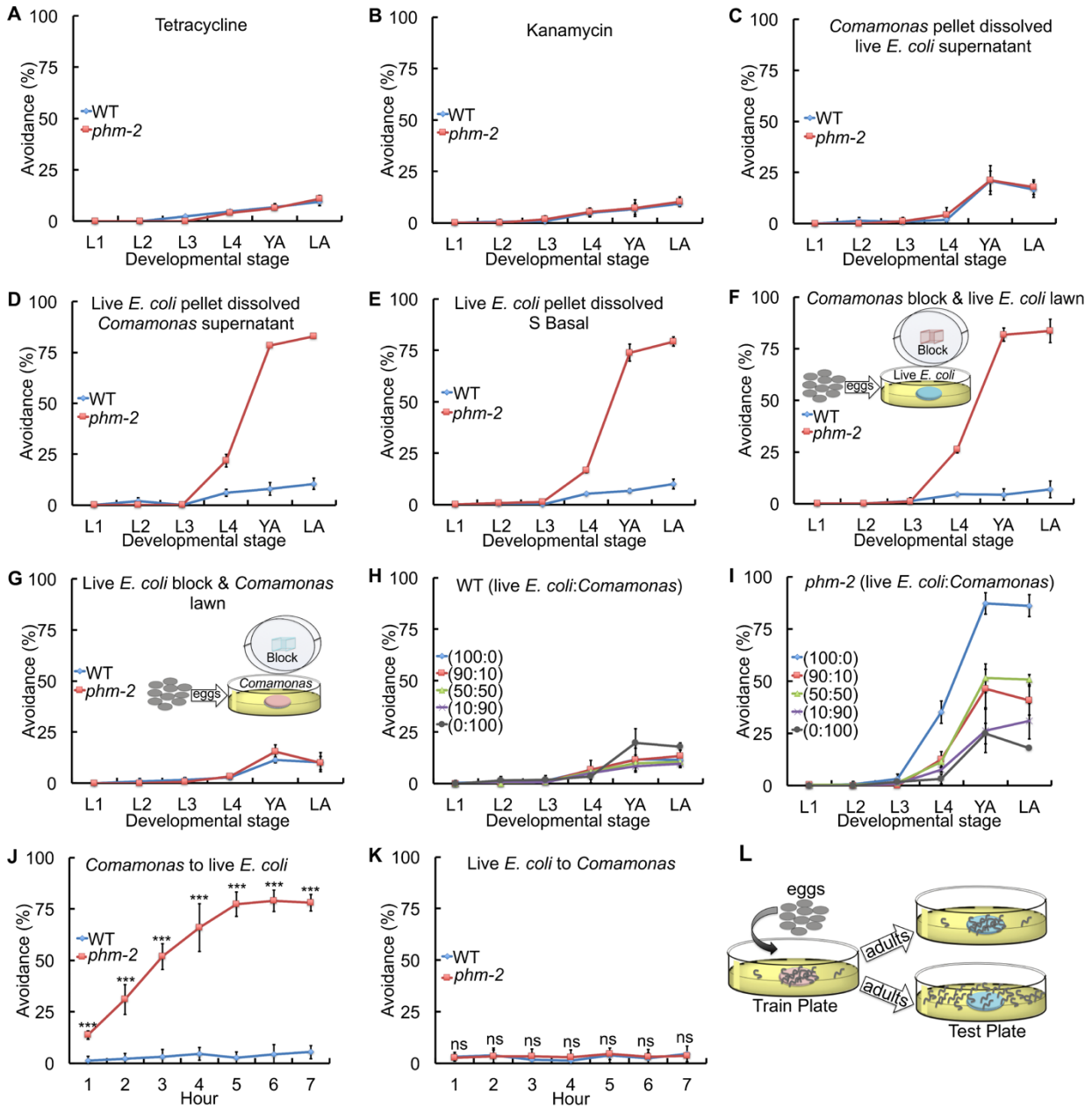

Figure S6. *phm-2(lf)* bacterial avoidance behavior does not appear to be mediated by a secreted factor

(A-K) "Avoidance" is the average percent of animals (+/- SD) outside the bacterial lawn at the larval stages L1, L2, L3, L4, day 1 adult (YA), and day 2 adult (LA). The *phm-2* allele was *am117*. **(A,B)** The antibiotics tetracycline **(A)** or kanamycin **(B)** were added to the NGM medium. Values are the average of three biological replicates, N=120-152 animals. WT and *phm-2* were not significantly different, $P > 0.05$, by Student's *t*-test.

(C) Concentrated *Comamonas* bacteria were dissolved in supernatant from live *E. coli* OP50. Values are the average of three to five biological replicates, N=139-295 animals. WT and *phm-2* were not significantly different, $P > 0.05$, by Student's *t*-test.

(D) Concentrated live *E. coli* OP50 were dissolved in supernatant from *Comamonas* bacteria. Values are the average of three to five biological replicates, N=139-295 animals. WT and *phm-2* were significantly different, $P < 0.001$, by Student's *t*-test.

(E) Concentrated live *E. coli* OP50 were dissolved in S medium buffer. Values are the average of three biological replicates, N=148-150 animals. WT and *phm-2* were significantly different, $P < 0.001$, by Student's *t*-test.

(F) A block of NGM agar with *Comamonas* bacteria was attached to the inside of the lid, and animals were cultured with live *E. coli* OP50. Values are the average of two biological replicates, N=89-100 animals. WT and *phm-2* were significantly different, $P < 0.001$, by Student's *t*-test.

(G) A block of NGM agar with live *E. coli* OP50 was attached to the inside of the lid, and animals were cultured with *Comamonas* bacteria. Values are the average of three biological replicates, N=89-100 animals. WT and *phm-2* were not significantly different, $P > 0.05$, by Student's *t*-test.

(H-I) Wild-type **(H)** and *phm-2(am117)* **(I)** animals were cultured with a mixture of live *E. coli* OP50 and *Comamonas* DA1877 in the following ratios*:* 100:0, 90:10, 50:50, 10:90 and 0:100. Values are the average of three or four biological replicates, N≥100 animals. Tukey post hoc HSD showed *phm-2(am117)* animals cultured with 50:50 was significantly different than 100:0 and 0:100 ($P < 0.01$).

(J-K) WT and *phm-2(am117*) animals were grown on either *Comamonas* or live *E. coli* OP50 bacteria from embryo to the young adult stage and then tested on live *E. coli* OP50 or *Comamonas*. Only *phm-2(am117*) animals on live *E. coli* OP50 displayed bacterial avoidance behavior (N=119-200 animals, 5-6 biological replicates, significance Student's *t*-test; n.s., not significant, $P > 0.05$).

(L) Schematic of learning paradigm.

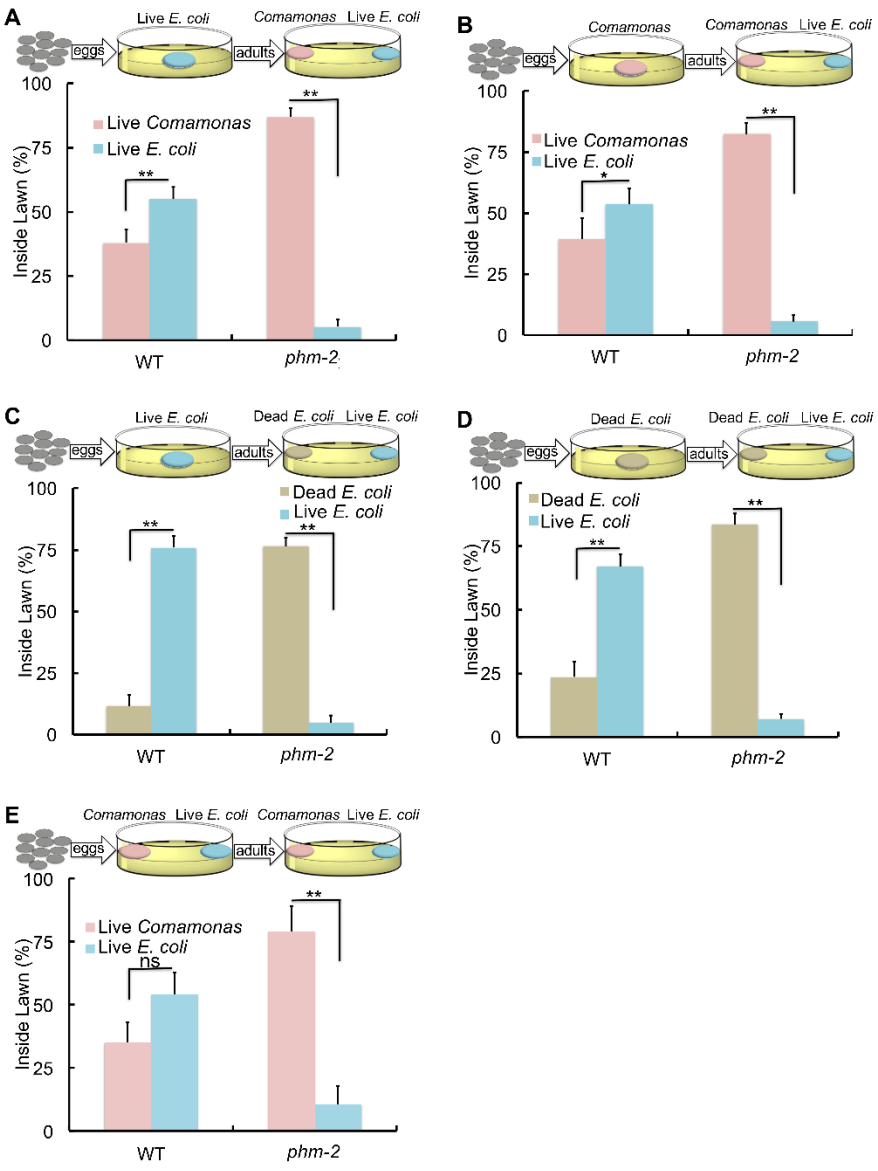

Figure S7. *phm-2(lf)* and wild type displayed different food preferences but no evidence of learning in a food choice learning assay

(A-E) "Inside Lawn" is the average percent of animals (+/- SD) inside the specified bacterial lawn 24 hours after transfer to the test dish. Schematics (top) illustrate the method and bacteria used in each panel. Wild-type and *phm-2(am117)* eggs were transferred to the training dish and allowed to develop to adults. Adult animals were transferred to the test dish containing two small bacterial lawns, and the number of animals inside each lawn was scored after 24 hours. **(A-D)** Values are the average of four biological replicates (N=149-180 animals: Tukey post hoc HSD; *, $P < 0.05$; **, $P < 0.01$.) **(E)** The training dish contained two small bacterial lawns. Values are the average of three biological replicates, (N=77-114 animals: Tukey post hoc HSD; ns, not significant, P>0.05; **, $P < 0.01$

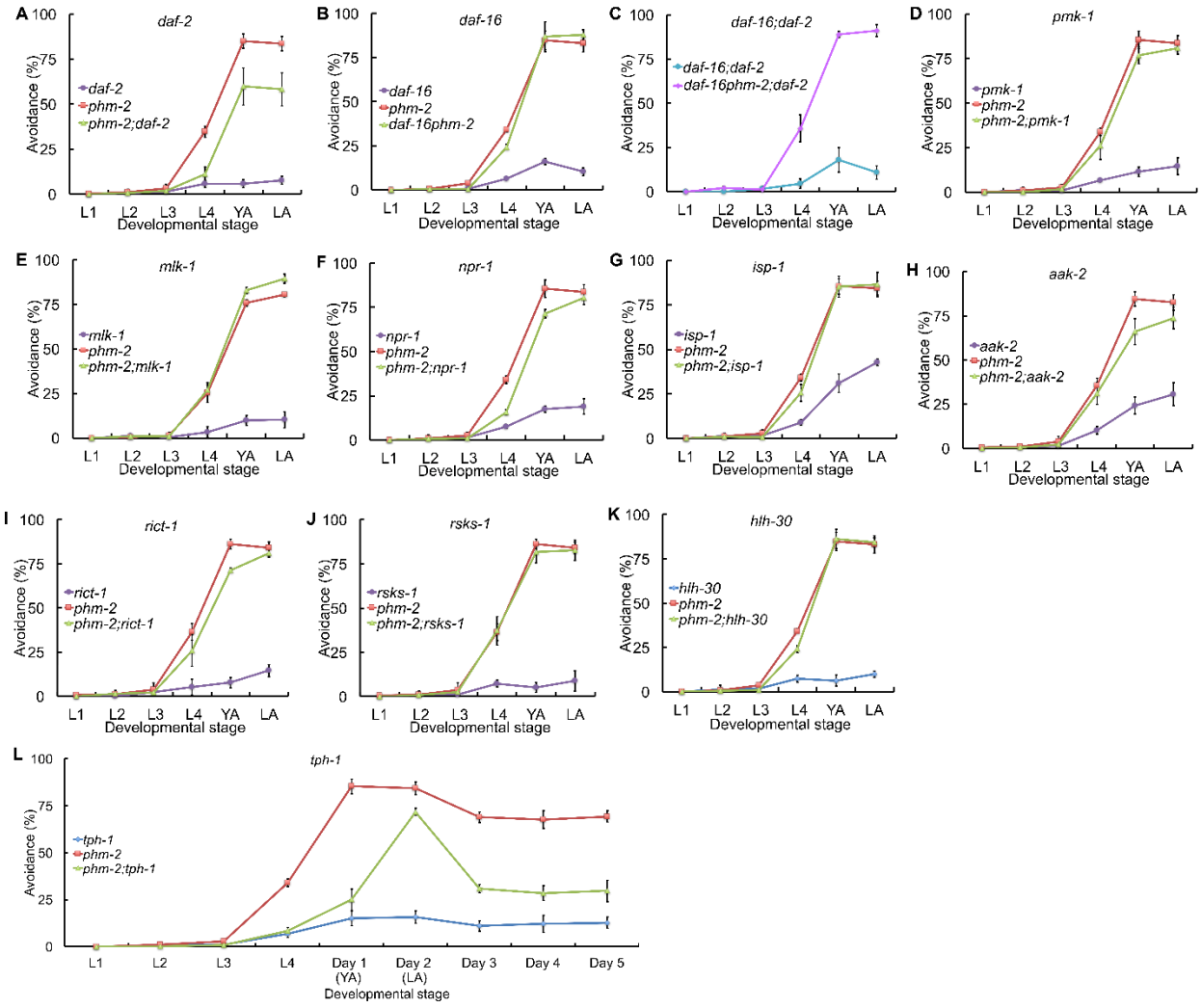

Figure S8. Genetic analysis of *phm-2(lf)* bacterial avoidance behavior

(A-L) "Avoidance" is the average percent of animals (+/- SD) outside the bacterial lawn at the larval stages L1, L2, L3, L4, day 1 adult (YA), and day 2 adult (LA). Panel L also shows results for day 3, 4 and 5 adults - the data for earlier stages are identical to **Figure 4K**. Hermaphrodites were cultured with live *E. coli* OP50 on NGM dishes at 20°C. The alleles were *phm-2(am117), daf-2(e1370), daf-16(mu86), pmk-1(km25), mlk-1(ok2471), npr-1(ur89), isp-1(qm150)*, *aak-2(ok524)*, *rict-1(mg360)*, *rsks-1(ok1255)*, *hlh-30(tm1978),* and *tph-1(mg280)*. See **Table S5** for summary statistics, number of animals and number of independent experiments.

Table S1. *phm-2(lf)* extended mean and maximum life span

Genotype[1]	Mean[2,3] lifespan ± SD (days)	% Change in mean	Maximum[2,3] lifespan ± SD (days)	% Change in maximum	N (n)[4]
WT 20°C	15.8±3.7		21.9±1.2		316 (6)
phm-2(am117) 20°C	21.1±3.1**	+34	27.3±1.2**	+24	279 (6)
WT 15°C	20.5±4.3		28.2±1.4		99 (2)
phm-2(am117) 15°C	30.5±5.4**	+49	38.2±1.0**	+36	140 (2)
WT 25°C	9.8±3.0		15.6±1.1		185 (3)
phm-2(am117) 25°C	16.7±26**	+71	21.2±0.6**	+36	140 (3)
WT	16.1±3.4		22.2±1.3		171 (3)
phm-2(ad538)	21.0±4.0**	+30	28.5±1.2**	+28	148 (3)
phm-2(ad597)	21.4±3.3**	+33	28.2±0.8**	+27	192 (3)
phm-2(am117)	21.8±3.1		27.7±1.4		154 (3)
daf-2(e1370)	36.3±9.9		53.3±3.4		239 (3)
phm-2;daf-2	58±24.6**	+60	100.1±5.6**	+88	156 (3)
phm-2(am117)	21.1±3.1		27.4±1.4		193 (4)
daf-16(mu86)	11.7±2.3		16.3±1.1		219 (4)
daf-16 phm-2	18.5±2.7**	+58	23.3±0.9**	+43	183 (4)
daf-16(mu86)	11.6±2.4		16.3±1.1		104 (2)
daf-16;daf-2	13.0±2.2		16.7±0.8		128 (2)
daf-16 phm-2;daf-2	21.9±3.3**	+68	26.8±0.7**	+60	168 (2)
phm-2(am117)	21.4±2.5		27.2±1.3		180 (4)
isp-1(qm150)	21.3±6.8		33.3±1.4		106 (4)
phm-2;isp-1	28.8±9.9**	+35	43.8±1.2**	+32	91 (4)
phm-2(am117)	21.3±3.1		27.7±1.2		144 (3)
aak-2(ok524)	14.3±2.3		19.6±0.7		178 (3)
phm-2;aak-2	20.4±2.7**	+42	27.1±0.9**	+38	133 (3)
phm-2(am117) FudR[5]	26±4.4		32.5±1.0		83 (2)
eat-2(ad1116) FudR[5]	23.2±3.8		29.5±1		112 (2)
phm-2;eat-2 FudR[5]	22.9±4.5[ns]	-1	30±0.9[ns]	+2	90 (2)
phm-2(am117)	21.3±3.6		27.5±0.9		254 (3)
rict-1(mg360)	10.2±2.2		14.2±0.6		138 (3)
phm-2;rict-1	19.7±2.8**	+93	24.2±0.9**	+70	220 (3)
phm-2(am117)	21.3±3.6		27.5±0.9		254 (3)
rsks-1(ok1255)	17.9±4.4		25.3±1.2		232 (3)
phm-2;rsks-1	18.3±3.6[ns]	+2	25.4±1.5[ns]	+1	179 (3)

phm-2(am117)	20.2±3.1		26.4±1.0		117 (2)
hlh-30(tm1978)	14.8±2.2		18.9±0.8		232 (2)
phm-2;hlh-30[6]	17.3±2.7**	-14	21.7±1.5**	-18	154 (2)
phm-2(am117)	17.2±0.45		22.85±0.26		86 (2)
raga-1(ok386)	17.3±0.48		27.4±0.57		100 (2)
phm-2;raga-1	18.1±0.38 [ns]	+5	26.2±0.62 [ns]	-4	113 (2)
phm-2(am117)	21.2±4.1		28.0±1.0		47
phm-2(am117);amEx321[7]	16.2±3.0**	-23	21.7±1.1**	-22	25
phm-2(am117);amEx322[7]	16.2±3.6**	-23	23.0±1.0**	-18	26
phm-2(am117);amEx324[7]	18.3±4.4**	-14	24.7±0.6**	-12	22
phm-2(am117);amEx328[7]	16.6±4.5**	-21	23.7±1.4**	-15	64
phm-2(am117);amEx331[7]	17.1±3.5*	-19	22.2±0.9**	-20	35

[1]Genotype: Wild-type hermaphrodites or the indicated mutant strains were analyzed.

[2]Lifespan: L4 stage animals were cultured on standard NGM dishes with a small lawn of live *E. coli* OP50 bacteria at 20°C, except those labeled 25°C and 15°C.

[3]Mean, Maximum, % Change: Maximum adult lifespan is the mean lifespan of the 10% of the population that had the longest lifespans. Comparisons are to the matched WT control (rows 1-9), the non-*phm-2* single mutant strain (rows 10-15, 19-33, and 37-39) or to *daf-16; daf-2* (rows 16-18). The statistical test was one-way ANOVA with Tukey post hoc HSD; *, $P < 0.05$; **, $P < 0.01$; ns, not significant, P>0.05.

[4]*N(n)*: Total number of hermaphrodites analyzed, and the number of independent experiments.

[5]Hermaphrodites were exposed FudR, a drug that prevents embryos from hatching, to avoid matricidal hatching and allow the observation of aging.

[6]In rows 34-36, comparison is to *phm-2(am117)*.

[7]Transgenic animals contained the chromosomal mutation *phm-2(am117)* and an extrachromosomal array composed of plasmid pSK2 with the upstream *phm-2* promoter driving the F32B4.4a cDNA and the plasmid pRF4 that causes a dominant Rol phenotype used to identify transgenic animals. Five independently-derived transgenic lines were analyzed, named *amEx321*, *amEx322*, *amEx324*, *amEx328*, and *amEx331*.

Table S2. Avoidance behavior is influenced by bacteria

Genotype[1]	**Bacteria**[2]	**Live/ Dead**[2]	**% Avoidance**[3] **± SD Young adult (YA)**	**% Avoidance**[3] **± SD Late adult (LA)**	**N (n)**[4]
WT *phm-2(am117)*	*E. coli* OP50	Live Live	11.6±5.4 87.2±5.0**	11.4±4.2 88.1±5.2**	410 (9) 453 (9)
WT *phm-2(ad538)* *phm-2(ad597)*	*E. coli* OP50	Live Live Live	9.2±3.7 78.7±3.9** 83.0±4.7**	10.7±2.4 82.2±0.9** 85.3±3.1**	136 (3) 185 (3) 160 (3)
WT *phm-2(am117)*	*E. coli* HB101	Live Live	8.6±4.1 62.9±7.2**	9.4±4.0 70.4±4.1**	273 (5) 296 (5)
WT *phm-2(am117)*	*Comamonas* DA1877	Live Live	19.7±6.9 25.0±4.9^{ns}	18.0±1.7 17.9±3.6^{ns}	252 (5) 269 (5)
WT *phm-2(am117)*	*B. subtilis*	Live Live	15.1±3.9 13.4±3.4^{ns}	13.7±4.4 17.4±7.2^{ns}	284 (5) 257 (5)
WT *phm-2(am117)*	*E. coli* OP50	Dead Dead	13.0±2.9 12.7±0.7^{ns}	16.6±1.4 16.9±0.6^{ns}	162 (3) 155 (3)
WT *eat-2(ad465)*	*E. coli* OP50	Live Live	9.1±2.9 44.5±2.3**	11.5±2.3 54.1±3.5**	307 (7) 334 (7)
WT *eat-2(ad465)*	*Comamonas* DA1877	Live Live	19.5±3.9 20.9±5.0^{ns}	19.9±4.0 21.3±2.8^{ns}	123 (3) 118 (3)
WT *eat-2(ad465)*	*E. coli* OP50	Dead Dead	11.4±2.2 13.3±3.0^{ns}	14.1±2.4 11.6±0.7^{ns}	203 (5) 249 (5)

[1]Genotype: Wild-type hermaphrodites or the indicated mutants were analyzed.

[2]Bacteria: Bacteria of the indicated species and strain were spotted in the center of the NGM dish to form a small lawn. To generate dead *E. coli*, we spotted bacteria on the dish and then treated with UV light.

[3]Avoidance: Animals were scored as inside or outside the bacterial lawn (Avoidance=N_{out}/N_{total}) as one day old adults (YA) and two day old adults (LA); Comparisons are to the matched WT, and the statistical test was one-way ANOVA with Tukey post hoc HSD; *, $P < 0.05$; **, $P < 0.01$; ns, not significant, P>0.05.

[4]*N(n)*: Total number of hermaphrodites analyzed, and the number of independent experiments.

Table S3. Pharyngeal pumping rate of *phm-2* and *eat-2* mutants

Day	Genotype[1]	Pharyngeal pumps per minute ± SD[2]	N (n)[3]
2	WT *phm-2(am117)* *eat-2(ad1116)*	279±25 263±23** 74±17**	55(2) 50(2) 49(2)
4	WT *phm-2(am117)* *eat-2(ad1116)*	253±22 216±26** 51±14**	46(2) 47(2) 57(2)
6	WT *phm-2(am117)* *eat-2(ad1116)*	201±34 205±35^{ns} 45±15**	45(2) 44(2) 44(2)
8	WT *phm-2(am117)* *eat-2(ad1116)*	138±47 196±33** 44±16**	45(2) 43(2) 43(2)
10	WT *phm-2(am117)* *eat-2(ad1116)*	127±43 189±35** 29±18**	47(2) 44(2) 50(2)
12	WT *phm-2(am117)* *eat-2(ad1116)*	65±43 168±40** 25±17**	43(2) 46(2) 46(2)
14	WT *phm-2(am117)* *eat-2(ad1116)*	36±47 105±29** 15±13*	37(2) 36(2) 35(2)
16	WT *phm-2(am117)* *eat-2(ad1116)*	12±16 96±44** 16±14^{ns}	33(2) 30(2) 34(2)
18	WT *phm-2(am117)* *eat-2(ad1116)*	3±5 58±46** 7±8^{ns}	15(2) 24(2) 16(2)

[1]Genotype: Wild-type hermaphrodites or the indicated mutants were analyzed.

[2]Pharyngeal pumps per minute: Pharyngeal pumping rate was measured by counting using a dissecting microscope for 10 seconds. The results were multiplied by 6 to calculate the number of pharyngeal pumps per minute. Comparisons are to the matched WT control. Statistical test was Student's *t*-Test; *, $P < 0.05$; **, $P < 0.01$; ns, not significant, $P>0.05$.

[3]*N(n)*: Total number of hermaphrodites analyzed, and the number of independent experiments.

Table S4. *pha-4* RNAi affected Mean and Maximum life span

Genotype[1]	**RNAi[2]**	**Mean[3] lifespan ±SD (days)**	**%Change in mean**	**Maximum[3] lifespan ± SD (days)**	**% Change in maximum**	**N (n)[4]**
WT	Control	16.5±3.5		22.6±0.9		234 (5)
WT	*pha-4*	12.2±2.9**	-26	18.0±1.3**	-20	203 (5)
phm-2(am117)	Control	20.7±4.8		30.2±1.2		128 (5)
phm-2(am117)	*pha-4*	11.5±2.7**	-44	16.2±1.2**	-46	267 (5)
WT	*pha-4*	12.2±2.9		18.0±1.3		203 (5)
phm-2(am117)	*pha-4*	11.5±2.7^{ns}	-6	16.2±1.2**	-10	267 (5)
daf-2(e1370)	Control	39.3±9.6		53.3±2.7		117 (3)
daf-2(e1370)	*pha-4*	39.9±11.2^{ns}	+2	57.0±2.0**	+7	115 (3)

[1]Genotype: Wild-type hermaphrodites or the indicated mutant strains were analyzed.

[2]RNAi: Animals were cultured with bacteria containing the control RNAi plasmid (L4440) or the *pha-4* RNAi plasmid starting at the L4 stage.

[3]Mean, Maximum, % Change: Maximum adult lifespan is the mean lifespan of the 10% of the population that had the longest lifespans. Comparisons are between rows 1 and 2, 3 and 4, 5 and 6, or 7 and 8. Statistical test was one-way ANOVA with Tukey post hoc HSD; *, $P < 0.05$; **, $P < 0.01$; ns, not significant, P>0.05.

[4]*N(n)*: Total number of hermaphrodites analyzed, and the number of independent experiments.

Table S5. Bacterial avoidance behavior of mutant strains

Genotype[1]	**% Avoidance**[2] **± SD Young adult (YA)**	**% Avoidance**[2] **± SD Late adult (LA)**	**N (n)**[3]
tph-1(mg280)	15.1±3.9	15.8±3.3	292 (5)
phm-2(am117)	85.3±4.2	84.3±3.9	250 (5)
phm-2;tph-1	25.0±5.7**	71.7±1.9**	304 (5)
daf-2(e1370)	5.8±2.2	7.7±2.3	431 (9)
phm-2(am117)	85.0±3.9	83.5±3.9	465 (9)
phm-2;daf-2	59.8±10.3**	58.2±9.0**	485 (9)
daf-16(mu86)	16.0±1.7	10.3±2.2	258 (3)
phm-2(am117)	84.8±5.2	83.2±5.0	135 (3)
daf-16 phm-2	86.9±8.4^{ns}	87.9±3.0^{ns}	210 (3)
daf-16;daf-2	17.9±6.9	10.8±3.8	199 (3)
daf-16 phm-2;daf-2	88.9±1.6**	91.0±3.2**	190 (3)
isp-1(qm150)	31.0±5.2	42.7±1.8	266 (4)
phm-2(am117)	85.4±4.3	84.3±3.9	250 (4)
phm-2;isp-1	85.2±5.9^{ns}	86.5±6.8^{ns}	212 (4)
aak-2(ok524)	24.2±4.8	30.7±6.5	210 (4)
phm-2(am117)	84.6±4.0	82.5±4.3	215 (4)
phm-2;aak-2	66.1±7.3**	73.7±6.0^{ns}	213 (4)
rict-1(mg360)	7.7±3.0	14.6±3.5	177 (3)
phm-2(am117)	86.2±2.9	84.2±2.9	166 (3)
phm-2;rict-1	71.4±1.4**	81.0±2.2^{ns}	174 (3)
rsks-1(ok1255)	5.1±2.8	8.8±5.8	176 (3)
phm-2(am117)	86.2±2.9	84.2±2.9	166 (3)
phm-2;rsks-1	81.7±6.0^{ns}	82.8±5.7^{ns}	181 (3)
hlh-30(tm1978)	6.4±3.2	10.0±1.7	159 (3)
phm-2(am117)	84.8±5.2	83.2±4.9	135 (3)
phm-2;hlh-30	86.4±5.3^{ns}	84.4±2.6^{ns}	165 (3)
pmk-1(ok2471)	11.4±2.6	14.4±4.7	240 (4)
phm-2(am117)	85.5±4.9	83.6±4.1	204 (4)
phm-2;pmk-1	76.8±4.7*	80.7±3.3^{ns}	229 (4)
mlk-1(ok2471)	9.8±2.8	10.3±4.6	183 (4)
phm-2(am117)	75.8±1.8	80.6±1.1	191 (4)
phm-2;mlk-1	82.9±1.9**	89.5±2.6**	211 (4)
npr-1(ur89)	17.5±1.9	18.9±4.4	183 (4)
phm-2(am117)	85.5±4.9	83.7±4.1	191 (4)
phm-2;npr-1	71.3±2.4**	80.3±3.7^{ns}	211 (4)

[1]Genotype: The indicated mutant strains were cultured with a small lawn of live *E. coli* OP50 bacteria on NGM dishes at 20°C.

[2]Avoidance: Animals were scored as inside or outside the bacterial lawn (Avoidance=N_{out}/N_{total}) as one day old adults (YA) and two day old adults (LA); Comparisons are to the *phm-2* single mutant, and the statistical test was one-way ANOVA with Tukey post hoc HSD; *, $P < 0.05$; **, $P < 0.01$; ns, not significant, $P > 0.05$.

[3]*N(n)*: Total number of hermaphrodites analyzed, and the number of independent experiments.

Table S6. The bacterial strain and lawn size affected mean and maximum life span

Genotype[1]	Bacteria[2]	Mean[3] lifespan ± SD (days)	% Change in mean	Maximum[3] lifespan ± SD (days)	% Change in maximum	N (n)[4]
WT *phm-2(am117)*	Live *E. coli* OP50	15.8±3.7 21.1±3.1**	+34	21.9±1.2 27.3±1.2**	+24	316 (6) 279 (6)
WT *phm-2(am117)*	Live *E. coli* HB101	15.2±2.7 20.6±3.5**	+36	19.8±0.9 26.7±0.8**	+35	158 (3) 93 (3)
WT *phm-2(am117)*	Live *Comamonas*	14.7±2.4 15.2±2.4[ns]	+4	18.8±0.6 19.3±0.5*	+3	83 (2) 141 (2)
WT *phm-2(am117)*	Live *B. subtilis*	20.4±4.7 20.5±4.4 [ns]	+1	27.7±1.4 27.6±1.2 [ns]	-1	68 (3) 59 (3)
WT *phm-2(am117)*	Dead *E. coli* OP50	17.9±3.6 16.2±3.1**	-10	24.5±1.1 22.0±0.8**	-10	78 (2) 69 (2)
WT *phm-2(am117)*	Begin on Live *E. coli* OP50, transfer to Live *E. coli* OP50	15.2±0.4 21.1±0.6**	+39	24.2±0.4 29.8±0.3**	+23	97 (2) 103 (2)
WT *phm-2(am117)*	Begin on Live *Comamonas*, transfer to Live *E. coli* OP50	14.5±0.4 19.96±0.4**	+32	22.0±0.5 26.4±0.5**	+20	87 (2) 100 (2)
WT *eat-2(ad465)*	Live *E. coli* OP50	17.0±3.7 22.2±4.7**	+30	23.0±1.0 31.0±2.4**	+36	116 (2) 115 (2)
WT *eat-2(ad465)*	Live *Comamonas*	14.4±2.8 14.8±2.8 [ns]	+3	19.4±1.0 20.1±0.9 [ns]	-1	72 (2) 76 (2)
WT *eat-2(ad465)*	Dead *E. coli* OP50	20.1±4.8 22.3±7.1**	+11	27.4±1.1 34.0±1.8**	+24	231 (5) 275 (5)
WT[5] *phm-2(am117)* [5]	Live *E. coli* OP50, Large Lawn	12.6±4.4 8.6±3.8**	-31	19.6±1.3 16.9±2.3**	-14	146 (6) 172 (6)
phm-2(am117) [5] *tph-1(mg280)* [5] *phm-2;tph-1*[5]	Live *E. coli* OP50, Small Lawn	18.8±5.5 13.3±4.3 11.9±6.9*	-37	28.6±1.0 21±1.4 24.4±1.5**	-15	163 (3) 275 (3) 142 (3)

[1]Genotype: Wild-type hermaphrodites or the indicated mutants were analyzed.

[2]Bacteria: Bacterial species of the indicated strains were spotted in the center of the NGM dish to form a small lawn, except rows 21-22 where bacteria were spread to form a large lawn. To generate dead *E. coli*, we spotted bacteria on the dish and then treated with UV light. For rows 11-14, animals were cultured on one bacterial strain from egg to adulthood, and then transferred to a second strain for the remainder of the lifespan.

[3]Mean, Maximum, % Change: Maximum adult lifespan is the mean lifespan of the 10% of the population that had the longest lifespans. Comparisons are to the matched WT control; row 25 was compared to row 23. Statistical test was one-way ANOVA with Tukey post hoc HSD; *, $P < 0.05$; **, $P < 0.01$; ns, not significant, $P > 0.05$.

[4]*N(n)*: Total number of hermaphrodites analyzed, and the number of independent experiments.

[5]For rows 21-25, animals that died due to matricidal hatching were not censored from the data.

Appendix 3: Supplemental data for Chapter 6

Supplemental
Figure 1

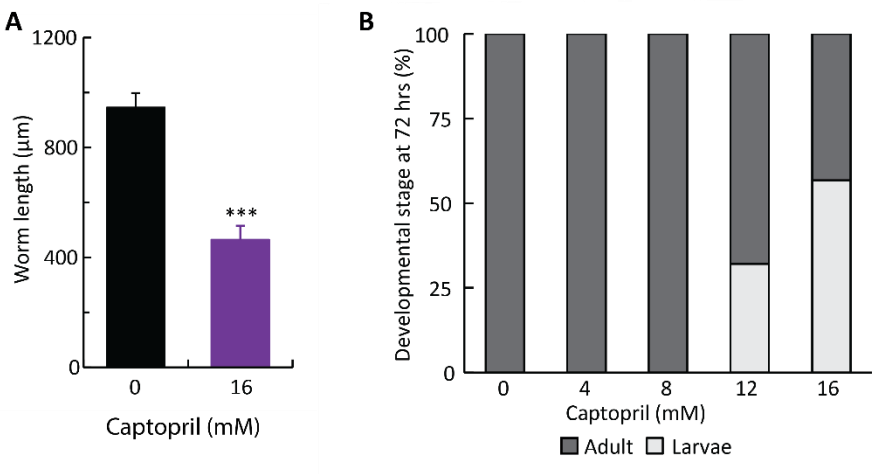

Figure S1: Captopril caused dose-dependent developmental delays.

(A) Wild-type embryos were cultured on medium containing 0 (black) or 16 (purple) mM captopril for 72 hrs, and length of individuals was scored using Wormsizer [716]. 16 mM captopril significantly reduced growth rate. Values are average length and s.d. n=13-32 animals, Student's *t*-test, ***, $p<0.001$. **(B)** Wild-type embryos were cultured on medium containing 0, 4, 8, 12, or 16 mM captopril for 72 hrs at 20°C, and the developmental stage of each animal was classified as adult (dark gray) or larva (light gray) based on morphological criteria. Bars indicate the percentage of animals at each stage and total 100%. Captopril caused a dose-dependent reduction in the rate of development. Whereas 100% of animals matured to adults when cultured with 0, 4, or 8 mM captopril, ~70% matured to adults with 12 mM captopril and ~45% with 16 mM captopril. n=4 trials, N=96-119 animals.

Supplemental
Figure 2

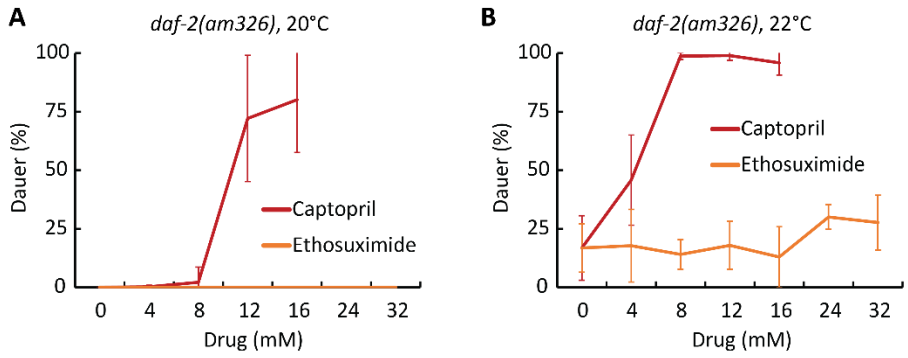

Figure S2: Captopril but not ethosuximide promoted dauer formation.

(A,B) *daf-2(am326)* embryos were cultured at 20°C **(A)** or 22°C **(B)** on medium containing the indicated concentrations of captopril (red) or ethosuximide (orange). Values are the average percentage of animals in the dauer stage and s.d. (see **Table S2 and S6** for statistics). The captopril data is identical to **Fig. 5A** and is displayed here to facilitate comparison to the ethosuximide data. Ethosuximide is an FDA-approved anticonvulsant that extends nematode lifespan at a similar concentration to that of captopril [681,682]. In contrast to captopril, ethosuximide did not promote dauer formation.

Supplemental
Figure 3

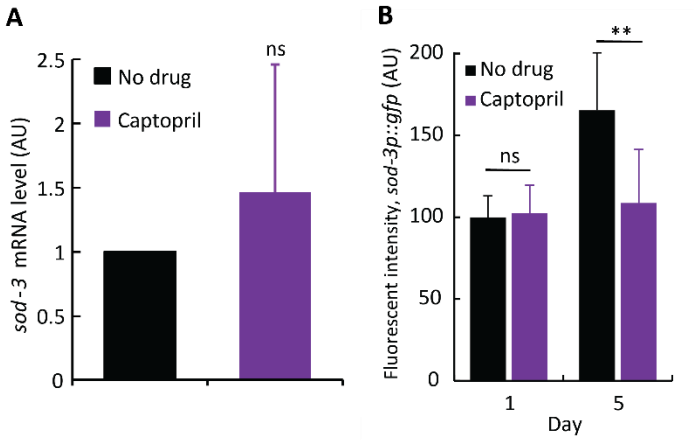

Figure S3: Captopril did not activate expression of *sod-3*, a DAF-16 target gene.

(A) Wild-type embryos were cultured at 20°C on medium containing 0 mM (No drug, black) or 2.5 mM captopril (purple). After three days (day 1 of adulthood), animals were harvested for total RNA, and *sod-3* mRNA levels were measured using qPCR. *ama-1* mRNA levels were used as an internal control, and the mRNA level in 0 mM was set equal to 1.0. Values are mRNA levels in arbitrary units (AU) and s.d. No significant difference was observed. N=4 biological replicates, Student's *t*-test. **(B)** Transgenic animals that contain a *sod-3p::gfp* transcriptional reporter were cultured at 20°C on medium containing 0 mM (No drug, black) or 2.5 mM captopril (purple). Young adult (Day 1) and middle-aged adult (Day 5) animals were analyzed by fluorescence microscopy. Values are total fluorescence quantified in arbitrary units (AU) and s.d. Captopril-treated animals did not display a significant increase in fluorescent intensity. n=3 trials, N=26-38 animals, Student's *t*-test. ns, non-significant, $p \geq 0.05$; **, $p < 0.01$.

Table S1: Effect of captopril on WT lifespan

Genotype[a]	Captopril (mM)[b]	Mean lifespan (days±s.e.)[c]	Change vs. 0 mM (%)[d]	N (n)[e]
WT	0	17.7±0.5		136 (5)
WT	0.3	17.5±0.9	-1.1[ns]	25 (1)
WT	1.6	20.0±0.6	+13.0*	63 (2)
WT	1.9	19.2±2.1	+8.5[ns]	14 (2)
WT	2.5	23.7±1.1	+33.9***	27 (1)
WT	3.2	19.7±0.4	+11.3*	126 (5)
WT	3.8	22.5±0.8	+27.1***	33 (1)
WT	5.7	17.5±0.5	-1.1[ns]	79 (3)
WT	7.6	14.8±0.8	-16.4**	27 (1)

[a] All animals were wild type (WT).

[b] Animals were cultured with this concentration of captopril in the medium beginning at the L4 larval stage.

[c] Mean lifespan and standard error (s.e.) determined by Kaplan-Meier survival function.

[d] Percent change in lifespan compared to 0 mM captopril; negative values indicate lifespan reduction, and positive values indicate lifespan extension. ns, non-significant, $p \geq 0.05$; *, $p < 0.05$; **, $p < 0.01$; ***, $p < 0.001$ by log-rank (Mantel-Cox) test.

[e] N, total number of animals; n, number of independent trials.

Table S2: Effect of genotype, captopril, and temperature on dauer formation

Genotype[a]	Captopril (mM)[b]	Temperature (°C)[c]	Dauer (%±s.d.)[d]	N (n)[e]
WT	0	20	0±0	775 (22)
	4		0±0	743 (21)
	8		0±0	784 (22)
	12		0±0	640 (22)
	16		0±0	620 (23)
	0	22	0±0^{ns}	468 (8)
	4		0±0^{ns}	334 (7)
	8		0±0^{ns}	438 (9)
	12		0±0^{ns}	375 (9)
	16		0.8±2.0 ^{ns}	188 (7)
	0	25	0±0^{ns}	519 (9)
	4		0±0^{ns}	444 (9)
	8		0±0^{ns}	369 (8)
	12		2.5±5.6 ^{ns}	313 (9)
	16		3.9±9.6 ^{ns}	119 (6)
	0	27	0±0^{ns}	128 (3)
	4		0±0^{ns}	137 (3)
	8		0±0^{ns}	140 (3)
	12		0±0^{ns}	123 (3)
	16		12.8±1.4**	62 (3)
daf-2(am326)	0	20	0±0^{ns}	400 (9)
	4		0.2±0.7^{ns}	367 (9)
	8		2.2±6.5^{ns}	343 (9)
	12		72.1±27.0**	189 (8)
	16		80.0±22.5**	137 (9)
	0	22	16.8±13.8*	341 (8)
	4		45.8±19.2***	384 (9)
	8		98.7±1.4***	348 (9)
	12		98.9±2.1**	369 (12)
	16		95.8±5.2 ^{ns}	254 (11)
	0	25	90.0±15.2***	377 (9)
	4		100±0***	380 (9)
	8		100±0***	370 (9)
	12		97.7±7.4**	366 (10)
	16		80.1±20.7 ^{ns}	345 (10)
daf-16(mu86)	0	20	0±0^{ns}	231 (8)
	4		0±0^{ns}	239 (8)
	8		0±0^{ns}	215 (8)
	12		0±0^{ns}	181 (8)

	16		0±0[ns]	111 (8)
daf-2(am326);daf-16(mu86)	0	20	0±0[ns]	222 (8)
	4		0±0[ns]	217 (8)
	8		0±0[ns]	189 (8)
	12		0±0[ns]	156 (8)
	16		0±0[ns]	78 (8)
daf-2(syb4952)	0	20	0±0[ns]	118 (4)
	4		0±0[ns]	104 (4)
	8		12.1±7.1**	117 (4)
	12		94.8±4.2**	102 (4)
	16		75.3±14.9**	60 (4)
daf-2(e1370)	0	20	8.9±15.6 [ns]	543 (13)
	4		1.5±3.0 [ns]	364 (10)
	8		1.4±1.9 [ns]	358 (10)
	12		26.6±16.0**	278 (10)
	16		68.5±27.5**	163 (10)
daf-2(e1370);daf-16(mu86)	0	20	0±0[ns]	111 (4)
	4		0±0[ns]	115 (4)
	8		0±0[ns]	87 (4)
	12		0±0[ns]	98 (4)
	16		0±0[ns]	30 (4)

[a] Animals were wild type (WT) or had the indicated alleles of *daf-2* and *daf-16*.

[b] Animals were cultured with this concentration of captopril in the medium beginning at the embryo stage.

[c] Culture temperature beginning at the embryo stage.

[d] The percentage of dauer larvae was determined by counting the number of dauer larvae and dividing by the total number of surviving animals. Animals were analyzed 2-4 days after the embryo stage, and dauer was defined using visual inspection and morphological criteria. Wild type cultured at 22, 25, and 27°C were compared to the same captopril concentration at 20°C. Mutant genotypes at 20°C were compared to WT at the same concentration of captopril. *daf-2(am326)* animals at 22 and 25°C were compared to *daf-2(am326)* animals at 20°C. s.d., standard deviation. ns, non-significant, $p \geq 0.05$; *, $p < 0.05$; **, $p < 0.01$; ***, $p < 0.001$ by one-way ANOVA with post-hoc Tukey HSD.

[e] N, total number of animals; n, number of independent trials.

Table S3: Effect of captopril, oxidative stress, and heat stress on *daf-2(am326)* mutant lifespan and survival

	Genotype[a]	Treatment[b]	Mean lifespan (days±s.e.)[c]	Survival time under stress (hrs±s.e.)[d]	Change (%)[e]	N (n)[f]
1	WT	None	14.5±0.2			365 (6)
2	WT	Captopril (2.5 mM)	15.5±0.3		+6.9***	219 (4)
3	*daf-2(am326)*	None	25.3±0.5		+74.5***	351 (6)
4	*daf-2(am326)*	Captopril (2.5 mM)	29.5±0.8		+16.6***	227 (4)
5	WT	Oxidation (40 mM paraquat)		33.2±1.26		47 (3)
6	*daf-2(am326)*	Oxidation (40 mM paraquat)		70.9±3.7	+114***	57 (3)
7	WT	Heat (35°C)		6±0		87 (3)
8	*daf-2(am326)*	Heat (35°C)		15.7±1.0	+162***	85 (3)

[a] Animals were wild type (WT) or *daf-2(am326)*

[b] Embryos were cultured with standard medium at 20°C; beginning at the L4 larval stage, animals were transferred to standard medium at 20°C (lines 1,3), medium containing 2.5 mM captopril at 20°C (lines 2,4), medium containing 40 mM paraquat at 20°C (lines 5,6), or standard medium at 35°C (lines 7,8).

[c] Mean lifespan and standard error (s.e.) determined by Kaplan-Meier survival function.

[d] Survival time after transition of L4 animals to medium containing paraquat or high heat and standard error (s.e.) determined by Kaplan-Meier survival function.

[e] Percent change in lifespan or survival time. Lines 2 and 3 compared to line 1. Line 4 compared to line 3. Line 6 compared to line 5. Line 8 compared to line 7. ***, $p<0.001$ by log-rank (Mantel-Cox) test.

[f] N, total number of animals; n, number of independent trials.

Table S4: Unique base pair variants correlated with the position of *am326*.

Chromosome[a]	Position[b]	Region affected[c]	Gene[d]	Reference Base[e]	Mutant Base[f]	Predicted amino acid change[g]
I	3990093	Intergenic	N/A	T	A	
I	5153878	Intron	C05D2.16	A	T	
I	10207580	Intergenic	N/A	A	C	
III	2501655	Intron	D2030.14	A	T	
III	2501656	Intron	D2030.14	T	C,G,A	
III	2501657	Intron	D2030.14	G	T	
III	2596005	Intron	*apb-1*	T	A	
III	2609341	Exon	Y71H2B.5	G	A	D147N
III	2616752	Intron	Y71H2B.5	G	A	
III	2627506	5'UTR	Y71H2B.5	T	C	
III	2833819	5'UTR	Y71H2AM.1	T	C	
III	2883947	Intron	F56F11.2	T	G	
III	2932661	Exon	*cdh-1*	G	A	D2353N
III	2960916	5'UTR	H05C05.1	G	T,C	
III	2967423	Intergenic	N/A	T	C	
III	2989344	Intron	Y55D5A.4	A	T	
III	3015386	Exon	*daf-2*	G	A	A261V
III	3027523	Intron	*daf-2*	T	A	
III	3151035	lincRNA	*linc-19*	G	A	
III	3176041	Exon	R148.3	G	A	E143K
III	3209991	Intron	*frm-8* and Y41C4A.28	T	A	
III	3209994	Intron	*frm-8* and Y41C4A.28	G	A	
III	3230687	Intron	Y41C4A.28	T	C	
III	3427844	Intron	Y41C4A.28 and Y92C3A.8 and *metl-18*	G	A	
III	3549790	Exon	C54C6.5	G	A	A14T
III	3717368	Intron	*nrde-1*	T	A	
III	3852545	Intergenic	N/A	C	T	
III	3856303	Intron	*brc-1*	T	C	
III	3996847	Intergenic	N/A	G	A	
III	4386389	Exon	*pals-28*	G	A	R220K
III	4466409	Intron	*ndg-4*	T	A	
III	4546277	Intergenic	N/A	G	A	

III	4873286	Intron	C35D10.12	G	A	
III	4907433	Intron	*rom-1*	G	A	
III	5132742	Intron	*tbx-2*	G	A	
III	5208540	Exon	*syx-16*	C	T	R58Q
III	5208869	Intron	*syx-16*	G	A	
III	5570359	Intergenic	N/A	G	A	
III	5592934	Exon	*ucr-1*	G	A	G173A
IV	8580492	Intergenic	N/A	A	T,G	
V	14755854	Intergenic	N/A	T	C	
V	16707257	Intron	*clec-9*	C	T	
V	16707293	Intron	*clec-9*	C	T,A	
X	7078104	Intergenic	N/A	G	A,T,C	
X	10368098	Intergenic	N/A	C	A,T	

[a] The chromosome containing the base pair variant (I, III, IV, V, or X).
[b] The number assigned to the nucleotide position of the base pair variant by the WS220.64/ce10 *C. elegans* reference genome, measured from the end of the chromosome.
[c] The predicted relationship of the position of the base pair variant to coding regions (Intergenic, Intron, Exon, lincRNA, or 5'UTR).
[d] The name of the gene affected by the base pair variant; N/A indicates an intergenic region.
[e] The nucleotide base present in the reference strain at that position, defined as wild type.
[f] The nucleotide base(s) present in the *am326* strain at that position, defined as mutant. At some positions, multiple different bases were present in the mutant strains.
[g] Eight base pair variants are predicted to cause an amino acid substitution. Red indicates the A261V substitution in *daf-2* that is the *am326* mutation. Yellow indicates the seven missense mutations that are linked, but are not the *am326* mutation.

Table S5: Effect of captopril treatment on WT and mutant lifespan

Genotype[a]	Treatment[b]	Mean lifespan (days±s.e.)[c]	Change (%)[d]	N (n)[e]
WT	None	14.5±0.4		105 (2)
WT	Captopril (2.5 mM)	17.5±0.5	20.6***	114 (2)
daf-16(mu86)	None	12.2±0.3	-15.9***	118 (2)
daf-16(mu86)	Captopril (2.5 mM)	12.2±0.3	0^{ns}	120 (2)
daf-2(am326);daf-16(mu86)	None	14.1±0.4	-2.8^{ns}	121 (2)
daf-2(am326);daf-16(mu86)	Captopril (2.5 mM)	14.6±0.4	3.5^{ns}	120 (2)
WT	None	15.8±0.2		534 (6)
WT	Captopril (2.5 mM)	17.8±0.5	12.7**	185 (3)
daf-2(syb4952)	None	30.4±0.6	92.4***	356 (5)
daf-2(syb4952)	Captopril (2.5 mM)	34.5±0.9	13.5***	160 (3)
WT	None	15.5±0.5		173 (3)
WT	Captopril (2.5 mM)	17.8±0.5	14.8**	185 (3)
daf-12(rh61rh411)	None	14.8±0.4	-4.5^{ns}	138 (3)
daf-12(rh61rh411)	Captopril (2.5 mM)	13.8±0.3	-6.8*	169 (3)
WT	None	17.2±0.6		154 (2)
acn-1(am314/+)	None	19.8±0.7	15.1**	187 (2)

[a] Animals were wild type (WT) or had the indicated alleles of *daf-2*, *daf-12*, *daf-16*, or *acn-1*.

[b] Embryos were cultured with standard medium at 20°C; beginning at the L4 larval stage, animals were transferred to standard medium at 20°C or medium containing 2.5 mM captopril at 20°C.

[c] Mean lifespan and standard error (s.e.) determined by Kaplan-Meier survival function.

[d] Percent change in lifespan. Mutants with no drug are compared to WT with no drug. Animals treated with captopril are compared to the same genotype with no drug. Negative values indicate lifespan reduction, and positive values indicate lifespan extension. ns, non-significant, $p \geq 0.05$; *, $p < 0.05$; **, $p < 0.01$; ***, $p < 0.001$ by log-rank (Mantel-Cox) test.

[e] N, total number of animals; n, number of independent trials.

Table S6: Effect of ethosuximide treatment on dauer formation

Genotype[a]	Ethosuximide (mM)[b]	Temperature (°C)[c]	Dauer (%±s.d.)[d]	N (n)[e]
WT	0	20	0±0	152 (3)
	4		0±0[ns]	148 (3)
	8		0±0[ns]	152 (3)
	12		0±0[ns]	141 (3)
	16		0±0[ns]	131 (3)
	24		0±0[ns]	142 (3)
	32		0±0[ns]	144 (3)
WT	0	22	0±0	162 (3)
	4		0±0[ns]	142 (3)
	8		0±0[ns]	143 (3)
	12		0±0[ns]	138 (3)
	16		0±0[ns]	139 (3)
	24		0±0[ns]	132 (3)
	32		0±0[ns]	139 (3)
WT	0	25	0±0	152 (3)
	4		0±0[ns]	143 (3)
	8		0±0[ns]	144 (3)
	12		0±0[ns]	140 (3)
	16		0±0[ns]	139 (3)
	24		0±0[ns]	141 (3)
	32		0±0[ns]	142 (3)
daf-2(am326)	0	20	0±0	400 (9)
	4		0±0[ns]	150 (3)
	8		0±0[ns]	156 (3)
	12		0±0[ns]	159 (3)
	16		0±0[ns]	153 (3)
	24		0±0[ns]	145 (3)
	32		0±0[ns]	146 (3)
daf-2(am326)	0	22	16.8±13.8	341 (8)
	4		17.7±15.5[ns]	156 (3)
	8		14.0±6.4[ns]	143 (3)
	12		17.9±10.2[ns]	150 (3)
	16		12.9±12.9[ns]	151 (3)
	24		30.0±5.3[ns]	150 (3)
	32		27.6±11.7[ns]	155 (3)
daf-2(am326)	0	25	100±0	151 (3)
	4		100±0[ns]	148 (3)
	8		100±0[ns]	146 (3)
	12		100±0[ns]	151 (3)
	16		100±0[ns]	155 (3)
	24		100±0[ns]	150 (3)

	32		100±0[ns]	149 (3)

[a] Animals were wild type (WT) or *daf-2(am326)*.

[b] Animals were cultured with this concentration of ethosuximide in the medium beginning at the embryo stage.

[c] Culture temperature beginning at the embryo stage.

[d] The percentage of dauer larvae was determined by counting the number of dauer larvae and dividing by the total number of surviving animals. Animals were analyzed 2-4 days after the embryo stage, and dauer was defined using visual inspection and morphological criteria. Animals cultured with ethosuximide were compared to 0 mM ethosuximide with the same genotype and temperature. Ethosuximide did not significantly promote dauer formation in any condition. s.d., standard deviation. ns, non-significant, $p \geq 0.05$ by one-way ANOVA with post-hoc Tukey HSD.

[e] N, total number of animals; n, number of independent trials.

Table S7: Effect of *acn-1* RNAi on dauer formation

Genotype[a]	RNAi[b]	Temperature (°C)[c]	Dauer (%±s.d.)[d]	N (n)[e]
WT	Control	20	0±0	151 (3)
		22	0±0	152 (3)
		25	0±0	152 (3)
	acn-1	20	0±0[ns]	158 (3)
		22	0±0[ns]	162 (3)
		25	0±0[ns]	152 (3)
daf-2(am326)	Control	20	0±0	167 (3)
		22	13.8±6.4	155 (3)
		25	100±0	155 (3)
	acn-1	20	0±0[ns]	144 (3)
		22	31.5±7.4**	149 (3)
		25	100±0[ns]	154 (3)

[a] Animals were wild type (WT) or *daf-2(am326)*.

[b] Animals were cultured with *E. coli* HT115 bacteria containing plasmid L4440 modified to encode *acn-1* dsRNA or plasmid L4440 with no insert as a control.

[c] Culture temperature beginning at the embryo stage.

[d] The percentage of dauer larvae was determined by counting the number of dauer larvae and dividing by the total number of surviving animals. Animals were analyzed 2-4 days after the embryo stage, and dauer was defined using visual inspection and morphological criteria. Values for *acn-1* RNAi were compared to control at the same temperature and genotype. s.d., standard deviation. ns, non-significant, $p \geq 0.05$; **, $p < 0.01$ by one-way ANOVA with post-hoc Tukey HSD

[e] N, total number of animals; n, number of independent trials.